Caspase-dependent signaling as an inductive cue for cardiac hypertrophy

Charis Putinski

Thesis submitted to the Faculty of Graduate and Postdoctoral Studies
in partial fulfillment of the requirements for the
Doctorate in Philosophy degree in Cellular and Molecular Medicine

Department of Cellular and Molecular Medicine
Faculty of Medicine
University of Ottawa

© Charis Putinski, Ottawa, Canada, 2018

Authorization

Permission for reproduction of material from Hill J.A., and Olson E.N., Cardiac Plasticity. The New England Journal of Medicine. 358(13): 1370-80, © 2008 Massachusetts Medical Society in a thesis/dissertation was freely provided at no additional cost.

Permission for reproduction of material from Molketin, J.D., Parsing Good Versus Bad Signaling Pathways in the Heart. Circulation Research. 113:16-19, © 2013 Wolters Kluwer Health, Inc in a thesis/dissertation was freely provided at no additional cost.

Permission for reproduction of material from Best, S.A. Viral Subversion of Apoptotic Enzymes: Escape from Death. Annual Review of Microbiology. 62: 171-192, © 2008 Annual Reviews in a thesis/dissertation was freely provided at no additional cost.

Permission for the reproduction, as part of a thesis dissertation, of Putinski, C. et al. Intrinsic-mediated caspase activation is essential for cardiomyocyte hypertrophy. Proceedings of the National Academy of Sciences USA. 110(43):E4079-87, © 2013 is provided by the authors and the National Academy of Sciences.

Permission to include the paper Abdul-Ghani, M. et al. Cardiotrophin 1 stimulates beneficial myogenic and vascular remodeling of the heart. Cell Research. 27(10): 1195-1215, © 2017 is provided by the authors and Springer Nature.

Permission to include the paper Dick, SA. et al. Caspase 3 cleavage of Pax7 inhibits self-renewal of satellite cells. Proceedings of the National Academy of Sciences, USA 112(38):E5246-52, © 2015 is provided by the authors and National Academy of Sciences.

Abstract

The heart has the remarkable ability to adjust in response to varying stress stimuli and myocardium enlargement, referred to as cardiac hypertrophy, is a common form of stress adaptation. Divergent forms of hypertrophy can occur depending on the type and duration of the insult. The beneficial physiological form of hypertrophy is reversible and leads to improved cardiac function, while the pathological form is a maladaptive process that often transitions to heart failure. As a result of the prominence of cardiac disease, investigations into methods of reducing this detrimental form of cardiac remodeling are sought. Interestingly, pathological cardiac hypertrophy shares common features with the regulated form of cell death referred to as apoptosis. Here, we describe an essential role for apoptotic caspase-dependent signaling in the induction of pathological cardiac hypertrophy. Initially, we discovered that primary cardiomyocytes treated with hypertrophy agonists display transient activation of intrinsic-mediated apoptotic-signaling, including caspase 9 and caspase 3 activity. The necessity of functional caspase activation in hypertrophic signaling was shown by both *in vitro* and *in vivo* methods. We further investigated caspase cleavage targets histone deacetylase 3 (HDAC3) and gelsolin (GSN). HDAC3 cleavage was observed during early stages of hypertrophy and reduced in the presence of a caspase inhibitor. Caspase-mediated GSN cleavage occurred at latter stages, coincident with the cytoskeletal alterations that occur during this process. We demonstrated the requirement of GSN and its caspase-mediated processing by use of GSN expressing adenoviruses (AdVs). Use of a non-cleavable GSN-AdV provided evidence for not only the requirement of GSN in the hypertrophic response, but also for caspase-mediated GSN cleavage. This body of work implicates caspase pathways and

their targets as inductive signaling cues for pathological cardiac hypertrophy. These observations suggest that inhibitors that mute or suppress caspase activity and/or activity of its cognate substrates may offer novel therapeutic targets to limit the development of pathological hypertrophy.

Table of Contents

Authorization……ii

Abstract……iii

Table of Contents……..v

List of Figures…..……viii

List of Tables……..x

List of Abbreviations……xi

Acknowledgments……....xv

Chapter 1: General Introduction……1

1.1 Cardiac physiology and adaptability……..……2
1.1.1 Physiological cardiac hypertrophy……..……5
1.1.2 Pathological cardiac hypertrophy…..……..8
1.2 Caspase proteases and apoptotic signaling……..……...11
1.2.1 Endogenous regulation of caspase-mediated apoptotic signaling…….……..…..14
1.3 Non-death roles of apoptotic signaling and caspases…….…16
1.3.1 Mechanisms to control/restrain caspases for non-death cell activities…….……...……18
1.3.2 Caspases and cardiac hypertrophy……..……..21
1.3.3 The potential roles of actin remodeling protein gelsolin in cardiac hypertrophy…….……25
1.4 The use of synthetic modulators of aspase activity in disease therapy……28
1.5 Hypothesis and Aims…….……..31
1.5.1 Hypothesis……..32
1.5.2 Aims……...……32

Chapter 2: Intrinsic-mediated caspase activation is essential for cardiomyocyte hypertrophy…….…..34

Contribution of Co-Authors…….……36
Significance……..……...37
Abstract……..38
Introduction……39
Results and Discussion……..……42
Activation of the Intrinsic Cell Death Pathway During Agonist-Induced Cardiomyocyte Hypertrophy……42

Activation of the Intrinsic Cell Death Pathway Is Required for Cardiomyocyte Hypertrophy……...51
Effector Caspase/Caspase 3 Activation Is Essential for Cardiomyocyte Hypertrophy *in Vitro* and *in Vivo*……...56
Caspase 3 Activation Is Sufficient to Induce Cardiomyocyte Hypertrophy……65
Materials and Methods……..……..73
Acknowledgements……74
Supporting Information……..75
SI Materials and Methods……..75
Cell Culture……75
Cardiomyocyte Treatments……75
Immunocytochemistry……...…76
Detection of Mitochondrial Membrane Potential……..77
Cardiomyocyte Viability……78
Caspase and Calpain Activity Assays……79
Caspase 3-Specific Small Molecule Activation……79
Prohypertrophic Reporter Luciferase Assay……..79
In Vivo Cardiomyocyte Hypertrophy……80
Immunoblotting……..81
Statistical Analysis……82

Chapter 3: Caspase cleavage of gelsolin is an inductive cue for pathologic cardiac hypertrophy……83

Contribution of Collaborators……..…..……84
Abstract……..85
Introduction……..…….……86
Results ……..……88
Gelsolin is cleaved by effector caspases during pathological cardiac hypertrophy…….……..88
Gelsolin is essential for cardiomyocyte hypertrophy……91
Full-length or caspase cleaved N-terminal gelsolin induces cardiomyocyte hypertrophy……93
Full-length or caspase cleaved N-terminal gelsolin induces cardiomyocyte hypertrophy *in vivo*……96
Secreted gelsolin is a hypertrophy inductive cue……101
Discussion……...……104
Methods……108
Cell culture…….……..108
Immunoblotting……..…….……109
In vitro cleavage assay……..……..……109
Mass spectrometry……...……110
Immunofluorescence……110
Construction of gelsolin adenoviruses……...……..……111
Gelsolin adenovirus infection and cardiomyocyte treatments……114
Gelsolin siRNA knockdown and gelsolin reintroduction……116

Prohypertrophic reporter luciferase assay……116
In vivo gelsolin adenovirus analysis……..…….....117
Caspase inhibition and gelsolin adenovirus infection…….....118
Conditioned hypertrophy media analysis…….……..…118
Statistical analysis…….……..119

Chapter 4: General Discussion…….……120

4.0 General Discussion……..……..121
4.1 Apoptosis and the heart…….…….……121
4.2 The essential role of intrinsic-mediated caspase activation during pathological hypertrophy…….…….122
4.3 Timing and localization of caspase 3 activity during pathological cardiac hypertrophy……...……...126
4.4 Caspase-mediated gelsolin cleavage is required for pathological cardiac remodeling……...…..128
4.5 Future directions……...…131
4.6 Conclusions……133

References……...…135

References: Chapter 1, 3, and 4……...……135
References: Chapter 2……..153

Appendix I……...…..157

Figure 1: HDAC3 is cleaved by effector caspase 3 and 7…….…..158

Figure 2: End-point heart weight to body weight and heart weight to tibia length ratio analysis of intra-myocardial control GFP or gelsolin adenovirus injected rats…..159

Appendix II: Abdul-Ghani, M. et al. (2017) Cardiotrophin 1 stimulates beneficial myogenic and vascular remodeling of the heart. Cell Research. 27(10): 1195-1215 ….160

Appendix III: Dick, SA. et al. (2015) Caspase 3 cleavage of Pax7 inhibits self-renewal of satellite cells. Proceedings of the National Academy of Sciences, USA. 112(38):E5246-52……..…182

List of Figures

Chapter 1: General Introduction

Figure 1: The divergent outcomes of physiological and pathological cardiac hypertrophy……4

Figure 2: Signaling events governing pathologic and physiologic cardiac hypertrophy..……..……..7

Figure 3: The caspase cascade can be activated by intrinsic and extrinsic signals……13

Chapter 2: Intrinsic-mediated caspase activation is essential for cardiomyocyte hypertrophy

Figure 1: Increased caspase 3 and 9 activation during early stages of PE- and ISO-induced cardiomyocyte hypertrophy……..……43

Figure S1: Increased caspase 3 and 9 activation during early stages of agonist-induced cardiomyocyte hypertrophy…….45

Figure S2: Increased caspase 3 activation and localization during PE-induced cardiomyocyte hypertrophy…….……..46

Figure S3: Increased caspase 9 activation during agonist-induced cardiomyocyte hypertrophy……..….47

Figure S4: z-Stack confocal imaging indicates specificity of nuclear-localized active caspase 3 during PE-induced cardiomyocyte hypertrophy……..……49

Figure S5: Global/total caspase activity remained unchanged during PE-induced cardiomyocyte hypertrophy…….……50

Figure 2: The intrinsic mitochondrial/caspase 9 cell death pathway is required for PE- and ISO-induced cardiomyocyte hypertrophy……...53

Figure S6: Cardiomyocyte cell size and ANP levels are reduced by Mcl-1-AdV during 24 h agonist-induced hypertrophy……..55

Figure 3: Caspase 3 activation is required for PE- and ISO-induced cardiomyocyte hypertrophy……57

Figure S7: Effector caspase 3 is required for agonist-induced hypertrophy……..59

Figure S8: Qualitative analysis of paracrine effects during p35-AdV infection……..…61

Figure 4: Inhibition of caspase 3 activity attenuates cardiomyocyte hypertrophy in the intact myocardium……..……....…….66

Figure S9: Cardiomyocyte viability is maintained after low-dose PAC-1 treatment……67

Figure 5: Caspase 3 activation is sufficient to induce cardiomyocyte hypertrophy……..69

Chapter 3: Caspase cleavage of gelsolin is an inductive cue for pathologic cardiac hypertrophy

Figure 1: Gelsolin is an essential caspase cleavage substrate during cardiomyocyte hypertrophy……..…….89

Figure S1: Cytoplasmic and plasma gelsolin start sites within the precursor *Rattus norvegicus* Gelsolin amino acid sequence……..92

Figure 2: Expression of wild-type or N-terminal gelsolin can induce hypertrophy in primary cardiomyocytes…….…94

Figure S2: Expression of wild-type or N-terminal gelsolin can rescue the hypertrophy response reduced by caspase inhibition……...……..97

Figure 3: Wild-type or N-terminal gelsolin overexpression can induce a hypertrophy response in the intact myocardium……..……..98

Figure S3: Left ventricular posterior wall thickness, fractional shortening and cardiac output measured throughout gelsolin adenovirus *in vivo* study……..……100

Figure 4: Gelsolin secreted by hypertrophic cardiomyocytes may be involved in the induction of hypertrophy……...…….103

Figure S4: Confirmation of proper expression from gelsolin adenoviruses……..…..115

Appendix I:

Figure 1: HDAC3 is cleaved by effector caspase 3 and 7…….……..158

Figure 2: End-point heart weight to body weight and heart weight to tibia length ratio analysis of intra-myocardial control GFP or gelsolin adenovirus injected rats.…159

List of Tables

Chapter 3: Caspase cleavage of gelsolin is an inductive cue for pathologic cardiac hypertrophy

Table 1: Primers used for gelsolin adenovirus construction……..……..112

List of Abbreviations

A	Alanine
AA	Amino Acid
ab	Antibody
ABP	Actin-binding Proteins
ACEI	Angtiotensin-converting Enzyme Inhibitor
AdV	Adenovirus
Akt	Protein Kinase B
AngII	Angiotensin II
ANP	Atrial Natriuretic Peptide
Apaf-1	Apoptotic Protease Activating Factor 1
ARB	Angiotensin II Receptor Blocker
ARTS	Sept4_i2
ATP	Adenosine Triphosphate
ATPase	Adenosine Triphosphatase
Bad	Bcl-2-associated death protein
Bak	Bcl-2-antagonist/Killer 1
Bax	Bcl-2-associated X protein
Bcl-2	B-cell CLL/Lymphoma 2
Bcl-xL	B-cell lymphoma-extra large
BH	Bcl-2 Homology
Bid	BH3-interacting domain death agonist
Bim	Bcl-2-interacting mediator of cell death
BIR	Baculoviral inhibitor of apoptosis protein repeat
BNP	B-Type Natriuretic Peptide
BSA	Bovine Serum Albumin
BW	Body Weight
CAD	Caspase-activated DNase
CaM	Calmodulin
CAMK	Ca^{2+}/Calmodulin-dependent Kinase
CARD	Caspase Recruitment Domain
Caspase	Cysteinyl-aspartate specific protease
CCT	Chaperonin Containing Tcp-1
CHAPS	3-(3-cholamidopropyl)-dimethyl-ammonio)-propanesulfonate
CK2	Casein Kinase 2
Cn	Calcineurin
CnA	Calcineurin A
CnB	Calcineurin B
CnT	Cardiac Troponin T
CT1	Cardiotrophin 1
Cyt *c*	Cytochrome *c*
CO	Cardiac Output
D	Aspartic Acid
DAG	Diacylglycerol
DAPI	4’,6-diamidino-2-phenylindole

DED	Death Effector Domain
DISC	Death-inducing Signaling Complex
DMEM	Dulbecco's Modified Eagle Medium
DMSO	Dimethyl Sulfoxide
DNA	Deoxyribonucleic Acid
DTT	Dithiothreitol
E	Glutaminc Acid
ECL	Enhanced Chemiluminescence
ECHO	Echocardiography
EF	Ejection Fraction
EGTA	Ethylene glycol-bis(2-aminoethylether)-*N,N,N′,N′*-tetraacetic acid
ERK	Extracellular-regulated Protein Kinase
ESC	Embryonic Stem Cell
ET1	Endothelin 1
FADD	Fas-associated Death Domain
FBS	Fetal Bovine Serum
FITC	Fluorescein isothiocyanate
fmk	Fluoromethylketone
GFP	Green Fluorescent Protein
gp130	Glycoprotein 130
GPCR	G-Protein Coupled Receptors
GSN	Gelsolin
hCT1	Human Cardiotrophin 1
HDAC	Histone Deacrtylase
HDAC3	Histone Deacetylase 3
HDAC4	Histone Deacetylase 4
HF	Heart Failure
HR	Heart Rate
HRP	Horseradish Peroxidase
Hsps	Heat Shock Proteins
HW	Heart Weight
ICAD	Inhibitor of Caspase-activated DNase
IGF-1	Insulin-like Growth Factor 1
IAP	Inhibitors of Apoptosis
IκBα	Inhibitor of Kappa B Alpha
IL-1β	Interleukin-1β
IP3	Inositol-triphosphate
IRES	Internal Ribosome Entry Site
ISO	Isoproterenol
IVS	Interventricular Septum
J-MEM	Joklik's modified Eagle medium
JNK-1	c-Jun N-terminal Kinase
LC-MS/MS	Liquid chromatography-mass spectrometry
LV	Left Ventricle
LVID	Left Ventricular Internal Diameter
LVPW	Left Ventricular Posterior Wall

MAPK	Mitogen-activated Protein Kinase
Mcl-1	Myeloid Cell Leukemia
MDM2	Mouse Double Minute 2 Homolog
MEF2	Myocyte Enhancer Factor-2
MHC	Myosin Heavy Chain
MI	Myocardial Infarction
MKs	Megakaryocytes
MOI	Multiplicity of Infection
MOMP	Mitochondrial Outer Membrane Permeabilization
MST1	Mammalian Sterile Twenty-like Kinase
mTOR	Mechanistic target of rapamycin
MyBP C	Myosin Binding Protein C
MyoD	Myoblast Determination Protein
NFAT	Nuclear Factor of Activated T Cells
NF-κB	Nuclear Factor Kappa B
NLS	Nuclear Localization Signal
Omi	Protein HtrA2
p53	Tumor Protein p53
PAAC	Partial Abdominal Aortic Constriction
PAC-1	Procaspase Activating Compound 1
PAH	Pulmonary Hypertension
PARP	Poly (ADP-ribose) Polymerase
Pax7	Paired-box 7
PBS	Phosphate-Buffered Saline
PCD	Programmed Cell Death
PCR	Polymerase chain reaction
PE	Phenylephrine
PFA	Paraformaldehyde
PI	Propidium Iodide
PI3K	Phosphoinositide 3-kinase
PIP_2	Phosphatidylinositol 4,5-biphosphate
PLC	Phospholipase C
PP2B	Protein Phosphatase 2B
PVDF	Polyvinylidene Fluoride
Rac	Ras-related C3 botulinum toxin substrate
RasGAP	Ras GTPase Activating Protein
RNA	Ribonucleic Acid
SAPK	Stress-activated protein kinase
SEM	Standard Error of the Mean
SF	Serum Free
siRNA	Small Interfering RNA
SRF	Serum Response Factor
SDS/PAGE	Sodium Dodecyl Sulfate/Polyacrylamide Gel Electrophoresis
SMAC	Second Mitochondrial-derived Activator of Caspases
STS	Staurosporine
SV	Stroke Volume

TL	Tibia Length
TNF	Tumor Necrosis Factor
TNF-α	Tumor Necrosis Factor Alpha
TUNEL	Terminal Deoxynucleotidyl Transferase dUTP Nick End Labeling
Wnt	Wingless
WT	Wild-type
XIAP	X-linked Inhibitor of Apoptosis
Yca1	Yeast Caspase 1
z-DEVD-fmk	*N*-benzyloxycarbonyl-Asp-Glu-Val-Asp-fluomethylketone
z-LEHD-fmk	*N*-benzyloxycarbonyl-Leu-Glu-His-Asp-fluoromethylketone
z-VAD-fmk	*N*-benzyloxycarbonyl-Val-Ala-Asp-fluoromethylketone

Acknowledgments

Firstly, thank you to my supervisor, Dr. Lynn Megeney, for your unwavering support over the years. Thank you for guiding me throughout this journey and for teaching me many important lessons, both in and outside of the lab. I consider myself extremely fortunate to have completed my studies in Dr. Megeney's laboratory and will be forever grateful for his mentorship. I would like to express sincere gratitude towards all of the past and present Megeney Lab members. You were all instrumental to my progress. Thank you for all of your crucial guidance, technical support, and for always being there to lend a helping hand. Furthermore, thank you to my thesis advisory committee members, both past and present, for keeping me on track throughout both my Master's and Doctorate studies; Drs. Marjorie Brand, Patrick Burgon, Pasan Fernando, Duncan Stewart, and Valerie Wallace.

I would like to thank my friends for their support. Thank you for always being there, especially during the tough times, and for understanding my limited availability over the past few months. Thank you, Jason. Thank you for always keeping a smile on my face and for standing by my side. I cannot thank you enough for your encouragement and support. Finally, I want to acknowledge my family. To my parents, Diane and Steve, my sister, Ashley, and my brother, Shawn; thank you for putting up with my necessity for silence over the years (Dad that means you can now leave your subwoofer on). Thank you for believing in me and for pushing me to achieve my goals. Thank you to everyone who played a role, no matter how big or how small, in enriching my life over the duration of my graduate studies. This road has been filled with many challenges, but it has been brimming with even more wonderful memories, and for that I am truly grateful.

Chapter 1:

General Introduction

1.1 Cardiac physiology and adaptability

The mammalian heart is constructed of four chambers, consisting of two atria and two ventricles, and has evolved from the two- and three-chambered heart of fish and amphibians, respectively (Olson 2006). Separation of the pulmonary and systemic circulatory systems is achieved through the structure of the four-chambered heart, enabling more efficient transport of oxygenated blood. Here, deoxygenated blood is received through the right atrium and travels to the right ventricle via the atrioventricular valve. Blood then enters the lungs through the pulmonary artery where it receives oxygen and expels carbon dioxide. This oxygenated blood then enters the left atrium and subsequently the left ventricle through the mitral valve. The left ventricle is responsible for pumping this oxygenated blood to the rest of the body. The sequence of events occurring when the heart beats is called the cardiac cycle and includes diastolic and systolic phases. In the diastole phase, the ventricles are relaxed and filling with blood. Conversely, the ventricles contract and pump out blood to the arteries during the systole phase.

The heart is the most fatigue-resistant striated muscle in the body and continues to pump oxygen and nutrients via the bloodstream to the tissues of the body without rest. This continuous contractile activity is managed by cardiomyocytes, which are specialized muscle cells comprised of myofibrils with repeating sarcomeric units (McMullen & Jennings 2007). The sarcomere is the region of the myofilament in which the thin actin filaments are anchored to adjacent filaments by α-actinin at the Z-disc. The thick filaments, referred to as myosin, use Adenosine Triphosphatase (ATPase)-generated force to pull the thin filaments causing the sarcomere length to shorten. This sliding

action is synonymous with muscle contraction. In turn, cardiomyocytes are highly resistant to fatigue, with a high mitochondrial density to enable continuous production of ATP (McFalls et al. 2003).

The heart is among the first organs to develop during embryogenesis, in order to meet the developing organism's demand for continuous supply of oxygenated blood. As such, cardiomyocytes are one of the earliest cell lineages to be specified. Cardiac progenitor cells arise early in gastrulation from the anterior lateral mesoderm and migrate to the cranial and cranio-lateral regions of the embryo. This population of epithelial progenitor cells is referred to as the cardiac crescent, which expresses cardiac specific markers (Harvey 2002). For instance, the mammalian ortholog of the *Drosophila* gene *Wingless*, *Wnt*, is one of the earliest markers of cardiac specification in mesodermal progenitors (Wu et al. 1995). The formation of the mammalian heart is initiated by these committed mesodermal precursor cells, which develop into the primitive linear heart tube. This structure undergoes cardiac looping, which places the four chambers and vessels in alignment to that of the adult heart (Zaffran & Frasch 2002). The heart becomes functional, beating and pumping blood, within three weeks post fertilization, emphasizing its early specification and development. These events rely on specific cardiogenic transcription factors. Some of the major players in the early stages of cardiogenesis include Myocyte Enhancer Factor-2 (MEF2), GATA4, Nkx2.5, Hand1, Hand2, and Tbx5 (Olson & Srivastava 1996; Bruneau 2002).

In response to environmental demands, the post-natal heart has a remarkable capability to remodel, with a variety of stimuli inducing growth or atrophy of the myocardium (Figure 1) (Hill & Olson 2008). Cardiac atrophy is accompanied by a

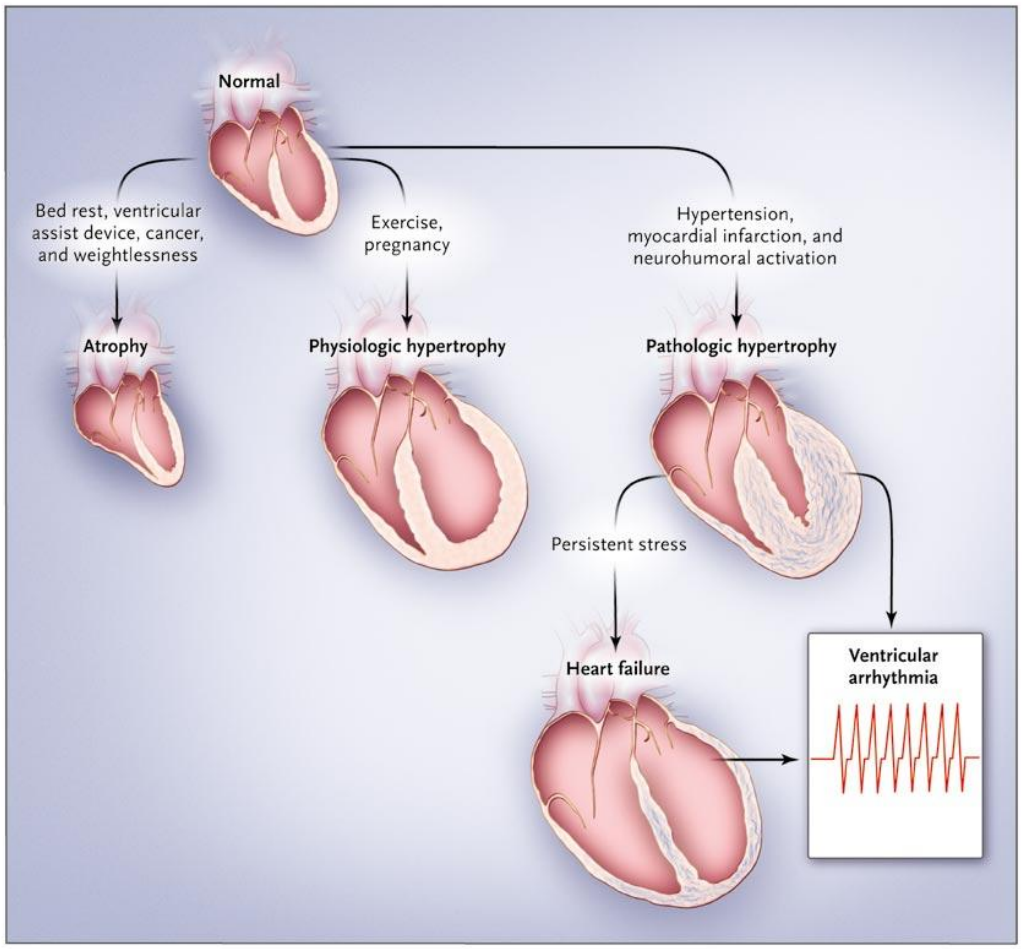


Figure 1. The divergent outcomes of physiological and pathological cardiac hypertrophy. The heart is an adaptive organ, which responds to stress stimuli by increasing or decreasing in size, referred to as hypertrophy and atrophy, respectively. Cardiac hypertrophy can be induced by varying forms of stimuli leading to divergent outcomes. Physiological hypertrophy occurs as a result of exercise or pregnancy while hypertension, myocardial infarction, and neurohumoral activation can lead to pathological hypertrophy. Persistent pathological stress can often transition into heart failure. Figure reprinted by permission from Massachusetts Medical Society: Hill, J.A. and Olson, E.N. Cardiac Plasticity. The New England Journal of Medicine. 358(13):1370-80©2008.

reduction in the size of the heart and can be induced by reduced workload due to extended bed rest, immobilization, cancer, malnutrition, or aging. Alternatively, cardiac hypertrophy is typically associated with an increase in the size of the left ventricle allowing the heart to maintain cardiac output (CO) at times of stress. As cardiomyocytes are terminally differentiated, myocardial growth results from an increase in the size of the existing cardiomyocyte population rather than by an increase in cell number. Hypertrophy is initially a beneficial adaptive response to acute cardiac stress; however, chronic stress on the heart is a maladaptive process that often leads to an unproductive form of hypertrophy, which may transition to heart failure (HF) and ultimately death (McMullen & Jennings 2007). Cardiac hypertrophy may be physiological or pathological, which is generally considered to be a beneficial or detrimental adaptation, respectively. Although both forms of hypertrophy are stress adaptations, the cellular and molecular mechanisms that drive each process have unique attributes, which uniquely influence the structure and function of the heart itself (Figure 1).

1.1.1 Physiological cardiac hypertrophy

Physiological cardiac hypertrophy is a form of myocardial growth that is beneficial, reversible, and not associated with progress to HF. This form of hypertrophy is exemplified by an equal increase in ventricular wall thickness and chamber dimension. At the cellular level this growth is manifested by addition of sarcomeres in series and an overall increase in cardiomyocyte length. This is in contrast to concentric hypertrophy, which results in addition of sarcomeres in parallel leading to an increase in the cross-sectional area of cardiomyocytes (Heineke & Molkentin 2006; Barry & Townsend 2010). A variety of stimuli are associated with the induction of physiologic hypertrophy, with

pregnancy and endurance sports training being the most studied examples (Dorn 2007; Chung & Leinwand 2014; Roh et al. 2016). Under these circumstances, the heart responds to the increased demands for oxygenated blood by hypertrophy of cardiac myocytes, which is also matched with a corresponding increase in myocardial angiogenesis (Hudlicka et al. 1992; Shiojima & Walsh 2006). Additionally, normal growth of the heart after birth until adulthood is a form of developmental hypertrophy called eutrophy (Kerkela & Force 2006). With both physiological and developmental hypertrophy, the hearts response is adaptive. Here, the cardiac hypertrophy will initially normalize the increased tension and pressure in the cardiac chambers thereby eliminating the initial stress and maintaining CO to meet the systemic demands of the body.

Despite the importance of physiologic hypertrophy in maintaining and improving cardiac function, the cellular and molecular signals that manage this process are not well defined. Known factors involved in physiological hypertrophic induction include the Phosphoinositide 3-kinase/ Protein Kinase B (PI3K/Akt)- and Mitogen-activated Protein Kinase (MAPK)-mediated signaling cascades (Figure 2) (McMullen et al. 2003; McMullen et al. 2007; Dorn 2007). Further, an agonistic role for Insulin-like Growth Factor 1 (IGF-1) in the process of beneficial hypertrophy has emerged (McMullen et al. 2004). Although muscle hypertrophy is promoted through activation of several IGF-1-mediated pathways, the most prominent is dependent on activation of the PI3K/Akt/mechanistic target of rapamycin (mTOR) axis (Glass 2005). Further, IGF-1 has also been shown to signal through extracellular signal-regulated kinases (ERKs) and G-proteins 1eading to a hypertrophy response (Lavandero et al. 1998; Nakayama et al. 2010). Elevated IGF-1 levels have also been observed in the serum of athletes

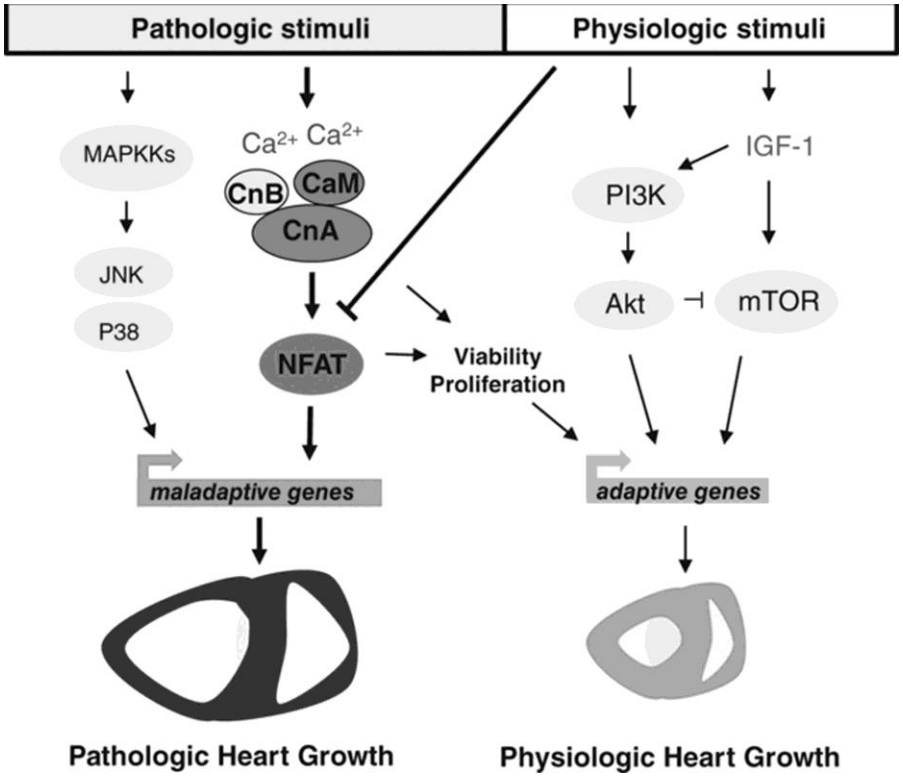


Figure 2. Signaling events governing pathologic and physiologic cardiac hypertrophy. The left panel illustrates factors involved in pathological hypertrophy. This includes mitogen activated protein kinases (MAPKs) c-Jun N-terminal kinase (JNK) or p38 kinase and the Ca^{2+}-calmodulin-activated phosphatise calcineurin (Cn). Elevated calcium levels leads to Cn activation via formation of the calcineurin B (CnB), calmodulin (CaM) and calcineurin A (CnA) complex. Cn dephosphorylates the nuclear factor of activated T cells (NFAT) transcription factor leading to its nuclear localization. This allows for activation of hypertrophic genes. Physiological hypertrophy, shown on the right, can be induced by insulin-like growth factor-1 (IGF-1) leading to phosphoinositide 3-kinase (PI3K), protein kinase B (Akt), and mammalian target of rapamycin (mTOR) activation. Physiologic hypertrophy can also downregulate calcineurin-NFAT signaling negatively impacting fetal gene activation. Figure reprinted by permission from Wolters Kluwer Health, Inc: Molkentin, J.D. Parsing Good Versus Bad Signaling Pathways in the Heart. Circulation Research. 113:16-19. ©2013.

experiencing physiological cardiac hypertrophy (Vitale et al. 2008; McMullen et al. 2007). Transgenic animal models have further implicated a role for IGF-1 solely in physiological cardiac hypertrophy and not pathological cardiac growth (McMullen et al. 2003; McMullen et al. 2004). Recently, the cytokine cardiotrophin 1 (CT1) was shown to engage a reversible physiological form of cardiac hypertrophy (Abdul-Ghani et al. 2017). Here, CT1 signaling led to an angiogenic response and compensatory cardiomyocyte vascular growth to facilitate improved blood supply. Further, this cytokine is a known pro-survival signal in cardiomyocytes and has been shown to interact with and engage glycoprotein 130 (gp130) receptor complexes, which also play an important role in cardiac survival (Fischer & Hilfiker-Kleiner 2007; Yoshida et al. 1996).

1.1.2 Pathological cardiac hypertrophy

The hypertrophic response is initially beneficial and compensatory even in many pathologic settings; however sustained stress on the heart will evolve into a detrimental and maladaptive process that causes pathological hypertrophy. Pathological hypertrophy can result from stress in the form of hypertension, myocardial infarction (MI), or genetic mutations (Hill & Olson 2008). The transition from adaptive into maladaptive hypertrophy is accompanied by several distinct changes that eventually impact cardiac metabolism and function (Frey & Olson 2003). Here, increased ventricular mass that is not matched with an increase in ventricular chamber size is observed (Heineke & Molkentin 2006). For instance, hypertension can cause pressure overload and produce concentric hypertrophy where cardiomyocytes increase in parallel resulting in ventricular wall thickening (Barry & Townsend 2010). Conversely, eccentric hypertrophy occurs during volume overload, isotonic exercise, or after infarct. Here, an increase in cardiac

mass with enlarged chamber volume is observed and longitudinal cell growth results due to addition of sarcomeres in series. With eccentric hypertrophy, wall thickness can range from being normal to decreased or increased. Thinning or dilation of the ventricular wall can occur after extended stress, which ultimately leads to HF (Hill & Olson 2008).

This form of hypertrophy is also associated with the upregulation of fetal genes, including atrial natriuretic peptide (ANP), B-type natriuretic peptide (BNP), and contractile proteins, such as skeletal α-actin and β-myosin heavy chain (β-MHC) (McMullen & Jennings 2007). ANP and BNP are secreted from the hypertrophied heart and initiate diuresis and vasodilation. This aids in regulating blood volume and lowering blood pressure (Hall 2004; Kuhn et al. 2002; Horio et al. 2000). Additionally, a decrease in heart metabolism via a switch from fatty acid oxidation to the lower energy-consuming process of glycolysis also occurs (Hill & Olson 2008).

Pathological hypertrophic agonists include Angiotensin II (AngII), Endothelin 1 (ET1), Isoproterenol (ISO), and Phenylephrine (PE), which signal via G-Protein Coupled Receptors (GPCRs). Downstream signaling includes activation of phospholipase C (PLC), which signals through diacylglycerol (DAG) activating MAPK or inositol-triphosphate (IP3) activating nuclear factor of activated T lymphocytes (NFAT), which converge on transcription factors, including GATA, MEF2 and Nkx2.5, to reengage the fetal genes and induce pathological hypertrophy (Figure 2) (Frey & Olson 2003; McMullen & Jennings 2007). Despite numerous pathways being implicated in this pathological process, the MAPK pathway has emerged as a common signaling cascade for most hypertrophic stimuli and subsequent progression to HF (Sugden & Clerk 1998; Haq et al. 2001). Here, genes involved in cardiac hypertrophy are enhanced through

activation of kinases and downstream effector kinases. Two families of effector kinases are known to be activated through MAPK signaling: the extracellular-regulated protein kinase (ERK) and the stress-activated protein kinase (SAPK) family, which includes p38 kinase and c-Jun N-terminal kinase (JNK-1), respectively. Activation of ERK (Bueno et al. 2000; Nicol et al. 2001), p38 (Sopontammarak et al. 2005) and JNK-1 (Ramirez et al. 1997) have been detected in cardiac hypertrophy *in vivo*.

In addition, elevated intracellular calcium levels are linked to hypertrophic induction (Karliner et al. 1990; Sadoshima et al. 1993; Sadoshima & Izumo 1993; Leite et al. 1994). Molkentin et al. demonstrated that a calcineurin (Cn)-dependent pathway, which is activated by elevated calcium, is an essential driver of cardiac hypertrophy (Molkentin et al. 1998). Here, activated Cn dephosphorylates the transcription factor NFAT, which interacts with GATA4 leading to subsequent activation of the fetal gene program. Interestingly, the Cn inhibitors cyclosporine and FK506 have been shown to prevent pathological hypertrophy and dilated cardiomyopathy in mouse models (Sussman et al. 1998; Taigen et al. 2000). Further, mutations of genes encoding sarcomeric proteins have been shown to be associated with altered calcium-dependent tension generation in sarcomeres. This severely affects cardiac function and the balance between mechanical force and calcium-cycling. These mutations can lead to hypertrophy or dilation. Recently, Davis et al. determined a computational tension-based model that predicts cardiac phenotypes associated with these mutations based on calcium binding properties, which may have significant impact on treatment planning for cardiomyopathy patients (Davis et al. 2016).

One interesting and significant feature of pathological cardiac hypertrophy is the extent to which it overlaps with the process of programmed cell death or apoptosis. The following introductory sections will discuss apoptosis, caspase proteases, and the various roles they play in cell death and beyond, including its emergent role in cardiac hypertrophy and remodeling.

1.2 Caspase proteases and apoptotic signaling

Caspases (cysteinyl aspartate-specific proteases) have been well characterized for their role in the highly regulated form of cell death referred to as apoptosis. This signaling pathway is called the caspase cascade. These enzymes possess a cysteine residue in their active site and cleave their substrates by hydrolyzing peptide bonds on the carboxyl end of an aspartic acid (D) residue within the recognition consensus sequence (Earnshaw et al. 1999). Caspases are synthesized in their inactive zymogen form consisting of three domains: an N-terminal prodomain and the large (p20) and small (p10) domains. Caspases are activated by two subsequent cleavage events, where proteolytic processing occurs between p20 and p10, and between the prodomain and p20 (Earnshaw et al. 1999). Once activated the caspase enzyme forms a heterotetramer composed of two p20/p10 heterodimers and two active sites (Opferman & Korsmeyer 2003). This same caspase-mediated cleavage occurs in the activation of the downstream effector caspases 3, 6, and 7 by action of the initiator caspases. Initiator caspases, including caspase 8/10 and caspase 9 or caspase 2, contain a death effector domain (DED) or a caspase recruitment domain (CARD), respectively, which are responsible for initiating the caspase cascade and mediating protein interactions. Initiator caspase 8 is activated via induced proximity, which refers to caspase activation by high

concentrations of the pro-enzyme allowing numerous pro-caspases to mutually process and activate one another (Muzio et al. 1998). Alternatively, activation of initiator caspase 9 involves association with regulatory cofactor apoptosis activating compound 1 (Apaf-1), resulting in the formation of the caspase 9 holoenzyme, referred to as the apoptosome (Earnshaw et al. 1999).

The effector caspase cascade can be activated via two mechanisms, which are initiated by either intrinsic or extrinsic signals (Figure 3). The intrinsic pathway involves death signals arising from an intrinsic source originating from the mitochondria. The mitochondria contains several proapoptotic proteins, including cytochrome *c* (cyt *c*), and antiapoptotic proteins, and permeability of the mitochondria is controlled by these pro- and anti-apoptotic proteins. Sensors activate proapoptotic proteins Bcl-2-antagonist/Killer 1 (Bak) and Bcl-2-associated X protein (Bax), which insert into the mitochondrial membrane post-dimerization forming pores. Cyt *c* and other mitochondrial proteins are subsequently released into the cytosol. Further, the antiapoptotic roles of B-cell CLL/Lymphoma 2 (Bc1-2) and B-cell lymphoma-extra large (Bcl-xL) can be inhibited by proapoptotic sensors, which can form inhibitory heterodimeric complexes promoting pore formation and subsequent cyt *c* release. The binding of cyt *c* and Apaf-1 leads to apoptosome formation and initiator caspase 9 activation (Hengartner 2000).

The extrinsic pathway involves signals being received through a death receptor, such as Fas of the tumor necrosis factor (TNF) family of receptor, followed by caspase 8 or 10 activation. Transduction of the signal into the cell is completed by an adaptor

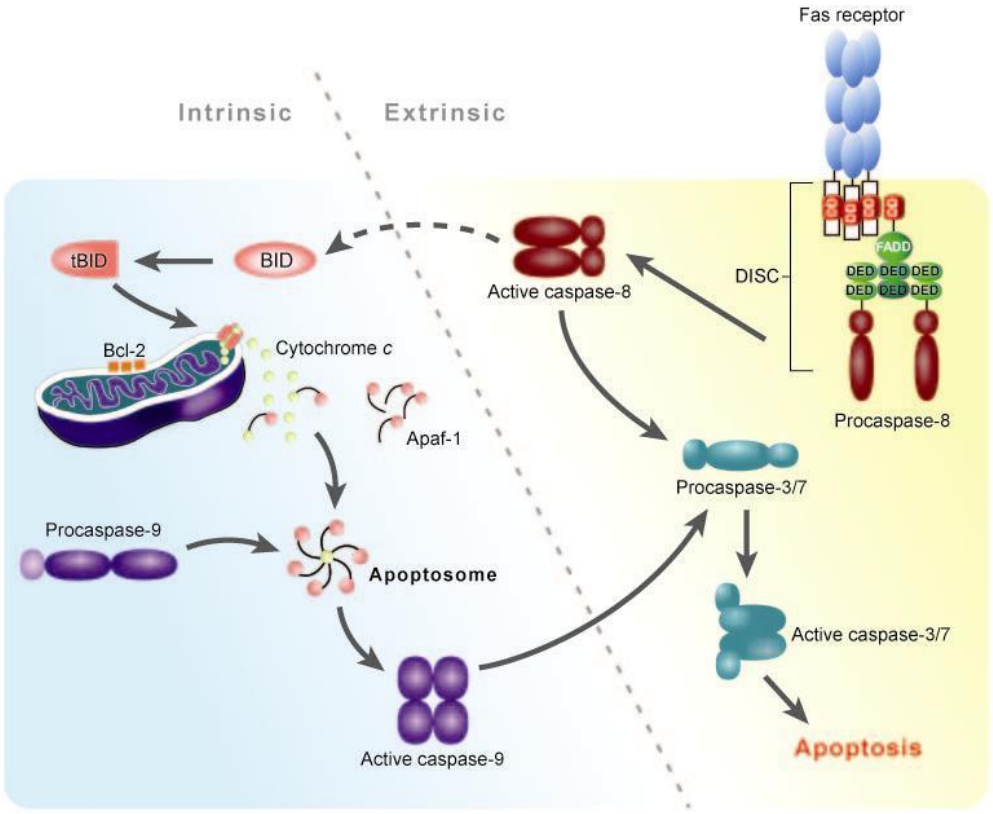


Figure 3. The caspase cascade can be activated by intrinsic and extrinsic signals. Intrinsic activation of apoptosis is initiated by localization of proapoptotic proteins, including Bcl-2 family member Bid, to the mitochondria. Pore formation leads to membrane permeabilization and subsequent cytochrome *c* (cyt *c*) release. Cyt *c* binds to apoptotic protease activating factor 1 (Apaf-1) leading to apoptosome formation, caspase 9 activation, and downstream effector caspase 3 and 7 activation. Extrinsic activation of apoptosis involves localization of caspase 8 to the death effector domain (DED) of the adaptor protein Fas-associated death domain (FADD). This forms the death-inducing signaling complex (DISC) and leads to caspase 8 followed by effector caspase activation. Figure reprinted by permission from Annual Reviews: Best, S.M. Viral Subversion of Apoptotic Enzymes: Escape from Death Row. Annual Review of Microbiology. 62:171-192©2008.

protein containing a DED within its cytoplasmic tail. For example, Fas-associated death domain (FADD) recruits procaspase 8 through interactions with the DED and caspase 8 is activated by autocatalysis (Aggarwal 2003). Interestingly, activation of proapoptotic protein Bid occurs via caspase 8-mediated processing, which connects the extrinsic to the intrinsic apoptotic pathways (Gross et al. 1999).

Regardless of the pathway utilized the downstream activation of effector caspases leads to subsequent proapoptotic proteolytic events, cell shrinkage, membrane blebbing, and formation of apoptotic bodies ultimately resulting in cell death (Hengartner 2000). While certain caspases, including caspase 4, 12 and 14, are limited to a single proteolytic substrate, effector caspase 3 can target over 300 substrates and this list is still growing (Burgon & Megeney 2017). The ability alone to cleave such a large number of targets within a limited time frame can have detrimental effects on cell viability. One key apoptotic caspase 3 substrate is the inhibitor of caspase-activated DNase (ICAD), which upon processing leads to release and nuclear localization of caspase activated DNase (CAD) causing DNA degradation (Cory 1998; McIlroy et al. 1999).

1.2.1 Endogenous regulation of caspase-mediated apoptotic signaling

A prominent mode of regulating apoptotic caspase signaling is through the action of the inhibitors of apoptosis protein family (IAPs). IAPs comprise a group of E3 ubiquitin ligases, which are capable of regulating caspase enzymes through direct protein-protein interaction. Here, baculoviral IAP repeat (BIR) domains provide the point of caspase interaction and inhibition (Berthelet & Dubrez 2013). Mammalian X-linked IAP (XIAP) has been shown to inhibit caspase 3, 7, and 9 activity (O'Riordan et al. 2008). Alternatively, inhibitors of IAPs can antagonize the action of these proteins,

releasing caspase function to promote apoptosis. During activation of the intrinsic apoptotic pathway, inhibitors of IAPs are released from the mitochondria following mitochondrial outer membrane permeabilization (MOMP). These IAP inhibitors include second mitochondrial-derived activator of caspases (SMAC), Protein HtrA2 (Omi), and Sept4_i2 (ARTS), which have been shown to bind to the BIR domain of IAPs, which then limits IAP interaction with caspases (Yang & Du 2004; Mandel-Gutfreund et al. 2011) Given the potent capacity of inhibitors of IAPs in promoting apoptosis, considerable efforts have focused on the use of these proteins (and small molecule mimetics) including SMAC and ARTS, for targeted killing of tumor cells and as novel cancer treatments (Bai et al. 2014; Beug et al. 2014; García-Fernández et al. 2010).

An additional source of caspase regulation is accomplished through the Bcl-2 family of proteins, which can both inhibit and promote apoptosis (Saelens et al. 2004). These proteins either exert pro or antiapoptotic functions through interacting with components of the apoptotic cascade (Regula & Kirshenbaum 2005; Biala & Kirshenbaum 2014). Ultimately, these proteins play roles in inducing or blocking mitochondrial cyt *c* release. As previously discussed, cyt *c* release leads to apoptosome formation followed by caspase 9 and subsequent caspase 3 activation. These proteins share Bcl-2 homology (BH) domains, including BH1, BH2, BH3, and BH4. The combination of these BH domains within the Bcl-2 protein determines whether it has a pro or antiapoptotic function. Antiapoptotic members contain at least BH1 and BH2 but most contain all four BH domains (Adams & Cory 1998). These antiapoptotic proteins include Bcl-2, Bcl-XL, and Myeloid Cell Leukemia 1 (Mcl-1). Here, the highly conserved BH4 domain is essential for the stabilization of the BH1-3 domains and

indispensable for the antiapoptotic action of these proteins (Hirotani et al. 1999). These proteins aid in preserving the integrity of the mitochondrial membrane by inhibiting the action of proapoptotic proteins. The proapoptotic Bcl-2 proteins can be subdivided by those containing several BH domains, such as Bax and Bak, and those that solely contain the BH3 domain, including Bcl-2-interacting mediator of cell death (Bim), BH3-interacting domain death agonist (Bid) and Bcl-2-associated death protein (Bad). All proapoptotic proteins contain a BH3 domain, as it is essential for dimerization with other proteins of the Bcl-2 family (Adams & Cory 1998).

In addition to direct protein modifiers of the Bcl-2 family, other classes of protein interactions have been identified as potent regulatory steps in managing caspase function. Heat shock proteins (Hsps) are a family of proteins which act as molecular chaperones ensuring proper folding and assembly of proteins (Young et al. 2004). Cell stress has been shown to upregulate Hsp activity and this form of endogenous caspase regulation has been observed during cardiac pathology (Heads et al. 1994; Jayakumar et al. 2001; Kamradt et al. 2002). Further, Hsps can interact with components of the caspase cascade thus blocking cell death progression. For example, Hsp27 can bind cyt *c* (Garrido et al. 2000), αB-cystallin binds caspase 3 preventing autocatalysis (Kamradt et al. 2001), and Hsp70 can bind Apaf-1 preventing apoptosome formation and caspase 9 activation (Saleh et al. 2000; Beere et al. 2000).

1.3 Non-death roles of apoptotic signaling and caspases

Although typically associated with cell death, programmed cell death (PCD) or apoptosis signaling pathways are also vital in maintaining organism homeostasis. A growing body of literature has provided evidence for non-death roles of apoptotic

machinery and caspase proteases. Notably, caspase-dependent pathways have been implicated as essential drivers of cell differentiation. For instance, the upregulation of caspase 3 activity was demonstrated to be synonymous with skeletal muscle differentiation and inhibition of caspase 3 resulted in a significant reduction in formation of mature myofibers (Fernando et al. 2002). Caspases 3, 9, 7, and 2 are transiently activated during erythrocyte differentiation and inhibition of these proteases leads to blunted erythroid maturation (Zermati et al. 2001). A series of caspase inspired biochemical and morphological events that resemble apoptosis have been observed during terminal lens fiber cell differentiation (Bassnett 2002). Further, an essential role for the intrinsic cell death pathway in the initiation of differentiation in the developing lens has also been shown (Weber & Menko 2005). Here, elevated expression of proapoptotic proteins, mitochondrial cyt *c* release, and caspase 3 activation were observed in the developing lens. This study also demonstrated that during lens fiber epithelial cell differentiation heightened expression of antiapoptotic genes regulates caspase activity levels thus preventing the transition to apoptosis. The differentiation of cardiac progenitor cells has also been shown to be caspase-dependent (Abdul-Ghani et al. 2011). Abdul-Ghani et al. determined that Wnt11-mediated cardiomyocyte development is dependent on caspase driven β-catenin inhibition. Aspects of the mitochondrial cell death pathway, including drICE (the *Drosophila* homolog of caspase 3) activation, have also been observed during sperm terminal differentiation (Arama et al. 2003). In this study, caspase inhibition prevented the removal of the bulk cytoplasm *in vivo*, a key step in the maturation of sperm, leading to male sterility, suggesting that caspase activation is essential to spermatid differentiation. The involvement of the intrinsic cell death pathway

has been observed in the maturation of numerous cell types, including neurons and skeletal muscle (Dick et al. 2015; Ohsawa et al. 2010; Murray et al. 2008). Effector caspases have also been implicated in early stages of cell differentiation, specifically at the stage of stem cell self-renewal versus commitment to differentiation. It has been reported that caspase-mediated Nanog cleavage is required in order to stop the self-renewal process and initiate differentiation of embryonic stem cells (ESCs) (Fujita et al. 2008). Caspase 3 activity has also been implicated in muscle stem/progenitor cell self-renewal (Dick et al. 2015). Beyond these early observations, the differentiation of most mature somatic cells have been linked to transient activation of caspase signaling (Dick & Megeney 2013; Bell & Megeney 2017).

Caspases also play roles in the innate immune response, which is the first line of defense against infectious agents. Caspases 1, 4, 5, 11, and 12, each containing a CARD domain, are involved in cytokine activation. These caspases are essential to the proinflammatory response through activation in interleukin-1β (IL-1β) and IL-18 within the cell. Studies have confirmed the role of caspase 1 and 11 in the regulation of inflammation and cytokine maturation (Fernández & Lamkanfi 2015). Here, caspase 1, activated by caspase 11 processing, has been shown to cleave IL-1β (Kang et al. 2002). Caspase 11 has also been implicated in cell migration during inflammation. Li et al. demonstrated that caspase 11 plays a role in actin dynamics and that lymphocytes deficient in caspase 11 have migration defects (Li et al. 2007).

1.3.1 Mechanisms to control/restrain caspases for non-death cell activities

In broad terms, the primary determinants in the death versus non-death role of caspase proteases are the level and duration of caspase activation. Unrestrained elevated

caspase activation can engage cell death whereas a more transient and spatially restrained activation is associated with non-death outcomes, such as cell differentiation. For example, Adams et al. observed low levels of transient caspase activity during neurohormonal agonist induced hypertrophy where adenoviral (AdV) expression of wild-type Gαq induced hypertrophy after 24 hours. Alternatively, constitutively active mutant Gαq rapidly progressed to cell death (Adams et al. 1998). Similarly, the Ras GTPase activating protein (AP) (RasGAP) can respond to varied levels of caspase activity. Low levels of apoptotic-stimuli lead to partial RasGAP cleavage with no negative effect on cell viability. Alternatively, high levels of caspase activity resulted in RasGAP-induced cell death (Yang & Widmann 2001; Yang et al. 2004). During neural stem cell differentiation a similar transient caspase 3 activation is observed which peaks at 24 hours followed by reduced caspase activity levels (Fernando et al. 2005). Additionally, prolonged caspase 3 activated mammalian sterile twenty-like kinase (MST1) is associated with apoptosis while temporal MST1 activation induces myoblast differentiation (Fernando et al. 2002). Caspase activity during lens fiber differentiation has also been noted to be lower compared to levels observed during bona fide apoptosis (Weber & Menko 2005).

The sub-cellular localization of cleaved/activated caspases also plays a regulatory role in controlling cell fate. Confining caspase activity to specific sub-cellular compartments can effect whether or not apoptosis is induced. During platelet formation punctate cytoplasmic active caspase 3 is observed in maturing megakaryocytes (MKs) whereas more diffuse caspase 3 is noted during apoptosis (De Botton et al. 2002). Similarly, activated caspase 8 has also been shown to reside in aggregates within lipid

rafts during T-cell activation. During apoptosis, high levels of diffuse caspase 8 is observed (Koenig et al. 2008). These studies suggest that during non-death processes active caspases are sequestered to specific sub-cellular compartments, providing access to a limited and specific pool of substrates (Feinstein-Rotkopf & Arama 2009; Fernando & Megeney 2007).

Specific protein/protein interactions may also be involved in restraining and positioning caspases in the required sub-cellular localization during non-death processes. An interaction between caspase 3 and the small Hsp αB-crystallin has been observed. This physical association was shown to be involved in directing caspase 3 to specific sub-cellular locations and restraining its proteolytic activity in both skeletal muscle and cardiomyocytes (Kamradt et al. 2002; Chis et al. 2012). As previously stated, caspases can also be regulated by action of IAPs. A potent IAP, the XIAP, has been shown to inhibit activities of caspase 3, 7, and 9 (O'Riordan et al. 2008). XIAP contains E3 ubiquitin ligase activity permitting it to further regulate caspase activity by promoting ubiquitination of the target caspase (O'Riordan et al. 2008). In cardiomyocytes, XIAP has been observed to physically interact with and inhibit caspase 3 activity (Potts et al. 2005; Piacentino et al. 2012). XIAP can also modify caspase activity during myoblast differentiation (Murray et al. 2008; Smith et al. 2009). This capacity to localize and direct caspase function to a specific sub-cellular compartment may have been an early evolutionary adaptation in eukaryotes, as evidenced by the yeast metacaspase Yca1. During stress, Yca1 colocalizes with chaperone remodeling proteins to control protein aggregation (Lee et al. 2010). There is debate in the literature as to whether caspases are

directly evolved from metacaspase proteases (Minina et al. 2017), however there is agreement that these proteases act as functional homologues (Bell & Megeney 2017).

The post-translational modification of caspases, and their substrates, is an additional mode of regulation in the non-death deployment of caspase function. Altering peptides within or in the flanking regions of caspase recognition sequences can have profound effects on caspase targeting. For example, regulatory phosphorylation of caspase proteins have been demonstrated to be capable of altering protease activity, which in turn impacts cell functions (Kurokawa & Kornbluth 2009; Desagher et al. 2001; Turowec et al. 2014). For example, casein kinase 2 (CK2) has been shown to phosphorylate serine residues in close proximity to the caspase 3 cleavage site, including the autocatalysis site on caspase 3 itself, which leads to steric inhibition of caspase cleavage (Duncan et al. 2011; Turowec et al. 2014). Subsequently, Dick et al. demonstrated that CK2-mediated phosphorylation of paired-box 7 protein (Pax7) inhibits caspase cleavage of this lineage determination factor, which promotes satellite cell self-renewal and restrains induction of the differentiation program (Dick et al. 2015). Additionally, altering the essential aspartic acid residue(s) within the caspase cleavage site negatively impacts the occurrence of caspase-mediated processing. Caspase cleavage site mutated Pax7 inhibited caspase-mediated cleavage, forcing satellite cell self-renewal and limiting the induction of the myogenic differentiation program (Dick et al. 2015).

1.3.2 Caspases and cardiac hypertrophy

The involvement of caspases as active cellular stress sensing agents is an emergent area of investigation, spanning a diverse biology. Stress adaptations can be physiological, which consists of cellular reactions to normal stimulation by endogenous

chemical mediators or hormones. Conversely, pathological adaptations include alterations that allow cells to evade injury by structural and functional modulations. If prolonged and/or severe, pathological stress adaptations can have detrimental outcomes. Pathological cardiac hypertrophy induced by hypertension, as previous discussed, is an example of a pathological stress adaptation.

One study provided evidence suggesting a potential role for caspases in pathological cardiac hypertrophy (Balakumar & Singh 2006). Here, inhibition of effector caspase activity abrogated cardiac hypertrophy and ventricular dysfunction induced by partial abdominal aortic constriction (PAAC). Further, pharmacologic caspase inhibition has shown promising results, including reducing left ventricular cardiac remodeling following MI (Yarbrough et al. 2003; Yarbrough et al. 2010). A role for CAD in the regulation of pathological cardiac hypertrophy has also been observed (Gao et al. 2015). This caspase 3-activated endonuclease plays an important role in the induction of DNA fragmentation during apoptosis. Gao et al. showed that disruption of CAD results in pressure overload-induced cardiac hypertrophy, fibrosis, and cardiac dysfunction. However, the role of CAD in this context appeared to be independent of caspase activity per se.

Caspase activity can also promote the reorganization of sub-cellular structures during differentiation without reducing cell viability (Abdul-Ghani & Megeney 2008; Fuchs & Steller 2011). Similarly, caspases have been shown to be involved in hypertrophic remodeling of the cytoskeleton and contractile proteins (Communal et al. 2002). During β-adrenergic stimulation, caspase-mediated processing of α-actin, α-

actinin, and cardiac troponin T (CnT) have been observed prior to the onset of apoptosis (Communal et al. 2002).

Although a role for caspases in the process of pathological cardiac hypertrophy has been suggested, the precise caspase-dependent signaling pathways and cleavage targets involved in propagating cardiac hypertrophy remain elusive. Interestingly, an overlap between apoptotic and non-apoptotic caspase substrate specificity exists and numerous cleavage substrates with defined roles in apoptosis induction have also been separately implicated in the process of pathologic hypertrophy.

The MEF2 family functions as a point of convergence for a variety of hypertrophic signals, including activation of the fetal gene program (Olson et al. 2006; Zhang et al. 2002; Han & Molkentin 2000). MEF2 transcriptional activity has been demonstrated to be modulated by lysine acetylation and overall MEF2 transcription is suppressed by the binding of histone deacetylases (HDACs). Histone deacetylation by HDACs promotes chromatin condensation favouring transcriptional repression. The relief of this suppression is well documented as a key step in the hypertrophic response (Olson et al. 2006). A class I HDAC, HDAC3, has been demonstrated to efficiently deacetylate MEF2 and when bound to MEF2 is responsible for repressing MEF2-dependent transcription (Grégoire et al. 2007). HDAC3 targets MEF2 by direct deacetylation and by physical association. Interestingly, caspase 3 has been shown to cleave HDAC3 and HDAC4, a class IIa HDAC, leading to their cytoplasmic relocalization during apoptosis signaling (Escaffit et al. 2007; Liu et al. 2004; Paroni et al. 2004). In context of hypertrophy, nuclear export of HDAC3 may relieve MEF2 transcriptional repression leading to hypertrophic induction. Therefore, caspase-directed HDAC3 cleavage may

serve as a novel regulatory mechanism to alleviate MEF2 suppression during hypertrophy. It has also been observed that under stress lysine acetylation of MHC leads to increased cardiac function (Samant et al. 2015). This may also be accomplished via caspase-mediated HDAC3 cleavage effectively inhibiting HDAC3-mediated MHC deacetylation and allowing for MHC acetylation. Furthermore, cardiac specific deletion of HDAC3 has also been shown to lead to pronounced cardiac hypertrophy (Montgomery et al. 2008).

An additional hypertrophic signaling pathway that may respond to and translate caspase activity is the nuclear factor kappa B (NF-κB) pathway. NF-κB is a transcription factor that responds to stress signaling and is also a prominent feature of pathological hypertrophy (Gordon et al. 2011). In its inactive state, NF-κB exists in the cytosol as a complex composed of a NF-κB heterodimer Rel (p65) and p50 bound by the inhibitor of kappa B alpha (IκBα). IκBα kinase (IKK) phosphorylates IκBα leading to its dissociation from the NF-κB heterodimer allowing liberated NF-κB to translocate to the nucleus and engage in transcription. Interestingly, caspase proteases have been shown to activate NF-κB signaling by cleavage of IKK and the IκBα inhibitor protein (Lamkanfi et al. 2006; Rathore et al. 2004).

Cn, also referred to as protein phosphatase 2B (PP2B), may also be involved in caspase-mediated hypertrophic signaling. Activated Cn dephosphorylates transcription factor NFAT, which translocates into the nucleus to regulate transcription of genes involved in cardiac hypertrophy. Cn is made up of two subunits: CnA (60 kDa) and CnB (19 kDa). Interestingly, CnA has been shown to be proteolytically activated by caspases during apoptosis (Mukerjee et al. 2000). Mukerjee et al. showed that CnA is cleaved by

caspase 3 into an N-terminal 45 kDa fragment and a C-terminal 12 kDa fragment. Although not yet thoroughly investigated, a similar caspase-mediated Cn activation mechanism may also occur during cardiac hypertrophy induction.

Furthermore, as previously mentioned, caspase activity can be localized to promote dismantling of specific sub-cellular structures during cellular differentiation and remodeling (Abdul-Ghani & Megeney 2008; Fuchs & Steller 2011; Communal et al. 2002). During hypertrophy, caspases may trigger the reorganization of cytoskeletal and contractile protein components, allowing for the subsequent addition to and growth of sarcomeres. A potential caspase substrate which may be involved in the morphological changes noted during cardiac hypertrophy is gelsolin (GSN) and its involvement will be discussed in the following section.

1.3.3 The potential roles of actin remodeling protein gelsolin in cardiac hypertrophy

The actin cytoskeleton has vital roles in numerous cellular processes including maintaining cellular structure and organization. As such, actin is crucial to cell motility and processes involving structural rearrangements. Actin monomers, referred to as G-actin, can associate to form filaments (F-actin). The assembly and overall organization of actin filaments is regulated by interactions with actin-binding proteins (ABPs). ABPs play roles in regulating actin polymerization by nucleating filaments, capping filaments, cross-linking filaments to form networks, or disassembling filaments through severing or depolymerization (Nag et al. 2013). Gelsolin (GSN) is a widely distributed ABP and a key regulator of actin filament assembly and disassembly (Li et al. 2009). GSN was initially discovered as a protein that could sever F-actin and transform macrophage

extracts from a more solid ‘gel’ state to a fluid ‘sol’ state, hence the name gelsolin (Yin & Stossel 1979; Yin et al. 1981).

GSN contains six homologous repeat segments called G1 to G6. GSN activation is typically regulated by calcium levels where efficient severing of actin by GSN occurs in high calcium environments. The calcium regulation of GSN mainly resides in the carboxyl-terminal domain (G4-G6) while actin severing capabilities reside in the N-terminus (G1-G3). Until activated, GSN remains in its inactive state through the presence of three latches: the C-terminal latch, G1-G3 latch, and G4-G6 latch (Ashish et al. 2007; Burtnick et al. 1997; Burtnick et al. 2004; Choe et al. 2002; Way et al. 1989). The binding of calcium ions activates GSN by opening the latches allowing the rearrangement of GSN to its active state and thus exposing its actin-binding sites (Nag et al. 2013). Major actin-binding domains are located on G1 and G4-G6, with the highest affinity actin binding located on G2-G3 (Way & Weeds 1988). Overall, the severing of actin by GSN requires the GSN domains to cooperatively bind actin and a pincer movement resulting from competitive binding events between G1 and G4. At the minimum, actin severing requires the N-terminal G1 domain and the G1-G2 linker (Nag et al. 2013). Following actin severing, the G1 and G4-G6 GSN fragments can cap on to the severed actin monomers. Capped actin can be further primed to nucleate and promote filament growth by uncapping agents, including phosphatidylinositol 4,5-bisphosphate (PIP_2) and Ras-related C3 botulinum toxin substrate (Rac) (Hartwig et al. 1995; Janmey & Stossel 1989).

Transcription of GSN occurs at two distinct sites in the GSN gene giving rise to two isoforms, intracellular (cytoplasmic) or extracellular (plasma) GSN. Plasma GSN

contains a signaling peptide and N-terminal extension, which consequently makes it slightly larger than the cytoplasmic form. Although plasma GSN is mainly expressed in muscle cells, cytoplasmic GSN is ubiquitously expressed in cell and tissues. Cytoplasmic GSN levels have been shown to be altered during different stages of life and during cell differentiation (Ahn et al. 2003; Chaponnier et al. 1990; Kwiatkowski 1988; Paunio et al. 1997; Scholz & Hinssen 1995). Increased cytoplasmic GSN has also been detected during cardiac diseases such as HF (Li et al. 2009; Yang et al. 2000) while a downregulation has been observed in many forms of cancer, including bladder (Tanaka et al. 1995), lung (Dosaka-Akita et al. 1998), gastric (Kim et al. 2004), and breast cancer (Winston et al. 2001). Plasma GSN acts as an actin scavenger removing circulating actin, such as after tissue damage. A downregulaton of plasma GSN has been noted in many pathological conditions including septic shock, MI, and acute liver failure (Lee et al. 2007; Suhler et al. 1997; Wang et al. 2008). Conversely, elevated plasma GSN is observed in the Finnish type of familial amyloidosis (Smith et al. 1987) and pediatric multiple sclerosis (Rithidech et al. 2009).

GSN has been identified as a substrate of caspase 3, 7, and 9 (Geng et al. 1998; Azuma et al. 2000; Li et al. 2012). Interestingly, the full-length and resulting C-terminal fragment have been demonstrated to be antiapoptotic while the N-terminal cleavage fragment has proapoptotic roles (Li et al. 2009; Li et al. 2012). Furthermore, caspase mediated GSN cleavage is proposed to separate the N-terminal portion from the C-terminus, which in turn allows activation of N-terminal GSN severing capabilities independent of calcium levels (Selden et al. 1998; Burtnick et al. 2004). As previously mentioned, GSN can remain attached to the barbed end of the severed filament as a cap

preventing actin elongation. While this can lead the actin network to disassemble, severing has also been shown to have a constructive effect due to increased number of filaments. The dissociation or uncapping of GSN from filaments generates polymerization-competent ends from which actin can grow and rebuild the cytoskeleton (Sun et al. 1999; Yin & Stull 1999). Interestingly, uncapping agents have also been shown to be activated during cardiac hypertrophy (Li et al. 2014). Therefore, during hypertrophy, GSN severing may be activated by caspase cleavage followed by GSN uncapping allowing for subsequent actin elongation. GSN is known to bind tightly to myofibrils and its involvement in cardiomyocyte remodeling has been established (Matsudaira & Janmey 1988; Rouayrenc et al. 1984).

More recently, a role for GSN in the process of cardiac hypertrophy has emerged. It was demonstrated that GSN knockout mice subjected to left anterior descending coronary artery ligation had significantly reduced hypertrophy, mortality, and overall enhanced cardiac function compared to wild-type littermates (Li et al. 2009). Furthermore, overexpression of full-length GSN in H9C2 rat cardiac cells induces cardiac hypertrophy through p38 signaling and GATA4 transcription factor activation (Hu et al. 2014).

1.4 The use of synthetic modulators of caspase activity in disease therapy

Modulation of caspase activity has been a focal point of biologic investigation over the preceding two decades, with an equivalent interest in identifying factors that activate or repress protease activation. For example, Apaf-1 can be inhibited by use of small molecules, including a class of trialkylglycine-based molecules (Malet et al. 2006) and the small molecule competitive inhibitor leonurine-10-O-β-D-glucuronide (ZYZ-488) (Wang et al. 2016). These compounds disrupt the interaction between Apaf-1 and

procaspase 9 thus inhibiting apoptosome formation and intrinsic pathway activation. This will in turn effect activation or functionality of downstream caspase cleavage targets. Synthetic molecules have also been constructed to directly target and inhibit caspase activity. For example, peptide-based small molecular inhibitors of caspases, which were developed based on the recognition sequence of caspases, including the DEVD site of poly (ADP-ribose) polymerase (PARP) (Boulares et al. 1999). These peptide inhibitors are constructed based on the sequence specificity of each individual caspase to certain amino acids, referred to as the recognition sequence. As previously mentioned, common to all caspases is the specificity for an aspartic acid (D) residue in the primary specificity position (P_1). P_2 and P_4 are variable between caspases while P_3 is consistently a glutamic acid residue (E) (Timmer & Salvesen 2007; Salvesen & Riedl 2008). For instance, caspase 3 and 7 are specific to DEVD, caspase 8 to IETD, and caspase 9 to LEHD. Peptide caspase inhibitors have a benzyloxycarbonyl group on then N-terminus, referred to as the Z motif, which allows increased cell permeability. The fluoromethylketone (fmk) on the C-terminus acts to irreversibility inhibit caspases through alkylation of the cysteine residue present within the active site of the caspase (Schotte et al. 1999). Pan caspase inhibitors, including z-valine-alanine-aspartate-fmk (z-VAD-fmk), target a broad spectrum of caspases as opposed to a specific targeted protease (Van Noorden 2001; Rodriguez et al. 1996). This also encompasses the molecular inhibitor p35 (Clem 2001), which is commonly expressed using a p35 adenovirus (p35-AdV). Here, a caspase recognition sequence (D-Q-M-D87↓G) within the reactive site loop is recognized by a target caspase forming a thioester bond between the active cysteine residue and the P_1 residue resulting in an irreversibly inhibited enzyme (Fuentes-Prior & Salvesen 2004).

Small molecule activators of caspases have also been constructed. Notably, procaspase 3 activating compound 1 (PAC-1) activates caspase 3 through relief of zinc-mediated inhibition (Putt et al. 2006; Peterson et al. 2009). This compound is capable of directly activating procaspase 3 to caspase 3 by sequestering inhibitory zinc ions from the catalytic site of procaspase 3 (Peterson et al. 2009). Other small molecules activate caspases by promoting apoptosome formation (Nguyen & Wells 2003) or inhibiting the pro-survival action of the antiapoptotic protein Bcl-2 (Oltersdorf et al. 2005).

The loss or gain of caspase activity is a major contributor to the evolving pathology in a number of diseases. Cancer is a key example of a pathologic state which is associated with the lack or reduction of caspase activity (Hensley et al. 2013). Activators of caspase activity, including PAC-1, are therefore prominent potential therapeutics (Putt et al. 2006; Botham et al. 2016; Chen et al. 2016; Roth & Hergenrother 2016). Additionally, tumor protein p53 (p53), which positively regulates expression of proapoptotic factors (Vazquez et al. 2008; Green & Kroemer 2009), is mutated or negatively regulated by endogenous inhibitors, including mouse double minute 2 homolog (MDM2) and Hsps, in many forms of cancer (Vazquez et al. 2008; Jego et al. 2013; Rérole et al. 2011). Moreover, neurodegenerative diseases such as Alzheimer's and Parkinson's, are associated with increased levels of apoptosis and caspase activity (Ghavami et al. 2014). Similarly, the use of caspase inhibitors also shows promise in the treatment of ischemia. Ischemia is the restriction of blood flow to tissues, where the anoxic environment can trigger activation of caspase signaling and cell death. Indeed, delivery of caspase inhibitors protect neurons against ischemic cell death in a rodent focal ischemia model (Hara et al. 1997).

The use of caspase inhibitors in cardiac disease has also been explored. *In vivo* animal studies observed reduced cardiomyocyte apoptosis and preserved cardiac function following MI in rats treated with a broad spectrum caspase inhibitor (Chandrashekhar et al. 2004). Reduced infarct size and left ventricular (LV) pressure in rat (Yaoita et al. 1998) and rabbit (Holly et al. 1999) animal models, and reduced LV remodeling (Yarbrough et al. 2003) have been observed as a result of prolonged treatment with caspase inhibitors. The general consensus of these studies has been that suppression of caspase activity results in diminished cell death/apoptosis, preserving the existing myocardium.

Despite the therapeutic impact of limiting cell death, the development and use of caspase therapeutics is not without concern. As previously discussed, caspases play a wide array of roles in cell death and beyond and therefore the use of modulators of caspase activity may elicit off-target effects. As such, the introduction of caspase therapeutics must be selective to target cells, and non-target cells monitored for deleterious outcomes. Additionally, as discussed above, the timing of caspase activation is critical in determining whether a normal/physiological or disease/pathological state ensues. As such, the therapeutic window for administration will also be a key consideration for use of caspase modifying compounds.

1.5 Hypothesis and Aims

This thesis aims to further explore the role and requirement of caspase proteases in the development of pathological cardiac hypertrophy. Here, the role and requirement of intrinsic-apoptotic signaling in pathological cardiac hypertrophy will be discussed in Chapter 2. In Chapter 3, GSN is investigated as a key caspase substrate and inductive cue

for cardiac hypertrophy. This work will contribute to establishing a better understanding of pathological cardiac remodeling and the role that caspase signaling plays in this process. Importantly, these observations may aid in identifying inhibitors that can suppress the progression of cardiac hypertrophy, including inhibitors of caspase activity and/or activity of its cleavage targets.

1.5.1 Hypothesis

We hypothesized that cardiac hypertrophy is mediated by the activation of caspase-dependent signaling pathways. We further hypothesized that caspase-mediated cleavage events induce hypertrophic transcription/gene expression programs and propel cytoskeletal remodeling during the hypertrophy process.

1.5.2 Aims

Using *in vitro* and *in vivo* assessment determine:

1) if an increase in caspase activity occurs during the early stages of cardiac hypertrophy.
2) if caspase activation is required for the development of cardiac hypertrophy.
3) if caspase activation is sufficient to induce cardiac hypertrophy.
4) potential caspase cleavage substrate(s) that promote cardiac hypertrophy. Determine:
    a) whether the proposed substrate is cleaved by a caspase-dependent mechanism during hypertrophy.

b) whether caspase-mediated substrate cleavage is necessary to induce cardiac hypertrophy.

c) whether caspase-mediated substrate cleavage is sufficient to induce hypertrophy in the absence of any additional prohypertrophic stimulation.

Chapter 2:

Intrinsic-mediated caspase activation is essential for cardiomyocyte hypertrophy

Intrinsic-mediated caspase activation is essential for cardiomyocyte hypertrophy

Charis Putinski[a,b], Mohammad Abdul-Ghani[a,b] , Rebecca Stiles[a,b] , Steve Brunette[a], Sarah A. Dick[a,b], Pasan Fernando[b,c,d], and Lynn A. Megeney[a,b,e]

[a]Ottawa Hospital Research Institute, Sprott Centre for Stem Cell Research, Regenerative Medicine Program, Ottawa Hospital, Ottawa, ON, Canada K1H 8L6

[b]Department of Cellular and Molecular Medicine, Faculty of Medicine

[e]Department of Medicine, University of Ottawa, Ottawa, ON, Canada K1H 8M5;

[c]Division of Cardiology, Canadian Molecular Imaging Centre of Excellence, University of Ottawa Heart Institute, Ottawa, ON, Canada K1Y 4W7

[d]Nordion, Ottawa, ON, Canada K2K 1X8

Published: October 22, 2013, Proceedings of the National Academy of Science, volume 110, number 43, pages E4079-E4087

Contribution of Co-Authors

Dr. Mohammad Abdul-Ghani contributed to designing and performing experiments, completing data analysis, and writing the paper. Rebecca Stiles completed preliminary analysis, laying the foundation for this study. Steve Brunette provided technical support throughout this study, and assisted with the *in vivo* work and collection of the hearts. Dr. Sarah A. Dick assisted with data analysis of the fragmented apoptotic nuclei (Figure 1D). Dr. Pasan Fernando assisted with coordination and experimental design of the *in vivo* study completed at the University of Ottawa Heart Institute. Dr. Lynn A. Megeney contributed in experimental design, data analysis, and writing of the manuscript.

Significance

Cardiac hypertrophy is a pathologic enlargement of the heart, an alteration that leads to contractile dysfunction and eventual organ failure. The hypertrophy phenotype originates from concentric growth of heart muscle cells and shares many biochemical features with programmed cell death, implying a common molecular origin. Here, we show cell-autonomous activation of a mitochondrial cell death pathway during initial stages of muscle cell hypertrophy, a signal that is essential and sufficient to promote hypertrophy. Targeting individual cell death proteins may offer an effective means to limit the initial stage of cardiac disease, and forgo the transition to heart failure.

Abstract

Cardiomyocyte hypertrophy is the cellular response that mediates pathologic enlargement of the heart. This maladaptation is also characterized by cell behaviors that are typically associated with apoptosis, including cytoskeletal reorganization and disassembly, altered nuclear morphology, and enhanced protein synthesis/translation. Here, we investigated the requirement of apoptotic caspase pathways in mediating cardiomyocyte hypertrophy. Cardiomyocytes treated with hypertrophy agonists displayed rapid and transient activation of the intrinsic-mediated cell death pathway, characterized by elevated levels of caspase 9, followed by caspase 3 protease activity. Disruption of the intrinsic cell death pathway at multiple junctures led to a significant inhibition of cardiomyocyte hypertrophy during agonist stimulation, with a corresponding reduction in the expression of known hypertrophic markers (atrial natriuretic peptide) and transcription factor activity [myocyte enhancer factor-2, nuclear factor kappa B (NF-κB)]. Similarly, *in vivo* attenuation of caspase activity via adenoviral expression of the biologic effector caspase inhibitor p35 blunted cardiomyocyte hypertrophy in response to agonist stimulation. Treatment of cardiomyocytes with procaspase 3 activating compound 1, a small-molecule activator of caspase 3, resulted in a robust induction of the hypertrophy response in the absence of any agonist stimulation. These results suggest that caspase-dependent signaling is necessary and sufficient to promote cardiomyocyte hypertrophy. These results also confirm that cell death signal pathways behave as active remodeling agents in cardiomyocytes, independent of inducing an apoptosis response.

Introduction

The vertebrate heart is structurally complex, yet this organ retains a remarkable ability to adjust intrinsic cell properties to alterations in the exterior milieu. A most critical aspect of this phenomenon is hypertrophic growth of individual cardiomyocytes. This form of cell adaptation is a vital feature that matches physiologic enlargement of the heart to the growth of the organism, yet compensatory hypertrophy is also a prominent feature of cardiac disease. Consequently, disease hypertrophy has been intensely studied, resulting in the identification of a consistent cellular pathology. In general, the pathologic condition derives from an agonist or trigger that stimulates key intracellular signaling pathways, which converge on transcription factors to reengage the fetal gene expression program in cardiomyocytes. Prominent examples of this molecular circuit are agonist-induced mitogen-activated protein kinase (MAPK)/CAMK (Ca^{2+}/calmodulin-dependent kinase) activation of myocyte enhancer factor-2 (MEF2) transcription and calcineurin activation of nuclear factor of activated T cells (NFAT) transcription (1–3).

Despite the success in identifying the key transcription control events during cardiomyocyte hypertrophy, the pathways or proteins that couple the fetal gene expression program with the structural reorganization of the cell remain largely unknown. One notable facet of hypertrophy is the degree to which this cell morphology shares overlapping features of programmed cell death or apoptosis. For example, hypertrophy is characterized by standard hallmarks of programmed cell death, including cytoskeletal reorganization and disassembly, altered nuclear morphology, and enhanced protein synthesis/translation (4, 5). Moreover, although cardiomyocyte hypertrophy is initially adaptive, hypertrophy often transits to a myopathic response that results in dilation, a latter event that is concurrent with an increased incidence of caspase-mediated cell death

(6, 7). Therefore, a reasonable supposition is that activation of canonical cell death pathways may contribute to the initiation and/or progression of hypertrophy.

In addition to these general features, a number of proapoptotic agonists have been directly implicated in the development of cardiac hypertrophy, including tumor necrosis factor alpha (TNF-α) and the cognate FAS receptor. Antibody blockade of TNF-α leads to diminished overload-induced hypertrophy (8), and mice with genetic deletion of TNF-α display similar attenuation of an overload-induced hypertrophy response (9). Similarly, Fas ligand activation of the Fas receptor has been noted to prompt the induction of cardiomyocyte hypertrophy, and loss of the Fas receptor in vivo was reported to result in a dramatic reduction in compensatory hypertrophy through an as yet undefined signal (10). Interestingly, the apoptotic endonuclease EndoG has recently been shown to play a critical nonapoptotic role in maintaining mitochondrial bioenergetics, and defects in EndoG have directly been linked to the subsequent development of maladaptive hypertrophy (11).

These phenotypic and biochemical intersections raise the provocative hypothesis that a caspase signaling mechanism may propagate or direct the hypertrophy response in cardiomyocytes. This is not an unreasonable premise, as a growing body of literature has demonstrated that caspase-dependent apoptosis pathways act as essential drivers of cell differentiation, including the differentiation of cardiac progenitor cells (12, 13). Canonical cell death pathways derive from an intrinsic source originating from the mitochondria, or an extrinsic source as mediated by prodeath ligand/receptor interactions. Once engaged, these pathways ultimately converge, activating caspase proteases (such as caspase 3), which cleave vital protein substrates that usher in the cell death response.

Here, we demonstrate that agonist-induced cardiomyocyte hypertrophy is associated with and critically dependent on the transient activation of the mitochondrial/intrinsic cell death pathway. Inhibition of the intrinsic pathway (at multiple levels) led to a dramatic attenuation of hypertrophy, whereas small-molecule induction of caspase activation alone was sufficient to recapitulate the phenotypic and biochemical characteristics of cell hypertrophy.

Results and Discussion

Activation of the Intrinsic Cell Death Pathway During Agonist-Induced Cardiomyocyte Hypertrophy.

To begin to address the role of caspase-mediated signaling in cardiomyocyte adaptation, we used immunofluorescence microscopy to detect caspase activity during agonist-induced hypertrophy (Fig. 1 and Figs. S1-S3). Given the prominent role of caspase 3 as a mediator of cell fate determination, we initially examined the activity kinetics for this effector protease. Treatment of primary cardiomyocytes with the hypertrophy agonist phenylephrine (PE) resulted in rapid formation of active caspase 3 foci in the cytoplasm and within a nuclear/perinuclear compartment (Fig 1 *A*, *c* and *d*). Similar to PE, isoproterenol (ISO) treatment also resulted in nuclear localized active caspase 3 foci (Fig. 1 *A*, *e* and *f*). Caspase 3 activation and localization was also analyzed for additional hypertrophic agonists, including angiotensin II (AngII) and endothelin 1 (ET1), which displayed a similar caspase 3 activation pattern (Fig. S1 *A*, *c* and *d* and *e* and *f*, respectively). Within only 30 min of PE treatment, the number of cardiomyocytes expressing active caspase 3 increased compared with cells not treated with PE (Fig. S2, green, *e* and *f* vs. *g* and *h*; white arrows indicate nuclear and perinuclear localization patterns). Similar caspase 3 activation and localization was observed at 1 h (Fig. 1 *A*, *a* and *b* vs. *c* and *d*) and 3 h (Fig. S2, *i* and *j* vs. *k* and *l*) of PE exposure. Following 24 h of PE treatment, the caspase 3 activation pattern was detectable yet diminished, with limited cytoplasmic and perinuclear/nuclear activity (Fig. S2, green, *m* and *n* vs. *o* and *p*). Caspase 3 localization was quantified based on the number of

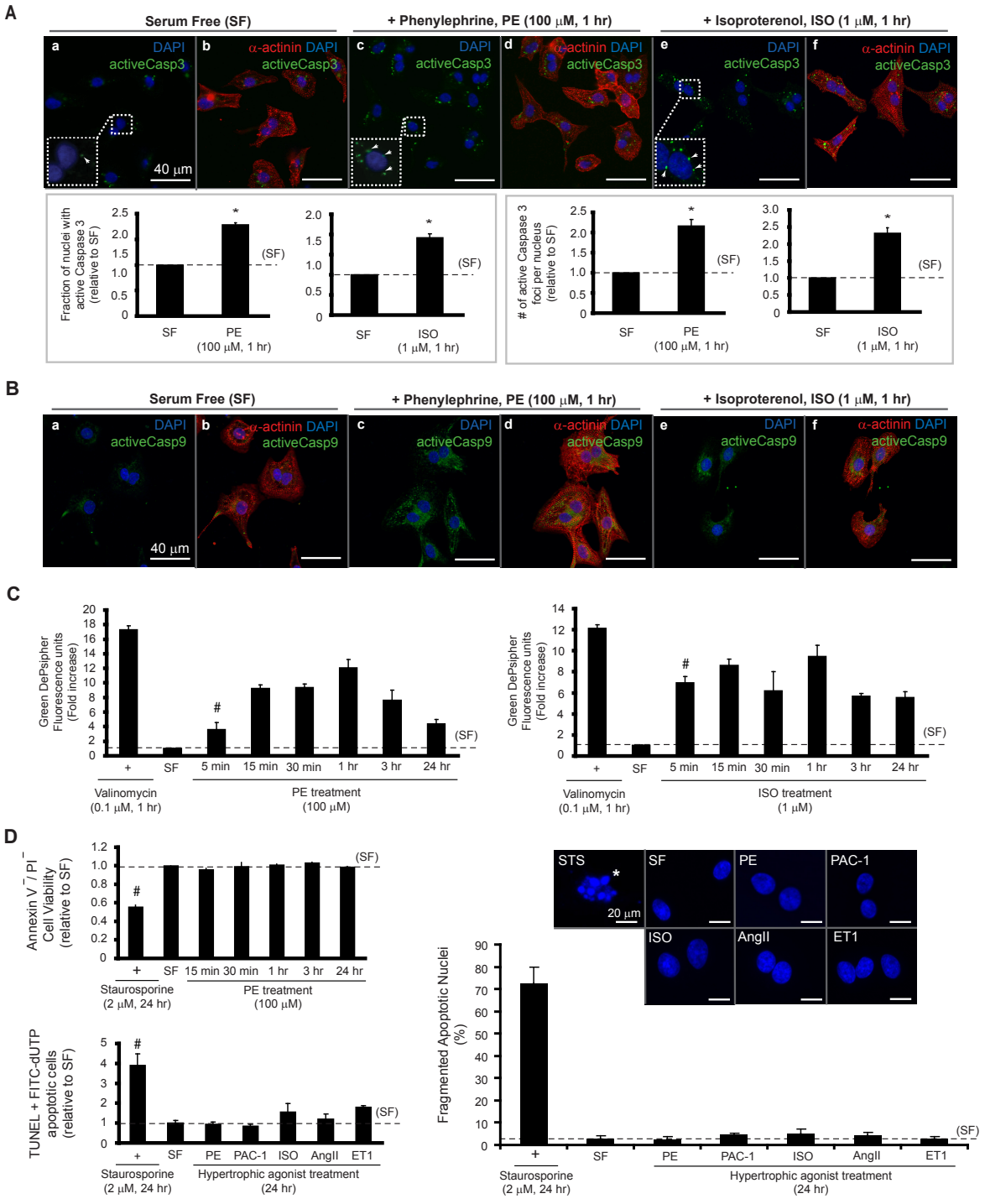

A
Serum Free (SF)
+ Phenylephrine, PE (100 μM, 1 hr)
+ Isoproterenol, ISO (1 μM, 1 hr)
a DAPI activeCasp3
b α-actinin DAPI activeCasp3
c DAPI activeCasp3
d α-actinin DAPI activeCasp3
e DAPI activeCasp3
f α-actinin DAPI activeCasp3
40 μm
Fraction of nuclei with active Caspase 3 (relative to SF)
# of active Caspase 3 foci per nucleus (relative to SF)
SF
PE (100 μM, 1 hr)
ISO (1 μM, 1 hr)
(SF)
B
Serum Free (SF)
+ Phenylephrine, PE (100 μM, 1 hr)
+ Isoproterenol, ISO (1 μM, 1 hr)
a DAPI activeCasp9
b α-actinin DAPI activeCasp9
c DAPI activeCasp9
d α-actinin DAPI activeCasp9
e DAPI activeCasp9
f α-actinin DAPI activeCasp9
40 μm
C
Green DePsipher Fluorescence units (Fold increase)
+
SF
5 min
15 min
30 min
1 hr
3 hr
24 hr
Valinomycin (0.1 μM, 1 hr)
PE treatment (100 μM)
ISO treatment (1 μM)
D
Annexin V⁻ / PI⁻ Cell Viability (relative to SF)
Staurosporine (2 μM, 24 hr)
PE treatment (100 μM)
TUNEL + FITC-dUTP apoptotic cells (relative to SF)
PE
PAC-1
ISO
AngII
ET1
Hypertrophic agonist treatment (24 hr)
STS
20 μm
Fragmented Apoptotic Nuclei (%)

Fig 1. Increased caspase 3 and 9 activation during early stages of PE- and ISO-induced cardiomyocyte hypertrophy. (*A*) Cardiomyocytes were treated with hypertrophic agonists PE (100 μM; *c* and *d*) or ISO (1 μM; *e* and *f*) to induce hypertrophy for 1 h. Immunofluorescence was used to detect activated caspase 3 (green), α-actinin (red), and DAPI (blue). Exposure to PE or ISO for only 1 h resulted in a significant increase in the number of cardiomyocytes expressing activated caspase 3 (green; PE, *c* and *d*; ISO, *e* and *f*) compared with SF media-treated cells (*a* and *b*). Activated caspase 3 displayed localization to the perinuclear and nuclear regions during hypertrophic induction (compare *c* and *d* and *e* and *f* vs. *a* and *b*). Magnified views are shown in boxed regions (white arrows; *a* and *c* vs *a* and *e*). The fraction of nuclei with active caspase 3 and the fraction of active caspase 3 foci per nucleus during PE and ISO treatment significantly increased after 1 h compared with SF controls ($n = 3$; $^{*}P < 0.05$; Figs. S1*A* and S2). (*B*) Cardiomyocytes were treated as in *A* and stained for activated caspase 9 (green). Caspase 9 activation was readily detected during PE and ISO treatment (green; *c* and *d* and *e* and *f*) compared with SF media-treated control cells (*a* and *b*; Figs. S1*B* and S3). (Scale bars: 40 μm.) (*C*) Activation of the intrinsic (caspase 9-mediated) pathway was also evaluated by use of the DePsipher kit. Green DePsipher fluorescence was quantified during PE- and ISO-induced hypertrophy from 5 min to 24 h. A significant increase in green fluorescence was observed after only 5 min of hypertrophic induction, suggesting early intrinsic pathway activation ($n = 3$; $^{\#}P < 0.05$). (*D*) Caspase activation during agonist-induced hypertrophy occurs in viable cardiomyocytes. Cardiomyocyte viability was evaluated by analysis of annexin V/PI double-negative cell population, fragmented apoptotic nuclei quantifications (asterisk), and TUNEL assay. Staurosporine treatment led to a significant reduction in cardiomyocyte viability ($n = 3$; $^{\#}P < 0.05$). Cardiomyocyte viability remained intact after 24 h hypertrophic induction with PE (100 μM), PAC-1 (25 μM), ISO (1 μM), AngII (100 nM), and ET1 (20 nM). (Scale bars: 20 μm.)

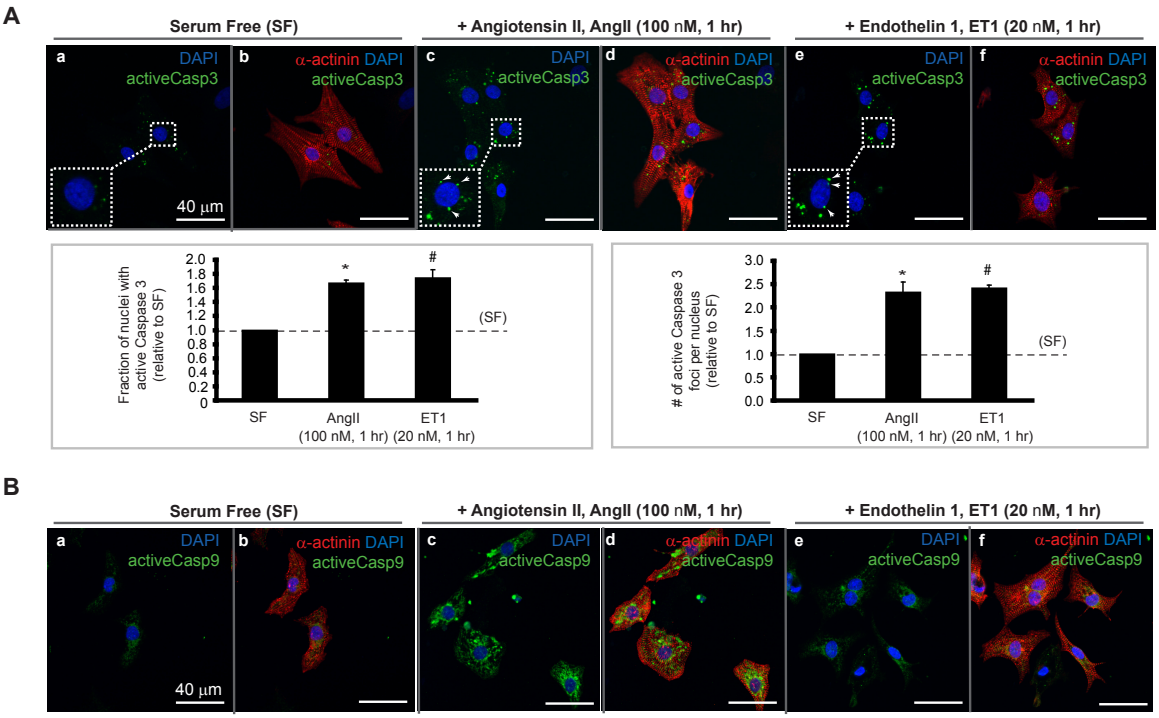


Fig S1. Increased caspase 3 and 9 activation during early stages of agonist-induced cardiomyocyte hypertrophy. (A) Primary cardiomyocytes were treated with AngII (100 nM; c and d) or ET1 (20 nM; e and f) for 1 h. Immunofluorescence was used to detect activated caspase 3 (green) and α-actinin (red). Nuclei were stained with DAPI (blue). Exposure to AngII and ET1 for 1 h resulted in an increase in the number of cardiomyocyte nuclei expressing activated caspase 3 (green; c and d and e and f; respectively) compared with cells not treated with agonist (a and b). Activated caspase 3 displayed a perinuclear and nuclear localization (white arrows). Magnified views of nuclear and perinuclear regions are shown in boxed regions. Fraction of nuclei with active caspase 3 and the number of active caspase 3 foci per nucleus were quantified for each hypertrophic agonist. (B) Cardiomyocytes were treated with AngII or ET1 as in A. Immunofluorescence was used to detect activated caspase 9 (green) and α-actinin (red). Nuclei were stained with DAPI (blue). Exposure to AngII or ET1 for 1 h resulted in a prominent increase in caspase 9 activity (green; c and d and e and f, respectively) compared with cells not treated with agonist (a and b). (Scale bars: 40 μm.)

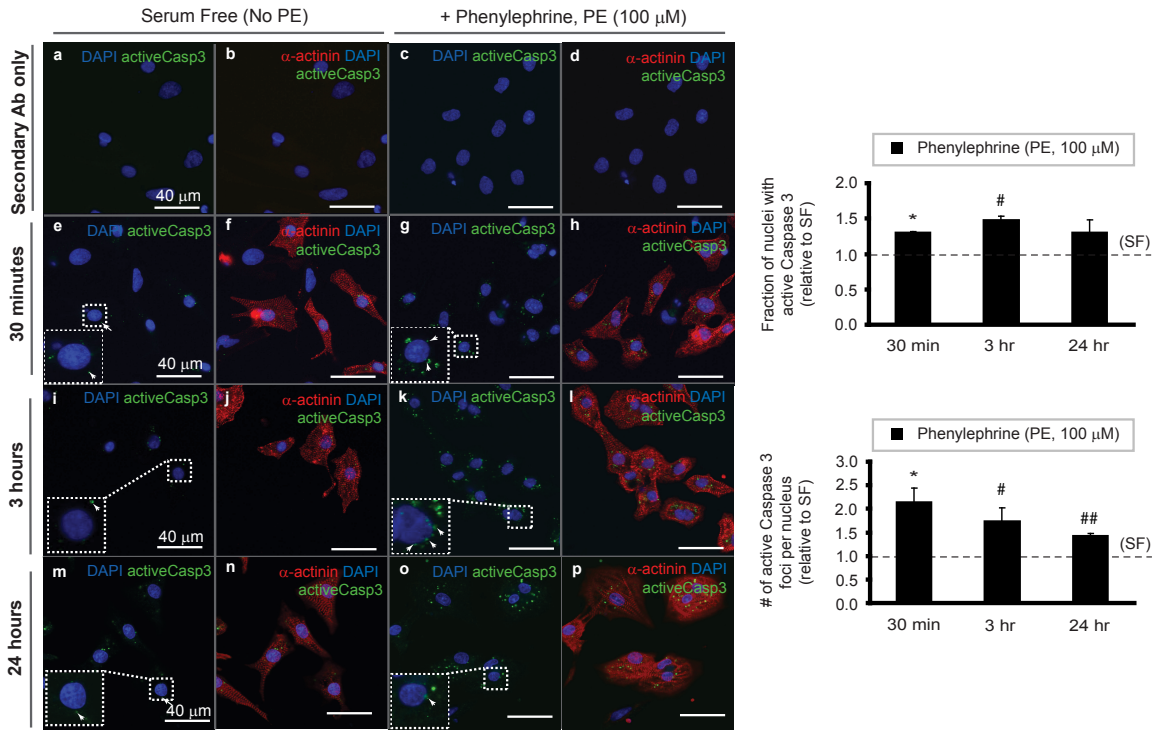


Fig S2. Increased caspase 3 activation and localization during PE-induced cardiomyocyte hypertrophy. (A) Primary cardiomyocytes were treated with PE (100 μM) to induce hypertrophy for 30 min (g and h), 3 h (k and l), and 24 h (o and p). Immunofluorescence was used to detect activated caspase 3 (green) and α-actinin (red). Nuclei were stained with DAPI (blue). Negative control samples (i.e., cells incubated with secondary antibody only) confirmed the absence of background fluorescent staining (a–d). Exposure to PE for 30 min, 3 h, and 24 h resulted in an increase in the number of cardiomyocyte nuclei expressing activated caspase 3 (green; g and h, k and l, and o and p, respectively) compared with cells not treated with PE (e and f, i and j, and m and n; respectively). Interestingly, activated caspase 3 also displayed a notable localization to the perinuclear and nuclear regions (white arrows; e–p). Magnified views of nuclear and perinuclear regions for PE treatments are shown in boxed regions (compare e and g, i and k, and m and o). The fraction of nuclei with active caspase 3 was significantly increased during early time points (n = 3; *P < 0.05). The number of active caspase 3 foci per nucleus significantly increased during PE-induced hypertrophy (n = 3; *P < 0.05). (Scale bars: 40 μm.)

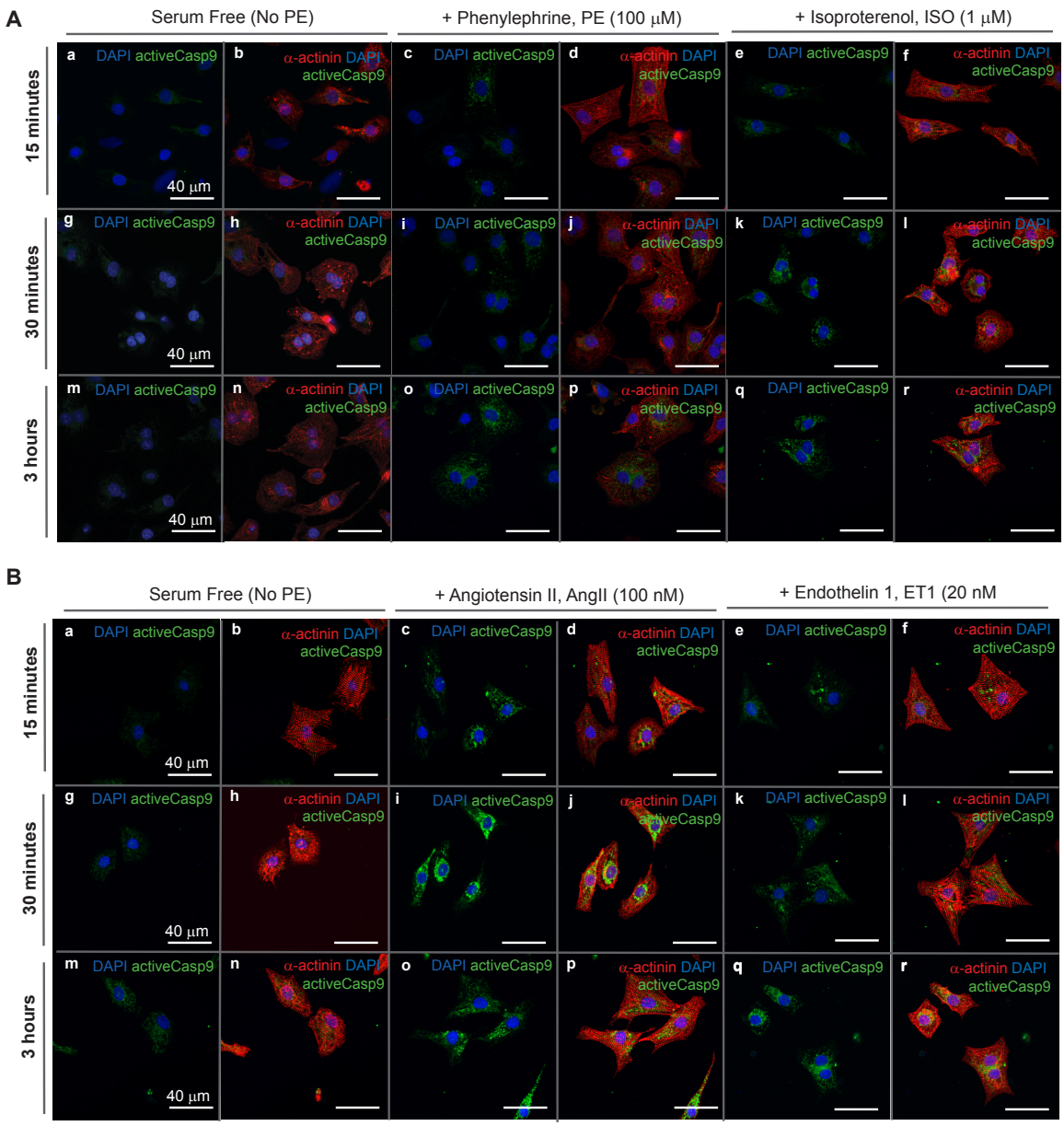


Fig S3. Increased caspase 9 activation during agonist-induced cardiomyocyte hypertrophy. (A) Primary cardiomyocytes were treated with PE (100 μM) or ISO (1 μM) for 15 min, 30 min, or 3 h. Immunofluorescence was used to detect activated caspase 9 (green) and α-actinin (red). Nuclei were stained with DAPI (blue). Exposure to PE and ISO for 15 min resulted in a prominent increase in caspase 9 activity (green; c and d and e and f, respectively) compared with SF mediumtreated cells (a and b). Activated caspase 9 displayed a punctate and diffuse staining pattern throughout the cell. Similar observations were noted at 30 min and 3 h. (B) Caspase 9 activation was also evaluated in cardiomyocytes treated with AngII (100 nM) or ET1 (20 nM) as done in A. Similarly, caspase 9 activation was observed as early as 15 min after hypertrophic induction. After 30 min and 3 h, caspase 9 activation was also detected. (Scale bars: 40 μm.)

cardiomyocytes expressing nuclear activated caspase 3 and the number of active caspase 3 foci per nuclei (Fig. 1*A*). A significant increase in the number of nuclei with active caspase 3 as well as total foci number was observed during agonist-induced hypertrophy (Fig. 1*A* and Fig. S1*A*). Furthermore, caspase 3 nuclear specificity was demonstrated by *z*-stack confocal imaging (Fig. S4). The focal activity pattern for caspase 3 suggested that the cardiomyocyte may restrict the protease activity to discrete compartments to engage nonapoptotic cellular functions. Indeed, otherwise lethal caspase activity can be refocused and restrained to effect targeting of particular cellular structures during remodeling and differentiation (14–16). Preliminary experiments indicate that caspase 3 activity in the total soluble protein fraction/lysate does not change during PE-induced hypertrophy (Fig. S5), suggesting that the active protease may be directed to a unique insoluble compartment within the cell.

α-Adrenergic stimulation via PE exposure has been reported to alter mitochondrial calcium leak and membrane potential (17, 18). As such, we reasoned that the source of caspase 3 activation during hypertrophy stimulation may originate from transient activation of the intrinsic/mitochondrial cell death pathway rather than the ligand-associated extrinsic-mediated cell death pathway. Caspase 9 activity represents an immediate downstream proxy for mitochondrial-derived signals whereby, in response to an apoptogen, the mitochondria releases cytochrome *c* (cyt *c*), promoting activation of procaspase 9 within the multiprotein apoptosome complex. Immunofluorescence analysis revealed a caspase 9 activation pattern as early as 15 min post hypertrophic induction (Fig. S3 *A*, *a* and *b* vs. *c* and *d*), with a peak of activation at 1 to 3 h after PE exposure in healthy, intact cardiomyocytes (Fig. 1 *B*, *a* and *b* vs. *c* and *d*; and Fig S3 A, *m* and *n* vs. *o* and *p*).

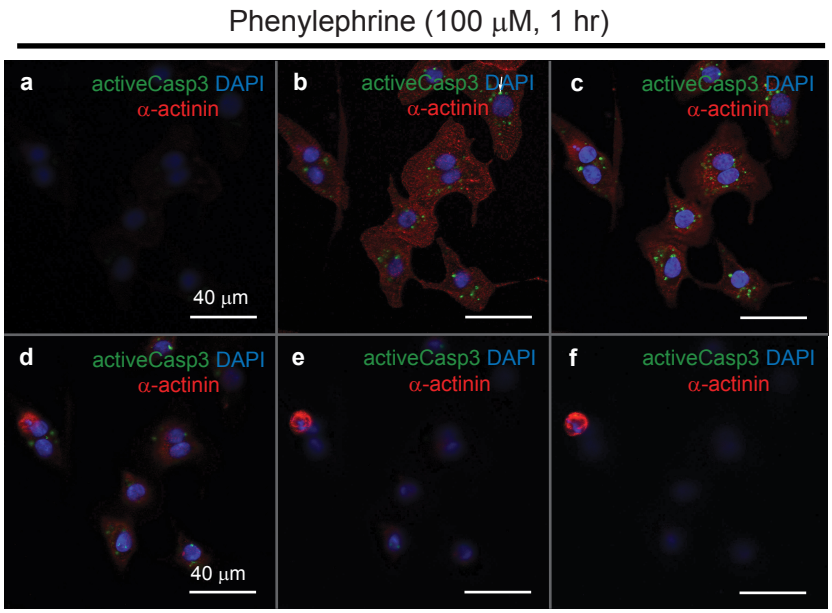


Fig S4. z-Stack confocal imaging indicates specificity of nuclear-localized active caspase 3 during PE-induced cardiomyocyte hypertrophy. Primary cardiomyocytes were treated with PE (100 μM) to induce hypertrophy for 1 h (a–f). Immunofluorescence was used to detect activated caspase 3 (green) and α-actinin (red). Nuclei were stained with DAPI (blue). Specificity of nuclear-localized active caspase 3 was confirmed by z-stack confocal imaging starting at the top of the nucleus (a) and successively imaging toward the bottom of the nucleus (f). Optical/imaging sections (2 μm thickness each) were taken. (Scale bars: 40 μm.)

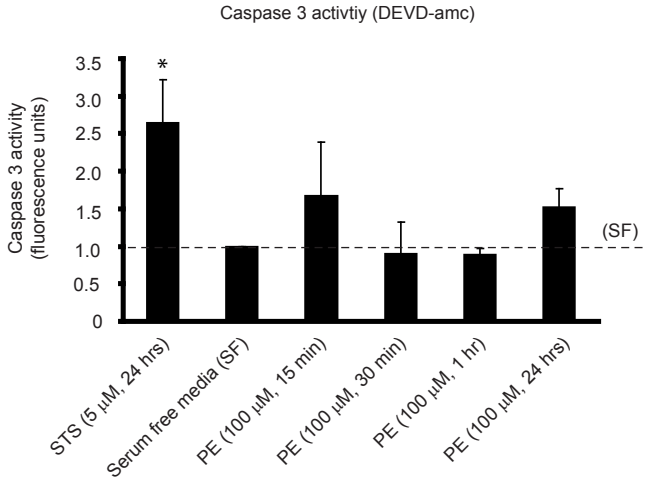


Fig S5. Global/total caspase activity remained unchanged during PE-induced cardiomyocyte hypertrophy. Primary cardiomyocytes were treated with PE (100 μM) for 15 min, 30 min, 1 h, and 24 h. STS (5 μM) treatment was used as a positive control for caspase activation, and SF media was used as a baseline control. Caspase 3 activity was measured in whole-cell lysates using the Ac-DEVD-amc fluorogenic substrate. STS positive control treatment resulted in the expected increase in caspase 3 (approximately 2.5-fold increase) compared with SF baseline control ($n = 3$; $^*P < 0.05$). However, no significant changes in global/total caspase 3 activity was detected in any of the PE treatments conducted. Twenty micrograms of total protein lysates were used for caspase activity assays, and the resulting fluorescence intensity (caspase activity) was measured at 460 nm. All values were normalized to the SF control ($n = 3$).

Additional hypertrophic agonists ISO (Fig. 1 *B*, *a* and *b* vs. *e* and *f*; and Fig. S3*A*), AngII (Fig. S1 *B*, *a* and *b* vs. *c* and *d*; and Fig. S3*B*), and ET1 (Fig S1 *B*, *a* and *b* vs. *e* and *f*; and Fig. S3*B*) showed similar caspase 9 activation patterns. With all hypertrophic agonists, caspase 9 activity was dispersed throughout the cell, reminiscent of a typical mitochondrial distribution pattern. Activation of the intrinsic (caspase 9-mediated) pathway was further confirmed by measuring the drop in mitochondrial membrane potential, which is an early essential step in this pathway. PE and ISO treatments led to a similar induction of the intrinsic pathway as early as 5 min after hypertrophic induction (see number symbols in Fig. 1 *C*, *Left* and *Right*, respectively). Together, these data demonstrate that agonist-induced hypertrophy leads to activation of the intrinsic cell death signal pathway in a temporally restricted manner.

It is important to note that this initiation signal (caspase 9 and caspase 3 activation) is not followed by induction of apoptosis per se. Extensive analysis of cardiomyocyte viability during agonist-induced hypertrophy was conducted by annexin V/propidium iodide (PI) labeling, TUNEL labeling of apoptosis-induced DNA damage, and analysis of nuclear integrity via DAPI staining (Fig. 1*D*). These efforts indicate that there is no significant increase in apoptotic cell death during hypertrophic agonist stimulation.

Activation of the Intrinsic Cell Death Pathway Is Required for Cardiomyocyte Hypertrophy.

Next, we investigated the requirement of the intrinsic mediated cell death pathway for mediating the hypertrophy response. Presumably, if the agonist-induced

hypertrophy response required sequential activation of the intrinsic pathway, inhibition of this signal should reduce or block hypertrophy. Primary cardiomyocytes were treated with PE in the presence or absence of the caspase 9 peptide inhibitor *N*-benzyloxycarbonyl-Leu-Glu-His-Asp-fluoromethylketone (z-LEHD-fmk). A significant attenuation of cardiomyocyte cell size (~39%) was noted after caspase 9 inhibition (Fig. 2 *A*, *b* vs. *c*). In addition to cell size, a significant reduction in the expression of the prohypertrophic marker atrial natriuretic peptide (ANP; ~62%) (19) was also observed following caspase 9 inhibition (Fig. 2 *A*, *e* vs. *f*). Although caspase 9 represents an accurate proxy for intrinsic pathway activation, we sought to confirm the mitochondria as the de facto initiation signal. Here, the intrinsic pathway was inhibited during agonist stimulation by infection with an adenovirus (AdV) expressing the myeloid cell leukemia 1 (Mcl-1) protein. Mcl-1 binds to various proapoptotic Bcl-2 homology 3 (BH3)-only proteins such as Bid and Bim and multiple BH domain proteins Bax and Bak, inhibiting BH3 pore formation in the mitochondrial membrane, squelching cyt *c* release, and effectively blocking activation of the intrinsic apoptotic pathway (20, 21). A significant decrease in cell size (~33%) and ANP levels (~61%) was noted in Mcl-1-AdV–infected cardiomyocytes compared with PE treatment alone (Fig. 2 *B*, *b* and *h* vs. *c* and *i*). ISO treatment (Fig. 2 *C*, *b* and *h* vs. *c* and *i*) and additional hypertrophic agonists, AngII and ET1, yielded similar reductions in cell size and ANP levels (Fig. S6). The decrease in cell size and ANP levels resulting from Mcl-1-AdV infection mirrors the observations with caspase 9 peptide inhibition, suggesting an essential role for the intrinsic cell death pathway in promoting hypertrophic induction.

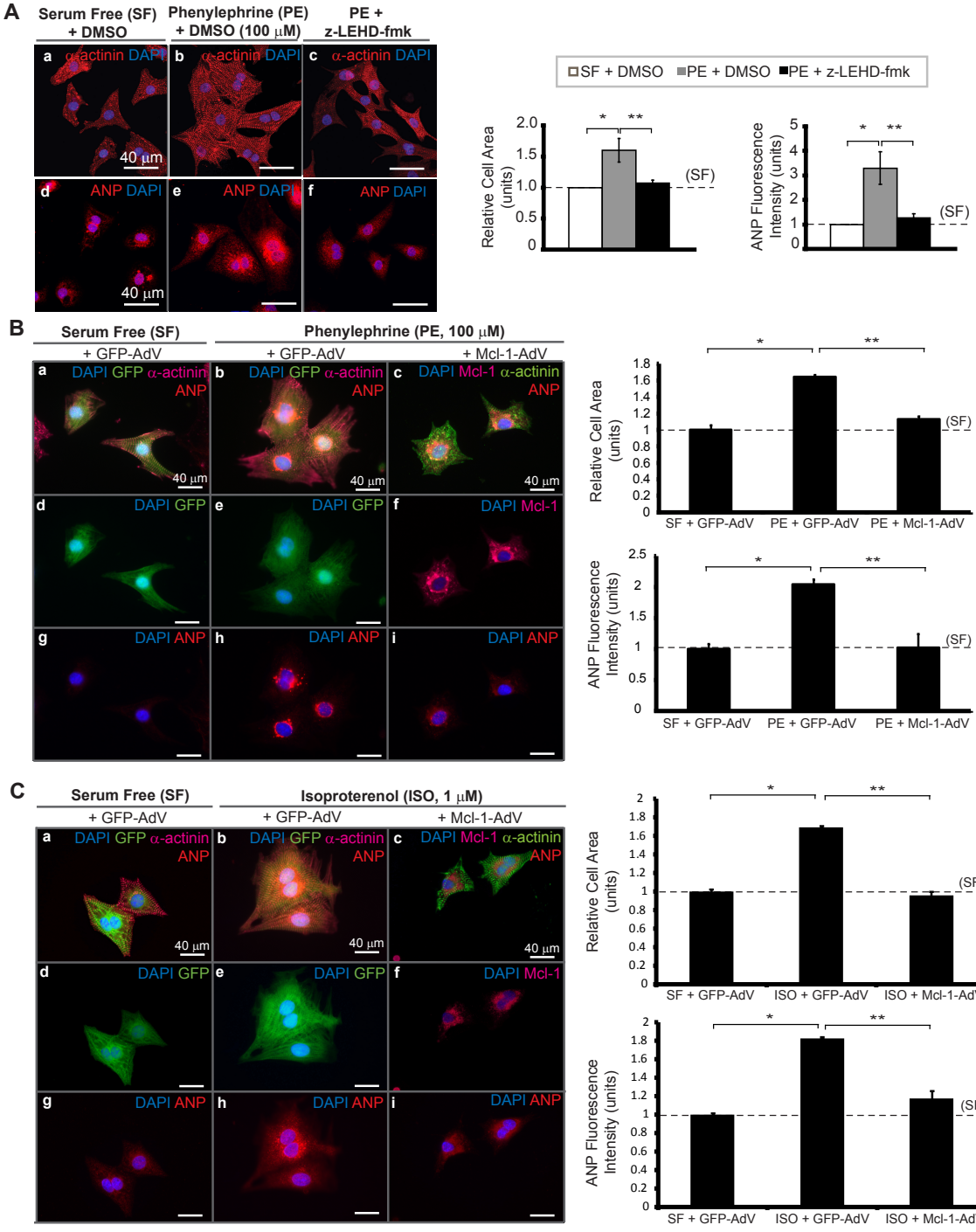

A
Serum Free (SF) + DMSO
Phenylephrine (PE) + DMSO (100 μM)
PE + z-LEHD-fmk
a α-actinin DAPI
b α-actinin DAPI
c α-actinin DAPI
40 μm
d ANP DAPI
e ANP DAPI
f ANP DAPI
40 μm
SF + DMSO
PE + DMSO
PE + z-LEHD-fmk
Relative Cell Area (units)
2.0
1.5
1.0
0.5
0
(SF)
ANP Fluorescence Intensity (units)
5
4
3
2
1
0
(SF)
B
Serum Free (SF)
Phenylephrine (PE, 100 μM)
+ GFP-AdV
+ GFP-AdV
+ Mcl-1-AdV
a DAPI GFP α-actinin ANP
b DAPI GFP α-actinin ANP
c DAPI Mcl-1 α-actinin ANP
40 μm
d DAPI GFP
e DAPI GFP
f DAPI Mcl-1
g DAPI ANP
h DAPI ANP
i DAPI ANP
Relative Cell Area (units)
1.8
1.6
1.4
1.2
1
0.8
0.6
0.4
0.2
0
(SF)
SF + GFP-AdV
PE + GFP-AdV
PE + Mcl-1-AdV
ANP Fluorescence Intensity (units)
2.5
2
1.5
1
0.5
0
(SF)
SF + GFP-AdV
PE + GFP-AdV
PE + Mcl-1-AdV
C
Serum Free (SF)
Isoproterenol (ISO, 1 μM)
+ GFP-AdV
+ GFP-AdV
+ Mcl-1-AdV
a DAPI GFP α-actinin ANP
b DAPI GFP α-actinin ANP
c DAPI Mcl-1 α-actinin ANP
40 μm
d DAPI GFP
e DAPI GFP
f DAPI Mcl-1
g DAPI ANP
h DAPI ANP
i DAPI ANP
Relative Cell Area (units)
2
1.8
1.6
1.4
1.2
1
0.8
0.6
0.4
0.2
0
(SF)
SF + GFP-AdV
ISO + GFP-AdV
ISO + Mcl-1-AdV
ANP Fluorescence Intensity (units)
2
1.8
1.6
1.4
1.2
1
0.8
0.6
0.4
0.2
0
(SF)
SF + GFP-AdV
ISO + GFP-AdV
ISO + Mcl-1-AdV

Fig 2. The intrinsic mitochondrial/caspase 9 cell death pathway is required for PE- and ISO-induced cardiomyocyte hypertrophy. (*A*) Cardiomyocytes were treated for 24 h with SF medium (*a* and *d*), 100 μM PE (*b* and *e*), and PE plus 20 μM caspase 9 inhibitor z-LEHD-fmk (*c* and *f*). PE treatment increased cell size, which was significantly attenuated in the presence of z-LEHD-fmk (*Left*; $n = 3$, $^{**}P < 0.05$). ANP levels were significantly reduced in the presence of z-LEHD-fmk compared with PE-treated cells (*Right*; $n = 3$, $^{**}P < 0.05$). (*B*) Mcl-1-AdV inhibition of the intrinsic caspase 9 pathway, with GFP-AdV used as a control. Infection with Mcl-1-AdV significantly decreased cell size and ANP levels compared with PE plus GFP-AdV–treated cardiomyocytes ($n = 3$; $^{**}P < 0.05$). (*C*) Cardiomyocytes were treated as in *B* except ISO was the hypertrophic agonist (1 μM). Similarly, intrinsic pathway inhibition by Mcl-1-AdV infection led to significantly reduced cell size and ANP levels ($n = 3$; $^{**}P < 0.05$). For *B* and *C*, Mcl-1 expression was detected with anti-myc antibody and an Alexa 647 (pink)-conjugated secondary antibody (Fig. S6). Cell sizes analyzed by using ImageJ software. (Scale bars: 40 μM.)

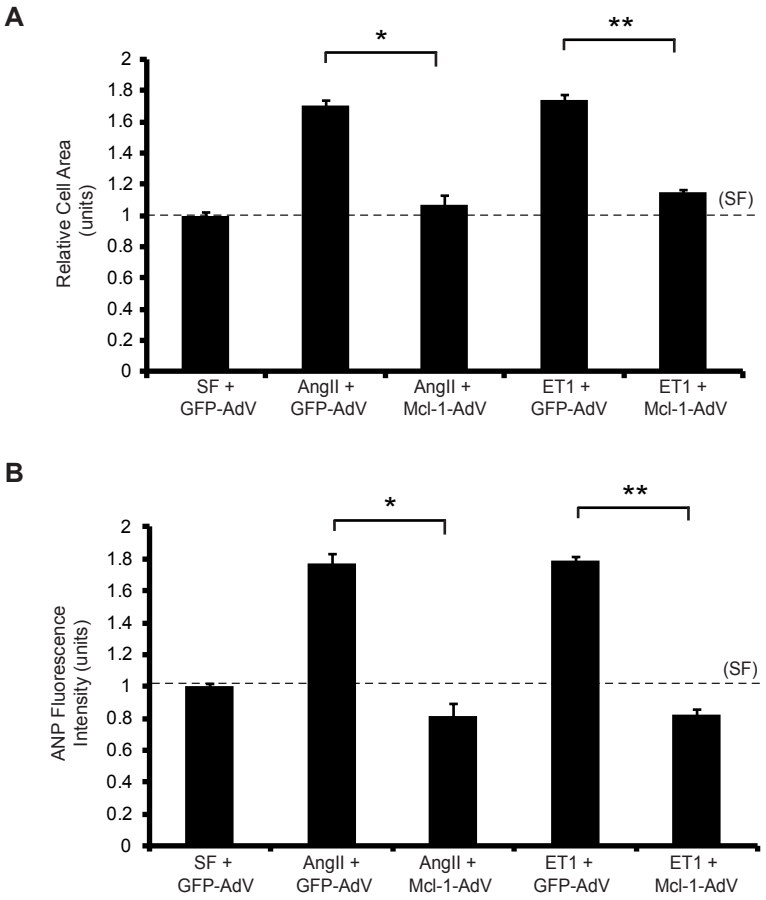


Fig S6. Cardiomyocyte cell size and ANP levels are reduced by Mcl-1-AdV during 24 h agonist-induced hypertrophy. Primary cardiomyocytes were treated with control SF media plus GFP-AdV, AngII (100 nM) plus GFP-AdV, AngII plus Mcl-1-AdV, ET1 (20 nM) plus GFP-AdV, or ET1 plus Mcl-1-AdV. Cell size (A) and ANP levels (B) were evaluated during each treatment. Cardiomyocyte size and ANP levels were significantly reduced by Mcl-1-AdV compared with control GFPAdV ($n = 3$; $^*P < 0.05$).

Effector Caspase/Caspase 3 Activation Is Essential for Cardiomyocyte Hypertrophy in Vitro and in Vivo.

We next examined the requirement of caspase 3 activity in the development of the hypertrophy response. Primary cardiomyocytes were treated with the caspase 3-specific peptide inhibitor N-benzyloxycarbonyl-Asp-Glu-Val-Asp-fluoromethylketone (z-DEVD-fmk), followed by cell size and ANP quantifications. The PE-induced hypertrophic phenotype was abrogated by caspase 3 inhibition, as demonstrated by reduced cell size (~36%) and ANP levels (~42%; Fig. 3 *A*, *b* and *e* vs. *c* and *f*). Caspase 3 inhibition was also accomplished by infection of primary cardiomyocytes with an AdV expressing the baculoviral protein p35 (22). p35 acts to competitively inhibit effector caspases by an irreversible chemical process. The caspase recognition sequence of p35 is targeted by the effector caspase (3, 6, 7), forming a thioester bond between the active cysteine and the P_1 residue, resulting in a completely disabled enzyme (23). p35 is the most potent inhibitor of caspases identified to date, providing an irreversible inhibition of all caspase enzymes except caspase 9 (23, 24). Importantly, the infection of cardiomyocytes with p35-AdV led to a similar reduction in the hypertrophic response following exposure to PE and ISO (decreased ANP levels in Fig. 3*B*), as well AngII and ET1 (decreased ANP and cell size in Fig. S7 *A*–*C*). Finally, we demonstrate that, within the same cardiomyocyte culture, cells that are infected with caspase signaling inhibitors (p35-AdV) do not respond to hypertrophy agonists, whereas the uninfected cardiomyocytes in the same culture undergo hypertrophy (Fig. S8). Taken together, these data confirm that secondary paracrine effects of caspase activity in adjacent apoptotic cells do not significantly impact the hypertrophy response.

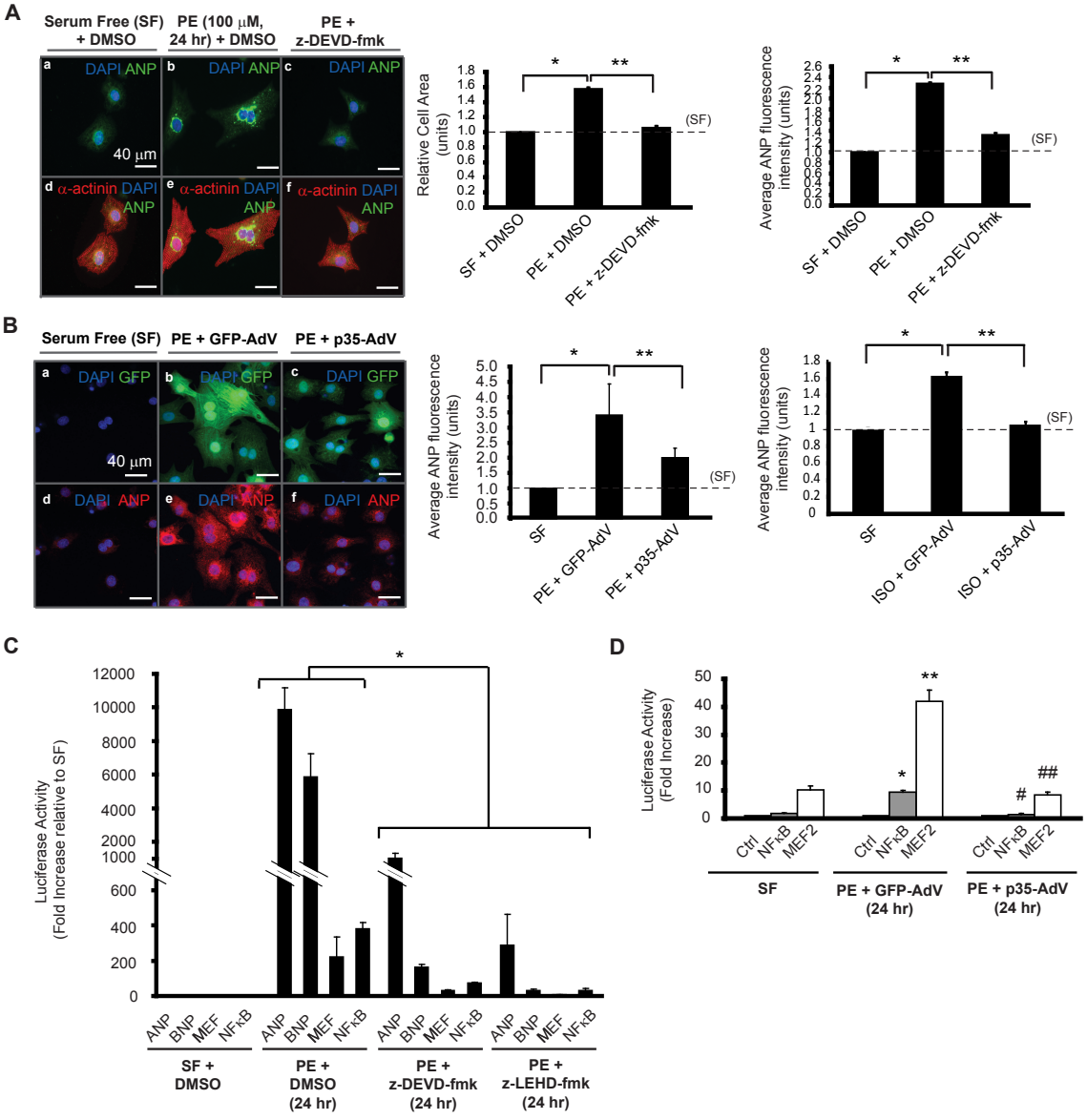

A
Serum Free (SF) + DMSO
PE (100 μM, 24 hr) + DMSO
PE + z-DEVD-fmk
DAPI ANP
40 μm
α-actinin DAPI ANP
Relative Cell Area (units)
Average ANP fluorescence intensity (units)
(SF)
SF + DMSO
PE + DMSO
PE + z-DEVD-fmk
B
Serum Free (SF)
PE + GFP-AdV
PE + p35-AdV
DAPI GFP
SF
PE + GFP-AdV
PE + p35-AdV
ISO + GFP-AdV
ISO + p35-AdV
C
Luciferase Activity (Fold Increase relative to SF)
ANP
BNP
MEF
NFκB
SF + DMSO
PE + DMSO (24 hr)
PE + z-DEVD-fmk (24 hr)
PE + z-LEHD-fmk (24 hr)
D
Luciferase Activity (Fold Increase)
Ctrl
NFκB
MEF2
SF
PE + GFP-AdV (24 hr)
PE + p35-AdV (24 hr)

Fig 3. Caspase 3 activation is required for PE- and ISO-induced cardiomyocyte hypertrophy. (*A*) Cardiomyocytes were treated for 24 h with SF medium (*a* and *d*), 100 μM PE (*b* and *e*), and PE plus 20 μM caspase 3 inhibitor z-DEVD-fmk (*c* and *f*). PE induced a significant increase in cell size, which was inhibited by z-DEVD-fmk (*Left*; $n = 3$; $^{**}P < 0.05$). PE also increased the levels of ANP, whereas the presence of z-DEVD-fmk reduced ANP expression (*Right*; $n = 3$; $^{**}P < 0.05$). (*B*) Cardiomyocytes were treated with SF medium (*a* and *d*), 100 μM PE plus GFP-AdV (*b* and *e*), and PE plus p35-AdV (*c* and *f*). During PE treatment, a significant increase in ANP was detected, whereas p35-AdV decreased ANP levels (*Left*; $n = 3$; $^{**}P < 0.05$). p35-AdV infection also led to significantly reduced ANP levels during ISO-induced hypertrophy (*Right*; $n = 3$, $^{**}P < 0.05$; Fig. S7). (*C*) Cardiomyocytes were transfected with luciferase reporter plasmids for prohypertrophic markers (ANP, BNP, MEF2, and NF-κB), and reporter activity was measured after treatments with SF plus DMSO, PE plus DMSO, and PE plus z-DEVD-fmk or z-LEHD-fmk inhibitors for 24 h. PE plus z-DEVD-fmk or z-LEHD-fmk inhibition led to a significant reduction in PE-induced reporter activation ($n = 3$; $^{*}P < 0.05$). (*D*) Cardiomyocytes were transfected with NF-κB, MEF2, or control luciferase hypertrophic reporter plasmids followed by infection with GFP-AdV or p35-AdV. PE-induced hypertrophy resulted in a significant increase in NF-κB ($n = 3$, $^{*}P < 0.05$) and MEF2 ($n = 3$, $^{**}P < 0.05$) activation compared with SF control. Caspase inhibition with p35-AdV infection suppressed NF-κB ($n = 3$, $\#P < 0.05$) and MEF2 ($n = 3$, $\#\#P < 0.05$) activation. (Scale bars: 40 μm.)

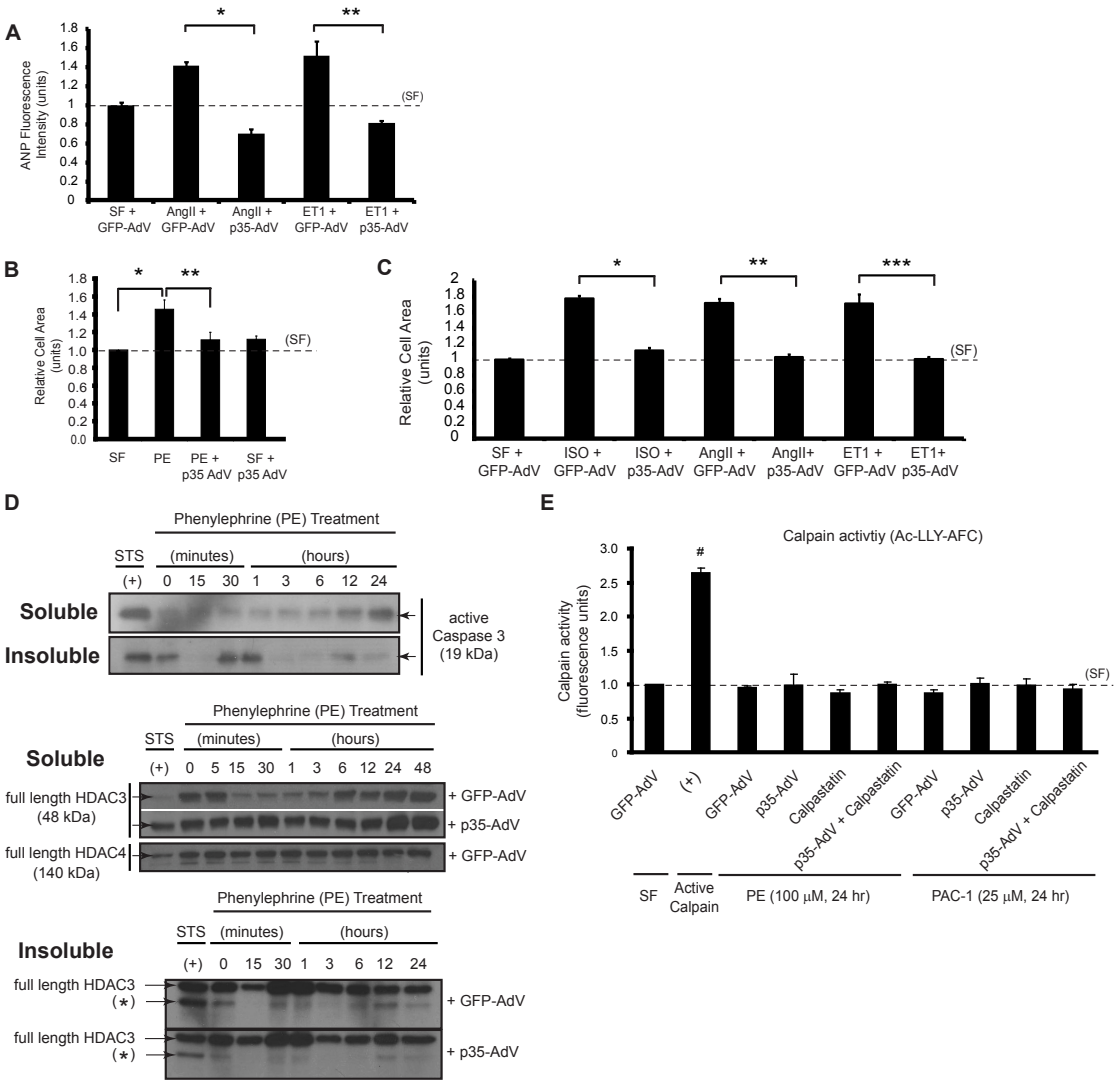

A
ANP Fluorescence Intensity (units)
(SF)
SF + GFP-AdV
AngII + GFP-AdV
AngII + p35-AdV
ET1 + GFP-AdV
ET1 + p35-AdV
B
Relative Cell Area (units)
SF
PE
PE + p35 AdV
SF + p35 AdV
C
Relative Cell Area (units)
SF + GFP-AdV
ISO + GFP-AdV
ISO + p35-AdV
AngII + GFP-AdV
AngII+ p35-AdV
ET1 + GFP-AdV
ET1+ p35-AdV
D
Phenylephrine (PE) Treatment
STS
(minutes)
(hours)
Soluble
Insoluble
active Caspase 3 (19 kDa)
full length HDAC3 (48 kDa)
full length HDAC4 (140 kDa)
+ GFP-AdV
+ p35-AdV
full length HDAC3 (*)
E
Calpain activtiy (Ac-LLY-AFC)
Calpain activity (fluorescence units)
GFP-AdV
Calpastatin
p35-AdV + Calpastatin
SF
Active Calpain
PE (100 μM, 24 hr)
PAC-1 (25 μM, 24 hr)

Fig S7. Effector caspase 3 is required for agonist-induced hypertrophy. (A) Cardiomyocytes were treated with hypertrophic agonists AngII (100 nM) or ET1 (20 nM) for 24 h with a GFP control AdV (GFP-AdV) or a potent effector caspase inhibitor p35-AdV. ANP fluorescence intensity significantly decreased when cardiomyocytes were infected with p35-AdV compared with GFP-AdV ($n = 3$; $^{*}P < 0.05$). (B) Cardiomyocyte cell size was also significantly decreased by p35-AdV during 24 h PE-induced hypertrophy. Cardiomyocytes were treated with control SF medium or 100 μM PE only for 24 h with or without p35-AdV. Cardiomyocyte cell size ($n = 3$; $^{**}P < 0.05$) was dramatically reduced in the presence of p35-AdV. The p35-AdV in SF media was found to not significantly affect the size of cardiomyocytes compared with SF media alone. (C) As in B, cell size was analyzed during ISO (1 μM), AngII (100 nM), and ET1 (20 nM) treatment with control GFP-AdV or p35-AdV. A significant reduction in cell size was noted for all agonists in the presence of p35-AdV ($n = 3$; $^{*}P < 0.05$). (D) Active caspase 3 levels were evaluated during PE-induced hypertrophy (0 min to 24 h) in soluble and insoluble fractions. Caspase 3 activation is observed at 15 min and increases at later time points (12–24 h) within the soluble fraction. Interestingly, high active caspase 3 levels are observed during 30 min to 1 h of PE treatment within the insoluble fraction, which correlates with the caspase 3 foci analysis. HDAC3 levels were also evaluated in soluble and insoluble fractions. Cardiomyocytes were infected with p35-AdV or control GFP-AdV followed by treatment with PE (100 μM) for various time points and subjected to immunoblot. Within the soluble fraction, full-length HDAC3 levels decreased during the early stages of hypertrophy in control GFP-AdV–infected cardiomyocytes (15 min to 3 h), whereas the presence of p35-AdV inhibited this decrease (arrows). Levels of full-length HDAC4 did not change. Treatment with 2 μM STS for 24 h was used as a positive (+) control. The insoluble fraction also contained significant levels of full-length HDAC3 (arrows) that was also associated with a potential HDAC3 fragment (asterisk). The addition of p35-AdV reduced levels of this potential cleavage fragment, suggesting the presence of a caspase-dependent cleavage event. (E) Calpain activation was assessed during the following treatments to exclude the involvement of the calpain pathway: SF plus GFP-AdV, active calpain, PE plus GFP-AdV, PE plus p35-AdV, PE plus calpastatin, PE plus p35-AdV plus calpastatin, PAC-1 plus GFP-AdV, PAC-1 plus p35-AdV, PAC-1 plus calpastatin, and PAC-1 plus p35-AdV plus calpastatin. Calpain pathway was not activated during PE- or PAC-1–induced hypertrophy, and calpain inhibition with calpastatin (200 nM; 1 h) had no effect. Treatment with active calpain showed significantly increased calpain activity ($n = 3$; $\#\ P < 0.05$).

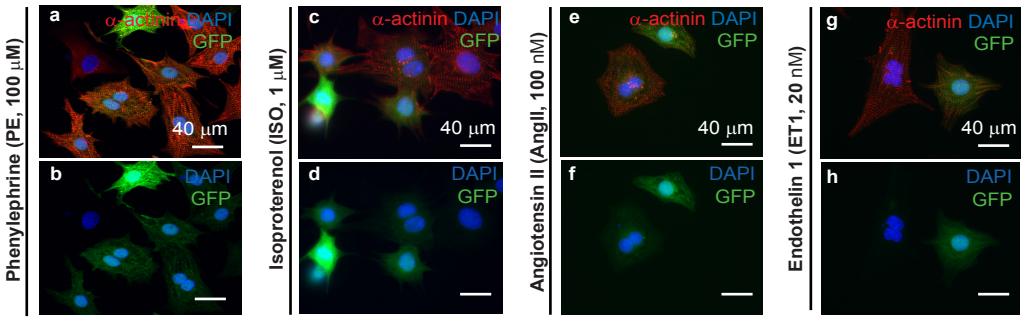


Fig S8. Qualitative analysis of paracrine effects during p35-AdV infection. Primary cardiomyocytes were treated with hypertrophic agonists PE (100 μM; a and b), ISO (1 μM; c and d), AngII (e and f), and ET1 (20 nM; g and h) with p35-AdV (green) for 24 h. Immunofluorescence was used to detect α-actinin (red), and nuclei were stained with DAPI (blue). Cardiomyocytes infected with p35-AdV are bright green and have reduced size, whereas those that were not infected (or infected to a lower extent) are responsive to agonist stimulation and become larger in size (i.e., hypertrophic). This analysis is an internal control for qualitatively addressing paracrine effects.

To further confirm the caspase 3-induced hypertrophy response, we measured the transcriptional response of known prohypertrophic markers [MEF2, NF-κB, ANP, (B-type natriuretic peptide (BNP)]. Primary cardiomyocytes were transfected with MEF2, NF-κB, ANP, or BNP plasmids (with a *Renilla* luciferase internal control plasmid) and monitored for the response to agonist and caspase activation (SF plus DMSO, PE plus DMSO, PE plus z-DEVD-fmk or z-LEHD-fmk). PE treatment resulted in a significant increase in all hypertrophic markers compared with cardiomyocytes treated with SF plus DMSO media (Fig. 3*C*), whereas PE treatment followed by caspase 3 or caspase 9 inhibition led to a dramatic reduction in reporter activation compared with PE plus DMSO treatment (Fig. 3*C*).

We next sought to identify a molecular cascade whereby caspase 3 activity engages the hypertrophy response. In this regard, the MEF2 pathway was of considerable interest. The MEF2 family functions as a point of convergence for a variety of hypertrophic signals, including the fetal gene program (3, 25). MEF2 transcriptional activity is suppressed by the binding of histone deacetylases (HDACs), and relief of this repression has been well documented as a key step in the hypertrophic response (3). Of interest, caspase 3 has been shown to cleave HDAC3 and HDAC4, resulting in their cytoplasmic relocalization during apoptotic signaling (26–28). Moreover, cardiac-specific deletion of HDAC3 is synonymous with a pronounced cardiac hypertrophy phenotype (29). To address our supposition that caspase 3 activity is restrained in insoluble foci, we first examined levels of activated caspase 3 in the soluble and insoluble fractions. We observed a significant increase in the level of active caspase 3 within the insoluble fraction of PE-treated cardiomyocytes as early as 30 min, followed by a transient

decrease and then a latter-stage increase in activity (Fig. S7*D*). We observed a specific and temporal decline in levels of full-length HDAC3 at early time points following PE-induced hypertrophy in the soluble fraction, whereas HDAC4 protein levels remained unchanged (Fig. S7*D*). Furthermore, infection of cardiomyocytes with p35-AdV blocked the temporal decline in HDAC3 protein levels, suggesting that the HDAC3 decrease was caspase 3-dependent (Fig. S7*D*). Finally, we noted a large concentration of full-length HDAC3 (~48 kDa) within the insoluble protein fraction, which was associated with a cleavage event that was attenuated with p35-AdV (Fig. S7*D*, asterisk). The size of the putative fragment (~44 kDa) corresponds to the predicted size of the caspase 3-mediated large C-terminal cleavage fragment of HDAC3 observed by others (26). Interestingly, a classic caspase 3 cleavage site is present at Asp-391 of the C terminus of HDAC3 that would produce this putative large HDAC3 fragment. Prior observations in the literature also suggest that HDAC proteins do segregate and associate with an insoluble fraction (30, 31). Liu et al. noted that Hos2 (yeast HDAC) and Yca1 (yeast metacaspase) were contained within insoluble stress granules (30). Our group has previously demonstrated that the core molecular function of Yca1 is to limit protein aggregate formation in response to stress (16). As such, a reasonable conjecture is that the colocalization of caspase 3 and HDAC3 (and the caspase-mediated processing of HDAC3) may represent an adaptive stress response in cardiomyocytes, a response that has been conserved from single-celled eukaryotes. This is a topic of considerable interest and will require additional experimental validation to confirm this hypothesis.

Consistent with a model of caspase-mediated derepression of MEF2, we also observed that MEF2 transcriptional activity (via an MEF2-dependent reporter assay) was

dramatically attenuated (~80%) in cardiomyocytes with impaired caspase activation via p35-AdV during PE stimulation (Fig. 3*D*). An additional hypertrophic transcription signal that may respond to and translate caspase activity is the NF-κB pathway. NF-κB is a transcription factor that responds to stress signaling to promote or enhance cell survival, yet this factor is also a prominent feature in pathological cardiac hypertrophy (32). Interestingly, caspase proteases have been shown to activate NF-κB signaling in a variety of noncardiac settings, steps that involve cleavage-activation of the inhibitor of kappa B kinase (IKK) kinases, as well as targeted cleavage and removal of the inhibitor of kappa B alpha (IκBα), the NF-κB inhibitor protein (33–35). PE-treated cardiomyocytes displayed a significant increase in NF-κB reporter activity, yet caspase inhibition via p35-AdV infection resulted in complete blockade of the NF-κB–induced response (~84%; Fig. 3*D*). These results suggest that the hypertrophy-associated engagement of NF-κB activity is caspase 3-responsive, yet we have been unable to identify the precise caspase 3 substrate that is targeted in this pathway.

Caspase 3-mediated induction of cardiomyocyte hypertrophy was also examined in the intact myocardium. PE control and experimental groups were subject to ultrasound-guided microinjection of the left ventricle wall with control GFP-AdV or p35-AdV expressing AdVs. After 3 d, osmotic minipumps were implanted in rats containing saline solution (control) or PE (PE control and experimental groups) to induce pathologic hypertrophy. Subsequently, hearts were retrieved at 3 wk after treatment, to coincide with the early stages of adaptive hypertrophy. Hearts treated with PE and infected with p35-AdV displayed a significant reduction in heart weight to body weight (HW/BW) ratio (~12%) and cardiomyocyte cell size (~37%) compared with the PE-treated GFP-AdV–

infected group (Fig. 4*A*). Similarly, ISO-induced hypertrophy in vivo (2 wk) was significantly blunted in the presence of p35-AdV, with a decreased HW/BW ratio (~12%) and cardiomyocyte cell size (~42%) compared with the ISO-treated GFP-AdV–infected group (Fig. 4*B*). Therefore, similar to the in vitro experimental observations, inhibition of effector caspase activity (caspase 3) attenuates cardiomyocyte hypertrophy in the intact heart.

Caspase 3 Activation Is Sufficient to Induce Cardiomyocyte Hypertrophy.

The combination of peptide and biologic inhibitor experiments demonstrate that intrinsic-mediated cell death signaling is required for the development of cardiomyocyte hypertrophy. As such, we next examined whether caspase activation was sufficient to engage hypertrophy, independent of any agonist stimulation. To test this premise, we used a small molecule that specifically stimulates caspase 3 activation, termed procaspase 3 activating compound 1 (PAC-1). PAC-1 is a potent and specific activator of procaspase 3 that acts via sequestration of the inhibitory zinc ions at the catalytic site on the pro form of caspase 3 (36, 37). As unrestricted caspase 3 activation leads to induction of apoptosis, we conducted a dose range experiment to establish a concentration of PAC-1 that was compatible with maintaining cell viability. Primary cardiomyocytes treated with high doses of PAC-1 (100 μM) displayed decreased viability (i.e., increased cell death) relative to control cells, an outcome that was comparable to a standard apoptotic treatment with staurosporine (Fig. S9). However, low-dose PAC-1 administration (12.5–25 μM) maintained cell viability (i.e., no significant decrease in cell viability) while

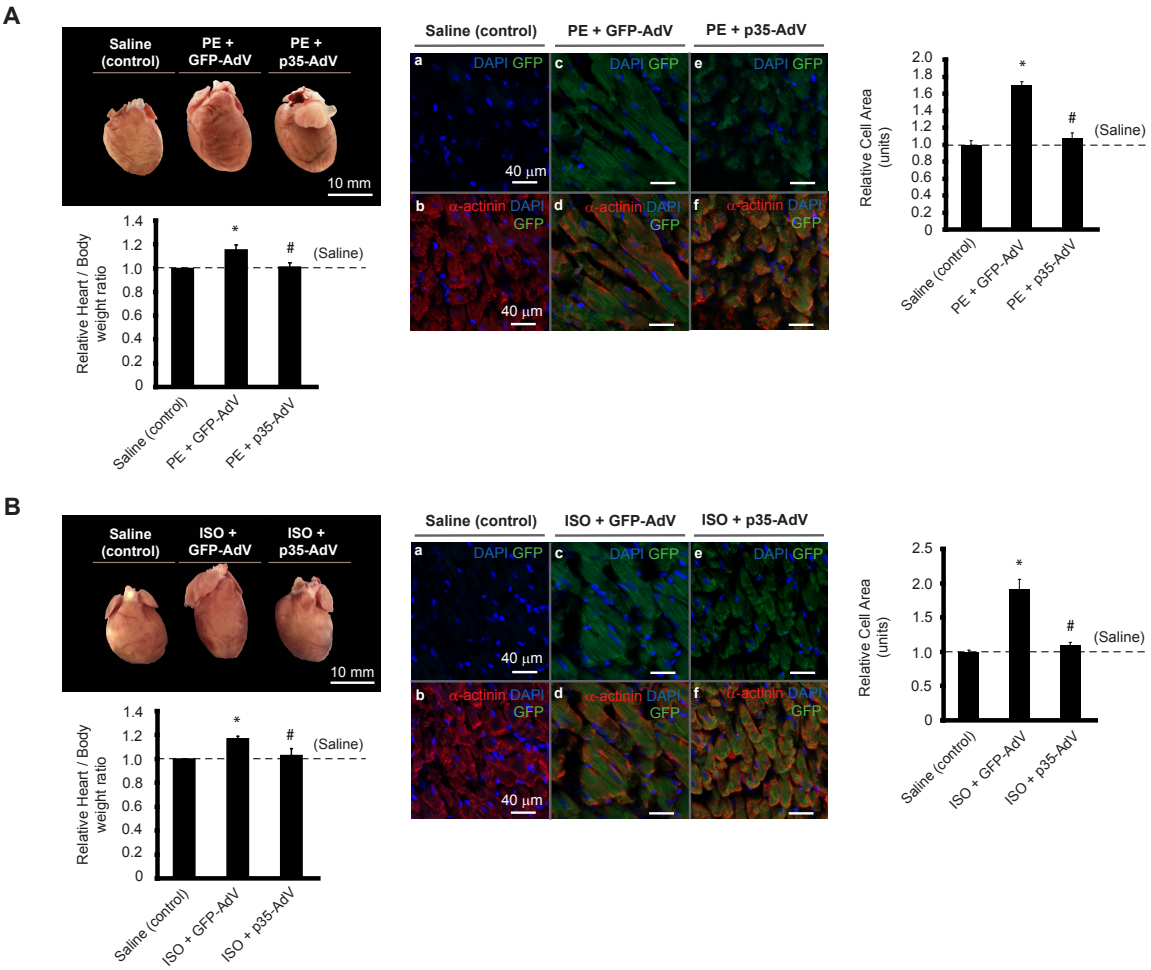


Fig 4. Inhibition of caspase 3 activity attenuates cardiomyocyte hypertrophy in the intact myocardium. (*A*) Osmotic minipumps were implanted in rats containing saline solution (control) or PE (PE control and experimental) to induce hypertrophy over 3 wk at 10 mg/kg/d. PE control and experimental groups were subjected to GFP-AdV or a GFP tagged p35 expressing AdV (p35-AdV) infection via echo-directed microinjections into the ventricle wall. After 3 wk, whole hearts were isolated, cryosectioned, and stained for α-actinin (red) and DAPI (blue). PE induced an increase in HW/BW ratio of 15% and an increase in cardiomyocyte cell area of 69% compared with control ($n = 3$; $^{*}P < 0.05$) whereas p35-AdV significantly reduced these effects ($n = 3$; $^{\#}P < 0.05$). (*B*) Hypertrophy was induced (as described earlier) using ISO at 1 mg/kg/d for 2 wk. HW/BW ratio and cell size were increased (17% and 90%, respectively) compared with control ($n = 3$; $^{*}P < 0.05$), and p35-AdV treatment led to a significant reduction in these hypertrophic effects ($n = 3$; $^{\#}P < 0.05$). Cell area of GFP (green)-positive cardiomyocytes was evaluated by using ImageJ software. (Scale bars: 40 μm.)

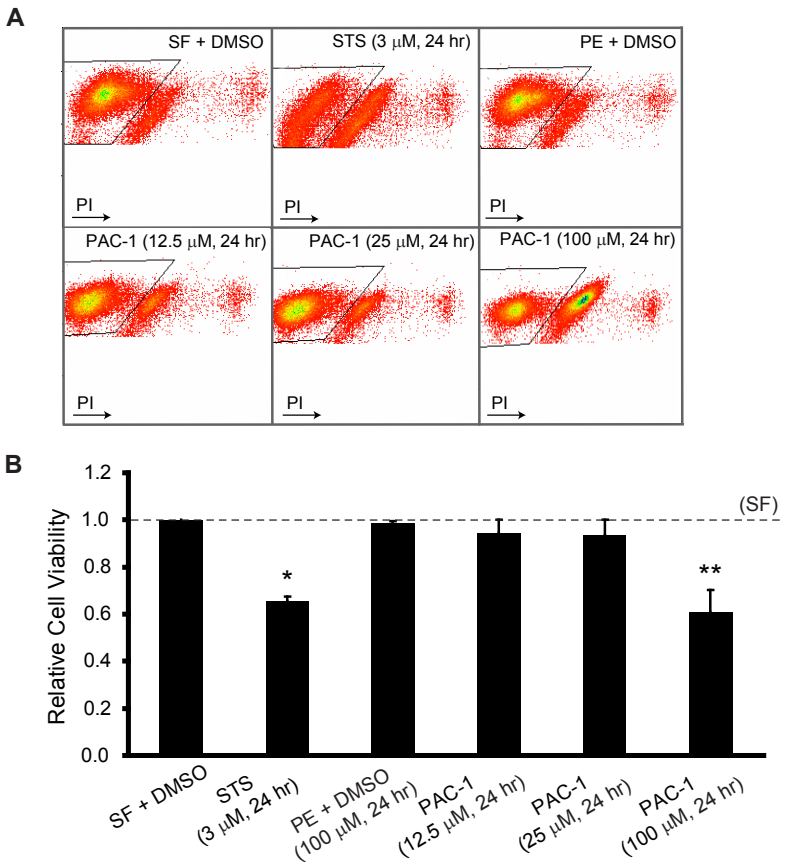


Fig S9. Cardiomyocyte viability is maintained after low-dose PAC-1 treatment. Primary cardiomyocytes were treated with SF media, STS (3 μM; 24 h), PE (100 μM; 24 h), and 12.5 to 100 μM of PAC-1 for 24 h. Cardiomyocyte viability was determined by PI staining and flow cytometry (488-nm excitation/617-nm emission). PI cell viability plots are shown in A, and overall viability quantifications are shown in the graph (B). Cardiomyocytes treated with high-dose PAC-1 (100 μM) displayed similar viability to STS treatment (i.e., significantly reduced viability; n = 3, * $P < 0.05$). Low-dose PAC-1 (12.5–25 μM) administration resulted in maintained cell viability, comparable to SF and PE treatments (i.e., viable cardiomyocytes).

inducing cardiomyocyte hypertrophy, a response that was comparable with the hypertrophic agonist PE (Fig. S9 and Fig. 5*A*). Specifically, cardiomyocytes treated with low PAC-1 concentrations (25 μM, 24 h) displayed a significant increase in cell size (~65%) and ANP expression (approximately threefold; Fig. 5 *A*, *a* and *f* vs. *c*and *h*). To further validate the PAC-1/caspase 3-induced hypertrophy response, we measured the transcriptional response of known prohypertrophic markers (MEF2, NF-κB, ANP, BNP) after 1 h, 3 h, and 24 h of PAC-1 (25 μM) treatment. Similar to PE treatment, PAC-1 administration resulted in a significant increase in all hypertrophic markers compared with cardiomyocytes treated with SF plus DMSO media as early as 1 h after exposure to PAC-1 (Fig. 5*B*, *Left*). After 3 h of PAC-1 treatment, significant elevations in reporter activity were observed which were comparable to those following PE exposure (Fig. 5*B*, *Center*). Significant reporter activity after 24 h of PAC-1 treatment was also observed (Fig. 5*B*, *Right*). The differences in the fold activation noted at the 24-h time point in PE treated vs. PAC-1–treated cardiomyocytes may derive from the probability that PE engages additional signaling events, signals that extend beyond the intrinsic cell death pathway and that converge to amplify the hypertrophic gene expression program.

Finally, to confirm specificity of action for PAC-1, we conducted two additional experiments. Assuming PAC-1 stimulates cardiomyocyte hypertrophy through a strict activation of caspase 3, then (*i*) use of an irreversible inhibitor of caspase 3 activity should block the ability of PAC-1 to induce hypertrophy, and (*ii*) limiting activation of the intrinsic pathway should not impact the ability of PAC-1 to promote hypertrophy. Importantly, a significant reduction in cell size (~39%) and ANP expression (~56%) was observed in cardiomyocytes treated with the caspase 3 inhibitor during PAC-1

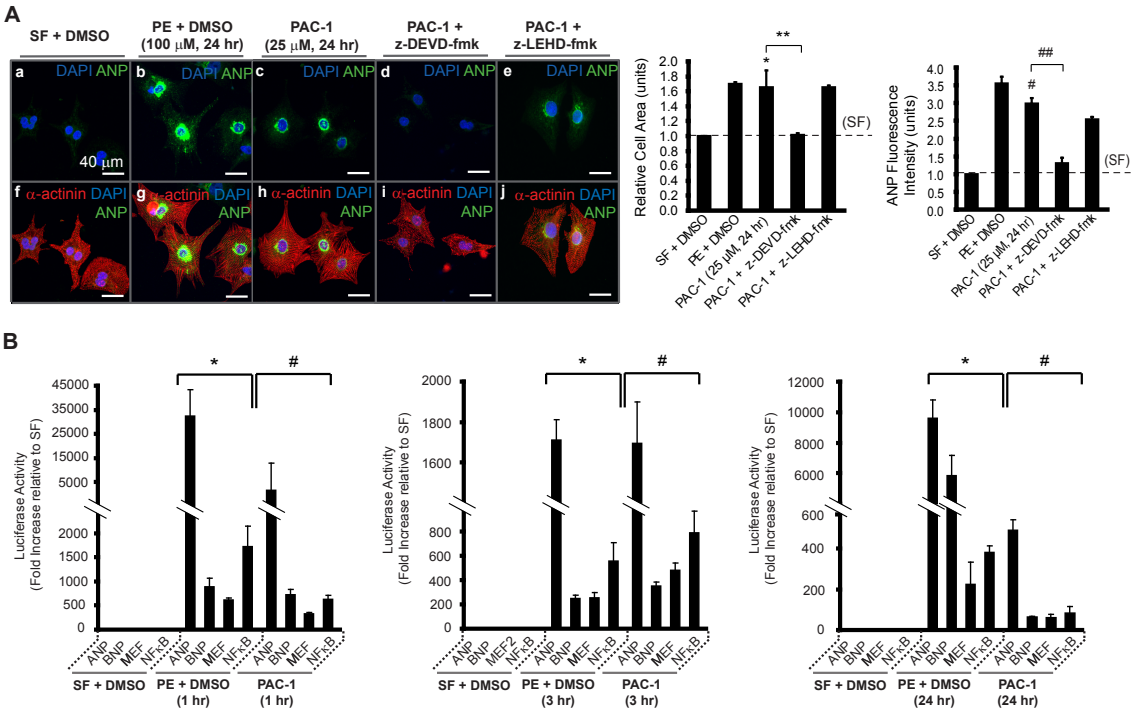


Fig 5. Caspase 3 activation is sufficient to induce cardiomyocyte hypertrophy. (*A*) Cardiomyocytes were treated with SF media (*a* and *f*), PE (100 μM; 24 h; *b* and *g*), PAC-1 (25 μM; 24 h; *c* and *h*), PAC-1 and caspase 3 inhibitor z-DEVD-fmk (*d* and *i*), or PAC-1 and caspase 9 inhibitor z-LEHD-fmk (*e* and *j*). Cells were stained for α-actinin (red), ANP (green), and DAPI (blue). PAC-1 treatment resulted in a significant increase in cell area and ANP levels, whereas inhibition with z-DEVD-fmk resulted in a significant reduction in cell size ($n = 3$, $^{**}P < 0.05$) and ANP levels ($n = 3$, $^{\#\#}P < 0.05$). Conversely, caspase 9 inhibition was not able to significantly reduce the hypertrophic phenotype induced by PAC-1 treatment (compare *c* and *h* vs. *e* and *j*). (Scale bars: 40 μm.) (*B*) The transcriptional response of known prohypertrophic markers was evaluated following 1, 3, and 24 h of PAC-1 treatment. Cardiomyocytes were transfected with luciferase reporter plasmids for prohypertrophic markers (MEF2, NF-κB, ANP, and BNP), and reporter activity was measured after treatments with SF, PE, and PAC-1. PAC-1 treatment resulted in a significant increase ($n = 3$; $^{\#}P < 0.05$) in all hypertrophic markers compared with SF media during early (1–3 h) and late (24 h) time points.

administration (Fig. 5 *A*, *c* and *h* vs. *d* and *i*). Conversely, caspase 9 inhibition was not able to significantly reduce the hypertrophic phenotype induced by PAC-1 treatment, demonstrating that PAC-1 activates caspase 3 downstream of caspase 9 (Fig. 5 *A*, *c* and *h* vs. *e* and *j*). These results establish that small molecule induction of caspase 3 activation is sufficient to recapitulate the phenotypic and biochemical characteristics of cardiomyocyte hypertrophy, independent of any agonist costimulation. To address the involvement of nonspecific protease activity or other calcium activated proteases as probable contributors to caspase induction of hypertrophy, we analyzed calpain activity during PE- and PAC-1–induced hypertrophy in the presence of caspase and calpain inhibitors (p35-AdV and calpastatin, respectively; Fig. S7*E*). Neither PE stimulation nor PAC-1 treatment of primary cardiomyocytes leads to any appreciable increase in calpain activity at later time points in the hypertrophy cycle (Fig. S7*E*). Although our observations do not preclude a role for calpains in the hypertrophic remodeling process, the data and reagents used in this study demonstrate a caspase specific role that cannot be attributed directly to calpain activity.

The present study establishes the intrinsic/mitochondrial cell death pathway as a central conduit for adrenergic-induced cardiomyocyte hypertrophy. To date, cell death signal pathways have been associated with the transition to end-stage heart failure. For example, long-term caspase inhibition has been reported to reduce cardiomyocyte apoptosis, attenuate cardiac remodeling, while preserving myocardial function in models of cardiomyopathy and pressure overload (6, 38–40). Here, our observations indicate that elevated caspase 3 activity is an early and essential step in the promotion of cardiomyocyte hypertrophy, a cellular response that is not associated with the apoptosis

program per se. The ability of caspase signaling to induce hypertrophy or apoptosis may appear to be an incompatible feature for a single pathway, yet may simply reflect alterations in signal intensity or duration. In such a model, transient and low-level activation of intrinsic signaling would be predicted to promote the hypertrophic adaptation, whereas sustained and high level activation would result in apoptosis. Indeed, a similar dichotomy has been reported for many neurohormonal agonists that trigger adrenergic receptor signaling events in the myocardium (e.g., PE, norepinephrine, AngII, and ET1). AdV expression of WT Gαq has been reported to induce compensatory/adaptive hypertrophic growth in cultured cardiomyocytes at 24 h; however, expression of a constitutively active Gαq mutant produced hypertrophy, which rapidly progressed to apoptotic cell death (41). These observations were supported by in vivo studies where transgenic mice overexpressing WT Gαq developed compensatory hypertrophy that rapidly transitioned to progressive heart failure (41, 42). Although these studies did not investigate the requirement for caspase activity, adrenergic stimulation of intrinsic cell death signaling may explain the accelerated progression from hypertrophy to failure.

We favor the hypothesis that caspase 3 cleavage inactivation of MEF2 and NF-κB inhibitory proteins releases the respective transcription factors to induce the cardiomyocyte hypertrophy program. Nevertheless, it is reasonable to conclude that other caspase-related signaling events augment the hypertrophy transition. Caspase activity can be localized to promote dismantling of specific subcellular structures during cellular differentiation and remodeling (13, 14). In the context of prohypertrophic remodeling, localized/restricted caspase activity may trigger the dynamic reorganization of

cytoskeletal and contractile protein components, thus allowing for the subsequent addition to and growth of sarcomeres (43). Communal et al. (43) have reported that β-adrenergic stimulation via norepinephrine exposure in adult rat ventricular cardiomyocytes triggered a caspase 3 targeting of α-actin, α-actinin, and cardiac troponin T before the onset of apoptosis. More recently, other sarcomeric proteins have been shown to be direct caspase targets in apoptotic models including, myosin heavy chain and ventricular myosin light chain (44–46). The ability of caspase 3 to directly modify cellular structure while altering the activity of key gene expression programs implies that this protease (and the intrinsic pathway) may serve as a fulcrum for agonist-induced hypertrophy in general.

In summary, we have provided clear evidence that the mitochondrial/intrinsic caspase-mediated pathway is essential for cardiomyocyte hypertrophy. Currently, antagonists of the upstream adrenergic receptors (e.g., β-blockers) are one of several mainstay treatments of heart failure (47). Based on our results, targeting downstream components of the intrinsic pathway, specifically caspase 3 or 9 protease function, may allow for therapeutic intervention in patients at the earlier compensatory stage of the disease process, limiting cardiomyocyte cell size and forgoing the maladaptive transition to heart failure.

Materials and Methods

Primary neonatal rat cardiomyocytes were isolated from hearts of 2-d-old Sprague–Dawley rats, and ventricles were digested with collagenase II. Subsequently, cardiomyocytes were resuspended in DMEM. Cells were allowed to recover in DMEM culture media for 24 h, followed by a change to serum-free (SF) media for another 24 h before cardiomyocyte treatments with hypertrophic agonists: PE (100 μM), ISO (1 μM), AngII (100 nM), or ET1 (20 nM). Caspase 3 and 9 signaling was inhibited by using 20 μM of a chemical peptide inhibitor (z-DEVD-fmk and z-LEHD-fmk, respectively). Inhibition of the intrinsic and effector caspase pathways was accomplished by infecting primary cardiomyocytes with AdVs expressing the biological caspase inhibitors (Mcl-1-AdV and p35-AdV, respectively).

Additional details regarding materials and methods are provided in SI Materials and Methods.

Acknowledgements

The authors thank Drs. Duncan Stewart, Michael Rudnicki, and Peter Liu for helpful discussions; Rick Seymour and Ali Ahmadi for performing ultrasound-guided intracardiac injections (University of Ottawa Heart Institute); Paul Oleynik for assistance with flow cytometry analyses (StemCore); and Dr. Ruth Slack for providing the Mcl-1–expressing adenovirus. This work was supported by grants (to L.A.M.) from the Ontario Research Fund, The Heart and Stroke Foundation of Canada, and the Canadian Institutes of Health Research. L.A.M. held the Mach Gaensslen Chair in Cardiac Research.

Supporting Information

SI Materials and Methods

All animal studies (primary cell retrieval and in vivo analysis) were approved by the University of Ottawa Heart Institute and the University of Ottawa Animal Care Committee.

Cell Culture.

Primary neonatal rat cardiomyocytes were isolated from hearts of 2-d-old Sprague–Dawley rats (Charles River Canada). Briefly, hearts were excised and placed in Joklik modified Eagle medium (J-MEM). Ventricles were separated from the atria, minced, and digested with 0.1% collagenase II (Worthington) in J-MEM for five rounds of 15-min digestions at 37 °C with agitation. Cellular fractions were collected and supernatants were incubated with 10% (vol/vol) FBS (Gibco) to prevent further digestion and spun at 100 × g for 5 min. Cell pellets were resuspended in DMEM/10% (vol/vol) FBS/1% (vol/vol) penicillin–streptomycin (Gibco). Two 30-min preplating incubations removed noncardiomyocytes. The nonadherent cells were seeded on adherent culture dishes or collagen-coated 25-mm glass coverslips for immunocytochemistry. Cells were allowed to recover in DMEM culture media for 24 h at 37 °C with 5% CO_2. Media were changed to serum-free (SF) media for 24 h at 37 °C with 5% CO_2.

Cardiomyocyte Treatments.

Cardiomyocyte hypertrophy was induced by replacing SF media with hypertrophic agonists phenylephrine (PE; 100μM; Sigma), isoproterenol (ISO; 1μM; Sigma), angiotensin II (AngII; 100 nM; Sigma) or endothelin 1 (ET1; 20 nM; Sigma) in SF media

for time courses ranging from 0 to 24 h. Staurosporine (STS; 2μM; dissolved in DMSO; 24 h; BioVision) in SF media was used as a positive control for caspase activation. For caspase 9 inhibition, cardiomyocytes were pretreated with N-benzyloxycarbonyl-Leu-Glu-His-Asp-fluoromethylketone (z-LEHD-fmk) (BioVision; 20μM; dissolved in DMSO) for 2 h before the induction of hypertrophy by PE (100μM; 24 h) when fresh inhibitor was added. The intrinsic pathway was specifically inhibited by infection with a Myc-tagged Mcl-1 expressing adenovirus (AdV). Caspase 3 inhibition was completed by use of N benzyloxycarbonyl-Asp-Glu-Val-Asp-fluoromethylketone (z-DEVD-fmk) (BioVision), as described earlier. Effector caspase inhibition was also accomplished via infection of primary cardiomyocytes with a p35-expressing AdV with a GFP reporter followed by PE treatment. A GFP-expressing control AdV was additionally used as a control for the p35-AdV and Mcl-1-AdV experiments.

Immunocytochemistry.

Fluorescent staining of primary cardiomyocytes, at a density of 2.7×10^5 cells per coverslip, was conducted on collagen-coated 25-mm glass coverslips. Briefly, cells were washed in PBS solution and fixed with 4% (wt/vol) paraformaldehyde (PFA) for 30 min after indicated treatment. Cell permeabilization was completed by incubating in blocking buffer (1% BSA, 2% (wt/vol) normal goat serum, 0.4% Tx-100 in PBS solution) for 30 min. Cardiomyocyte specificity was verified by staining with mouse anti–α-actinin (Sigma) overnight at 4 °C and then with goat anti-mouse IgG Cy3 conjugate (Millipore) for 1.5 h. To detect caspase activation, rabbit anti-active caspase 3 (Cell Signaling) or rabbit anti-active caspase 9 (Abcam) were used followed by the goat anti-rabbit Alexa 488 secondary antibody (Invitrogen). For the intrinsic pathway inhibition using Myc

tagged Mcl-1-AdV, an anti-Myc antibody (Invitrogen) was used followed by donkey anti-goat Alexa 647 (Invitrogen). Hypertrophic induction was examined by staining with known hypertrophic marker atrial natriuretic peptide (ANP), rabbit anti-ANP (Abcam), followed by detection by the Cy3 or Alexa 488 secondary antibody. Nuclei were counterstained with DAPI (Sigma), and cells were mounted onto microscope slides with DakoCytomation fluorescent mounting media (DakoCytomation). Fluorescent images were obtained using the Zeiss LSM510 (Carl Zeiss MicroImaging). Hypertrophy was assessed by cardiomyocyte cell size analysis of α-actinin–positive cells using ImageJ software. ANP fluorescence intensity was determined by integrated density quantification also by using ImageJ software. All values were normalized to SF control treatments.

Detection of Mitochondrial Membrane Potential.

Activation of the intrinsic (caspase 9-mediated) cell death pathway was evaluated by use of the DePsipher Kit (Trevigen). This kit uses a cationic dye (5,5′,6,6′-tetraethylbenzimidazolyl-carbocyanine iodide) to detect the loss of mitochondrial potential, which is an early step in the intrinsic pathway. When the mitochondrial membrane collapses, indicating intrinsic pathway activation, the DePsipher reagent is localized in the cytoplasm in its monomeric green fluorescent form. Primary cardiomyocytes were treated with SF as a negative control or valinomycin as a positive control ionophore (0.1μM; 1 h) and with hypertrophy agonists PE (100μM; 5 min to 24 h) or ISO (1 μM; 5 min to 24 h) followed by light fixation (0.5% PFA for 5 min). Assays were completed according to manufacturer's instructions, and the resulting fluorescence was detected immediately by microscopic observation. Green fluorescence (emission, 530 nm) was quantified by use of ImageJ software.

Cardiomyocyte Viability.

The FITC Annexin V/Dead Cell Apoptosis Kit with FITC annexin V and propidium iodide (PI) for flow cytometry (Invitrogen) was used to evaluate cardiomyocyte viability during PE (100 μM; 15 min, 30 min, 1 h, 3 h, 24 h), STS (2 μM, 24 h), or SF treatment according to the manufacturer's instruction. The double negatives (negative annexin V and negative PI) were evaluated by flow cytometry by using 488-nm excitation and 617-nm emission (MoFlo instrument; Beckman Coulter). Analysis was conducted by using Summit version 4.3 software. Measurement of apoptotic nuclei was also used to assess cell viability by incorporation of FITC-dUTP into the ends of fragmented DNA using TUNEL assay kit according to the manufacturer's instructions (Abcam). Direct measurement of nuclear DNA fragmentation was also used to assess cell viability by using DAPI nuclear stain. Cardiomyocyte viability was also analyzed after the indicated treatment, SF plus DMSO, PE (100 μM, 24 h) plus DMSO, STS (2 μM, 24 h), procaspase 3 activating compound 1 (PAC-1; 25 μM, 24 h) using PI staining followed by flow cytometry. Briefly, following cardiomyocyte treatment, cells were incubated with 1× trypsin and diluted with 1×PBS solution. Cells were harvested by centrifugation at 250×g for 5 min and resuspended in 1 ×PBS solution. Incubation with PI (1mg/mL) for 5 min at 4°C was followed by analysis of PI-positive cells by flow cytometry using 488-nm excitation and 617-nm emission (MoFlo instrument; Beckman Coulter). Analysis was conducted by using Summit version 4.3 software.

Caspase and Calpain Activity Assays.

Caspase activity was measured by incubating cell lysates with caspase-specific fluorogenic substrates: acetyl-Asp-Glu-Val-Asp-7-amino-4-methylcoumarin (Ac-DEVD-amc), acetyl-Ile-Glu-Thr-Asp-7-amino-4-methyl-coumarin (Ac-IETD-amc) and acetyl-Leu-Glu-His-Asp-amino-4-methylcoumarin (Ac-LEHD-amc) for caspase 3, 8, and 9, respectively (Enzo Life Sciences). Cells were lysed in caspase lysis buffer (50 mM Tris-HCl, pH 7.5, 150 mM NaCl, 1% Nonidet P-40, 0.25% Na-deoxycholate, 1 mM EGTA) and incubated at 4 °C for 1 h. The supernatant was centrifuged at 17,000×g for 10 min, followed by incubating 50 μg of protein with 0.1 mM fluorogenic caspase substrate in caspase activity buffer (25 mM Hepes-NaOH, pH 7.5, 10% (wt/vol) sucrose, 1 mM EDTA, 0.1% CHAPS, and 10 mM DTT) for 1 h. The resulting fluorogenic intensity (caspase activity) was measured at 460 nm. Calpain activity was measured by fluorogenic detection of cleavage of the calpain substrate acetyl-Leu-Leu-Tyr-7-amino-4-tri fluoromethylcoumarin (Ac-LLY-AFC) at 505 nm using the Calpain Activity Assay Kit per manufacturer's instructions (BioVision).

Caspase 3-Specific Small Molecule Activation.

To examine the hypertrophy inducing capabilities of caspase 3 activation, cardiomyocytes were incubated with the small molecule procaspase 3 activating compound 1 [procaspase 3 activating compound 1 (PAC-1); BioVision; 25 μM; dissolved in DMSO; 24h] in SF media or DMSO as a control.

Prohypertrophic Reporter Luciferase Assay.

Primary cardiomyocytes were seeded onto 48-well plates (0.7×10^5 cells per well), and, the following day, cells were transfected by using Lipofectamine 2000 (Invitrogen), SF

Opti-MEM α (Gibco), 4 ng of internal Renilla luciferase internal control, and 200 ng of Fire fly luciferase reporter DNA containing the gene of interest (reporters: ANP, BNP, NF-κB, MEF2) for 5 h at 37 °C with 5% CO_2. The media was replaced with SF media, and cells were incubated overnight at 37 °C with 5% CO_2. The next day, cardiomyocytes were incubated with SF media and DMSO, PE (100 μM; 1 h, 3 h, and 24 h), and DMSO or PAC-1 (25 μM; 1 h, 3 h and 24 h). Luciferase activity (prohypertrophic reporter activation) was measured by using the Dual Luciferase Assay System per manufacturer's instructions (Promega). Luciferase values were normalized to Renilla luciferase internal control, empty pXP2 vector, and SF media and DMSO treatments. Prohypertrophic reporter luciferase assays were also conducted, as described earlier, after SF media incubation, PE (100 μM) plus DMSO, and PE plus and caspase 3 or caspase 9 peptide inhibitors (24 h). Additionally, assays were completed after SF media incubation and GFP-AdV infection, PE treatment and GFP-AdV infection, and PE treatment and p35-AdV infection.

***In Vivo* Cardiomyocyte Hypertrophy.**

Hypertrophy was induced in Sprague-Dawley rats (~450 g) by infusion of PE at 10 mg/kg/d (dissolved in 0.9% saline solution) with osmotic minipumps (0.25 μL/h; model 2004, Alzet; Durect). Rat treatments were as follows: control (saline pumps plus no AdV), PE control (PE pumps plus GFP-AdV), and experimental (PE pumps plus p35-AdV). Briefly, echocardiography (VisualSonics)-guided intra-myocardial injections of p35-AdV or GFP-AdV diluted in 0.9% saline solution, at 3.75×10^5 pfu/μL, was completed on day 0 by using a staged microinjector under parasternal long axis view. On day 3, minipumps were implanted s.c. followed by saline solution or PE delivery for 21

d. At 3 wk after initial PE delivery, a tail-vein injection of 2 M KCl was used to arrest hearts in diastole and preserve ultrastructure. A parallel experiment was conducted to induce hypertrophy by using minipump infusion of ISO at 1 mg/kg/d (0.50 μL/h) over 2 wk (model 2002, Alzet; Durect). Hearts were isolated and stored in 4% (wt/vol) PFA. Hearts were dehydrated with 25% (wt/vol) sucrose overnight at 4 °C and were embedded in optimal cutting temperature cryoembedding media for frozen sectioning. Hearts were cryosectioned (10-μm transverse sections) and tissue sections were washed in PBS solution and fixed in 0.2% glutaraldehyde for 10 min at room temperature. Fluorescent staining was completed on the heart tissues in a rehydration chamber by using mouse anti–α-actinin, goat anti-mouse IgG Cy3 conjugate, and DAPI as described earlier. Cell size analysis was completed on GFP-positive cardiomyocytes as indicated earlier.

Immunoblotting.

Cell lysates were obtained after GFP-AdV or p35-AdV infection followed by 0 to 24 or 48 h of PE treatment. STS and SF treatments served as positive and negative controls for caspase activation, respectively. Briefly, cells were washed in PBS solution and harvested by centrifugation at 1,500×g for 7 min. Cells were lysed in lysis buffer supplemented with protease inhibitors (0.5 M Hepes-NaOH, pH 7.5, 5.0 M NaCl, 80% (vol/vol) glycerol, 1% (vol/vol) Tx 100, 0.2 M EGTA, 1 M $MgCl_2$, 20 mM NaF, 10 mM sodium pyrophosphate, 2.0 mM sodium orthovanadate, 200μM PMSF) and incubated at 4 °C for1 h followed by centrifugation at 20,800×g for 10 min. Insoluble fractions were resuspended in lysis buffer and sonicated. Protein (10 μg) was separated by SDS/PAGE and transferred to PVDF membranes. Membranes were blocked with 10 mM Tris, pH 7.4, 150 mM NaCl, 0.05% Tween-20, 5% (wt/vol) nonfat powdered milk, and incubated

with rabbit anti-caspase 3 (Cell Signaling) or mouse anti-histone deacetylase 3 (HDAC3; Abcam) overnight at 4 °C followed by incubation with HRP-conjugated goat anti-rabbit or anti-mouse secondary antibody (BioRad). Mouse anti–β-tubulin (clone E7; Developmental Studies Hybridoma Bank) was used as a loading control and the secondary antibody used was HRP-conjugated goat anti-mouse (BioRad). The ECL detection kit (GE Healthcare) was used to detect protein expression.

Statistical Analysis.

All data are expressed as mean ± SEM. The Student t test was used for comparisons between treatments, with $P<0.05$ considered significant.

Chapter 3:

Caspase cleavage of gelsolin is an inductive cue for pathologic cardiac hypertrophy

Contribution of Collaborators

Dr. Mohammad Abdul-Ghani assisted in experimental design and data analysis (Ottawa Hospital Research Institute (OHRI)). Steve Brunette provided technical support and assisted with the construction of the gelsolin adenoviruses and completion of the *in vivo* work, including collecting the hearts (OHRI). Dr. Patrick G. Burgon assisted with the *in vivo* study experimental design and echocardiography data analysis (University of Ottawa Heart Institute (UOHI)). Rick Seymour performed the ultrasound-guided intracardiac injections and echocardiography measurements (UOHI). Dr. Lawrence Puente carried out the mass spectrometry (LC-MS/MS) analysis (Proteomics Core Facility, OHRI). Dr. Lynn A. Megeney contributed in experimental design and data analysis. All other works described were conducted by the author of the thesis.

Abstract

Cardiac hypertrophy is an adaptive remodeling event that may improve (physiologic) or diminish (pathologic) contractile performance of the heart. Physiologic and pathologic hypertrophy yield distinct outcomes, yet each growth process is dependent on caspase 3 mediated signaling. Here, we investigated the molecular basis by which caspase 3 directs the divergent forms of hypertrophy. Pathologic agonists induce biphasic caspase 3 activation, where late stage protease activity cleaves the actin capping/depolymerizing protein gelsolin. We demonstrate that expression of the N-terminal cleavage fragment of gelsolin is necessary and sufficient to cause pathologic remodeling in both isolated cardiomyocytes and the intact heart, while expression of a caspase non-cleavable form of gelsolin prevents cardiac remodeling. Further we observed that agonist stimulation of cardiomyocytes led to gelsolin secretion, which induced hypertrophy in naïve cells. These results suggest that cell autonomous cleavage of gelsolin is essential for pathologic hypertrophy and that cardiomyocyte secretion of gelsolin may systemically propagate and accelerate this negative remodeling response of the heart.

Introduction

Cardiac hypertrophy can occur in response to biomechanical and neurohormonal stimuli, which promotes growth of the intact heart (Kong et al. 2005; Hill & Olson 2008). Hypertrophy can be physiologic, such as the cardiac enlargement experienced during pregnancy or exercise (Dorn 2007; Chung & Leinwand 2014; Roh et al. 2016). Physiologic hypertrophy matches myocardial growth to increased vascularity and normalizes increased tension and pressure in the cardiac chambers to minimize stress and meet systemic demands of the body. Pathological cardiac hypertrophy is a consequence of disease-inducing stimuli, such as hypertension, and while initially adaptive, continued ventricular growth will lead to a decline in function resulting in heart failure (Hill & Olson 2008; Heineke & Molkentin 2006). The transition from adaptive to maladaptive hypertrophy is accompanied by several distinct changes including increased fibrosis, gross enlargement of cardiomyocytes, and prominent alterations in cytoskeletal/sarcomere assembly (Frey & Olson 2003; van Berlo et al. 2013).

Despite the overt difference in physiologic and pathologic cardiac hypertrophy, the cardiomyocyte growth for each condition requires activation of the same signaling cascade. Specifically, both forms of hypertrophy depend on stimulation of the intrinsic mediated cell death pathway, culminating in activation of caspase 3 (Abdul-Ghani et al. 2017; Putinski et al. 2013). Both physiologic and pathologic hypertrophy agonists, such as cardiotrophin 1 (CT1) and phenylephrine (PE) respectively, rapidly engage caspase 3. Once active, caspase 3 targets and cleaves HDAC3 to relieve repression on myocyte enhancer factor 2 (MEF2), a key factor that controls hypertrophy dependent transcription events in cardiomyocytes (Putinski et al. 2013). During physiologic hypertrophy, this

pathway is rapidly curtailed through concurrent stimulation of casein kinase 2 (CK2) (Abdul-Ghani et al. 2017). CK2 phosphorylates the cleavage site on caspase 3 and its substrates to render the pathway ineffective.

These observations suggest the critical step in transition to pathologic hypertrophy and heart failure is sustained caspase 3 activity. Here, we sought to define the mechanism by which caspase 3 promotes adverse cardiomyocyte/cardiac hypertrophy and whether this is dependent on a unique enzyme substrate cleavage event. Caspase sensitive transcriptional responses are similar in physiologic and pathologic hypertrophy (Abdul-Ghani et al. 2017), therefore we focused our investigation on potential caspase substrates that may modify cytoskeletal/sarcomeric components. Inspection of literature and substrate databases suggested that the actin binding/severing protein gelsolin (GSN) may be a pathologic conveyer of caspase 3 activity during late stages of hypertrophy. In apoptotic cells, the N-terminal fragment of caspase cleaved GSN can dramatically alter actin structure (Geng et al. 1998; Kothakota et al. 1997). In addition, GSN null mice have a blunted remodeling response in the post-infarct heart, although this was attributed to a loss in the full-length protein (Li et al. 2009).

Results

Gelsolin is cleaved by effector caspases during pathological cardiac hypertrophy.

First, we examined GSN integrity in primary cardiomyocytes treated with the hypertrophy agonist PE. GSN cleavage was observed at later stages (6-24hr) and was coincident with hypertrophy related cytoskeletal alterations that occur during this process (Figure 1A). GSN cleavage was blocked by caspase inhibition via infection of cardiomyocytes with the p35-AdV caspase inhibitor, demonstrating caspase dependence for this cleavage event. Importantly, the GSN cleavage fragments matched the size of caspase produced GSN fragments reported by previous groups (Geng et al. 1998; Martin et al. 2010; Kothakota et al. 1997). Note that baseline (PE 0 min) caspase activity is observed (Figure 1A) and has also previously been shown (Putinski et al. 2013). To confirm the enzyme substrate relationship we conducted *in vitro* cleavage assays using recombinant active caspase 3 and caspase 7, and recombinant GSN in the presence or absence of the peptide caspase inhibitor *N*-benzyloxycarbonyl-Asp-Glu-Val-Asp-fluomethylketone (z-DEVD-fmk). Both effector caspases cleaved GSN while caspase inhibition blocked the production of the GSN cleavage product (Figure 1B). Blots were probed with an antibody corresponding to the C-terminal portion of GSN and thus a single band was observed (~42 kDa C-terminal fragment), which also corresponded with the GSN fragments observed in hypertrophic cells. Next, we mapped the caspase cleavage site within GSN, by extracting N- and C-terminal GSN cleavage products from silver-stained gels followed by liquid chromatography-tandem mass spectrometry (LC-MS/MS) (Figure 1C). A non-tryptic cleavage event was observed at aspartic acid residue

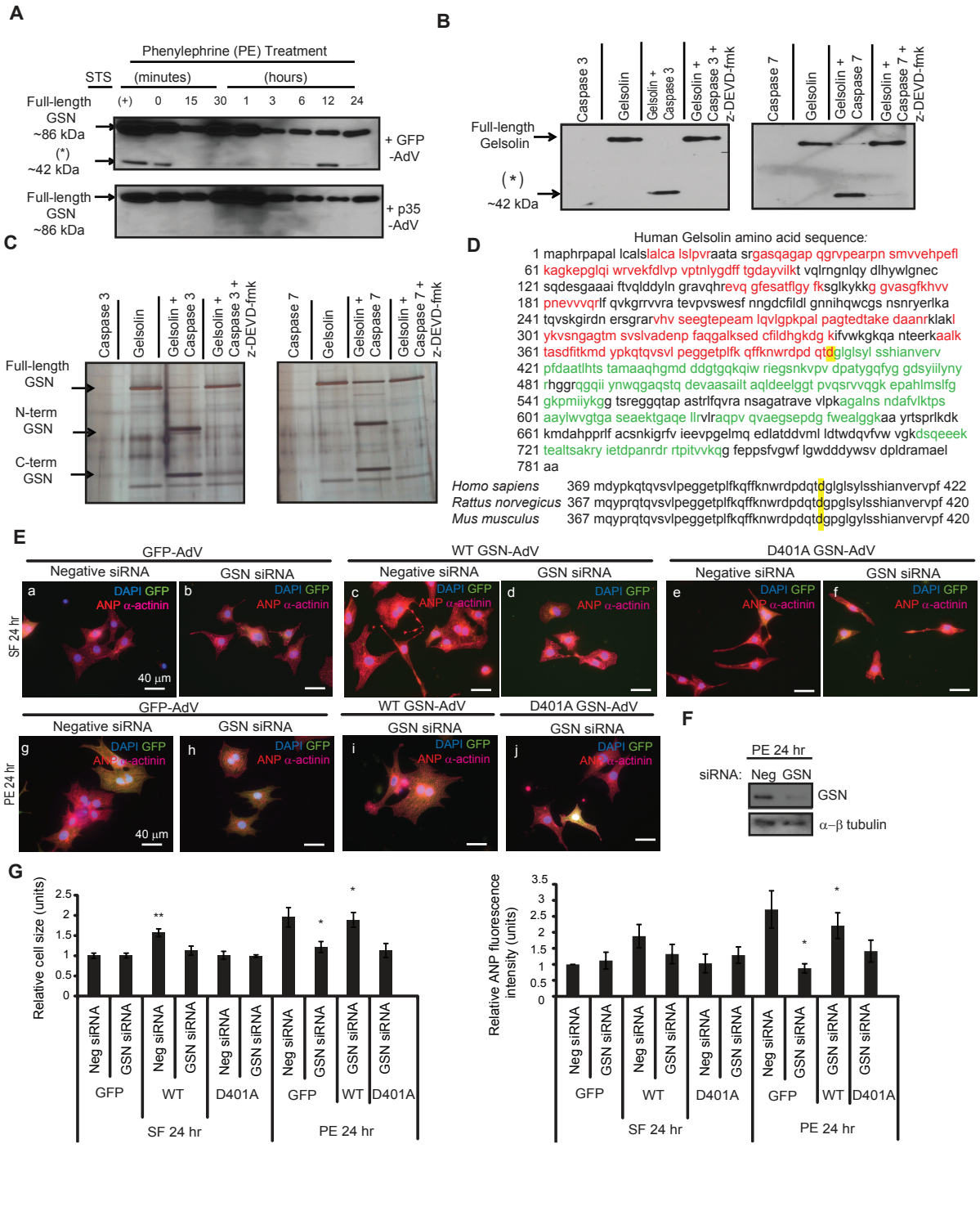

A
Phenylephrine (PE) Treatment
STS
(minutes)
(hours)
(+) 0 15 30 1 3 6 12 24
Full-length GSN ~86 kDa
(*) ~42 kDa
+ GFP -AdV
Full-length GSN ~86 kDa
+ p35 -AdV
B
Caspase 3
Gelsolin
Gelsolin + Caspase 3
Gelsolin + Caspase 3 + z-DEVD-fmk
Caspase 7
Gelsolin
Gelsolin + Caspase 7
Gelsolin + Caspase 7 + z-DEVD-fmk
Full-length Gelsolin
(*) ~42 kDa
C
Caspase 3
Gelsolin
Gelsolin + Caspase 3
Gelsolin + Caspase 3 + z-DEVD-fmk
Caspase 7
Gelsolin
Gelsolin + Caspase 7
Gelsolin + Caspase 7 + z-DEVD-fmk
Full-length GSN
N-term GSN
C-term GSN
D
Human Gelsolin amino acid sequence:
1 maphrpapal lcalslalca lslpvraata srgasqagap qgrvpearpn smvvehpefl
61 kagkepglqi wrvekfdlvp vptnlygdff tgdayvilkt vqlrngnlqy dlhywlgnec
121 sqdesgaaai ftvqlddyln gravqhrevq gfesatflgy fksglkykkg gvasgfkhvv
181 pnevvvqrlf qvkgrrvvra tevpvswesf nngdcfildl gnnihqwcgs nsnryerlka
241 tqvskgirdn ersgrarvhv seegtepeam lqvlgpkpal pagtedtake daanrklakl
301 ykvsngagtm svslvadenp faqgalksed cfildhgkdg kifvwkgkqa nteerkaalk
361 tasdfitkmd ypkqtqvsvl peggetplfk qffknwrdpd qtdglglsyl sshianverv
421 pfdaatlhts tamaaqhgmd ddgtgqkqiw riegsnkvpv dpatyggfyg gdsyiilyny
481 rhggrqgqii ynwqgaqstq devaasailt aqldeelggt pvqsrvvqgk epahlmslfg
541 gkpmiiykgg tsreggqtap astrlfqvra nsagatrave vlpkagalns ndafvlktps
601 aaylwvgtga seaektgaqe llrvlraqpv qvaegsepdg fwealggkaa yrtsprlkdk
661 kmdahpprlf acsnkigrfv ieevpgelmq edlatddvml ldtwdqvfvw vgkdsqeeek
721 tealtsakry ietdpanrdr rtpitvvkqg feppsfvgwf lgwdddywsv dpldramael
781 aa
Homo sapiens 369 mdypkqtqvsvlpeggetplfkqffknwrdpdqtdglglsylsshianvervpf 422
Rattus norvegicus 367 mqyprqtqvsvlpeggetplfkqffknwrdpdqtdgpglsylsshianvervpf 420
Mus musculus 367 mqyprqtqvsvlpeggetplfkqffknwrdpdqtdgpglgylsshianvervpf 420
E
GFP-AdV
WT GSN-AdV
D401A GSN-AdV
Negative siRNA
GSN siRNA
SF 24 hr
PE 24 hr
DAPI GFP
ANP α-actinin
40 μm
a
b
c
d
e
f
g
h
i
j
F
PE 24 hr
siRNA: Neg GSN
GSN
α–β tubulin
G
Relative cell size (units)
Relative ANP fluorescence intensity (units)
Neg siRNA
GSN siRNA
GFP
WT
D401A
SF 24 hr
PE 24 hr

Figure 1. Gelsolin is an essential caspase cleavage substrate during cardiomyocyte hypertrophy. (A) Cardiomyocytes infected with p35-AdV or GFP-AdV were treated with phenylephrine (PE) and subjected to immunoblot using a C-terminal gelsolin (GSN) antibody. GSN cleavage was observed with GFP-AdV while these fragments were not present with p35-AdV. Treatment with 2 μM staurosporine (STS) served as a positive (+) control. (B) GSN *in vitro* cleavage assays for caspase alone, GSN alone, GSN with caspase 3 or 7 or GSN with caspase and caspase inhibitor z-DEVD-fmk were probed with a C-terminal GSN antibody. A smaller molecular weight GSN fragment (asterisk) is observed when GSN is incubated with caspase 3/7 and is reduced with z-DEVD-fmk. (C) Recombinant GSN was subjected to an *in vitro* cleavage reaction followed by SDS/PAGE and silver stain. Protein fragments were isolated and processed by LC-MS/MS. (D) Red peptides represent those from the N-terminal fragment (44 kDa plus 26 kDa N-terminal GSN GST tag). Green peptides represent those from the C-terminal fragment (~42 kDa). The aspartic acid targeted by caspase 3/7 is highlighted in yellow. Consensus of the targeted aspartic acid residues (highlighted in yellow) in *Homo sapiens* (D403; NP_000168.1), *Rattus norvegicus* (D401; NP_001004080.1) and *Mus musculus* (D401; NP_666232.2). Amino acid sequences were obtained from the National Center for Biotechnology Information (NCBI). (E) Cardiomyocytes transfected with scrambled negative control siRNA or GSN siRNA followed by infection with GFP-AdV, wild-type (WT) GSN-AdV or D401A GSN-AdV (MOI=1) during serum-free (SF) or PE treatment. (F) GSN knockdown confirmed by western blotting where GSN siRNA led to reduced GSN levels compared to the negative scrambled siRNA. Alpha-β tubulin was the loading control. (G) During SF treatment, WT GSN-AdV infection after negative siRNA transfection led to increased cell size ($n=4$, $P<0.01$, **) while mutant D401A GSN-AdV infection did not. During PE treatment, GSN siRNA-mediated knockdown led to a significant reduction in hypertrophy ($n=4$, $P<0.05$, *). WT GSN-AdV infection after GSN siRNA treatment rescued the hypertrophy response ($n=4$, $P<0.05$, *). This hypertrophy rescue did not occur with the non-cleavable D401A GSN-AdV. Error bars represent standard error of the mean (SEM). (Scale bars: 40 μm).

401 (D401) within the rat GSN amino acid sequence (Figure 1D). This cleavage event is reflective of what has been observed in other studies (Martin et al. 2010; Kothakota et al. 1997; Geng et al. 1998). Note that these studies based their numbering on the cytoplasmic GSN sequence which lacks 49 N-terminal amino acids (AA) compared to the full GSN precursor or plasma GSN sequence (Figure S1) (Kwiatkowski et al. 1986; Nag et al. 2013).

Gelsolin is essential for cardiomyocyte hypertrophy.

We next examined whether GSN itself and GSN caspase-mediated cleavage was essential for cardiomyocyte hypertrophy. To test this supposition, we used GSN siRNA to knockdown GSN expression in primary cardiomyocytes during SF or PE treatment followed by reintroduction of the caspase-cleavable WT GSN or the non-cleavable D401A GSN-AdV (Figure 1E and 1F). As previously shown (Hu et al. 2014), we also observed that GSN siRNA knockdown during PE treatment leads to reduced hypertrophy. Cell size and hypertrophy marker atrial natriuretic peptide (ANP) levels were also reduced by GSN knockdown indicating a role for GSN protein in hypertrophy induction (Figure 1E and 1G). Cardiomyocytes transfected with GSN siRNA and infected with the WT GSN-AdV, during PE treatment, were enlarged compared to those infected with the control GFP-AdV demonstrating that the reintroduction of a caspase-cleavable GSN can rescue hypertrophy. Alternatively, GSN siRNA mediated knockdown followed by infection with the caspase cleavage site mutated GSN-AdV did not lead to a significant increase in cell size or ANP levels, suggesting that caspase cleavage of GSN may be a critical step in the development of the hypertrophy phenotype (Figure 1E and 1G).

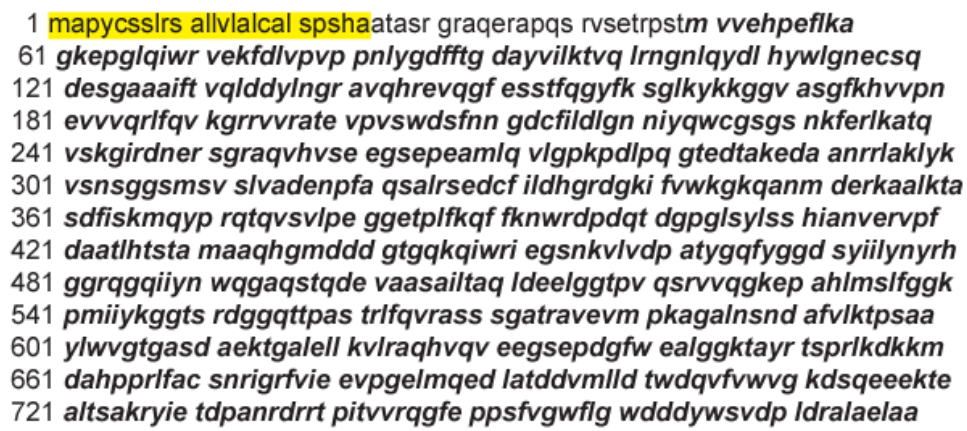


Figure S1. Cytoplasmic and plasma gelsolin start sites within the precursor *Rattus norvegicus* Gelsolin amino acid sequence. Precursor gelsolin (GSN) amino acid sequence (NP_001004080.1) was obtained from the National Center for Biotechnology Information (www.ncbi.nlm.nih.gov). The plasma GSN signal peptide is shown in yellow and corresponds to the first 25 amino acids. The start site of cytoplasmic GSN is shown in bold italics font at amino acid 50.

Full-length or caspase cleaved N-terminal gelsolin induces cardiomyocyte hypertrophy.

To investigate the biological role of caspase-mediated GSN cleavage in pathological cardiac hypertrophy, we compared a panel of GSN-AdV constructs, which included the WT and D401A (as noted above) along with N- and C-terminal caspase cleavage fragments. When comparing these AdV constructs, significant changes in cell size (SF 24hr, SF 48hr, PE 3hr) and ANP levels (SF 48hr) were observed. Each GSN AdV was further compared to the control GFP-AdV and interestingly, cardiomyocytes infected with the WT or N-terminal GSN-AdV in SF conditions were significantly enlarged compared to those infected with the GFP-AdV at 24 and 48 hours (Figure 2A and 2B). These same GSN-AdVs also elicited an increased expression of ANP. Limited PE treatment (3hr) further enhanced the hypertrophy response. Conversely, cardiomyocytes infected with the C-terminal GSN fragment or D401A GSN-AdV did not display any increase in size or ANP expression at any of the timepoints tested. We measured whether these same GSN constructs impacted transcriptional activity of known hypertrophy responsive genes. Here, primary cardiomyocytes were transfected with reporter plasmids for ANP, B-type natriuretic peptide (BNP), MEF2, nuclear factor kappa B (NF-κB) or serum response factor (SRF) (with a *Renilla* luciferase internal control) and monitored for the response to GSN expression during SF treatment. With each prohypertrophy marker, significant changes were observed among the AdV groups (Figure 2C). When compared to the control GFP-AdV, only WT and N-terminal GSN-AdV infection resulted in a significant increase in reporter activity during SF treatment, which were comparable to those observed during PE stimulation (Figure 2C). As GSN is

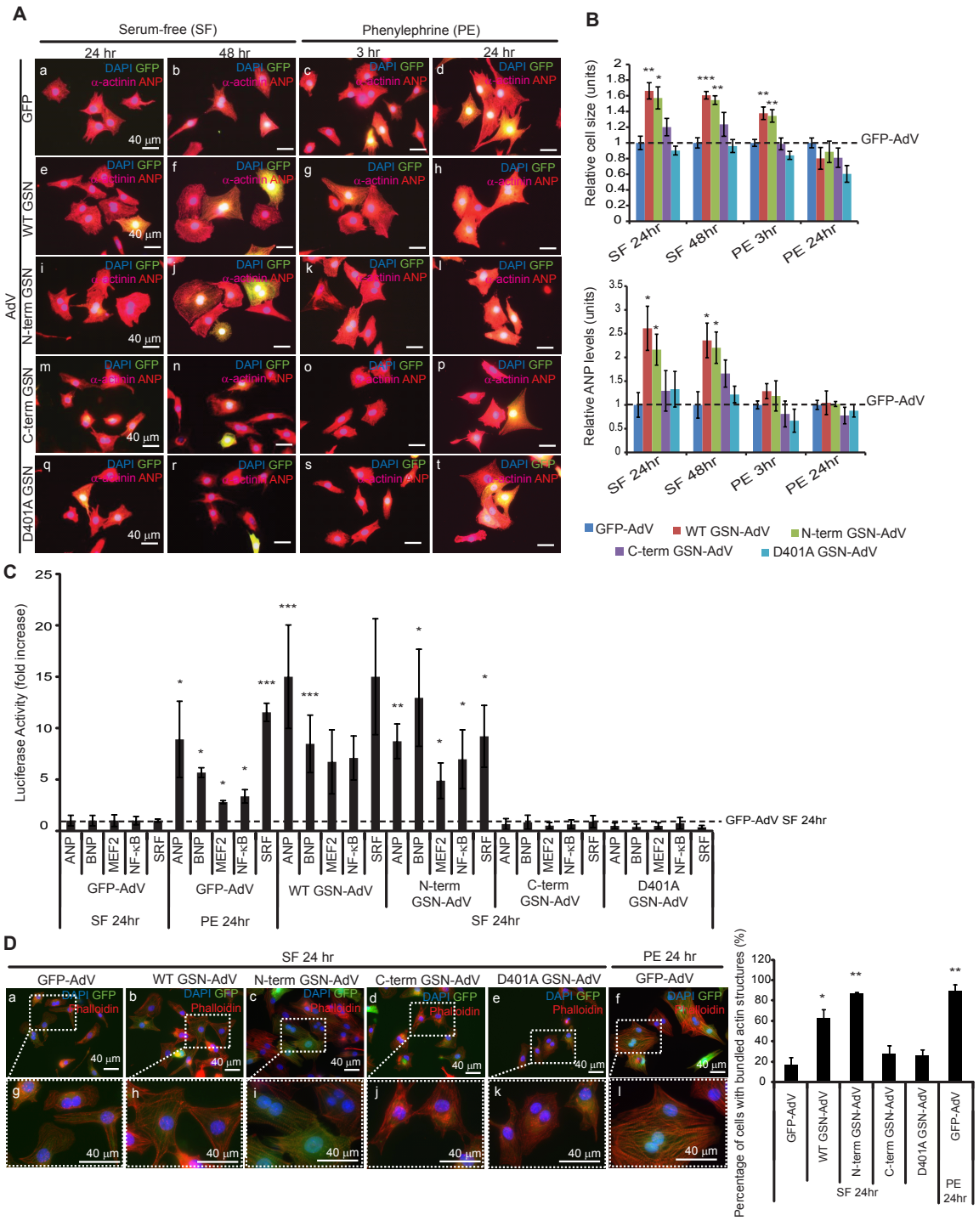

A
Serum-free (SF)
Phenylephrine (PE)
24 hr
48 hr
3 hr
24 hr
AdV
GFP
WT GSN
N-term GSN
C-term GSN
D401A GSN
DAPI GFP
α-actinin ANP
40 μm
B
Relative cell size (units)
Relative ANP levels (units)
GFP-AdV
SF 24hr
SF 48hr
PE 3hr
PE 24hr
GFP-AdV
WT GSN-AdV
N-term GSN-AdV
C-term GSN-AdV
D401A GSN-AdV
C
Luciferase Activity (fold increase)
GFP-AdV SF 24hr
ANP
BNP
MEF2
NF-κB
SRF
GFP-AdV
SF 24hr
GFP-AdV
PE 24hr
WT GSN-AdV
N-term GSN-AdV
C-term GSN-AdV
D401A GSN-AdV
SF 24hr
D
SF 24 hr
PE 24 hr
GFP-AdV
WT GSN-AdV
N-term GSN-AdV
C-term GSN-AdV
D401A GSN-AdV
GFP-AdV
DAPI GFP
Phalloidin
40 μm
Percentage of cells with bundled actin structures (%)
SF 24hr
PE 24hr

Figure 2. Expression of wild-type or N-terminal gelsolin can induce hypertrophy in primary cardiomyocytes. Primary cardiomyocytes were infected with either GFP control AdV, wild-type (WT) GSN-AdV, N-terminal GSN-AdV, C-terminal GSN-AdV or D401A GSN-AdV (MOI=1) during serum-free (SF) or phenylephrine (PE) treatment. Immunofluorescence analysis (A) was completed and cell size and ANP levels were evaluated (B). All values were normalized to the GFP-AdV infected cardiomyocytes within each treatment. A significant increase in cell size was observed after WT (n=3, **, $P<0.01$) or N-terminal GSN infection (n=3, *, $P<0.05$) during 24 hours of SF treatment, whereas the C-terminal GSN or D401A GSN-AdV did not significantly affect cell size. Similar results were observed after SF 48 hours (WT, n=3, ***, $P<0.001$; N-term, n=3, **, $P<0.01$) and PE 3 hours (WT, n=3, **, $P<0.01$; N-term, n=3, **, $P<0.01$). ANP levels were also significantly increased after WT and N-terminal GSN-AdV infection after 24 and 48 hours of SF treatment (n=3, *, $P<0.05$). (C) Cardiomyocytes were transfected with luciferase reporter plasmids for prohypertrophic markers (ANP, BNP, MEF2, NF-κB and SRF). Reporter activity was measured after cardiomyocytes were infected with either GFP control AdV, wild-type (WT) GSN-AdV, N-terminal GSN-AdV, C-terminal GSN-AdV or D401A GSN-AdV (MOI=1) during SF or PE treatment. WT (ANP, n=3, ***, $P<0.001$; BNP, n=3, ***, $P<0.001$) and N-terminal (ANP, n=3, **, $P<0.01$; BNP, n=3, *, $P<0.05$; MEF2, n=3, *, $P<0.05$; NF-κB, n=3, *, $P<0.05$; SRF, n=3, *, $P<0.05$) GSN-AdV infection, during SF treatment, led to a significant increase in hypertrophy reporter activation compared to the GFP-AdV control, similar to what is observed during PE-induced hypertrophy (PE 24 h). (D) Actin remodeling was evaluated in cardiomyocytes infected with GSN-AdV constructs during SF treatment by phalloidin staining followed by determination of the percentage of cells with bundled actin (%). Magnified views are shown in boxed regions. Significant increases in bundled actin were observed in cardiomyocytes treated with N-terminal GSN (n=3, **, $P<0.01$) and WT GSN-AdV (n=3, $P<0.05$, *). N-terminal GSN treatment led to a similar increase in actin remodeling to that observed during PE treatment (n=3, $P<0.01$, **). Error bars represent SEM. (Scale bars: 40 μm).

a potent actin-remodeling agent, we also measured the capacity of the various GSN-AdV constructs to modify cytoskeletal/sarcomeric structure. We noted that both WT and N-terminal GSN-AdV infected cardiomyocytes displayed a significant increase in bundled actin structures compared to all other AdV infected cells, a structural reorganization that was similar to that induced by the hypertrophy agonist PE (Figure 2D). Finally, we tested the ability of the various GSN-AdV constructs to remodel cardiomyocytes in the absence of caspase signaling. We noted that both the WT and N-terminal GSN-AdVs could induce hypertrophy when cardiomyocytes were exposed to the effector peptide caspase inhibitor z-DEVD-fmk (Figure S2), although the caspase cleaved N-terminal GSN provided a more significant rescue. This suggests both caspase dependent and independent GSN functions.

Full-length or caspase cleaved N-terminal gelsolin induces cardiomyocyte hypertrophy *in vivo.*

Next, we examined whether GSN and its cleavage products altered heart structure *in vivo*. We performed ultrasound guided intra-myocardial injections of the same GSN-AdV constructs as above, followed by echocardiography (ECHO) analysis over 28 days (Figure 3A). N-terminal GSN-AdV injections led to significant reductions in left ventricular internal diameter during diastole compared to the GFP-AdV (Figure 3B) (Day 28). Although no significant increase in left ventricular posterior wall thickness was observed (Figure S3), the interventricular septum thickness was significantly increased during systole (Day 14 and 21) and diastole (Day 21) in rats injected with the N-terminal GSN-AdV compared to the GFP-AdV (Figure 3B). As expected, full-length GSN (WT GSN-AdV) induced pathologic hypertrophy

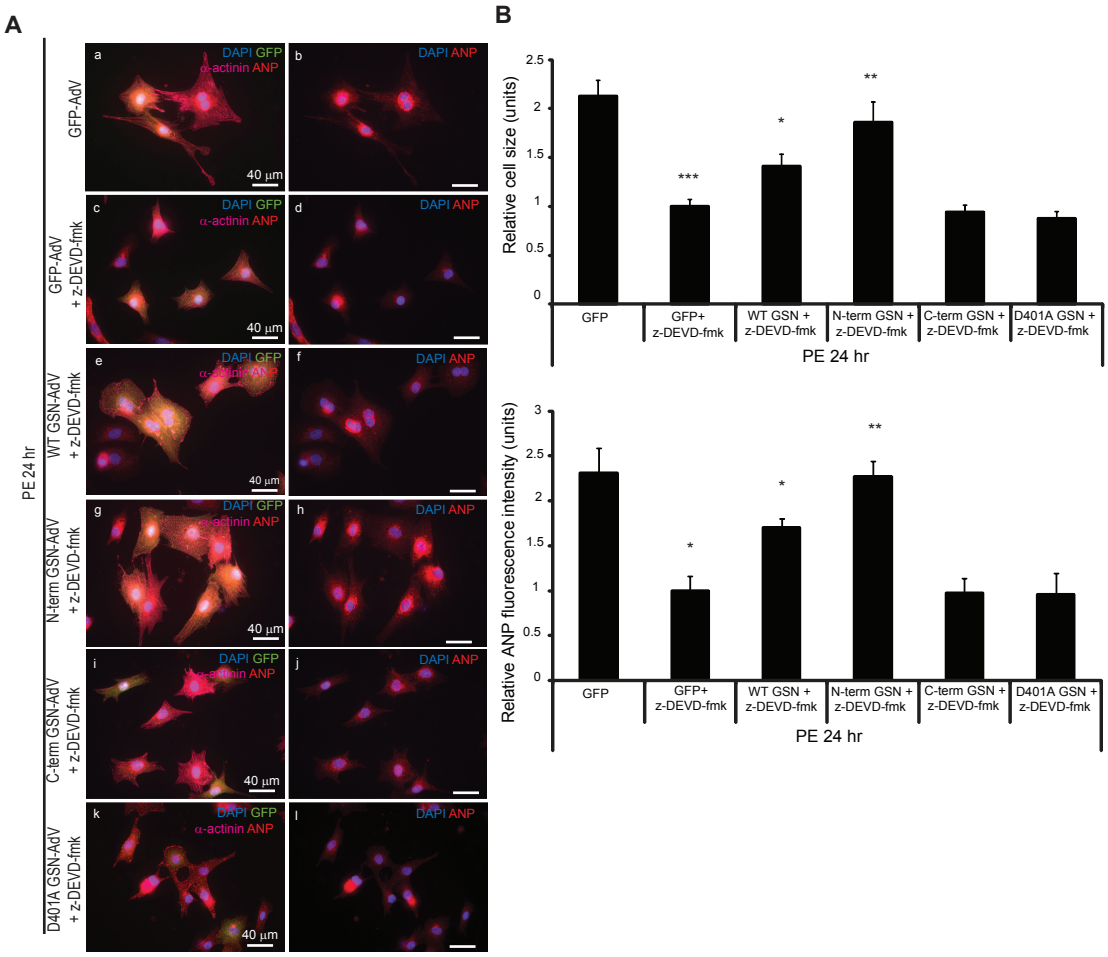


Figure S2. Expression of wild-type or N-terminal gelsolin can rescue the hypertrophy response reduced by caspase inhibition. Primary cardiomyocytes were treated with 20 μM of the caspase 3 inhibitor z-DEVD-fmk, infected with either GFP control AdV, wild-type (WT) GSN-AdV, N-terminal GSN-AdV, C-terminal GSN-AdV or D401A GSN-AdV (MOI=1) and treated with phenylephrine (PE) for 24 hours. Immunofluorescence analysis (A) was completed and cell size and ANP levels were evaluated (B). All values were normalized to the caspase inhibited and GFP-AdV infected cardiomyocytes, which were reduced in size and ANP levels compared to those lacking caspase inhibitor treatment (n=3, ***, $P<0.001$ and n=3, **, $P<0.01$, respectively). During caspase inhibition, a hypertrophy rescue was observed after WT (n=3, *, $P<0.05$) or N-terminal GSN infection (n=3, **, $P<0.01$) and identified by a significant increase in cell size and ANP levels compared to GFP-AdV infected cardiomyocytes (WT, n=3, **, $P<0.01$; N-term, n=3, **, $P<0.01$). The C-terminal GSN or D401A GSN-AdV infected cardiomyocytes did not significantly rescue cell size or ANP levels. Error bars represent SEM. (Scale bars: 40 μm).

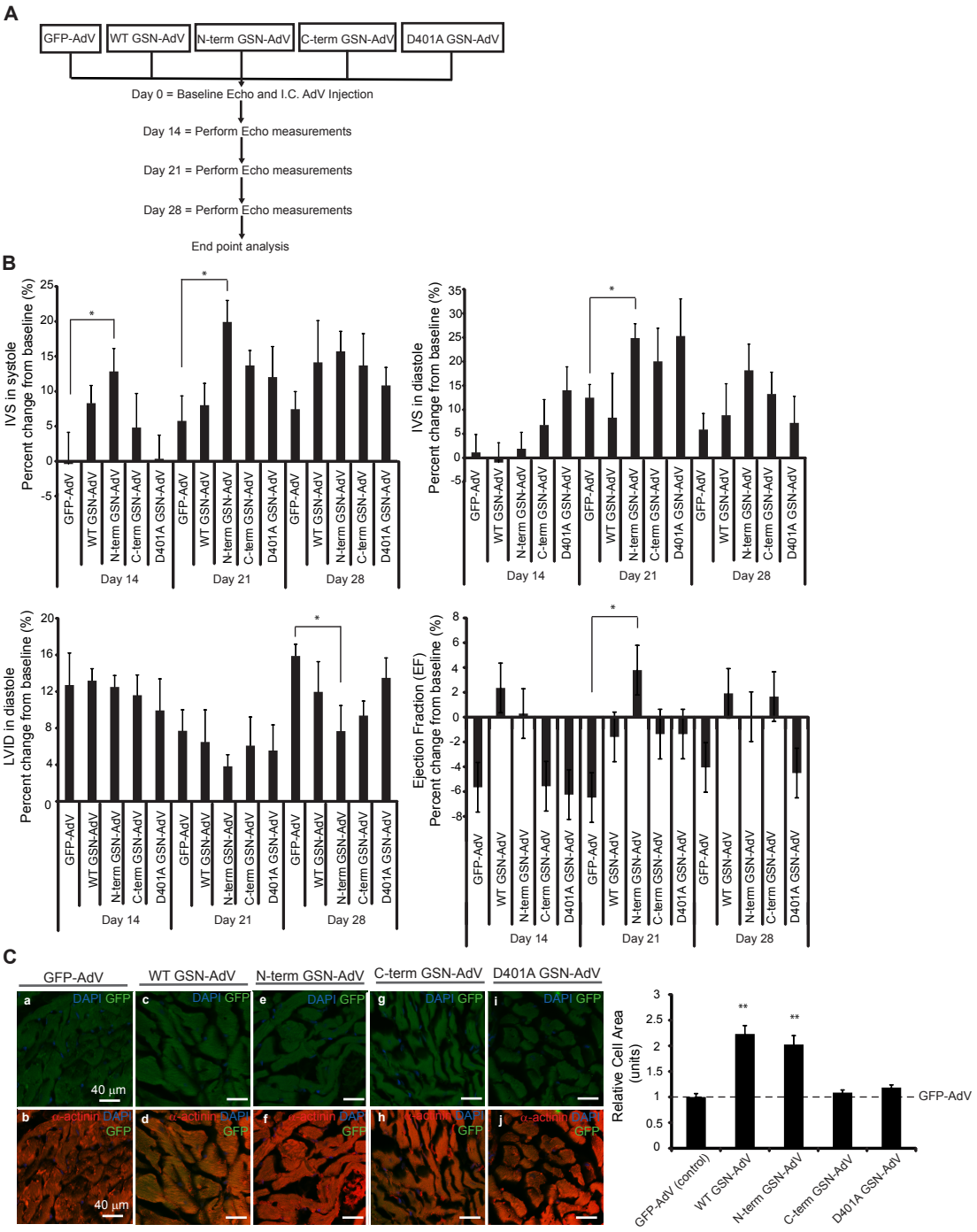

A
GFP-AdV
WT GSN-AdV
N-term GSN-AdV
C-term GSN-AdV
D401A GSN-AdV
Day 0 = Baseline Echo and I.C. AdV Injection
Day 14 = Perform Echo measurements
Day 21 = Perform Echo measurements
Day 28 = Perform Echo measurements
End point analysis
B
IVS in systole
Percent change from baseline (%)
IVS in diastole
Percent change from baseline (%)
LVID in diastole
Percent change from baseline (%)
Ejection Fraction (EF)
Percent change from baseline (%)
Day 14
Day 21
Day 28
C
GFP-AdV
WT GSN-AdV
N-term GSN-AdV
C-term GSN-AdV
D401A GSN-AdV
DAPI GFP
α-actinin DAPI GFP
40 μm
Relative Cell Area (units)
GFP-AdV (control)

Figure 3. Wild-type or N-terminal gelsolin overexpression can induce a hypertrophy response in the intact myocardium. (A) Outline of *in vivo* study. Sprague Dawley rats were echo-guided intra-myocardial injected with either the control GFP-AdV or one of the gelsolin (GSN) AdVs. Echocardiography (ECHO) was performed at day 0, 14, 21, and 28. Rats were sacrificed at day 35 and hearts and tibia were isolated. Three hearts per AdV group were OCT embedded and cryosectioned. (B) ECHO data was taken at day 0, 14, 21, and 28 and represent the percent change from the baseline measurement (%). Significant differences in these measurements were observed when comparing the GSN injected rats to those injected with the control GFP-AdV. Significantly reduced left ventricular internal diameter (LVID) was observed in rats injected with N-terminal GSN AdV compared to the GFP-AdV (Day 28) ($n=7$, $P<0.05$, *). Although no significant increase in left ventricular posterior wall thickness (LVPW, Figure S3) was observed, interventricular spetum (IVS) measurements showed thickening in N-terminal GSN rats compared to GFP during contraction (Day 14 and 21) ($n=7$, $P<0.05$, *). During relaxation, IVS thickening was also observed in N-terminal injected rats compared to GFP (Day 21) ($n=7$, $P<0.05$, *). Increased ejection fraction (EF) was observed in rats infected with the N-terminal GSN AdV at day 21 compared to the GFP-AdV ($n=7$, $P<0.05$, *). Cardiac output (CO) and fractional shortening (FS) data are shown in Figure S3. Note that no significant changes were observed when comparing the rats injected with C-terminal or D401A GSN-AdV to those injected with the GFP-AdV. (C) Heart sections were stained for α-actinin (red), GFP (green) and DAPI (blue). Cell size of GFP tagged GSN AdV-infected cardiomyocytes (green) was quantified. Hearts infected with WT or N-terminal GSN-AdVs were significantly enlarged compared to those infected with a GFP control AdV ($n=3$, *, $P<0.01$ and **, $P<0.01$, respectively). Hearts infected with C-terminal GSN or caspase cleavage mutant GSN (D401A GSN-AdV) did not induce the same hypertrophy response. Error bars represent SEM. (Scale bars: 40 μm).

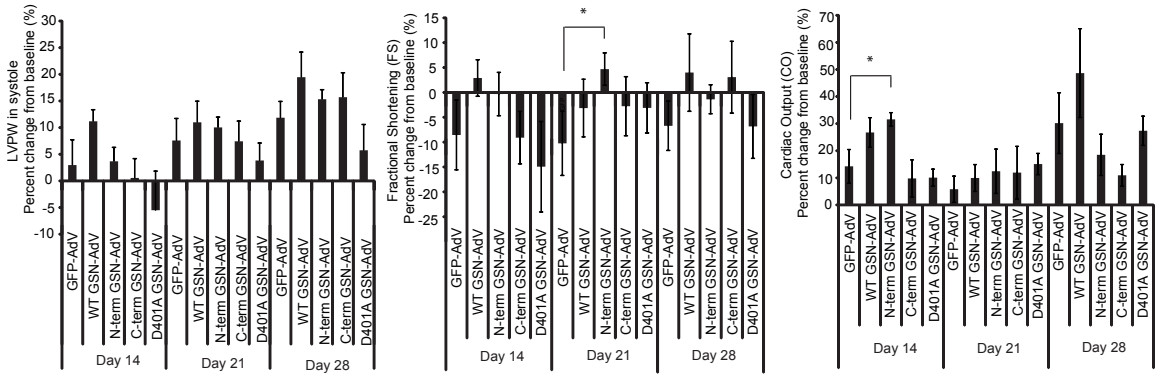


Figure S3. Left ventricular posterior wall thickness, fractional shortening and cardiac output measured throughout gelsolin adenovirus *in vivo* study. Echocardiography data obtained from control GFP or gelsolin (GSN) adenovirus (AdV) infected rats taken on day 0, 14, 21, and 28, represented as percent change from baseline (%). No significant changes in left ventricular posterior wall (LVPW) thickness during systole were observed (left). On day 21, a significant increase in fractional shortening (FS) was observed in rats infected with the N-terminal GSN AdV compared to the GFP control (n=7, $P<0.05$, *) (middle). A significant increase in cardiac output (CO) was also observed at day 14 in rats injected with N-terminal GSN compared to GFP (n=7, $P<0.05$, *) (right). Error bars represent SEM.

akin to N-terminal GSN-AdV, yet no significant changes in cardiac structure were noted in hearts injected with the C-terminal GSN-AdV or the D401A GSN-AdV. Cardiac function was also evaluated and N-terminal GSN-AdV injected animals displayed elevated ejection fraction (EF) (Day 21) (Figure 3B) and cardiac output (CO) (Day 14) (Figure S3) compared to GFP-AdV treatment. Fractional shortening (FS) was also increased in rats infected with N-terminal GSN compared to the control GFP-AdV (Day 21) (Figure S3). Moreover, long term N-terminal GSN expression (i.e. at day 28) led to a decline in EF, CO, FS measurements with no significant difference compared to GFP-AdV, consistent with a transition to decompensation and failure (Figure 3B and Figure S3). Cell structure was also evaluated and full-length and N-terminal GSN-AdV infections resulted in increased cardiomyocyte size compared to those infected with the GFP control AdV (Figure 3C). Conversely, hearts infected with the C-terminal or caspase cleavage mutant GSN-AdVs did not induce a similar cell hypertrophy response.

Secreted gelsolin is a hypertrophy inductive cue.

Compensatory hypertrophy can rapidly transition to decompensation/heart failure and may occur in segmental fashion (Hill & Olson 2008). This wave of decompensation is consistent with release of a factor(s) that may alter the structure and function of cardiomyocytes. Interestingly, GSN has been demonstrated to exist in multiple pools within other cells, one of which can be released into extracellular space (Ji et al. 2008; Welton et al. 2010). Here, we tested whether full-length and/or caspase activated GSN is secreted from cardiomyocytes to propagate the hypertrophy response in adjacent naïve cardiomyocytes. Primary cardiomyocytes were treated with

SF, PE or the procaspase-activating compound, referred to as PAC-1, for 24 hours to induce hypertrophy (Figure 4). Media was then aspirated, cells washed, and fresh SF media added and collected after 24 hours from each condition. Initial analysis showed significant changes in both cell size and ANP levels among the treatment groups (Figure 4B). Cardiomyocytes treated with conditioned PE or PAC-1 media were enlarged compared to SF treated cardiomyocytes demonstrating that secreted components within the media may induce hypertrophy. However, cardiomyocytes treated with conditioned PE or PAC-1 media in the presence of a GSN antibody did not display any increase in cell size or ANP levels compared to hypertrophy conditioned media treatment alone. Treatment with a blocking GSN peptide abrogated this GSN antibody-induced hypertrophy inhibition, confirming the specificity of GSN effect in propagating the pathologic hypertrophy response.

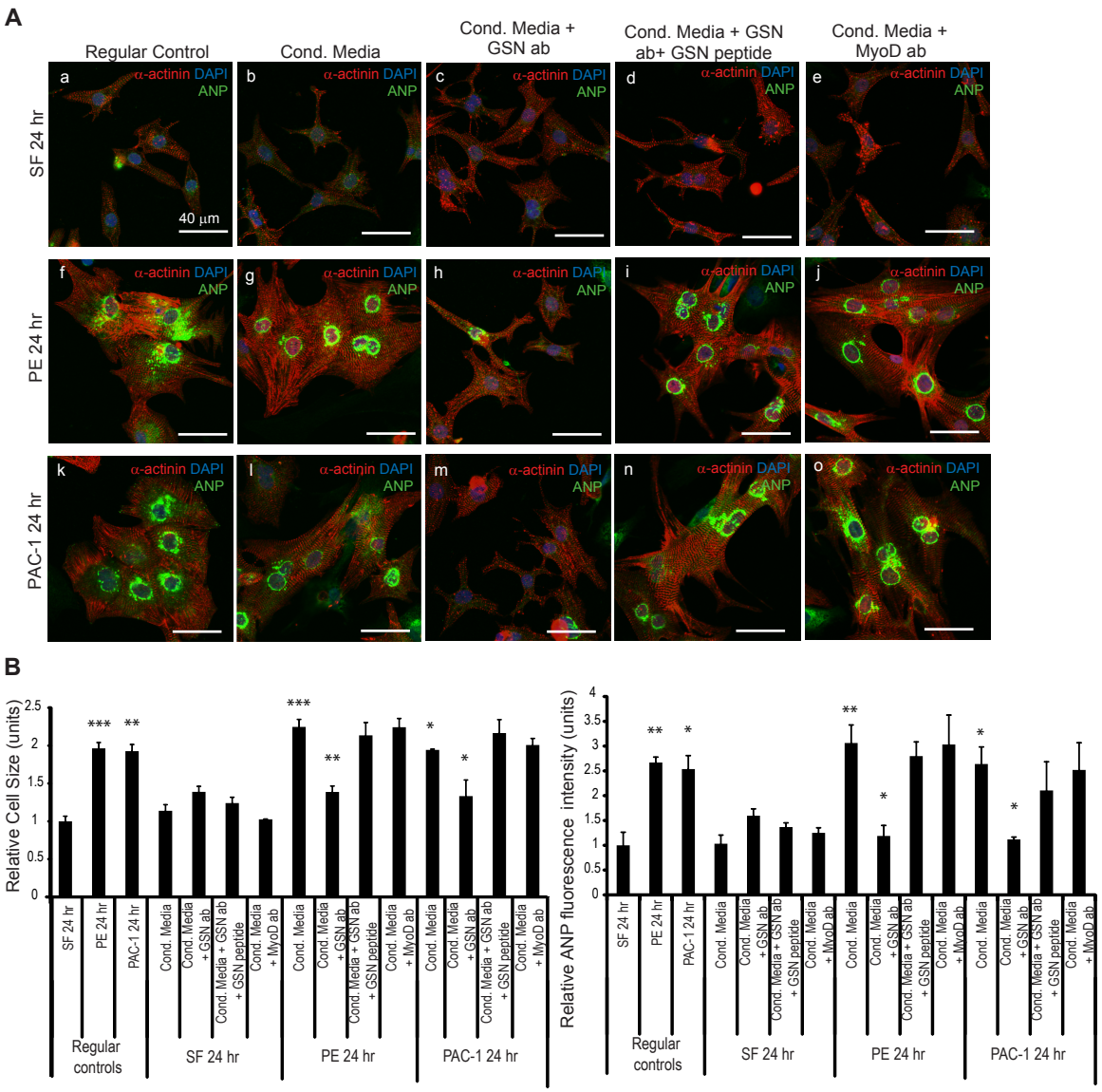


Figure 4. Gelsolin secreted by hypertrophic cardiomyocytes may be involved in the induction of hypertrophy. (A) Primary cardiomyocytes were treated with conditioned hypertrophic media (cond. media), from PE or PAC-1 treated cardiomyocytes, supplemented with Gelsolin (GSN) antibody (ab) to block secreted GSN, GSN ab plus GSN peptide or MyoD ab. Serum-free media treatment was used as a control. Cell size and ANP levels were analyzed and are quantified in (B). PE (size, n=3, ***, P<0.001; ANP, n=3, **, P<0.01) and PAC-1 (size, n=3, **, P<0.01; ANP, n=3, *, P<0.05) treatment (regular controls) resulted in hypertrophy induction. Treatment of cardiomyocytes with PE or PAC-1 conditioned media led to enlarged cardiomyocytes (PE, n=3, ***, P<0.001; PAC-1, n=3, **, P<0.01) and elevated ANP levels (PE, n=3, **, P<0.01; PAC-1, n=3, *, P<0.05) compared to the SF control. Conversely, cardiomyocytes treated with the conditioned PE (size, n=3, **, P<0.01; ANP, n=3, *, P<0.05) or PAC-1 (size, n=3, *, P<0.05; ANP, n=3, *, P<0.05) hypertrophy media plus a GSN ab reduced the hypertrophy induction (n=3, #, P<0.05). Preincubation with a GSN blocking peptide rescued the hypertrophy response. Error bars represent SEM. (Scale bars: 40 μm).

Discussion

Here, we have demonstrated that GSN is a caspase cleavage target during negative remodeling of cardiomyocytes and the resulting N-terminal domain is sufficient for the development of pathologic hypertrophy. Prior studies have demonstrated that elevated expression of full-length GSN is a trigger for pathologic hypertrophy (Li et al. 2009; Hu et al. 2014), yet our data suggests that caspase processing of GSN may be the requisite inductive cue. We observed that expression of the N-terminal GSN fragment leads to robust actin/cytoskeletal bundling in cardiomyocytes, which is remarkably similar to the actin reordering that occurs in response to pathologic agonists. These cytoskeletal modifications are the primary target of activated N-terminal GSN, yet we have also observed that the same GSN fragment engages the hypertrophy transcriptional program, with increased MEF2, NF-κB and SRF activity, along with elevations in BNP and ANP reporters (Figure 2). At this stage, we have not identified the mechanism by which N-terminal GSN relays the transcription signal, however MADS box transcription factors such as SRF and MEF2 are known to be responsive to perturbations in actin structure (Sotiropoulos et al. 1999; Kircher et al. 2015). We surmise that N-terminal GSN modifies the actin superstructure to engage a kinase dependent signal that terminates with activation of these MADS box factors.

Our observations indicate that caspase cleavage of GSN is a temporally restricted phenomenon. We have previously demonstrated that caspase 3 cleaves the histone deacetylase HDAC3 to relieve repression of MEF2 factors, which then propels the early transcriptional response in both pathologic and physiologic hypertrophy (Putinski et al. 2013; Abdul-Ghani et al. 2017). These prior observations and the current study suggest

that the GSN protein is only available for caspase 3 targeting at later stages, which coincides with an elevated enzymatic activity of the protease. The corollary to this hypothesis is that GSN protein is either inaccessible or actively protected from caspase 3 targeting in earlier stages of remodeling. Interestingly, there is precedent for active shielding of caspase 3 substrates. The kinase CK2 phosphorylates caspase 3 cleavage sites in prospective target proteins, inducing steric hindrance to the protease (Duncan et al. 2011). This post-translational control of caspase 3 targeting has been noted in both skeletal (Dick et al. 2015) and cardiac (Abdul-Ghani et al. 2017) muscle growth, however GSN has yet to be confirmed as a CK2 substrate during the early hypertrophy phase in cardiomyocytes. Alternatively, GSN may be sequestered by a chaperone like protein, a mechanism that is known to be utilized to protect proteins from effector caspase cleavage (Bell & Megeney 2017). Recently, the chaperone protein chaperonin containing Tcp-1 (CCT) has been shown to directly bind GSN, and repress its ability to induce actin polymerization (Svanström & Grantham 2016). Whether this chaperone/GSN protein interaction is operative in cardiomyocytes will require further investigation.

Unabated cardiac remodeling is often problematic, as it frequently leads to loss of function and heart failure. As such, there is a fine balance in the capacity of cardiomyocytes to sustain sarcomereic and cytoskeletal protein fluctuations. For example, altered distribution and expression of α-actinin and myocardial titin have been observed during cardiomyopathy (Kawaguchi et al. 1995), and the upregulation of microtubules and desmin filaments have been reported to be contributing factors to cardiac malfunction (Wang et al. 1999). Notably, β-adrenergic stimulation in cardiomyocytes leads to caspase-mediated cleavage of sarcomeric proteins, including α-

actin, α-actinin, and cardiac troponin T (Communal et al. 2002). Therefore, it is likely that continued caspase activation leads to decompensation/heart failure through combinatorial targeting of sarcomeric proteins and GSN, which acts to promote unrestrained actin polymerization. Clearly, long term expression of N-terminal GSN is consistent with this hypothesis, as our experiments demonstrate initial improvement in cardiac function, which was followed by a significant decline at 28 days post N-terminal GSN delivery (Figure 3B and S3).

We propose that paracrine mediated release of GSN may propel the transition from hypertrophy to decompensation and heart failure. In a physiologic hypertrophy setting, cardiomyocytes release paracrine factors to stimulate angiogenesis, ensuring that the growth in the myocardium is matched to appropriate vascular support (Abdul-Ghani et al. 2017). Here, our experiments demonstrate that GSN acts as a paracrine factor to induce a pathologic hypertrophy response in otherwise naïve cells. Therefore, it is reasonable to conjecture that cardiomyocyte hypertrophy induced by endogenous caspase activated GSN, coupled with the release of GSN would spur a global negative remodeling of the myocardium and accelerate the development of heart failure. In support of this concept, robust levels of GSN have been measured in exosomes released from non-cardiac cell types (Ji et al. 2008; Welton et al. 2010), while other studies have confirmed elevated serum concentrations of GSN in the post-infarct heart (Li et al. 2009; Li et al. 2012). Our observations suggest that antibodies directed against GSN may provide a means to titrate a GSN paracrine signal, limiting or reducing pathologic hypertrophy and its physiologic endpoint of heart failure.

In summary, our results show evidence indicating a crucial role for GSN and its caspase-mediated processing in pathologic cardiac hypertrophy. Our work suggests that caspase signaling acts to engage both the transcriptional program and cytoskeletal accommodations that characterize pathological cardiac hypertrophy. Importantly, this suggests that the identification of inhibitors that suppress caspase activity and/or activity of its substrates, including GSN, may offer novel therapeutic targets to limit the development of pathological cardiac hypertrophy and/or prevent the transition to fulminant heart failure.

Methods

All animal studies, including primary cardiomyocyte retrieval and *in vivo* analysis, were approved by the University of Ottawa Heart Institute and the University of Ottawa Animal Care Committee.

Cell culture

Primary neonatal rat cardiomyocytes were isolated from hearts of 2 day old Sprague–Dawley rats (Charles River Canada). Here, hearts were placed in Joklik modified Eagle medium (J-MEM) after excision and ventricles were separated from the atria. Ventricles were minced and digested with 0.1% collagenase II (Worthington) in J-MEM for five rounds of digestions (15 minutes each) at 37 °C with agitation. To prevent further digestion, supernatants from collected cellular fractions were incubated with 10% (vol/vol) fetal bovine serum (FBS) (Gibco). Cellular fractions were spun at 100×g for 5 minutes and the resulting cell pellets were resuspended in Dulbecco's modified Eagle medium (DMEM)/10% (vol/vol) FBS/1% (vol/vol) penicillin–streptomycin (Gibco). Noncardiomyocyte cells were removed via two 30 minute preplating incubations. All nonadherent cells were seeded on adherent culture dishes or collagen-coated 25-mm glass coverslips for immunocytochemistry. Cells were allowed to recover for 24 hours in DMEM culture media at 37 °C with 5% CO_2. Media were changed to serum-free (SF) media for 24 hours at 37 °C with 5% CO_2.

Immunoblotting

Cell lysates were obtained after GFP-AdV or p35-AdV infection (MOI=1) followed by 0 to 24 of hypertrophy induced by treatment with hypertrophic agonist phenylephrine (PE; 100 µM; Sigma). Staurosporine **(**STS; 2µM; 24hr; dissolved in DMSO; BioVision) and SF treatments (PE 0hr) served as positive and negative controls for caspase activation, respectively. Briefly, cells were washed in PBS solution and harvested by centrifugation at 1,500×g for 7 min. Cells were lysed in lysis buffer supplemented with protease inhibitors (0.5 M Hepes-NaOH, pH 7.5, 5.0 M NaCl, 80% (vol/vol) glycerol, 1% (vol/vol) Tx 100, 0.2 M EGTA, 1 M $MgCl_2$, 20 mM NaF, 10 mM sodium pyrophosphate, 2.0 mM sodium orthovanadate, 200µM PMSF) and incubated at 4 °C for 1 hour followed by centrifugation at 20,800×g for 10 minutes. Protein was separated by SDS/PAGE and transferred to PVDF membranes. Membranes were blocked with 10 mM Tris, pH 7.4, 150 mM NaCl, 0.05% Tween-20, 5% (wt/vol) nonfat powdered milk, and incubated with mouse anti-gelsolin (GSN) (Abcam) overnight at 4 °C followed by incubation with HRP-conjugated goat anti-mouse (BioRad). The ECL detection kit (GE Healthcare) was used to detect protein expression.

***In vitro* cleavage assay**

Recombinant gelsolin protein (100 ng; Abnova) and recombinant active caspase 3 (3 units; Chemicon) or active caspase 7 (3 units; BioVision) were incubated for 3 hours at 37°C in cleavage assay buffer (50 mM Hepes, pH 7.5; 0.1 M NaCl; 10% (vol/vol) glycerol; 0.1% Chaps; 10 mM DTT) containing either DMSO or the effector caspase peptide inhibitor *N*-benzyloxycarbonyl-Asp-Glu-Val-Asp-fluoromethylketone (z-DEVD-

fmk) (BioVision; 20 μM). Reactions were stopped by addition of Laemmli sample buffer and subjected to SDS/PAGE. Western blot analysis was performed using a GSN (Abcam) antibody.

Mass spectrometry

To confirm caspase 3 and/or caspase 7 cleavage of GSN protein (2 μg), an *in vitro* cleavage reaction, performed as previously described, was subjected to SDS/PAGE followed by silver stain using silver nitrate. The protein bands corresponding to the cleavage fragments were excised and processed for LC-MS/MS via trypsin digest. The results were analyzed by MASCOT 2.4 software (Matrix Science), and the identified peptides were mapped to either the N-terminus or the C-terminus of the GSN protein sequence (Figure 1D).

Immunofluorescence

Primary cardiomyocytes were seeded for fluorescent staining at a density of 2.7×10^5 cells per collagen-coated 25-mm glass coverslip. Briefly, cells were washed in PBS solution and fixed with 4% (wt/vol) paraformaldehyde (PFA) for 30 minutes after indicated treatment. Cell permeabilization was completed by incubating in blocking buffer (1% BSA, 2% (wt/vol) normal goat serum, 0.4% Tx-100 in PBS solution) for 30 minutes. Cardiomyocytes were stained mouse anti–α-actinin (Sigma) overnight at 4 °C and then with goat anti-mouse IgG Cy3 conjugate (Millipore) for 1.5 hours. To detect hypertrophy induction cardiomyocytes were stained with known hypertrophic marker atrial natriuretic peptide (ANP), rabbit anti-ANP (Abcam), followed by detection by the Cy3 or Alexa 488 secondary antibody (Invitrogen). Nuclei were counterstained with DAPI (Sigma), and

cells were mounted onto microscope slides with DakoCytomation fluorescent mounting media (DakoCytomation). Fluorescent images were obtained using the Zeiss LSM510 (Carl Zeiss) or the Zeiss Observer Z1 inverted fluorescence microscope (Carl Zeiss). Actin was visualized by Alexa Flour® 555 Phalloidin staining (Cell Signaling) and cardiomyocytes with organized/parallel lines of sarcomeres were quantified. Hypertrophy was assessed by cardiomyocyte cell size analysis of α-actinin–positive cells using ImageJ software. ANP fluorescence intensity was determined by integrated density quantification also by using ImageJ software.

Construction of gelsolin adenoviruses

Recombinant GSN adenoviruses (AdVs) for gene delivery of wild-type (WT), N-terminal GSN caspase cleavage fragment and C-terminal GSN caspase cleavage fragment were constructed by use of the AdEasy^{TM} XL Adenoviral Vector System (Agilent Technologies) according to the manufacturer's instructions. Primers were constructed based on the full-length GSN rat sequence and are detailed in Table 1. Note that all GSN-AdVs are encoding cytoplasmic GSN which starts at AA 50 within the *Rattus norvegicus* precursor GSN sequence (Figure S1; NP_001004080.1). Polymerase chain reactions (PCR) were completed using full-length GSN as a template (GE Healthcare). PCR products were run on agarose gels followed by DNA extraction/purification. Double digestion with restriction enzymes Sal I (New England Biolabs) and Xho I (New England Biolabs), selected within the multiple cloning site of the shuttle vector, were completed overnight at 37°C followed by heat inactivation. Purified and digested inserts were ligated into the pShuttle-IRES-hrGFP-2 vector (Agilent Technologies) using the Takara DNA ligation kit (Clontech) according to manufacturer's instructions.

Table 1: Primers used for gelsolin adenovirus construction

Gelsolin Primer	
Wild-type (WT)	FW: 5'-TTTGTCGACATGGTGGTGGAGCACCCCGAAGGG-3' RV: 5'-TTCTCGAGGGCAGCCAGCTCAGCCAACC-3'
N-terminal fragment	FW: 5'-TTTGTCGACATGGTGGTGGAGCACCCCGAAGGG-3' RV: 5'-TTCTCGAGGTCTGTCTGGTCTGGGTCCC-3'
C-terminal fragment	FW: 5'-TTTGTCGACATGGGCCCTGGCCTGAGCTACGGG-3' RV: 5'-TTCTCGAGGGCAGCCAGCTCAGCCAACC-3'
D401A caspase cleavage mutant	FW: 5'-CCAGACCAGACAG***C***CGGCCCTGGCCTG -3' RV: 5'-CAGGCCAGGGCCG***G***CTGTCTGGTCTGG-3'
Internal sequencing primers	WT and N-terminal FW: 5'-GGACGCCGTGTAGTCCGTGCC-3' WT and C-terminal RV: 5'-GGCGGCGGAGGGGGTTTTCAG-3' N-terminal RV: 5'-GGTGCCCTGAGGCAGATCCGG-3' C-terminal FW: 5'-GTCGCTGCTTCAGCCATCCTG-3'

Forward (FW) and reverse (RV) Wild-type, N-terminal and C-terminal GSN-AdV primers include Sal1 and Xhol restriction sites, respectively.
Mutated site identified in bold italics.

The resulting ligation mixtures were transformed into DH5α competent cells and selected for kanamycin resistance. Correct insert ligation was confirmed by enzyme digest, and sequencing (Applied Biosystems 3730 DNA Analyzer, StemCore Laboratories, Ottawa) and analysis of sequencing data using Chromas software. Forward and reverse GSN primers are detailed in Table 1, were used for sequencing and additional internal primers were used to facilitate full sequencing coverage. Plasmid DNA was linearized with Pme I (New England Biolabs) and transformed into BJ5183-AD-1 cells, which are pre-transformed with pAdEasy-1 plasmid (Agilent Technologies), followed by selection for kanamycin resistance. DNA mini-preps were digested with Pac I (New England Biolabs) and run on agarose gel in parallel to uncut mini-prep DNA and cut unrecombinant vector as controls. Positive recombinant AdV plasmids were transformed into XL10-Gold ultra-competent cells (Agilent Technologies) and then transfected into AD-293 cells allowing for recombinant AdV plasmid DNA amplification. Once amplified, AdVs were purified by cesium chloride gradients using ultracentrifugation and quantified by spectrophotometry.

WT GSN previously cloned, as detailed above, into the pShuttle-IRES-hrGFP-2 vector was used as a template to produce a single point mutation within the GSN caspase cleavage site using site-directed mutagenesis. The PCR was performed using primers (Table 1) containing the mutated nucleotide sequence corresponding to a single amino acid change (D401A). The resulting mutated PCR products were then processed as described above producing caspase cleavage site mutated GSN AdVs.

Correct GSN expression was further verified by western blotting of lysates collected from AdV infected primary cardiomyocytes. Cells were washed in PBS solution and

harvested by centrifugation at 1,500×g for 7 minutes. Whole cell lysates were obtained by cell lysis with lysis buffer supplemented with protease inhibitors (50 mM Tris-HCl, 150 mM NaCl, 1 mM EDTA, 1% (vol/vol) NP-40, 1% (vol/vol) glycerol, 20 mM NaF, 10 mM sodium pyrophosphate, 2.0 mM sodium orthovanadate, 200μM PMSF) and incubated at 4 °C for 1 hour followed by centrifugation at 12000×g for 2 minutes. Protein was separated by SDS/PAGE and transferred to PVDF membranes. Membranes were blocked as described above and incubated with C-terminal mouse anti-GSN (Abcam) or N-terminal goat anti-GSN (Santa Cruz) overnight at 4 °C followed by incubation with HRP-conjugated goat anti-mouse (BioRad) or anti-goat (BioRad). The ECL detection kit (GE Healthcare) was used to detect protein expression (Figure S4).

Gelsolin adenovirus infection and cardiomyocyte treatments

Primary cardiomyocytes were infected with either the control GFP-AdV, wild-type (WT) GSN-AdV, N-terminal GSN-AdV, C-terminal GSN-AdV or the non-caspase cleavable D401A GSN-AdV (MOI=1) either in SF media (24hr or 48hr) or during PE (100 μM) hypertrophy induction (3hr or 24hr). Cardiomyocytes were PFA fixed and immunofluorescent analysis was completed with mouse anti-α-actinin, rabbit anti-ANP followed by detection by the Cy3 and Alexa 647 secondary antibody (Invitrogen). Nuclei were counterstained with DAPI, and cells were mounted onto microscope slides with DakoCytomation fluorescent mounting media. Fluorescent images were obtained using the Zeiss Observer Z1 (Zeiss AxioVision SE64 Imaging software). Hypertrophy was assessed by cardiomyocyte cell size analysis of α-actinin–positive cells using ImageJ software. ANP fluorescence intensity was determined by integrated density quantification also by using ImageJ software. All values were normalized to SF plus GFP-AdV infected

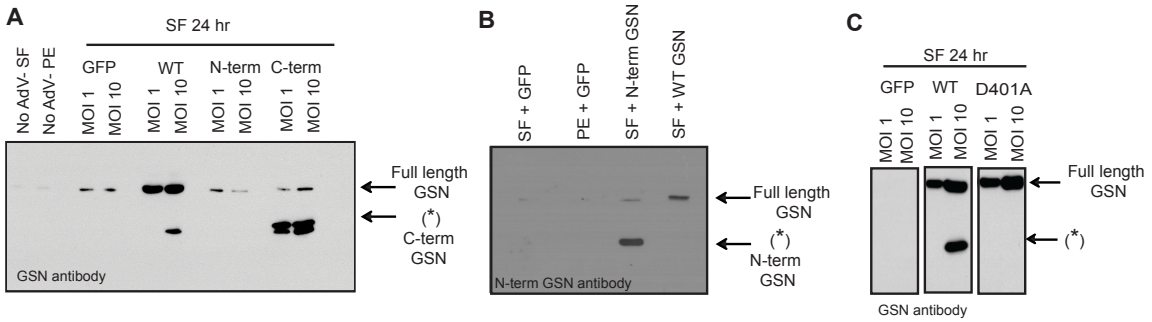


Figure S4. Confirmation of proper expression from gelsolin adenoviruses. Primary cardiomyocytes were infected with gelsolin (GSN) adenoviruses (AdVs) and correct GSN expression was confirmed by western blotting. (A) A C-terminal GSN antibody (Abcam) was used to detect GSN expression. Overexpression of full-length/wild-type (WT) was seen in cardiomyocytes infected with WT GSN at MOI=1 and MOI=10. Processing of GSN occurs at MOI=10. C-terminal GSN overexpression was observed (*). (B) An N-terminal GSN antibody (Santa Cruz) was used to verify N-terminal GSN overexpression in N-terminal GSN infected cardiomyocytes (*). (C) D401A GSN-AdV infected cardiomyocytes were null of GSN processing that was evident in WT infected cardiomyocytes (*).

control treatments.

Gelsolin siRNA knockdown and gelsolin reintroduction

Primary cardiomyocytes were transfected by using Lipofectamine 2000 (Invitrogen) and SF Opti-MEM α (Gibco), and GSN siRNA or negative control scrambled siRNA (Ambion) for 5 hours at 37°C with 5% CO_2. The media was replaced with SF media and cells were incubated overnight at 37 °C with 5% CO_2. The next day, cardiomyocytes were infected with either the control GFP-AdV, WT GSN-AdV or D401A caspase cleavage site mutant GSN-AdV (MOI=1). Cardiomyocytes were then incubated in SF (24 hr) or PE hypertrophy (24 hr) media and fresh siRNA was added. Cardiomyocytes were PFA fixed and immunofluorescence analysis and hypertrophy assessment was completed as described above. GSN knockdown was confirmed by western blotting using a GSN antibody (Abcam) where GSN siRNA treatment lead to reduced GSN levels during PE 24hr treatment compared to the negative scrambled control siRNA (Figure 1F). Equal loading is shown by α-β tubulin (Development Studies Hybridoma Bank).

Prohypertrophic reporter luciferase assay

At a density of 0.7×10^5 cells per well, primary cardiomyocytes were seeded onto 48-well plates and 24 hours later cells were transfected by using Lipofectamine 2000 (Invitrogen), SF Opti-MEM α (Gibco), 4 ng of internal Renilla luciferase internal control, and 200 ng of Fire fly luciferase reporter DNA containing the gene of interest (reporters: ANP, BNP, NF-κB, MEF2, SRF) for 5 hours at 37 °C with 5% CO_2. The media was replaced with SF media containing GFP control AdV or WT, N- or C-terminal GSN-AdV or the D401A GSN-AdV and cells were incubated overnight at 37 °C with 5% CO_2. The next day,

cardiomyocytes were incubated with SF media or PE (24 hr). Luciferase activity was measured by using the Dual Luciferase Assay System per manufacturer's instructions (Promega). Luciferase values were normalized to Renilla luciferase internal control, empty pXP2 vector, and SF media plus GFP-AdV.

In vivo gelsolin adenovirus analysis

Analysis was completed on Sprague-Dawley rats (~250 g at baseline). Echocardiography (VisualSonics)-guided intra-myocardial injections of GFP-AdV, wild-type GSN-AdV, N-terminal GSN-AdV, C-terminal GSN-AdV, or D401A GSN-AdV diluted in 0.9% saline solution, at 3.75×10^5 pfu/μL, was completed on day 0 by using a staged microinjector under parasternal long axis view. Hypertrophy progression was monitored by transthoracic echocardiography at room temperature using echocardiography-Doppler (Vevo 770 system; VisualSonics) with a probe RMV707B (15-45 MHz). Measurements were take on day 0, 14, 21, and 28. Here, the rats were slightly anesthetized with 0.5–1 % isoflurane in 100 % O_2. The two-dimensionally guided time motion mode recording of the LV provided the following measurements: interventricular septal wall thickness in diastole (IVS;d), posterior wall thickness in systole (LVPW;s), LV internal diameter during diastole (LVID;d), LV internal diameter during systole (LVID;s). Percentage of LV fractional shortening (FS) were calculated as follows: FS= (LVID;d - LVID;s)/ LVID;d multiplied by 100. Percentage of Ejection Fraction (EF) were calculated based on LV volume during diastole and systole (μL) where EF= (LV volume;d - LV volume;s/LV volume;d) multiplied by 100. Percentage of Cardiac Output (CO) were calculated based on heart rate (HR) measurements multiplied by Stroke Volume (SV), where SV was calculated by subtracting end systolic volume from end diastolic volume multiplied by

100. At 4 weeks, hearts were arrested in diastole by a tail-vein injection of 2 M KCl. Hearts were isolated and stored in 4% (wt/vol) PFA and dehydrated with 25% (wt/vol) sucrose overnight at 4 °C. Embedding and sectioning of hearts was completed by the Department of Pathology and Laboratory Medicine - Histology Core Facility (University of Ottawa, Ottawa). Tissue sections were washed in PBS solution and fixed in 0.2% glutaraldehyde for 10 minutes at room temperature. Fluorescent staining was completed on the heart tissues in a rehydration chamber by using mouse anti–α-actinin, goat anti-mouse IgG Cy3 conjugate, anti-GFP (Cell Signaling), goat anti-rabbit Alexa 488, and DAPI as described earlier. Fluorescent images were obtained using the Zeiss LSM510 (Carl Zeiss). Cell size analysis was completed on GFP-positive cardiomyocytes as described earlier.

Caspase inhibition and gelsolin adenovirus infection

Primary cardiomyocytes were infected with either the control GFP-AdV, wild-type (WT) GSN-AdV, N-terminal GSN-AdV, C-terminal GSN-AdV or the non-caspase cleavable D401A GSN-AdV (MOI=1) in SF media (24hr). The following day, primary cardiomyocytes were pretreated with z-DEVD-fmk for 2 hours before induction of hypertrophy by PE (100 μM; 24 hr) when additional fresh caspase 3 inhibitor was added. Cardiomyocytes were PFA fixed and immunofluorescence analysis and hypertrophy assessment was completed as described above. Fluorescent images were obtained using the Zeiss Observer Z1 (Zeiss AxioVision SE64 Imaging software).

Conditioned hypertrophy media analysis

Primary cardiomyocytes were treated with SF, PE (100 μM) or the procaspase activating

compound PAC-1 (25 μM; BioVision) for 24 hours. Hypertrophy media was aspirated and fresh SF media added. The media was collected after 24 hours and this conditioned media, in presence or absence of a GSN antibody, GSN antibody and GSN blocking peptide or control non-cardiac expression MyoD antibody, was used to treat additional dishes of primary cardiomyocytes. In more details, conditional media or conditioned media in presence of a GSN antibody (2 ug/mL; Abcam) was added to cardiomyocytes. GSN antibody (2 ug/mL) and GSN blocking peptide (6 ug/ mL; Abcam) were preincubated for 1 hour at room-temperature and then added to conditioned media and subsequently to cardiomyocytes. Additionally, an antibody for a non-cardiac expressing protein (MyoD; Cell Signaling) was used as a negative control and added to conditioned media to treat cardiomyocytes. Twenty-four hours later, cardiomyocytes were fixed and cell size and ANP levels were analyzed by immunofluorescence microscopy, as described above.

Statistical analysis

All data are expressed as mean ± SEM. Significance of multiple-group comparisons were completed by one-way ANOVA, where $P<0.05$ was considered significant (XLSTAT software). Pairwise comparisons of treatment groups or treatment groups with control groups were completed by the unpaired 2-tailed Student t test, with $P<0.05$ considered significant.

Chapter 4:

General Discussion

4. General Discussion

Caspase proteases have distinct roles in apoptosis, yet these proteins also have well defined roles in various non-death processes. The most widely studied non-death role of caspases are as essential regulators of cell differentiation and cell fate commitment (Zermati et al. 2001; Bassnett 2002; Fernando et al. 2002; Arama et al. 2003; Fujita et al. 2008; Abdul-Ghani et al. 2011; Dick et al. 2015). In addition to cell differentiation, caspase proteases have also been implicated in stress adaptation, where caspase 3 was suggested to modulate pathological cardiac hypertrophy (Balakumar & Singh 2006). Given that hypertrophy is initially a beneficial adaptation which can transit into a pathological state after prolonged stress, it is not an unreasonable premise to suggest that all forms of cardiac hypertrophy may be regulated by traditional apoptotic signaling mechanisms. For example, caspase activity may an essential inductive cue for cardiac remodeling, where the duration, intensity, and substrate selection determine the final cell state/phenotype. Here, we have investigated caspases and intrinsic apoptotic signaling as essential drivers of pathological cardiac hypertrophy. Relevant caspase cleavage targets were also analyzed for their roles in this pathological form of cardiac stress remodeling.

4.1 Apoptosis and the Heart

Cardiomyocyte cell death has been shown to be associated with numerous cardiac diseases, including heart failure (HF) and ischemic heart disease (Regula & Kirshenbaum 2005; Nishida & Otsu 2008; Clarke et al. 2007; Whelan et al. 2010). Traditionally, apoptosis has been demonstrated to play a role in the progression and detrimental

outcomes associated with these disease states, where caspase activation, DNA fragmentation, and programmed death of cardiomyocytes contributes to dysfunctional ventricular remodeling (Narula et al. 1996; Olivetti et al. 1997). Although apoptotic cell death is a bona fide feature of cardiac disease, many key biochemical features of apoptosis occur in surviving cardiomyocytes. Specifically, 'apoptotic' cardiomyocytes have been documented with intact and viable nuclei, while lacking classic downstream apoptotic caspase-mediated poly (ADP-ribose) polymerase (PARP) cleavage (Haider et al. 2002; Narula et al. 1996). Here, cell death was determined to be incomplete, suggesting that these apoptotic markers (including caspase activity) may be indicative of a physiologic response rather than cell death per se. Accordingly, it is reasonable to conjecture that caspase proteases may influence cardiomyocyte adaptation in other disease settings, such as pathologic hypertrophy.

4.2 The Essential Role of Intrinsic-Mediated Caspase Activation during Pathological Hypertrophy

We have identified a key requirement for the activation of the intrinsic-mediated apoptotic signaling cascade in the development of pathological cardiac hypertrophy. Treatment with prohypertrophy agonists, such as phenylephrine (PE), isoproterenol (ISO), angiotensin II (AngII), or endothelin 1 (ET1), resulted in transient caspase 3 activation in primary cardiomyocytes (Chapter 2: Figure 1A). The source of caspase 3 activation was determined to be mediated by the intrinsic pathway, which was reflected by a drop in mitochondrial membrane potential and activation of the initiator caspase, caspase 9 (Chapter 2: Figure 1B and C). Importantly, cell viability was not impaired when the activation of caspase 3 and 9 were elevated, strongly suggesting that these

proteases were moderating a non-death role during pathological hypertrophy (Chapter 2: Figure 1D). Indeed, this non-death activity is reminiscent of other vital cell functions attributed to the mitochondrial-mediated caspase cascade, which includes the stimulation of cell differentiation in a wide variety of cell lineages across the metazoan phyla (Abdul-Ghani & Megeney 2008; Murray et al. 2008; Dick & Megeney 2013; Fuchs & Steller 2011).

Peptide and biologic caspase inhibitors were used to investigate whether apoptotic signaling is required for and/or stimulates cardiac hypertrophy. Blocking the intrinsic pathway, by use of the caspase 9 peptide inhibitor z-LEHD-fmk, demonstrated that functional caspase 9 is required for induction of cardiac hypertrophy (Chapter 2: Figure 2A). Further, a myeloid cell leukemia 1 (Mcl-1) expressing AdV was used to blunt activation of the intrinsic pathway. Mcl-1 is an anti-apoptotic protein capable of binding to various BH3-only proteins and inhibiting their activity thus blocking mitochondrial pore formation, cyt *c* release, and downstream caspase 9 activation (Ploner et al. 2008; Zhuang & Brady 2006). PE treated cardiomyocytes infected with the Mcl-1-AdV were reduced in size and had significantly lowered ANP levels compared to those infected with a GFP control AdV (Chapter 2: Figure 2B and C). Effector caspase inhibited cardiomyocytes also displayed a similar reduction in agonist induced hypertrophy (Chapter 2: Figure 3). Additional prohypertrophy markers were analyzed by luciferase reporter assays further verifying that the intrinsic apoptotic pathway, and specifically functional caspase 9 and effector caspase 3, are essential to pathological hypertrophy (Chapter 2: Figure 3C). Here, we observed activation of the fetal gene program, including elevated ANP and BNP levels, and transcription factors known to be involved in cardiac

hypertrophy, namely MEF2 and NF-κB. Importantly, similar to our *in vitro* work, we also demonstrated that effector caspase inhibition attenuates hypertrophy in the intact myocardium (Chapter 2: Figure 4).

Having confirmed that caspase activity was necessary for the induction of pathological cardiomyocyte hypertrophy, we sought to determine whether caspase activation alone was sufficient for inducing hypertrophy. Here, we used the small molecule procaspase activating compound procaspase-activating compound 1 (PAC-1) to activate caspase 3. Since uncontrolled elevated active caspase proteases can have significant impact on cell viability, we determined a relevant concentration of PAC-1 to activate caspases, while maintaining cellular integrity. High PAC-1 doses (100 μM) induced a cell death response similar to that observed by apoptosis induction (STS treatment), yet lower PAC-1 doses (25 μM) engaged a hypertrophy response similar to PE treatment, with no decrease in cell viability (Chapter 2: Figure 5). These experiments highlight the delicate balance between the death and non-death function of an effector caspase. Although other inductive cues may be needed to recapitulate all aspects of the hypertrophy program, these results suggest that caspase activation alone can induce cardiomyocyte cell growth and activate relevant gene expression programs that are reflective of pathologic cardiac hypertrophy.

The majority of observations to date are consistent with the hypothesis that caspase activation is a conserved regulatory cue for pathologic cardiac hypertrophy. Given the very distinct morphologic and phenotypic variation between pathologic and physiologic cardiac growth/hypertrophy, it is a reasonable supposition that caspase signaling does not influence the latter form of beneficial remodeling. In support of this

concept, pathologic and physiologic growth of the myocardium have been linked to activation of distinct signaling pathways. This includes the phosphoinositide 3-kinase/protein kinase B (PI3K/Akt)-mediated signaling cascade as a physiological hypertrophy inductive cue (McMullen et al. 2003; McMullen et al. 2007; Dorn 2007) while fetal gene activation (McMullen & Jennings 2007) and calcineurin-mediated signaling are generally associated with pathological hypertrophy (Molkentin et al. 1998; van Berlo et al. 2013). Nevertheless, these variable patterns of cardiac remodeling may share a common biochemical signal. The early compensatory stages of pathological cardiac hypertrophy are often a beneficial adaptation to stress (Hill & Olson 2008) and both forms of cardiac growth have been shown to involve myocyte enhancer factor 2 (MEF2) transcriptional activation (Kolodziejczyk et al. 1999; Naya et al. 2002; van Rooij et al. 2010). Interestingly, one study recently observed limited/constrained caspase 3 activation during human cardiotrophin 1 (hCT1)-induced physiological cardiac hypertrophy (Abdul-Ghani et al. 2017). Here, caspase 3 activity was observed during physiological hypertrophy albeit this activation was notably reduced compared to pathological hypertrophy. Casein kinase 2 (CK2) activity was shown to constrain and limit caspase activity during physiological hypertrophy and prohibit progression to pathological hypertrophy. The CK2 phosphorylation site and caspase 3 cleavage site share an overlapping consensus sequence and CK2-mediated serine phosphorylation of caspase targets has been demonstrated to result in blunted caspase-mediated processing (Duncan et al. 2011; Turowec et al. 2014; Dick et al. 2015). Whether muted caspase activity is required for exercise and/or pregnancy induced physiologic hypertrophy will require further investigation.

Although the work presented in this thesis and other studies (Balakumar & Singh 2006; Putinski et al. 2013; Abdul-Ghani et al. 2017) demonstrate an essential role for caspase-mediated signaling in the induction of cardiac hypertrophy, it should be noted that a study by Cardona et al. showed the contrary (Cardona et al. 2015). This study however, focused on heart development in the caspase-deficient (not a complete knock-out) early post-natal myocardium.

4.3 Timing and Localization of Caspase 3 Activity during Pathological Cardiac Hypertrophy

What are the key determinants that dictate a death versus non-death outcome following effector caspase activation? As noted above, moderating the absolute level of caspase 3 activity via CK2 provides one mechanism. An additional conduit of control may be provided by altering the duration and localization of caspase activity and/or its substrate pool. Confined/restricted caspase localization has been observed during numerous non-death processes, whereas dispersed caspase activity is more typical of apoptosis (De Botton et al. 2002; Feinstein-Rotkopf & Arama 2009; Fernando & Megeney 2007; Koenig et al. 2008). Caspase regulation can be orchestrated through localization of caspase proteases and/or their substrates. For example, in healthy cells histone deacetylase 3 (HDAC3) resides in the nucleus whereas upon apoptotic stimulation, HDAC3 is cleaved resulting in its cytoplasmic relocalization (Escaffit et al. 2007). Escaffit et al. demonstrated that forced nuclear localization of HDAC3 blunts cell death progression, suggesting that HDAC3 localization regulates apoptosis induction. Although procaspase 3 is cleaved and activated in the cytoplasm, accumulation of active caspase 3 in apoptotic cells occurs in the nuclear fraction. Reports have shown that

cytoplasmic caspase targets, including caspase-activated DNase (CAD) and inhibitor of CAD (ICAD), translocate to the nucleus after cleavage resulting in nuclear morphological changes associated with apoptosis (Sahara et al. 1999; Lechardeur et al. 2000; Kamada et al. 2005). Similarly, our work indicates that caspases are positioned in the appropriate cellular milieu to obtain access to specific substrates at designated time points to initiate the hypertrophy program.

Here, we investigated two caspase cleavage substrates, HDAC3 and gelsolin (GSN), which may be involved in the induction and/or progression of pathological hypertrophy. At early hypertrophy time points, caspase 3 activity was localized to the nuclear/peri-nuclear regions of cardiomyocytes in distinct foci potentially enabling caspase access to nuclear targets (Chapter 2: Figure 1A). We observed HDAC3 cleavage at time points that overlap the endogenous peri-nuclear caspase 3 activation pattern (Chapter 2: Figure S7D). When present within the nucleus HDAC3 inhibits MEF2 activation subsequently suppressing hypertrophy induction. Nuclear localized caspase 3 may allow it to access a key target, HDAC3, enabling its processing. Effector caspases have previously been shown to cleave HDAC3 (Escaffit et al. 2007; Montgomery et al. 2008) and we further verified this protease substrate interaction using *in vitro* cleavage assays, as well as during a hypertrophy time course (Appendix I: Figure 1 and Chapter 2: Figure S7D, respectively). Of note, the prospective HDAC3 caspase cleavage site is found within the nuclear localization signal (NLS) present in the C-terminus of the protein (Yang et al. 2002; Escaffit et al. 2007). Thus upon caspase-mediated cleavage, the NLS is disrupted leading to nuclear export and relocalization of HDAC3 to the cytoplasm. Caspase-mediated cleavage and nuclear export of HDAC3 would establish

conditions, where suppression of MEF2 is removed, allowing for activation of prohypertrophic target genes. Indeed, we observed that caspase inhibition via p35-AdV infection significantly blunts MEF2 transcriptional activity (Chapter 2: Figure 3D).

In addition to an early activation pattern, caspase 3 signaling is also engaged at later time points in the hypertrophy program (6-24 hr) (Chapter 2: Figure S7D), albeit with a reduced number of nuclear localized caspase 3 foci (Chapter 2: Figure S2). Here, caspase 3 foci activity was mainly cytoplasmic, which coincided with caspase-mediated GSN cleavage (Chapter 3: Figure 1A). As previously discussed, GSN is an actin binding/severing protein and therefore maintains the same localization as actin (Unger & Hinssen 2010; Gonsior & Hinssen 1995; Rouayrenc et al. 1984). As such, the observed cytoplasmic caspase 3 localization may be necessary to allocate active caspase 3 in the correct sub-cellular localization to facilitate cleavage and activation of specific substrates, including GSN, which is involved in the cytoskeletal remodeling of cardiomyocytes. Other groups have also observed caspase-mediated cleavage of contractile components, including actin, α-actinin, and cTnT (Communal et al. 2002).

4.4 Caspase-mediated Gelsolin Cleavage is required for Pathological Cardiac Remodeling

Cytoskeletal remodeling is a prominent feature of the cardiomyocyte population during pathologic cardiac hypertrophy. Actin-binding protein (ABPs), including GSN, are known to be involved in this sarcomeric reorganizational process. Our findings that caspase-mediated GSN cleavage is involved in pathological cardiac remodeling build on the observation that caspase 3 activity (as discussed in Chapter 2; Putinski et al. 2013; Balakumar & Singh 2006) and GSN (Hu et al. 2014; Li et al. 2009) are essential to the

development of cardiac hypertrophy. Here, we have shown that the re-introduction of full-length but not caspase cleavage site mutated GSN (D401A) can rescue the hypertrophic response blunted by siRNA-mediated GSN inhibition (Chapter 3: Figure 1E and 1G). Further, the presence of the N-terminal portion of GSN, resulting from caspase-dependent processing, alone can initiate maladaptive actin severing, whereas introduction of the C-terminal portion of GSN did not induce cytoskeletal remodeling in primary cardiomyocytes. Consistent with a potent remodeling activity, we noted that expression of the N-terminal fragment of GSN induced numerous pro-hypertrophy markers and fetal genes, in addition to increasing cardiomyocyte cell size (Chapter 3: Figure 2).

Structural and functional changes reminiscent of pathological hypertrophy were recorded by echocardiography in rats injected with an N-terminal GSN expressing AdVs (Chapter 3: Figure 3B and S3). Although N-terminal GSN induced a hypertrophy response, as shown by increased interventricular septum thickness (IVS) and reduced left ventricular internal diameter (LVID) (Chapter 3: Figure 3B), no significant increase in organ size was observed. This was evaluated by analysis of both end stage heart weight to body weight (HW/BW) and heart weight to tibia length (HW/TL) ratios of all AdV injected rat groups (Appendix I: Figure 2). Although no significant change in HW/BW or HW/TL ratio was observed between the AdV groups, this may be in part due to early stages of hypertrophy being captured within this study time frame. A longer duration of exposure to N-terminal GSN-AdV may be necessary to induce an observable and more elevated increase in heart size. The significant increase in IVS thickness however is a known early indicator of hypertrophy and often precedes left ventricular posterior wall thickening and overall organ enlargement (Takahashi 1982; Verdecchia et al. 1994).

Also, additional AdV injections may be needed at later stages in order to induce a more robust hypertrophy phenotype. Alternatively, expression of N-terminal GSN may have induced decompensation which can affect and overall negatively impact the final HW. Indeed, we observed an initial improvement in cardiac function in rats injected with N-terminal GSN; however, at later stages declines in ejection fraction (EF), cardiac output (CO), and fractional shortening (FS) were observed (Chapter 3: Figure 3B and S3).

Other groups have demonstrated the presence of secreted GSN in exosomes during hypertrophy (Ji et al. 2008; Welton et al. 2010), suggesting that this actin severing protein may exert paracrine effects on adjacent cardiomyocytes. To directly test this supposition we examined whether GSN and/or its cleaved forms were secreted during exposure to hypertrophic agonists. Cardiomyocytes treated with conditioned media taken from PE or PAC-1 treated cells were enlarged compared to SF treated cardiomyocytes, demonstrating that secreted components within the media are hypertrophic (Chapter 3: Figure 4). Interestingly, the presence of a GSN antibody abrogated this hypertrophy response, suggesting that GSN secretion may propagate a hypertrophic signal to surrounding naïve cells. Although these observations require further verification *in vivo*, a pool of secreted and active GSN may explain why hypertrophied cardiomyocytes (and by extension the myocardium) are susceptible to further structural perturbations and failure. One group also demonstrated that GSN is released from the heart during ischemia and that secreted GSN may serve as a biomarker for cardiac injury (Li et al. 2012).

Taken together, these observations suggest that the N-terminal fragment of GSN is sufficient to promote cardiomyocyte remodeling. How actin severing of GSN leads to

altered gene expression and sarcomere structure in cardiomyocytes is not known. A reasonable explanation for these observations may be that disrupting the cytoskeleton engages a signaling pathway, which in turn directly enhances the hypertrophic gene expression program. In support of this hypothesis, we have noted that N-terminal GSN increases the expression of an SRF responsive promoter (Chapter 3: Figure 2C). Importantly, transcription factors, including as SRF and MEF2, have been shown to be responsive to cytoskeletal alterations (Sotiropoulos et al. 1999; Kircher et al. 2015). Studies have also demonstrated that SRF synergizes with transcription factors, such as NF-κB, GATA-4, and MEF2, to promote hypertrophic signaling further indicating the critical role of SRF in the regulation and induction of pathological cardiac hypertrophy (Belaguli et al. 2000; Kuwahara et al. 2007; Madonna et al. 2014).

4.5 Future Directions

In these studies we investigated the potential regulatory mechanisms for the non-death deployment of caspase activity during cardiac hypertrophy, including the timing, level, and localization of active caspases and their substrates. Collectively, these observations suggest that caspase signaling may be subject to both temporal and spatial control. For example, protein-protein interactions with IAPs or Hsps may contribute to constraining caspase 3 activation and preventing the induction of apoptosis. One candidate regulatory protein that may direct this non-death caspase activity is the Hsp αB-crystallin. A number of studies have confirmed that αB-crystallin suppresses caspase 3 activity through direct physical interaction in cardiomyocytes and skeletal muscle, and that αB-crystallin silencing during stress results in enhanced apoptosis (Chis et al. 2012; Kamradt et al. 2002). In preliminary studies we have observed that αB-crystallin

colocalizes with active caspase 3 during early stages of hypertrophy induction (unpublished results). Whether this protein interaction is a key to mitigating caspase activation during hypertrophy will require more direct experimentation. CK2-mediated caspase regulation may also provide a mechanism to restrain caspase activity in hypertrophic cardiomyocytes. CK2 mediated suppression of caspase 3 was recently noted in a model of physiologic hypertrophy, whether this same signal conduit is active to constrain pathological cardiac hypertrophy (and limit the transition to caspase induced apoptosis) remains to be examined (Abdul-Ghani et al. 2017).

Another interesting avenue to explore is whether effector caspases 3 and 7 play distinct roles in the execution of pathological cardiac hypertrophy. Substrate overlap between effector caspases 3 and 7 is evident but substrate specificity has been observed (Walsh et al. 2008). Similarly, both caspase 3 and caspase 7 can be inhibited by the peptide inhibitor z-DEVD-fmk or p35-AdV (Zhou et al. 1998) and activated by PAC-1 (Peterson et al. 2009). Compensation by either effector caspase provides evidence of their functional overlap. Also, the caspase 3/7 double knockout mouse is lethal at birth (Lakhani et al. 2006) and the outcome of the caspase $3^{-/-}$ mouse is highly dependent on the endogenous caspase 7 levels (Houde et al. 2004). To begin to address this, we completed all *in vitro* caspase cleavage assays for HDAC3 and GSN using both effector caspases 3 and 7 (Appendix I: Figure 1 and Chapter 3: Figure 1B and 1C, respectively). Interestingly, caspase 3 was observed to be more efficient at severing GSN while caspase 7 was more effective at HDAC3 processing. Indeed, others have shown that caspase 3 is primarily involved in the morphological changes associated with apoptosis whereas caspase 7 is essential to loss in cell viability and cell death progression (Lakhani et al.

2006). Similarly, GSN was cleaved more efficiently by caspase 3 and is proposed to be associated with the structural/cytoskeletal changes associated with cardiac hypertrophy, while HDAC3 severing is proposed to be involved in the induction/maintenance of hypertrophy signaling and showed more effective caspase 7-mediated processing.

We focused on evaluating HDAC3 and GSN as caspase cleavage substrates that influence the progression of pathological hypertrophy, however this does not preclude the potential of additional caspase targets, particularly those proteins discussed in section 1.3.2. Studies, similar to that detailed in Chapter 3, may provide critical information as to what role (if any) additional caspase substrates may have in conveying pathological cardiac remodeling. This could open the door to distinct caspase targets with essential roles in pathological cardiac hypertrophy induction and/or structural remodeling worth pursing with novel therapeutic potential.

4.6 Conclusions

We have provided evidence that the intrinsic apoptotic pathway is an essential driver of pathological cardiac hypertrophy. This cell-autonomous non-death activation of the caspase protease cascade may offer a route to moderating the early stages of pathological hypertrophy and/or may provide a potential therapeutic window for reversal of negative cardiac remodeling prior to the onset of HF. Inhibiting the intrinsic pathway at multiple junctures blocks downstream action of effector caspases and, in turn, limits pathologic hypertrophy. Examination of the caspase cleavage targets demonstrated that GSN and its caspase-mediated processing are critical aspects of pathological cardiac remodeling. Here, siRNA mediated GSN knockdown reduced hypertrophy and the reintroduction of caspase cleavage site mutated GSN was unable to sufficiently rescue

hypertrophy. Alternatively, expression of full-length GSN, capable of caspase processing, induced measurable hypertrophy. Similarly, expression of the N-terminal GSN caspase cleaved fragment, responsible for actin severing, resulted in a hypertrophy response both in primary cardiomyocytes and in the intact myocardium.

Our findings contribute to expanding the non-death roles of caspase proteases and importantly demonstrate the significance of intrinsic apoptotic signaling as an inductive cue for pathological cardiac hypertrophy. By targeting aspects of this signaling cascade, including caspases and/or their substrates, one may be able to effectively reduce the initial stages of cardiac hypertrophy, including pathological cardiac remodeling, and prevent the transition to HF.

References: Chapters 1, 3, and 4

Abdul-Ghani, M. et al., 2017. Cardiotrophin 1 stimulates beneficial myogenic and vascular remodeling of the heart. *Cell Research*, 27(10), pp.1195–1215.

Abdul-Ghani, M. et al., 2011. Wnt11 promotes cardiomyocyte development by caspase-mediated suppression of canonical Wnt signals. *Molecular and cellular biology*, 31(1), pp.163–178.

Abdul-Ghani, M. & Megeney, L.A., 2008. Rehabilitation of a contract killer: caspase-3 directs stem cell differentiation. *Cell stem cell*, 2(6), pp.515–516.

Adams, J.M. & Cory, S., 1998. The Bcl-2 protein family: arbiters of cell survival. *Science (New York, N.Y.)*, 281(5381), pp.1322–6.

Adams, J.W. et al., 1998. Enhanced Galphaq signaling: a common pathway mediates cardiac hypertrophy and apoptotic heart failure. *Proceedings of the National Academy of Sciences of the United States of America*, 95(17), pp.10140–10145.

Aggarwal, B.B., 2003. Signalling pathways of the TNF superfamily: a double-edged sword. *Nature reviews. Immunology*, 3(9), pp.745–56.

Ahn, J.S. et al., 2003. Aging-associated increase of gelsolin for apoptosis resistance. *Biochemical and biophysical research communications*, 312(4), pp.1335–41.

Arama, E., Agapite, J. & Steller, H., 2003. Caspase activity and a specific cytochrome C are required for sperm differentiation in Drosophila. *Developmental cell*, 4(5), pp.687–697.

Ashish et al., 2007. Global structure changes associated with Ca2+ activation of full-length human plasma gelsolin. *The Journal of biological chemistry*, 282(35), pp.25884–92.

Azuma, T. et al., 2000. Gelsolin in complex with phosphatidylinositol 4,5-bisphosphate inhibits caspase-3 and -9 to retard apoptotic progression. *The Journal of biological chemistry*, 275(6), pp.3761–3766.

Bai, L., Smith, D.C. & Wang, S., 2014. Small-molecule SMAC mimetics as new cancer therapeutics. *Pharmacology & Therapeutics*, 144(1), pp.82–95.

Balakumar, P. & Singh, M., 2006. The possible role of caspase-3 in pathological and physiological cardiac hypertrophy in rats. *Basic & clinical pharmacology & toxicology*, 99(6), pp.418–424.

Barry, S.P. & Townsend, P.A., 2010. What Causes a Broken Heart—Molecular Insights into Heart Failure. In pp. 113–179.

Bassnett, S., 2002. Lens organelle degradation. *Experimental eye research*, 74(1), pp.1–6.

Beere, H.M. et al., 2000. Heat-shock protein 70 inhibits apoptosis by preventing recruitment of procaspase-9 to the Apaf-1 apoptosome. *Nature cell biology*, 2(8), pp.469–75.

Belaguli, N.S. et al., 2000. Cardiac tissue enriched factors serum response factor and GATA-4 are mutual coregulators. *Molecular and cellular biology*, 20(20), pp.7550–8.

Bell, R.A. V & Megeney, L.A., 2017. Evolution of caspase-mediated cell death and differentiation: twins separated at birth. *Cell Death and Differentiation*, 24(8), pp.1359–1368.

van Berlo, J.H., Maillet, M. & Molkentin, J.D., 2013a. Signaling effectors underlying pathologic growth and remodeling of the heart. *Journal of Clinical Investigation*, 123(1), pp.37–45.

van Berlo, J.H., Maillet, M. & Molkentin, J.D., 2013b. Signaling effectors underlying pathologic growth and remodeling of the heart. *Journal of Clinical Investigation*, 123(1), pp.37–45.

Berthelet, J. & Dubrez, L., 2013. Regulation of Apoptosis by Inhibitors of Apoptosis (IAPs). *Cells*, 2(1), pp.163–187.

Beug, S.T. et al., 2014. Smac mimetics and innate immune stimuli synergize to promote tumor death. *Nature biotechnology*, 32(2), pp.182–90.

Biala, A.K. & Kirshenbaum, L.A., 2014. The interplay between cell death signaling pathways in the heart. *Trends in Cardiovascular Medicine*, 24(8), pp.325–331.

Botham, R.C. et al., 2016. Small-Molecule Procaspase-3 Activation Sensitizes Cancer to Treatment with Diverse Chemotherapeutics. *ACS Central Science*, 2(8), pp.545–559.

De Botton, S. et al., 2002. Platelet formation is the consequence of caspase activation within megakaryocytes. *Blood*, 100(4), pp.1310–1317.

Boulares, A.H. et al., 1999. Role of poly(ADP-ribose) polymerase (PARP) cleavage in apoptosis. Caspase 3-resistant PARP mutant increases rates of apoptosis in transfected cells. *The Journal of biological chemistry*, 274(33), pp.22932–40.

Bruneau, B.G., 2002. Transcriptional regulation of vertebrate cardiac morphogenesis. *Circulation research*, 90(5), pp.509–19.

Bueno, O.F. et al., 2000. The MEK1-ERK1/2 signaling pathway promotes compensated cardiac hypertrophy in transgenic mice. *The EMBO journal*, 19(23), pp.6341–50.

Burgon, P.G. & Megeney, L.A., 2017. Caspase signaling, a conserved inductive cue for metazoan cell differentiation. *Seminars in Cell & Developmental Biology*.

Burtnick, L.D. et al., 2004. Structure of the N-terminal half of gelsolin bound to actin: roles in severing, apoptosis and FAF. *The EMBO journal*, 23(14), pp.2713–2722.

Burtnick, L.D. et al., 1997. The crystal structure of plasma gelsolin: implications for actin severing, capping, and nucleation. *Cell*, 90(4), pp.661–70.

Cardona, M. et al., 2015. Executioner Caspase-3 and 7 Deficiency Reduces Myocyte Number in the Developing Mouse Heart. G.-C. Fan, ed. *PloS one*, 10(6), p.e0131411.

Chandrashekhar, Y. et al., 2004. Long-term caspase inhibition ameliorates apoptosis, reduces myocardial troponin-I cleavage, protects left ventricular function, and attenuates remodeling in rats with myocardial infarction. *Journal of the American College of Cardiology*, 43(2), pp.295–301.

Chaponnier, C., Kocher, O. & Gabbiani, G., 1990. Modulation of gelsolin content in rat aortic smooth muscle cells during development, experimental intimal thickening and culture. An immunohistochemical and biochemical study. *European journal of biochemistry*, 190(3), pp.559–65.

Chen, Y. et al., 2016. SM-1, a novel PAC-1 derivative, activates procaspase-3 and causes cancer cell apoptosis. *Cancer Chemotherapy and Pharmacology*, 78(3), pp.643–654.

Chis, R. et al., 2012. alpha-Crystallin B prevents apoptosis after H2O2 exposure in mouse neonatal cardiomyocytes. *American journal of physiology. Heart and circulatory physiology*, 303(8), pp.H967-78.

Choe, H. et al., 2002. The calcium activation of gelsolin: insights from the 3A structure of the G4-G6/actin complex. *Journal of molecular biology*, 324(4), pp.691–702.

Chung, E. & Leinwand, L.A., 2014. Pregnancy as a cardiac stress model. *Cardiovascular research*, 101(4), pp.561–70.

Clarke, M., Bennett, M. & Littlewood, T., 2007. Cell death in the cardiovascular system. *Heart*, 93(6), pp.659–664.

Clem, R.J., 2001. Baculoviruses and apoptosis: the good, the bad, and the ugly. *Cell death and differentiation*, 8(2), pp.137–43.

Communal, C. et al., 2002. Functional consequences of caspase activation in cardiac myocytes. *Proceedings of the National Academy of Sciences of the United States of America*, 99(9), pp.6252–6256.

Cory, S., 1998. Cell death throes. *Proceedings of the National Academy of Sciences of the United States of America*, 95(21), pp.12077–12079.

Davis, J. et al., 2016. A Tension-Based Model Distinguishes Hypertrophic versus Dilated Cardiomyopathy. *Cell*, 165(5), pp.1147–1159.

Desagher, S. et al., 2001. Phosphorylation of bid by casein kinases I and II regulates its cleavage by caspase 8. *Molecular cell*, 8(3), pp.601–611.

Dick, S.A. et al., 2015. Caspase 3 cleavage of Pax7 inhibits self-renewal of satellite cells. *Proceedings of the National Academy of Sciences of the United States of America*, 112(38), pp.E5246-52.

Dick, S.A. & Megeney, L.A., 2013. Cell death proteins: an evolutionary role in cellular adaptation before the advent of apoptosis. *BioEssays : news and reviews in molecular, cellular and developmental biology*, 35(11), pp.974–983.

Dorn, G.W., 2007. The Fuzzy Logic of Physiological Cardiac Hypertrophy. *Hypertension*, 49(5), pp.962–970.

Dosaka-Akita, H. et al., 1998. Frequent loss of gelsolin expression in non-small cell lung cancers of heavy smokers. *Cancer research*, 58(2), pp.322–7.

Duncan, J.S. et al., 2011. A Peptide-Based Target Screen Implicates the Protein Kinase CK2 in the Global Regulation of Caspase Signaling. *Science Signaling*, 4(172), p.ra30-ra30.

Duncan, J.S. et al., 2011. A peptide-based target screen implicates the protein kinase CK2 in the global regulation of caspase signaling. *Science signaling*, 4(172), p.ra30.

Earnshaw, W.C., Martins, L.M. & Kaufmann, S.H., 1999. Mammalian caspases: structure, activation, substrates, and functions during apoptosis. *Annual review of biochemistry*, 68, pp.383–424.

Escaffit, F. et al., 2007. Cleavage and cytoplasmic relocalization of histone deacetylase 3 are important for apoptosis progression. *Molecular and cellular biology*, 27(2), pp.554–67.

Feinstein-Rotkopf, Y. & Arama, E., 2009. Can't live without them, can live with them: roles of caspases during vital cellular processes. *Apoptosis : an international journal on programmed cell death*, 14(8), pp.980–995.

Fernández, D.J. & Lamkanfi, M., 2015. Inflammatory caspases: key regulators of inflammation and cell death. *Biological Chemistry*, 396(3), pp.193–203.

Fernando, P. et al., 2002. Caspase 3 activity is required for skeletal muscle differentiation. *Proceedings of the National Academy of Sciences of the United States of America*, 99(17), pp.11025–11030.

Fernando, P., Brunette, S. & Megeney, L.A., 2005. Neural stem cell differentiation is dependent upon endogenous caspase 3 activity. *FASEB journal : official publication of the Federation of American Societies for Experimental Biology*, 19(12), pp.1671–1673.

Fernando, P. & Megeney, L.A., 2007. Is caspase-dependent apoptosis only cell differentiation taken to the extreme? *FASEB journal : official publication of the Federation of American Societies for Experimental Biology*, 21(1), pp.8–17.

Fischer, P. & Hilfiker-Kleiner, D., 2007. Survival pathways in hypertrophy and heart failure: The gp130-STAT3 axis. *Basic Research in Cardiology*, 102(5), pp.393–411.

Frey, N. & Olson, E.N., 2003. Cardiac hypertrophy: the good, the bad, and the ugly. *Annual review of physiology*, 65(1), pp.45–79.

Fuchs, Y. & Steller, H., 2011. Programmed cell death in animal development and disease. *Cell*, 147(4), pp.742–758.

Fuentes-Prior, P. & Salvesen, G.S., 2004. The protein structures that shape caspase activity, specificity, activation and inhibition. *The Biochemical journal*, 384(Pt 2), pp.201–32.

Fujita, J. et al., 2008. Caspase activity mediates the differentiation of embryonic stem cells. *Cell stem cell*, 2(6), pp.595–601.

Gao, L. et al., 2015. Novel role for caspase-activated DNase in the regulation of pathological cardiac hypertrophy. *Hypertension (Dallas, Tex. : 1979)*, 65(4), pp.871–881.

García-Fernández, M. et al., 2010. Sept4/ARTS is required for stem cell apoptosis and tumor suppression. *Genes & development*, 24(20), pp.2282–93.

Garrido, C. et al., 2000. Hsp27 negatively regulates cell death by interacting with cytochrome c. *Nature Cell Biology*, 2(9), pp.645–652.

Geng, Y.J. et al., 1998. Caspase-3-induced gelsolin fragmentation contributes to actin cytoskeletal collapse, nucleolysis, and apoptosis of vascular smooth muscle cells exposed to proinflammatory cytokines. *European journal of cell biology*, 77(4), pp.294–302.

Ghavami, S. et al., 2014. Autophagy and apoptosis dysfunction in neurodegenerative disorders. *Progress in Neurobiology*, 112, pp.24–49.

Glass, D.J., 2005. Skeletal muscle hypertrophy and atrophy signaling pathways. *The International Journal of Biochemistry & Cell Biology*, 37(10), pp.1974–1984.

Gonsior, S. & Hinssen, H., 1995. Exogenous gelsolin binds to sarcomeric thin filaments without severing. *Cell motility and the cytoskeleton*, 31(3), pp.196–206.

Gordon, J.W., Shaw, J.A. & Kirshenbaum, L.A., 2011. Multiple Facets of NF-κB in the Heart. *Circulation Research*, 108(9), pp.1122–1132.

Green, D.R. & Kroemer, G., 2009. Cytoplasmic functions of the tumour suppressor p53. *Nature*, 458(7242), pp.1127–1130.

Grégoire, S. et al., 2007. Histone deacetylase 3 interacts with and deacetylates myocyte enhancer factor 2. *Molecular and cellular biology*, 27(4), pp.1280–95.

Gross, A. et al., 1999. Caspase cleaved BID targets mitochondria and is required for cytochrome c release, while BCL-XL prevents this release but not tumor necrosis factor-R1/Fas death. *The Journal of biological chemistry*, 274(2), pp.1156–63.

Haider, N., Narula, N. & Narula, J., 2002. Apoptosis in heart failure represents programmed cell survival, not death, of cardiomyocytes and likelihood of reverse remodeling. *Journal of cardiac failure*, 8(6 Suppl), pp.S512-7.

Hall, C., 2004. Essential biochemistry and physiology of (NT-pro)BNP. *European journal of heart failure*, 6(3), pp.257–60.

Han, J. & Molkentin, J.D., 2000. Regulation of MEF2 by p38 MAPK and its implication in cardiomyocyte biology. *Trends in cardiovascular medicine*, 10(1), pp.19–22.

Haq, S. et al., 2001. Differential activation of signal transduction pathways in human hearts with hypertrophy versus advanced heart failure. *Circulation*, 103(5), pp.670–7.

Hara, H. et al., 1997. Inhibition of interleukin 1beta converting enzyme family proteases reduces ischemic and excitotoxic neuronal damage. *Proceedings of the National Academy of Sciences of the United States of America*, 94(5), pp.2007–12.

Hartwig, J.H. et al., 1995. Thrombin receptor ligation and activated Rac uncap actin filament barbed ends through phosphoinositide synthesis in permeabilized human platelets. *Cell*, 82(4), pp.643–53.

Harvey, R.P., 2002. Patterning the vertebrate heart. *Nature reviews. Genetics*, 3(7), pp.544–56.

Heads, R.J., Latchman, D.S. & Yellon, D.M., 1994. Stable high level expression of a transfected human HSP70 gene protects a heart-derived muscle cell line against thermal stress. *Journal of molecular and cellular cardiology*, 26(6), pp.695–9.

Heineke, J. & Molkentin, J.D., 2006. Regulation of cardiac hypertrophy by intracellular signalling pathways. *Nature reviews. Molecular cell biology*, 7(8), pp.589–600.

Hengartner, M.O., 2000. The biochemistry of apoptosis. *Nature*, 407(6805), pp.770–776.

Hensley, P., Mishra, M. & Kyprianou, N., 2013. Targeting caspases in cancer therapeutics. *Biological Chemistry*, 394(7), pp.831–43.

Hill, J.A. & Olson, E.N., 2008. Cardiac plasticity. *The New England journal of medicine*, 358(13), pp.1370–1380.

Hirotani, M. et al., 1999. NH2-terminal BH4 domain of Bcl-2 is functional for heterodimerization with Bax and inhibition of apoptosis. *The Journal of biological chemistry*, 274(29), pp.20415–20.

Holly, T.A. et al., 1999. Caspase inhibition reduces myocyte cell death induced by myocardial ischemia and reperfusion in vivo. *Journal of molecular and cellular cardiology*, 31(9), pp.1709–15.

Horio, T. et al., 2000. Inhibitory regulation of hypertrophy by endogenous atrial natriuretic peptide in cultured cardiac myocytes. *Hypertension (Dallas, Tex. : 1979)*, 35(1 Pt 1), pp.19–24.

Houde, C. et al., 2004. Caspase-7 expanded function and intrinsic expression level underlies strain-specific brain phenotype of caspase-3-null mice. *The Journal of neuroscience : the official journal of the Society for Neuroscience*, 24(44), pp.9977–84.

Hu, W.-S. et al., 2014. Gelsolin (GSN) induces cardiomyocyte hypertrophy and BNP expression via p38 signaling and GATA-4 transcriptional factor activation. *Molecular and cellular biochemistry*, 390(1–2), pp.263–270.

Hudlicka, O., Brown, M. & Egginton, S., 1992. Angiogenesis in skeletal and cardiac muscle. *Physiological reviews*, 72(2), pp.369–417.

Janmey, P.A. & Stossel, T.P., 1989. Gelsolin-polyphosphoinositide interaction. Full expression of gelsolin-inhibiting function by polyphosphoinositides in vesicular form and inactivation by dilution, aggregation, or masking of the inositol head group. *The Journal of biological chemistry*, 264(9), pp.4825–31.

Jayakumar, J. et al., 2001. Heat shock protein 70 gene transfection protects mitochondrial and ventricular function against ischemia-reperfusion injury. *Circulation*, 104(12 Suppl 1), pp.I303-7.

Jego, G. et al., 2013. Targeting heat shock proteins in cancer. *Cancer letters*, 332(2), pp.275–85.

Ji, H. et al., 2008. Difference gel electrophoresis analysis of Ras-transformed fibroblast cell-derived exosomes. *Electrophoresis*, 29(12), pp.2660–71.

Kamada, S. et al., 2005. Nuclear translocation of caspase-3 is dependent on its proteolytic activation and recognition of a substrate-like protein(s). *The Journal of biological chemistry*, 280(2), pp.857–60.

Kamradt, M.C. et al., 2002. The small heat shock protein alpha B-crystallin negatively regulates apoptosis during myogenic differentiation by inhibiting caspase-3 activation. *The Journal of biological chemistry*, 277(41), pp.38731–38736.

Kamradt, M.C., Chen, F. & Cryns, V.L., 2001. The small heat shock protein alpha B-crystallin negatively regulates cytochrome c- and caspase-8-dependent activation of caspase-3 by inhibiting its autoproteolytic maturation. *The Journal of biological chemistry*, 276(19), pp.16059–63.

Kang, S.J. et al., 2002. Distinct downstream pathways of caspase-11 in regulating apoptosis and cytokine maturation during septic shock response. *Cell death and differentiation*, 9(10), pp.1115–25.

Karliner, J.S., Kagiya, T. & Simpson, P.C., 1990. Effects of pertussis toxin on alpha 1-agonist-mediated phosphatidylinositide turnover and myocardial cell hypertrophy in neonatal rat ventricular myocytes. *Experientia*, 46(1), pp.81–4.

Kawaguchi, N. et al., 1995. Pathological changes of myocardial cytoskeleton in cardiomyopathic hamster. *Molecular and cellular biochemistry*, 144(1), pp.75–9.

Kerkela, R. & Force, T., 2006. Recent insights into cardiac hypertrophy and left ventricular remodeling. *Current heart failure reports*, 3(1), pp.14–8.

Kim, J.-H. et al., 2004. Downregulation of gelsolin and retinoic acid receptor beta expression in gastric cancer tissues through histone deacetylase 1. *Journal of gastroenterology and hepatology*, 19(2), pp.218–24.

Kircher, P. et al., 2015. Filamin A interacts with the coactivator MKL1 to promote the activity of the transcription factor SRF and cell migration. *Science Signaling*, 8(402), p.ra112-ra112.

Koenig, A. et al., 2008. Spatial differences in active caspase-8 defines its role in T-cell activation versus cell death. *Cell death and differentiation*, 15(11), pp.1701–1711.

Kolodziejczyk, S.M. et al., 1999. MEF2 is upregulated during cardiac hypertrophy and is required for normal post-natal growth of the myocardium. *Current biology : CB*, 9(20), pp.1203–6.

Kong, S.W. et al., 2005. Genetic expression profiles during physiological and pathological cardiac hypertrophy and heart failure in rats. *Physiological Genomics*, 21(1), pp.34–42.

Kothakota, S. et al., 1997. Caspase-3-generated fragment of gelsolin: effector of morphological change in apoptosis. *Science (New York, N.Y.)*, 278(5336), pp.294–8.

Kuhn, M. et al., 2002. Progressive cardiac hypertrophy and dysfunction in atrial natriuretic peptide receptor (GC-A) deficient mice. *Heart (British Cardiac Society)*, 87(4), pp.368–74.

Kurokawa, M. & Kornbluth, S., 2009. Caspases and kinases in a death grip. *Cell*, 138(5), pp.838–854.

Kuwahara, K. et al., 2007. Modulation of adverse cardiac remodeling by STARS, a mediator of MEF2 signaling and SRF activity. *The Journal of clinical investigation*, 117(5), pp.1324–34.

Kwiatkowski, D.J. et al., 1986. Plasma and cytoplasmic gelsolins are encoded by a single gene and contain a duplicated actin-binding domain. *Nature*, 323(6087), pp.455–8.

Kwiatkowski, D.J., 1988. Predominant induction of gelsolin and actin-binding protein during myeloid differentiation. *The Journal of biological chemistry*, 263(27), pp.13857–62.

Lakhani, S.A. et al., 2006. Caspases 3 and 7: Key Mediators of Mitochondrial Events of Apoptosis. *Science*, 311(5762), pp.847–851.

Lamkanfi, M. et al., 2006. Caspases leave the beaten track: caspase-mediated activation of NF-kappaB. *The Journal of cell biology*, 173(2), pp.165–71.

Lavandero, S. et al., 1998. Effect of inhibitors of signal transduction on IGF-1-induced protein synthesis associated with hypertrophy in cultured neonatal rat ventricular myocytes. *FEBS letters*, 422(2), pp.193–6.

Lechardeur, D. et al., 2000. Determinants of the nuclear localization of the heterodimeric DNA fragmentation factor (ICAD/CAD). *The Journal of cell biology*, 150(2), pp.321–34.

Lee, P.-S. et al., 2007. Plasma gelsolin is a marker and therapeutic agent in animal sepsis. *Critical care medicine*, 35(3), pp.849–55.

Lee, R.E.C. et al., 2010. Metacaspase Yca1 is required for clearance of insoluble protein aggregates. *Proceedings of the National Academy of Sciences of the United States of America*, 107(30), pp.13348–13353.

Leite, M.F., Page, E. & Ambler, S.K., 1994. Regulation of ANP secretion by endothelin-1 in cultured atrial myocytes: desensitization and receptor subtype. *The American journal of physiology*, 267(6 Pt 2), pp.H2193-203.

Li, G.H. et al., 2009. Gelsolin regulates cardiac remodeling after myocardial infarction through DNase I-mediated apoptosis. *Circulation research*, 104(7), pp.896–904.

Li, G.H. et al., 2012. Multifunctional roles of gelsolin in health and diseases. *Medicinal research reviews*, 32(5), pp.999–1025.

Li, J. et al., 2007. Caspase-11 regulates cell migration by promoting Aip1-Cofilin-mediated actin depolymerization. *Nature cell biology*, 9(3), pp.276–86.

Li, J., Tanhehco, E.J. & Russell, B., 2014. Actin dynamics is rapidly regulated by the PTEN and PIP2 signaling pathways leading to myocyte hypertrophy. *AJP: Heart and Circulatory Physiology*, 307(11), pp.H1618–H1625.

Liu, F. et al., 2004. Caspase-mediated Specific Cleavage of Human Histone Deacetylase 4. *Journal of Biological Chemistry*, 279(33), pp.34537–34546.

Madonna, R. et al., 2014. Co-activation of nuclear factor-kappaB and myocardin/serum response factor conveys the hypertrophy signal of high insulin levels in cardiac myoblasts. *The Journal of biological chemistry*, 289(28), pp.19585–19598.

Malet, G. et al., 2006. Small molecule inhibitors of Apaf-1-related caspase- 3/-9 activation that control mitochondrial-dependent apoptosis. *Cell death and differentiation*, 13(9), pp.1523–32.

Mandel-Gutfreund, Y., Kosti, I. & Larisch, S., 2011. ARTS, the unusual septin: structural and functional aspects. *Biological chemistry*, 392(8–9), pp.783–90.

Martin, P. et al., 2010. Granzyme B-induced and Caspase 3-dependent Cleavage of Gelsolin by Mouse Cytotoxic T Cells Modifies Cytoskeleton Dynamics. *Journal of Biological Chemistry*, 285(24), pp.18918–18927.

Matsudaira, P. & Janmey, P., 1988. Pieces in the actin-severing protein puzzle. *Cell*, 54(2), pp.139–40.

McFalls, E.O. et al., 2003. Mitochondrial function: the heart of myocardial preservation. *Journal of Laboratory and Clinical Medicine*, 142(3), pp.141–148.

McIlroy, D. et al., 1999. Involvement of caspase 3-activated DNase in internucleosomal DNA cleavage induced by diverse apoptotic stimuli. *Oncogene*, 18(31), pp.4401–4408.

McMullen, J.R. et al., 2003. Phosphoinositide 3-kinase(p110alpha) plays a critical role for the induction of physiological, but not pathological, cardiac hypertrophy. *Proceedings of the National Academy of Sciences of the United States of America*, 100(21), pp.12355–60.

McMullen, J.R. et al., 2007. Protective effects of exercise and phosphoinositide 3-kinase(p110alpha) signaling in dilated and hypertrophic cardiomyopathy. *Proceedings of the National Academy of Sciences of the United States of America*, 104(2), pp.612–7.

McMullen, J.R. et al., 2004. The insulin-like growth factor 1 receptor induces physiological heart growth via the phosphoinositide 3-kinase(p110alpha) pathway. *The Journal of biological chemistry*, 279(6), pp.4782–93.

McMullen, J.R. & Jennings, G.L., 2007. Differences between pathological and physiological cardiac hypertrophy: novel therapeutic strategies to treat heart failure. *Clinical and experimental pharmacology & physiology*, 34(4), pp.255–262.

Minina, E.A. et al., 2017. Metacaspases versus caspases in development and cell fate regulation. *Cell death and differentiation*, 24(8), pp.1314–1325.

Molkentin, J.D. et al., 1998. A calcineurin-dependent transcriptional pathway for cardiac hypertrophy. *Cell*, 93(2), pp.215–28.

Montgomery, R.L. et al., 2008. Maintenance of cardiac energy metabolism by histone deacetylase 3 in mice. *Journal of Clinical Investigation*, 118(11), pp.3588–3597.

Mukerjee, N. et al., 2000. Caspase-mediated proteolytic activation of calcineurin in thapsigargin-mediated apoptosis in SH-SY5Y neuroblastoma cells. *Archives of biochemistry and biophysics*, 379(2), pp.337–43.

Murray, T.V.A. et al., 2008. A non-apoptotic role for caspase-9 in muscle differentiation. *Journal of cell science*, 121(Pt 22), pp.3786–3793.

Muzio, M. et al., 1998. An induced proximity model for caspase-8 activation. *The Journal of biological chemistry*, 273(5), pp.2926–30.

Nag, S. et al., 2013. Gelsolin: The tail of a molecular gymnast. *Cytoskeleton*, 70(7), pp.360–384.

Nakayama, H. et al., 2010. The IP3 receptor regulates cardiac hypertrophy in response to select stimuli. *Circulation research*, 107(5), pp.659–66.

Narula, J. et al., 1996. Apoptosis in Myocytes in End-Stage Heart Failure. *New England Journal of Medicine*, 335(16), pp.1182–1189.

Naya, F.J. et al., 2002. Mitochondrial deficiency and cardiac sudden death in mice lacking the MEF2A transcription factor. *Nature medicine*, 8(11), pp.1303–9.

Nguyen, J.T. & Wells, J.A., 2003. Direct activation of the apoptosis machinery as a mechanism to target cancer cells. *Proceedings of the National Academy of Sciences*, 100(13), pp.7533–7538.

Nicol, R.L. et al., 2001. Activated MEK5 induces serial assembly of sarcomeres and eccentric cardiac hypertrophy. *The EMBO journal*, 20(11), pp.2757–67.

Nishida, K. & Otsu, K., 2008. Cell death in heart failure. *Circulation journal : official journal of the Japanese Circulation Society*, 72 Suppl A, pp.A17-21.

Van Noorden, C.J., 2001. The history of Z-VAD-FMK, a tool for understanding the significance of caspase inhibition. *Acta histochemica*, 103(3), pp.241–51.

O'Riordan, M.X.D. et al., 2008. Inhibitor of apoptosis proteins in eukaryotic evolution and development: a model of thematic conservation. *Developmental cell*, 15(4), pp.497–508.

Ohsawa, S. et al., 2010. Maturation of the olfactory sensory neurons by Apaf-1/caspase-9-mediated caspase activity. *Proceedings of the National Academy of Sciences*, 107(30), pp.13366–13371.

Olivetti, G. et al., 1997. Apoptosis in the failing human heart. *The New England journal of medicine*, 336(16), pp.1131–41.

Olson, E.N., 2006. Gene Regulatory Networks in the Evolution and Development of the Heart. *Science*, 313(5795), pp.1922–1927.

Olson, E.N., Backs, J. & McKinsey, T.A., 2006. Control of cardiac hypertrophy and heart failure by histone acetylation/deacetylation. *Novartis Foundation symposium*, 274, pp.3-12–9, 152–5, 272–6.

Olson, E.N. & Srivastava, D., 1996. Molecular pathways controlling heart development. *Science (New York, N.Y.)*, 272(5262), pp.671–6.

Oltersdorf, T. et al., 2005. An inhibitor of Bcl-2 family proteins induces regression of solid tumours. *Nature*, 435(7042), pp.677–681.

Opferman, J.T. & Korsmeyer, S.J., 2003. Apoptosis in the development and maintenance of the immune system. *Nature immunology*, 4(5), pp.410–415.

Paroni, G. et al., 2004. Caspase-dependent regulation of histone deacetylase 4 nuclear-cytoplasmic shuttling promotes apoptosis. *Molecular biology of the cell*, 15(6), pp.2804–2818.

Paunio, T. et al., 1997. Tissue distribution and levels of gelsolin mRNA in normal individuals and patients with gelsolin-related amyloidosis. *FEBS letters*, 406(1–2), pp.49–55.

Peterson, Q.P. et al., 2009. PAC-1 Activates Procaspase-3 in Vitro through Relief of Zinc-Mediated Inhibition. *Journal of Molecular Biology*, 388(1), pp.144–158.

Piacentino, V. 3rd et al., 2012. X-linked inhibitor of apoptosis protein-mediated attenuation of apoptosis, using a novel cardiac-enhanced adeno-associated viral vector. *Human gene therapy*, 23(6), pp.635–646.

Ploner, C., Kofler, R. & Villunger, A., 2008. Noxa: at the tip of the balance between life and death. *Oncogene*, 27, pp.S84–S92.

Potts, M.B. et al., 2005. Reduced Apaf-1 levels in cardiomyocytes engage strict regulation of apoptosis by endogenous XIAP. *The Journal of cell biology*, 171(6), pp.925–930.

Putinski, C. et al., 2013. Intrinsic-mediated caspase activation is essential for cardiomyocyte hypertrophy. *Proceedings of the National Academy of Sciences of the United States of America*, 110(43), pp.E4079-87.

Putt, K.S. et al., 2006. Small-molecule activation of procaspase-3 to caspase-3 as a personalized anticancer strategy. *Nature Chemical Biology*, 2(10), pp.543–550.

Ramirez, M.T. et al., 1997. The MEKK-JNK pathway is stimulated by alpha1-adrenergic receptor and ras activation and is associated with in vitro and in vivo cardiac hypertrophy. *The Journal of biological chemistry*, 272(22), pp.14057–61.

Rathore, N., Matta, H. & Chaudhary, P.M., 2004. An Evolutionary Conserved Pathway of Nuclear Factor-κB Activation Involving Caspase-mediated Cleavage and N-end Rule Pathway-mediated Degradation of IκBα. *Journal of Biological Chemistry*, 279(38), pp.39358–39365.

Regula, K.M. & Kirshenbaum, L.A., 2005. Apoptosis of ventricular myocytes: a means to an end. *Journal of molecular and cellular cardiology*, 38(1), pp.3–13.

Rérole, A.-L., Jego, G. & Garrido, C., 2011. Hsp70: Anti-apoptotic and Tumorigenic Protein. In *Methods in molecular biology (Clifton, N.J.)*. pp. 205–230.

Rithidech, K.N. et al., 2009. Protein expression profiles in pediatric multiple sclerosis: potential biomarkers. *Multiple sclerosis (Houndmills, Basingstoke, England)*, 15(4), pp.455–64.

Rodriguez, I. et al., 1996. Systemic injection of a tripeptide inhibits the intracellular activation of CPP32-like proteases in vivo and fully protects mice against Fas-mediated fulminant liver destruction and death. *The Journal of experimental medicine*, 184(5), pp.2067–72.

Roh, J. et al., 2016. The Role of Exercise in Cardiac Aging. *Circulation Research*, 118(2), pp.279–295.

van Rooij, E. et al., 2010. Myocyte enhancer factor 2 and class II histone deacetylases control a gender-specific pathway of cardioprotection mediated by the estrogen receptor. *Circulation research*, 106(1), pp.155–65.

Roth, H.S. & Hergenrother, P.J., 2016. Derivatives of Procaspase-Activating Compound 1 (PAC-1) and their Anticancer Activities. *Current medicinal chemistry*, 23(3), pp.201–41.

Rouayrenc, J.F. et al., 1984. Muscle gelsolin: isolation from heart tissue and characterization as an integral myofibrillar protein. *FEBS letters*, 167(1), pp.52–8.

Sadoshima, J. et al., 1993. Autocrine release of angiotensin II mediates stretch-induced hypertrophy of cardiac myocytes in vitro. *Cell*, 75(5), pp.977–84.

Sadoshima, J. & Izumo, S., 1993. Signal transduction pathways of angiotensin II--induced c-fos gene expression in cardiac myocytes in vitro. Roles of phospholipid-derived second messengers. *Circulation research*, 73(3), pp.424–38.

Saelens, X. et al., 2004. Toxic proteins released from mitochondria in cell death. *Oncogene*, 23(16), pp.2861–2874.

Sahara, S. et al., 1999. Acinus is a caspase-3-activated protein required for apoptotic chromatin condensation. *Nature*, 401(6749), pp.168–173.

Saleh, A. et al., 2000. Negative regulation of the Apaf-1 apoptosome by Hsp70. *Nature cell biology*, 2(8), pp.476–83.

Salvesen, G.S. & Riedl, S.J., 2008. Caspase Mechanisms. In *Advances in experimental medicine and biology*. pp. 13–23.

Samant, S.A. et al., 2015. Histone Deacetylase 3 (HDAC3)-dependent Reversible Lysine Acetylation of Cardiac Myosin Heavy Chain Isoforms Modulates Their Enzymatic and Motor Activity. *Journal of Biological Chemistry*, 290(25), pp.15559–15569.

Scholz, A. & Hinssen, H., 1995. Biphasic pattern of gelsolin expression and variations in gelsolin-actin interactions during myogenesis. *Experimental cell research*, 219(2), pp.384–91.

Schotte, P. et al., 1999. Non-specific effects of methyl ketone peptide inhibitors of caspases. *FEBS letters*, 442(1), pp.117–21.

Selden, L.A. et al., 1998. Severing of F-actin by the amino-terminal half of gelsolin suggests internal cooperativity in gelsolin. *Biophysical journal*, 75(6), pp.3092–3100.

Shiojima, I. & Walsh, K., 2006. Regulation of cardiac growth and coronary angiogenesis by the Akt/PKB signaling pathway. *Genes & Development*, 20(24), pp.3347–3365.

Smith, D.B. et al., 1987. Quantitative measurement of plasma gelsolin and its incorporation into fibrin clots. *The Journal of laboratory and clinical medicine*, 110(2), pp.189–95.

Smith, M.I., Huang, Y.Y. & Deshmukh, M., 2009. Skeletal muscle differentiation evokes endogenous XIAP to restrict the apoptotic pathway. *PloS one*, 4(3), p.e5097.

Sopontammarak, S. et al., 2005. Mitogen-activated protein kinases (p38 and c-Jun NH2-terminal kinase) are differentially regulated during cardiac volume and pressure overload hypertrophy. *Cell biochemistry and biophysics*, 43(1), pp.61–76.

Sotiropoulos, A. et al., 1999. Signal-regulated activation of serum response factor is mediated by changes in actin dynamics. *Cell*, 98(2), pp.159–69.

Sugden, P.H. & Clerk, A., 1998. Regulation of mitogen-activated protein kinase cascades in the heart. *Advances in enzyme regulation*, 38, pp.87–98.

Suhler, E. et al., 1997. Decreased plasma gelsolin concentrations in acute liver failure, myocardial infarction, septic shock, and myonecrosis. *Critical care medicine*, 25(4), pp.594–8.

Sun, H.Q. et al., 1999. Gelsolin, a multifunctional actin regulatory protein. *The Journal of biological chemistry*, 274(47), pp.33179–82.

Sussman, M.A. et al., 1998. Prevention of cardiac hypertrophy in mice by calcineurin inhibition. *Science (New York, N.Y.)*, 281(5383), pp.1690–3.

Svanström, A. & Grantham, J., 2016. The molecular chaperone CCT modulates the activity of the actin filament severing and capping protein gelsolin in vitro. *Cell stress & chaperones*, 21(1), pp.55–62.

Taigen, T. et al., 2000. Targeted inhibition of calcineurin prevents agonist-induced cardiomyocyte hypertrophy. *Proceedings of the National Academy of Sciences of the United States of America*, 97(3), pp.1196–201.

Takahashi, H., 1982. [Echocardiographic observations of hypertensive heart disease: a follow-up study]. *Journal of cardiography*, 12(4), pp.953–961.

Tanaka, M. et al., 1995. Gelsolin: a candidate for suppressor of human bladder cancer. *Cancer research*, 55(15), pp.3228–32.

Timmer, J.C. & Salvesen, G.S., 2007. Caspase substrates. *Cell Death and Differentiation*, 14(1), pp.66–72.

Turowec, J.P. et al., 2014. An unbiased proteomic screen reveals caspase cleavage is positively and negatively regulated by substrate phosphorylation. *Molecular & cellular proteomics : MCP*, 13(5), pp.1184–1197.

Unger, A. & Hinssen, H., 2010. Electron-microscopical localization of gelsolin in various crustacean muscles. *Cell and Tissue Research*, 341(2), pp.313–323.

Vazquez, A. et al., 2008. The genetics of the p53 pathway, apoptosis and cancer therapy. *Nature Reviews Drug Discovery*, 7(12), pp.979–987.

Verdecchia, P. et al., 1994. Asymmetric left ventricular remodeling due to isolated septal thickening in patients with systemic hypertension and normal left ventricular masses. *The American journal of cardiology*, 73(4), pp.247–252.

Vitale, G. et al., 2008. Circulating IGF-I levels are associated with increased biventricular contractility in top-level rowers. *Clinical endocrinology*, 69(2), pp.231–6.

Walsh, J.G. et al., 2008. Executioner caspase-3 and caspase-7 are functionally distinct proteases. *Proceedings of the National Academy of Sciences of the United States of America*, 105(35), pp.12815–9.

Wang, H. et al., 2008. Time course of plasma gelsolin concentrations during severe sepsis in critically ill surgical patients. *Critical care (London, England)*, 12(4), p.R106.

Wang, X. et al., 1999. Chronic pressure overload cardiac hypertrophy and failure in guinea pigs: II. Cytoskeletal remodeling. *Journal of molecular and cellular cardiology*, 31(2), pp.319–31.

Wang, Y. et al., 2016. The discovery of a novel inhibitor of apoptotic protease activating factor-1 (Apaf-1) for ischemic heart: synthesis, activity and target identification. *Scientific Reports*, 6(1), p.29820.

Way, M. et al., 1989. Expression of human plasma gelsolin in Escherichia coli and dissection of actin binding sites by segmental deletion mutagenesis. *The Journal of cell biology*, 109(2), pp.593–605.

Way, M. & Weeds, A., 1988. Nucleotide sequence of pig plasma gelsolin. Comparison of protein sequence with human gelsolin and other actin-severing proteins shows strong homologies and evidence for large internal repeats. *Journal of molecular biology*, 203(4), pp.1127–33.

Weber, G.F. & Menko, A.S., 2005. The canonical intrinsic mitochondrial death pathway has a non-apoptotic role in signaling lens cell differentiation. *The Journal of biological chemistry*, 280(23), pp.22135–22145.

Welton, J.L. et al., 2010. Proteomics Analysis of Bladder Cancer Exosomes. *Molecular & Cellular Proteomics*, 9(6), pp.1324–1338.

Whelan, R.S., Kaplinskiy, V. & Kitsis, R.N., 2010. Cell death in the pathogenesis of heart disease: mechanisms and significance. *Annual review of physiology*, 72(1), pp.19–44.

Winston, J.S. et al., 2001. Downregulation of gelsolin correlates with the progression to breast carcinoma. *Breast cancer research and treatment*, 65(1), pp.11–21.

Wu, X., Golden, K. & Bodmer, R., 1995. Heart development in Drosophila requires the segment polarity gene wingless. *Developmental biology*, 169(2), pp.619–28.

Yang, J. et al., 2000. Decreased SLIM1 expression and increased gelsolin expression in failing human hearts measured by high-density oligonucleotide arrays. *Circulation*, 102(25), pp.3046–52.

Yang, J.-Y. et al., 2004. Partial cleavage of RasGAP by caspases is required for cell survival in mild stress conditions. *Molecular and cellular biology*, 24(23), pp.10425–10436.

Yang, J.Y. & Widmann, C., 2001. Antiapoptotic signaling generated by caspase-induced cleavage of RasGAP. *Molecular and cellular biology*, 21(16), pp.5346–5358.

Yang, Q.-H. & Du, C., 2004. Smac/DIABLO selectively reduces the levels of c-IAP1 and c-IAP2 but not that of XIAP and livin in HeLa cells. *The Journal of biological chemistry*, 279(17), pp.16963–70.

Yang, W.-M. et al., 2002. Functional Domains of Histone Deacetylase-3. *Journal of Biological Chemistry*, 277(11), pp.9447–9454.

Yaoita, H. et al., 1998. Attenuation of ischemia/reperfusion injury in rats by a caspase inhibitor. *Circulation*, 97(3), pp.276–81.

Yarbrough, W.M. et al., 2010. Caspase inhibition modulates left ventricular remodeling following myocardial infarction through cellular and extracellular mechanisms. *Journal of cardiovascular pharmacology*, 55(4), pp.408–16.

Yarbrough, W.M. et al., 2003. Pharmacologic inhibition of intracellular caspases after myocardial infarction attenuates left ventricular remodeling: a potentially novel pathway. *The Journal of thoracic and cardiovascular surgery*, 126(6), pp.1892–9.

Yin, H.L. et al., 1981. Ca2+ control of actin filament length. Effects of macrophage gelsolin on actin polymerization. *The Journal of biological chemistry*, 256(18), pp.9693–7.

Yin, H.L. & Stossel, T.P., 1979. Control of cytoplasmic actin gel-sol transformation by gelsolin, a calcium-dependent regulatory protein. *Nature*, 281(5732), pp.583–6.

Yin, H.L. & Stull, J.T., 1999. Proteins that regulate dynamic actin remodeling in response to membrane signaling minireview series. *The Journal of biological chemistry*, 274(46), pp.32529–30.

Yoshida, K. et al., 1996. Targeted disruption of gp130, a common signal transducer for the interleukin 6 family of cytokines, leads to myocardial and hematological disorders. *Proceedings of the National Academy of Sciences of the United States of America*, 93(1), pp.407–11.

Young, J.C. et al., 2004. Pathways of chaperone-mediated protein folding in the cytosol. *Nature reviews. Molecular cell biology*, 5(10), pp.781–91.

Zaffran, S. & Frasch, M., 2002. Early signals in cardiac development. *Circulation research*, 91(6), pp.457–69.

Zermati, Y. et al., 2001. Caspase activation is required for terminal erythroid differentiation. *The Journal of experimental medicine*, 193(2), pp.247–254.

Zhang, C.L. et al., 2002. Class II histone deacetylases act as signal-responsive repressors of cardiac hypertrophy. *Cell*, 110(4), pp.479–88.

Zhou, Q. et al., 1998. Interaction of the baculovirus anti-apoptotic protein p35 with caspases. Specificity, kinetics, and characterization of the caspase/p35 complex. *Biochemistry*, 37(30), pp.10757–65.

Zhuang, J. & Brady, H.J.M., 2006. Emerging role of Mcl-1 in actively counteracting BH3-only proteins in apoptosis. *Cell Death and Differentiation*, 13(8), pp.1263–1267.

References: Chapter 2

1. Kolodziejczyk SM, et al. (1999) MEF2 is upregulated during cardiac hypertrophy and is required for normal post-natal growth of the myocardium. *Curr Biol* 9(20):1203–6.

2. Liu Q, Chen Y, Auger-Messier M, Molkentin JD (2012) Interaction between NFκB and NFAT coordinates cardiac hypertrophy and pathological remodeling. *Circ Res* 110(8):1077–86.

3. Olson EN, Backs J, McKinsey TA (2006) Control of cardiac hypertrophy and heart failure by histone acetylation/deacetylation. *Novartis Found Symp* 274:3-12–9, 152–5, 272–6.

4. Nicol RL, Frey N, Olson EN (2000) From the sarcomere to the nucleus: role of genetics and signaling in structural heart disease. *Annu Rev Genomics Hum Genet* 1:179–223.

5. Oka T, Komuro I (2008) Molecular mechanisms underlying the transition of cardiac hypertrophy to heart failure. *Circ J* 72 Suppl A:A13-6.

6. Dorn GW (2009) Having a change of heart: reversing the suicidal proclivities of cardiac myocytes. *Trans Am Clin Climatol Assoc* 120:189–98.

7. van Berlo JH, Maillet M, Molkentin JD (2013) Signaling effectors underlying pathologic growth and remodeling of the heart. *J Clin Invest* 123(1):37–45.

8. Jobe LJ, et al. (2009) TNF-alpha inhibition attenuates adverse myocardial remodeling in a rat model of volume overload. *Am J Physiol Heart Circ Physiol* 297(4):H1462-8.

9. Sun M, et al. (2007) Tumor Necrosis Factor- Mediates Cardiac Remodeling and Ventricular Dysfunction After Pressure Overload State. *Circulation* 115(11):1398–1407.

10. Badorff C, et al. (2002) Fas receptor signaling inhibits glycogen synthase kinase 3β and induces cardiac hypertrophy following pressure overload. *J Clin Invest* 109(3):373–381.

11. McDermott-Roe C, et al. (2011) Endonuclease G is a novel determinant of cardiac hypertrophy and mitochondrial function. *Nature* 478(7367):114–118.

12. Abdul-Ghani M, et al. (2011) Wnt11 promotes cardiomyocyte development by caspase-mediated suppression of canonical Wnt signals. *Mol Cell Biol* 31(1):163–178.

13. Abdul-Ghani M, Megeney LA (2008) Rehabilitation of a contract killer: caspase-3 directs stem cell differentiation. *Cell Stem Cell* 2(6):515–516.

14. Fuchs Y, Steller H (2011) Programmed cell death in animal development and disease. *Cell* 147(4):742–758.

15. Larsen BD, et al. (2010) Caspase 3/caspase-activated DNase promote cell differentiation by inducing DNA strand breaks. *Proc Natl Acad Sci U S A* 107(9):4230–4235.

16. Lee REC, Brunette S, Puente LG, Megeney LA (2010) Metacaspase Yca1 is required for clearance of insoluble protein aggregates. *Proc Natl Acad Sci U S A* 107(30):13348–13353.

17. Coll KE, Joseph SK, Corkey BE, Williamson JR (1982) Determination of the matrix free Ca2+ concentration and kinetics of Ca2+ efflux in liver and heart mitochondria. *J Biol Chem* 257(15):8696–704.

18. Nagendran J, et al. (2008) A dynamic and chamber-specific mitochondrial remodeling in right ventricular hypertrophy can be therapeutically targeted. *J Thorac Cardiovasc Surg* 136(1):168–178.e3.

19. Garcia R, Thibault G, Cantin M (1987) Correlation between cardiac hypertrophy and plasma levels of atrial natriuretic factor in non-spontaneous models of hypertension in the rat. *Biochem Biophys Res Commun* 145(1):532–41.

20. Ploner C, Kofler R, Villunger A (2008) Noxa: at the tip of the balance between life and death. *Oncogene* 27:S84–S92.

21. Zhuang J, Brady HJM (2006) Emerging role of Mcl-1 in actively counteracting BH3-only proteins in apoptosis. *Cell Death Differ* 13(8):1263–1267.

22. Ryan CA, et al. (2002) Inhibitor specificity of recombinant and endogenous caspase-9. *Biochem J* 366(Pt 2):595–601.

23. FUENTES-PRIOR P, SALVESEN GS (2004) The protein structures that shape caspase activity, specificity, activation and inhibition. *Biochem J* 384(2):201–232.

24. Clem RJ (2001) Baculoviruses and apoptosis: the good, the bad, and the ugly. *Cell Death Differ* 8(2):137–43.

25. Zhang CL, et al. (2002) Class II histone deacetylases act as signal-responsive repressors of cardiac hypertrophy. *Cell* 110(4):479–88.

26. Escaffit F, et al. (2007) Cleavage and cytoplasmic relocalization of histone deacetylase 3 are important for apoptosis progression. *Mol Cell Biol* 27(2):554–67.

27. Liu F, Dowling M, Yang X-J, Kao GD (2004) Caspase-mediated Specific Cleavage of Human Histone Deacetylase 4. *J Biol Chem* 279(33):34537–34546.

28. Paroni G, et al. (2004) Caspase-dependent regulation of histone deacetylase 4 nuclear-cytoplasmic shuttling promotes apoptosis. *Mol Biol Cell* 15(6):2804–2818.

29. Montgomery RL, et al. (2008) Maintenance of cardiac energy metabolism by histone deacetylase 3 in mice. *J Clin Invest* 118(11):3588–3597.

30. Liu I-C, Chiu S-W, Lee H-Y, Leu J-Y (2012) The histone deacetylase Hos2 forms an Hsp42-dependent cytoplasmic granule in quiescent yeast cells. *Mol Biol Cell* 23(7):1231–1242.

31. Waltregny D, et al. (2005) Histone deacetylase HDAC8 associates with smooth muscle -actin and is essential for smooth muscle cell contractility. *FASEB J* 19(8):966–8.

32. Gordon JW, Shaw JA, Kirshenbaum LA (2011) Multiple Facets of NF-κB in the Heart. *Circ Res* 108(9):1122–1132.

33. Lamkanfi M, Declercq W, Vanden Berghe T, Vandenabeele P (2006) Caspases leave the beaten track: caspase-mediated activation of NF-kappaB. *J Cell Biol* 173(2):165–71.

34. Rathore N, Matta H, Chaudhary PM (2004) An Evolutionary Conserved Pathway of Nuclear Factor-κB Activation Involving Caspase-mediated Cleavage and N-end Rule Pathway-mediated Degradation of IκBα. *J Biol Chem* 279(38):39358–39365.

35. Su H, et al. (2005) Requirement for Caspase-8 in NF- B Activation by Antigen Receptor. *Science (80-)* 307(5714):1465–1468.

36. Peterson QP, et al. (2009) PAC-1 Activates Procaspase-3 in Vitro through Relief of Zinc-Mediated Inhibition. *J Mol Biol* 388(1):144–158.

37. Putt KS, et al. (2006) Small-molecule activation of procaspase-3 to caspase-3 as a personalized anticancer strategy. *Nat Chem Biol* 2(10):543–550.

38. Adams JW, et al. (2000) Cardiomyocyte apoptosis induced by Galphaq signaling is mediated by permeability transition pore formation and activation of the mitochondrial death pathway. *Circ Res* 87(12):1180–7.

39. Balakumar P, Singh M (2006) The possible role of caspase-3 in pathological and physiological cardiac hypertrophy in rats. *Basic Clin Pharmacol Toxicol* 99(6):418–424.

40. Balsam LB, Kofidis T, Robbins RC (2005) Caspase-3 inhibition preserves myocardial geometry and long-term function after infarction. *J Surg Res* 124(2):194–200.

41. Adams JW, et al. (1998) Enhanced Galphaq signaling: a common pathway mediates cardiac hypertrophy and apoptotic heart failure. *Proc Natl Acad Sci U S A* 95(17):10140–10145.

42. D'Angelo DD, et al. (1997) Transgenic Galphaq overexpression induces cardiac contractile failure in mice. *Proc Natl Acad Sci U S A* 94(15):8121–6.

43. Communal C, et al. (2002) Functional consequences of caspase activation in cardiac myocytes. *Proc Natl Acad Sci U S A* 99(9):6252–6256.

44. Fischer U, Jänicke RU, Schulze-Osthoff K (2003) Many cuts to ruin: a comprehensive update of caspase substrates. *Cell Death Differ* 10(1):76–100.

45. Moretti A, et al. (2002) Essential myosin light chain as a target for caspase-3 in failing myocardium. *Proc Natl Acad Sci U S A* 99(18):11860–5.

46. Solinet S, Vitale ML (2008) Isoform B of myosin II heavy chain mediates actomyosin contractility during TNFalpha-induced apoptosis. *J Cell Sci* 121(Pt 10):1681–92.

47. Deedwania PC, Carbajal E (2012) Evidence-Based Therapy for Heart Failure. *Med Clin North Am* 96(5):915–931.

Appendix I:

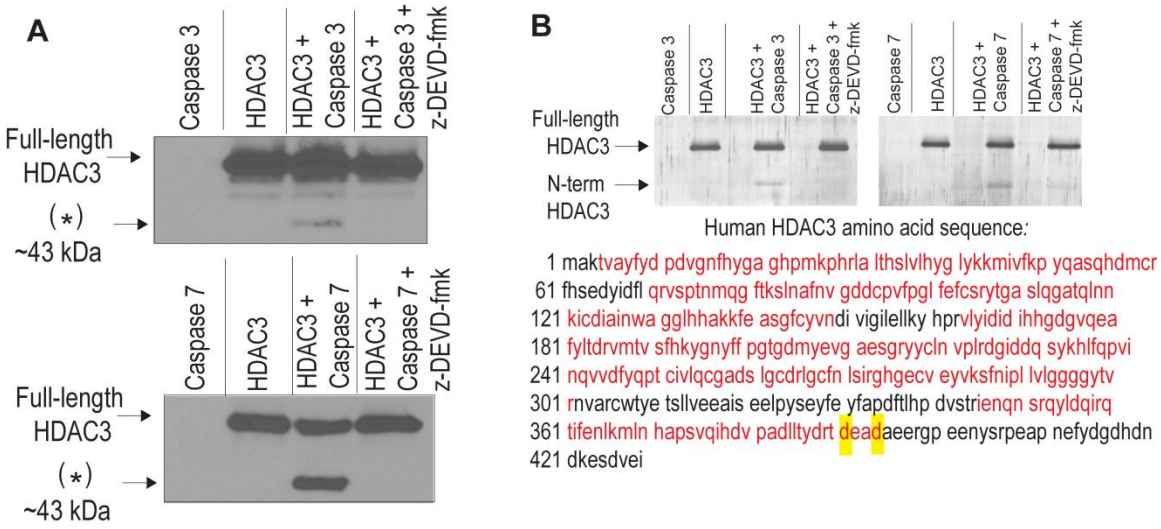


Figure 1. HDAC3 is cleaved by effector caspases 3 and 7. (A) HDAC3 *in vitro* cleavage assays using recombinant human HDAC3 and both caspase 3 and caspase 7. Blots were probed with an antibody against amino acids 309-425 of HDAC3 (C-terminus). Assays were completed for caspase alone, HDAC3 alone (full length HDAC3 ~50 kDa), HDAC3 with 3 units of active caspase 3 or caspase 7 (3 hr) or HDAC3 with caspase and effector caspase inhibitor z-DEVD-fmk. This depicts a smaller molecular weight HDAC3 fragment (asterisk, ~43 kDa) when HDAC3 is incubated with caspase 3 or 7 which is reduced with z-DEVD-fmk. More efficient cleavage by caspase 7 is proposed. (B) Similar to A recombinant HDAC3 was subjected to an *in vitro* caspase cleavage reaction followed by SDS/PAGE and silver stain (silver stained gel shown). The protein fragments were isolated and processed by LC-MS/MS. Analysis of the caspase cleavage site within the HDAC3 amino acid sequence. The red peptides represent those identified from the N-terminal fragment (~43 kDa fragment). The C-terminal fragment (~5 kDa) was not observed. The aspartic acid residues targeted by caspase 3/7 are highlighted in yellow. Note that mass spectrometry analysis showed that caspases 3 and 7 cleave at D394 while caspase 7 can additionally cleave at D391.

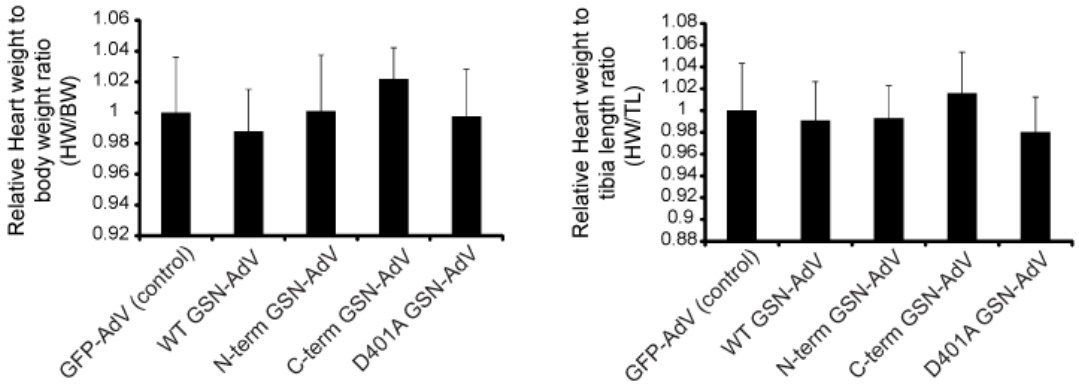


Figure 2. End-point heart weight to body weight and heart weight to tibia length ratio analysis of intra-myocardial control GFP or gelsolin adenovirus injected rats. End-point rat hearts were weighed and ratios were calculated compared to end-point rat weight (left) or tibia length (right). No significant differences were noted between rat groups suggesting no significant change in organ size as a result of AdV treatments. Values were normalized to the GFP-AdV control.

Appendix II:

Manuscript:

Abdul-Ghani, M. et al. (2017) Cardiotrophin 1 stimulates beneficial myogenic and vascular remodeling of the heart. Cell Research. 27(10): 1195-1215.

Open
ORIGINAL ARTICLE

Cell Research (2017) 27:1195-1215.
www.nature.com/cr

Cardiotrophin 1 stimulates beneficial myogenic and vascular remodeling of the heart

Mohammad Abdul-Ghani[1, 2, *], Colin Suen[1, 2, *], Baohua Jiang[1], Yupu Deng[1], Jonathan J Weldrick[2, 3], Charis Putinski[1, 2], Steve Brunette[1], Pasan Fernando[1, 4], Tom T Lee[5], Peter Flynn[5], Frans H H Leenen[2, 6, 3], Patrick G Burgon[2, 6, 3], Duncan J Stewart[1, 2, 6], Lynn A Megeney[1, 2, 6]

[1]Sprott Centre for Stem Cell Research, Regenerative Medicine Program, Ottawa Hospital Research Institute, Ottawa Hospital, Ottawa, Ontario K1H 8L6, Canada; [2]Department of Cellular and Molecular Medicine, Faculty of Medicine, University of Ottawa, Ottawa, Ontario K1H 8M5, Canada; [3]University of Ottawa Heart Institute, Ottawa, Ontario K1Y 4W7, Canada; [4]Department of Biology, Carleton University, Ottawa, Ontario K1S 5B6, Canada; [5]Fate Therapeutics Inc., 3535 General Atomics Court Suite 200, San Diego, CA 92121, USA; [6]Department of Medicine (Cardiology), Faculty of Medicine, University of Ottawa, Ottawa, Ontario K1H 8M5, Canada

The post-natal heart adapts to stress and overload through hypertrophic growth, a process that may be pathologic or beneficial (physiologic hypertrophy). Physiologic hypertrophy improves cardiac performance in both healthy and diseased individuals, yet the mechanisms that propagate this favorable adaptation remain poorly defined. We identify the cytokine cardiotrophin 1 (CT1) as a factor capable of recapitulating the key features of physiologic growth of the heart including transient and reversible hypertrophy of the myocardium, and stimulation of cardiomyocyte-derived angiogenic signals leading to increased vascularity. The capacity of CT1 to induce physiologic hypertrophy originates from a CK2-mediated restraining of caspase activation, preventing the transition to unrestrained pathologic growth. Exogenous CT1 protein delivery attenuated pathology and restored contractile function in a severe model of right heart failure, suggesting a novel treatment option for this intractable cardiac disease.

***Keywords*:** cardiotrophin 1; cardiac; hypertrophy; right heart failure; physiologic; reversible; caspase
Cell Research (2017) **27**:1195-1215. doi:10.1038/cr.2017.87; published online 8 August 2017

Introduction

Heart muscle growth, commonly referred to as cardiac hypertrophy, is a compensatory response that matches organ size to the systemic demands of the body. Hypertrophy can be a detrimental or beneficial adaptation, depending on the type of growth that occurs. In pathologic hypertrophy, heart muscle mass increases (wall thickness) without a corresponding improvement in function. Pathologic hypertrophy is generally irreversible and readily transitions to heart failure (HF), making this maladaptive process a leading cause of morbidity and mortality [1]. Given the prominence in disease etiology, the biochemical and molecular characteristics of pathologic hypertrophy have been intensely studied and documented [2, 3].

Physiologic cardiac hypertrophy is a form of beneficial remodeling, characterized by a modest increase in heart mass with improved contractile function that is reversible. Both pregnancy and endurance exercise provide well-documented means to engage this form of organ growth, a response that can also directly antagonize pathologic hypertrophy and the progression to HF [4, 5]. Akt- and MAPK-mediated signaling cascades appear to be consistent molecular signatures of physiologic hypertrophy, yet there is a paucity of definitive information regarding systemic factors that may initiate or propagate this healthy remodeling event [6-10]. Insulin-like growth factor has been examined as a probable physiologic hypertrophy agonist [11-13], yet the pleiotrophic effects of this hormone may preclude its use as a bona fide cardiac

*These two authors contributed equally to this work.
Correspondence: Lynn A Megeney[a], Duncan J Stewart[b]
[a]E-Mail: lmegeney@ohri.ca
[b]E-Mail: djstewart@ohri.ca
Received 18 December 2016; revised 6 March 2017; accepted 21 June 2017; published online 8 August 2017

restoration agent.

Cardiotrophin 1 (CT1) was originally identified as a promising hypertrophic agonist *in vitro* [14, 15], however its expression has been more recently linked to myocardial pathology, systemic elevated blood pressure, and cardiac failure in both animals and humans [16-19]. Despite these observational data implicating CT1 in certain cardiovascular diseases, this cytokine is known to bind and engage gp130 receptor complexes, a known pro-survival signal for cardiomyocytes [20-22]. Therefore, we reasoned that elevated expression of CT1 in human cardiac pathologies may simply reflect a compensatory response, which attempts to curtail disease progression through the biologic remodeling activity of CT1.

Here, we demonstrate that human CT1 protein (hCT1) engages a fully reversible form of myocardial growth, and that hCT1 attenuates the ongoing pathology and loss-of-function in an aggressive and unremitting model of right heart failure (RHF). hCT1 promotes cardiomyocyte growth in part by inducing a limited activation of an otherwise pathologic hypertrophy signal, as mediated by the caspase 3 protease. In addition, hCT1 engages a cardiomyocyte-derived vascular growth signal to ensure that the modest heart muscle growth is temporally matched with a supporting angiogenic response. Moreover, 2 weeks administration of hCT1 *in vivo* produced cardiac remodeling that was similar to that induced by exercise and, in a model of progressive RHF due to severe pulmonary arterial hypertension, improved cardiac function and reversed right ventricle (RV) dilatation. These data suggest that hCT1 fulfills the criteria as a beneficial remodeling agent, with a capacity to curtail or limit an intractable form of HF.

Results

hCT1 induces fully reversible cardiomyocyte cell growth through serial sarcomere addition

We hypothesized that CT1 may induce physiologic cardiomyocyte growth and beneficial myocardial adaptation. To test this hypothesis we examined whether human recombinant CT1 (hCT1) protein altered the structure of rodent neonatal ventricular cardiomyocytes. We reasoned that if CT1 was a conserved remodeling factor, then the human protein should engage a positive impact on rodent cardiomyocytes. Cardiomyocytes treated with hCT1 displayed a dramatic reorganization in cell architecture within 24 h, leading to a significant increase in the length to width ratio compared to untreated cardiomyocytes (Figure 1A-1C), as was reported previously for CT1 [15], but in contrast to the initial report of the discovery of CT1, which described a concentric growth pattern in treated cells [14]. The increase in the length to width ratio with hCT1 exposure, which was associated with adding sarcomeres in series, was in direct contrast to the morphologic alterations that occurred when cardiomyocytes were treated with pathologic hypertrophy agonists such as the α-adrenergic stimulant phenylephrine (PE) (Figure 1A). PE-treated cells engaged concentric growth, typically characterized by sarcomeres added in parallel, leading to increased cell size, but with a reduced length to width ratio (Figure 1A-1C).

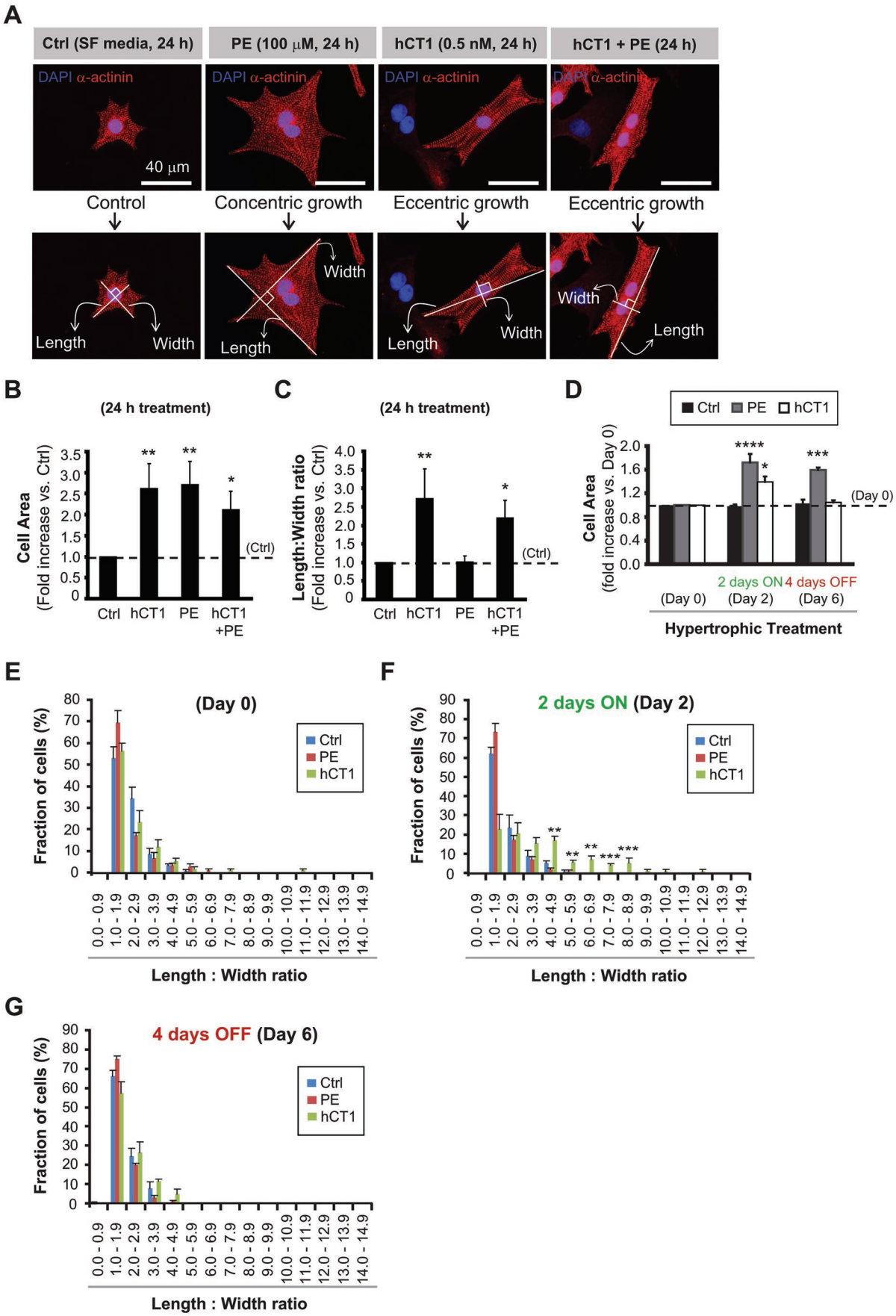
A defining characteristic of physiologic hypertrophy is the fact that the adaptation is fully reversible on cessation of the stress, with individual cardiomyocytes and the intact heart itself returning to pre-stress dimensions [5]. When cardiomyocytes were treated with hCT1 for a 48 h period, followed by removal of the cytokine, the cells rapidly resumed pre-treatment dimensions, similar to untreated cardiomyocytes (Figure 1D-1G). This reversible growth phenotype contrasted with PE-treated cells, where discontinuation of PE did not lead to a decrease in cell size over the same time period, a consistent feature of pathologic hypertrophy induction *in vivo* (Figure 1D-1G).

Aerobic exercise regimes can limit or lessen pathologic cardiac hypertrophy and negative remodeling [5], suggesting that beneficial growth factors (such as CT1) may similarly impede pathologic inductive cues. Notably, when cardiomyocytes were treated with both PE and hCT1, the cells displayed the growth characteristics of hCT1 alone (Figure 1A-1C). This observation suggests that hCT1 may recapitulate a key aspect of the exercise response, and limit or repress ongoing pathologic growth signals in heart muscle cells.

hCT1 stimulates a reversible and non-pathologic growth of the intact heart

To date, all extant *in vivo* observational studies of CT1 and heart function have shown negative correlation data, linking elevations in circulating/plasma CT1 to various forms of cardiac dysfunction [18, 19, 23]. A single study examining exogenous delivery of high concentrations of bolus-injected CT1 protein noted increased gross weight of the heart and morphology consistent with pathologic hypertrophy [17]. However, carefully monitored dose-response studies in both mouse and pig have shown that administration of CT1 protein protects the liver against ischemia reperfusion injury [24, 25], while other studies have reported that chronic CT1 protein delivery augments fatty acid metabolism and reduces insulin resistance [26], all of which suggest that CT1 conveys a beneficial systemic response.

Given these considerations, we chose to examine


A
Ctrl (SF media, 24 h)
PE (100 μM, 24 h)
hCT1 (0.5 nM, 24 h)
hCT1 + PE (24 h)
DAPI α-actinin
40 μm
Control
Concentric growth
Eccentric growth
Eccentric growth
Length
Width
B
(24 h treatment)
Cell Area
(Fold increase vs. Ctrl)
Ctrl hCT1 PE hCT1 +PE
C
(24 h treatment)
Length:Width ratio
(Fold increase vs. Ctrl)
D
Ctrl PE hCT1
Cell Area
(fold increase vs. Day 0)
2 days ON 4 days OFF
(Day 0) (Day 2) (Day 6)
Hypertrophic Treatment
E
(Day 0)
F
2 days ON (Day 2)
G
4 days OFF (Day 6)
Fraction of cells (%)
Length : Width ratio

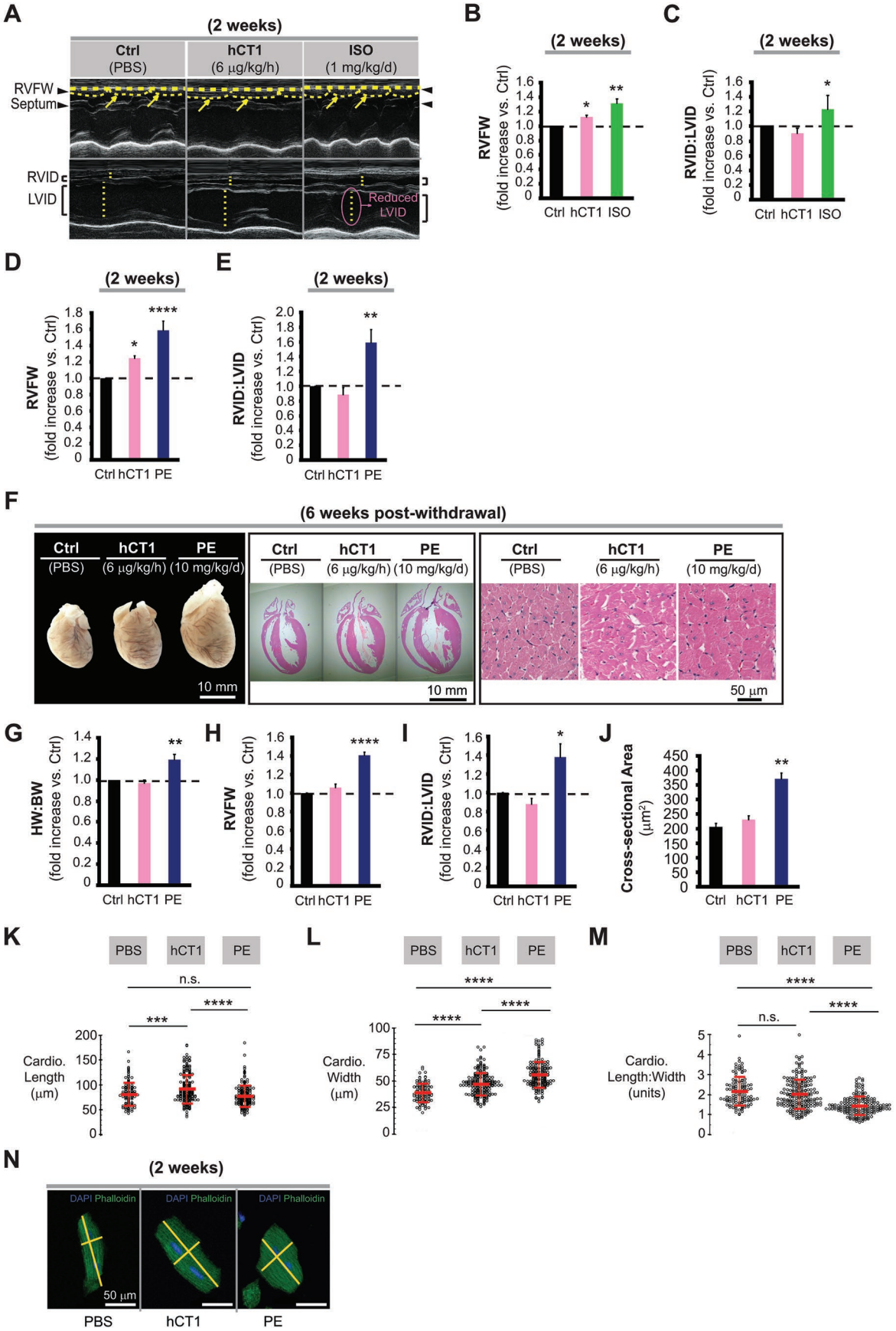
whether sustained 2 weeks delivery of hCT1 was beneficial or harmful to cardiac morphology and function. The decision to test 2 weeks of protein delivery was predicated on the hypothesis that the capacity of a biologic agent (hCT1 protein) to engage cardio-adaptive measures would most likely require sustained exposures, akin to the systemic changes which occur during exercise and pregnancy. hCT1-loaded osmotic minipumps were surgically implanted into rodents and protein was delivered for a continuous 14-day period (at 6 μg/kg/h, a hCT1 concentration within the dose range noted above). Animals subjected to this hCT1 dosing regimen displayed a cardiac remodeling that was reminiscent of exercise adaptation, with a modest yet significant increase in ventricle wall thickness and no alteration in right to left ventricle internal diameter ratio (RVID:LVID) (Figure 2A-2C). Different alterations were observed in isoproterenol (ISO) or PE-treated animals, which displayed a dramatic increase in wall thickness, with concomitant severe change in the RVID:LVID ratio (Figure 2B-2E). Importantly, we noted a complete reversion of cardiac growth/remodeling at 6 weeks following discontinuation of hCT1 after a 2-week exposure. Here, the overall heart mass of hCT1-treated animals was similar to control animals, with ventricle wall thickness and RVID:LVID ratios reverting to baseline levels (Figure 2F-2I). However, animals treated with PE for a similar 2-week period, followed by 6 weeks of recovery, continued to display a cardiac morphology that is consistent with a pathologic state, i.e., elevated wall thickness and RVID:LVID ratios (Figure 2F-2I). Moreover, changes in myocardial wall thickness were paralleled by a corresponding change in cardiomyocyte cross-sectional area (Figure 2F and 2J), consistent with the CT1-inspired *in vitro* adaptations.

We next examined isolated cardiomyocyte morphology from adult rodent (murine) hearts, which is representative of conditions where true physiologic adaptation occurs. We treated adult mice for 2 weeks with phosphate-buffered saline (PBS), hCT1 (6 μg/kg/h) or PE (10 mg/kg/d), observing that hCT1 caused an increased lengthening of isolated mouse cardiomyocytes versus PE or PBS control (Figure 2K-2N). Furthermore, the length to width ratio of PE-treated cardiomyocytes was significantly less than those for both hCT1 and PBS control, where hCT1 and PBS treatments resulted in similar length to width ratios (Figure 2K-2N). These data are similar to what we observed for isolated and cultured neonatal primary cardiomyocytes (Figure 1), the only notable difference is that in the *in vitro* model there was a significant increase in the length to width ratio and not just length following hCT1 treatment, as was the case in the *in vivo* assessments (Figure 2K-2N). The greater length changes *in vitro* with hCT1 administration may be attributed to a lack of physical constraints within this system, which allows the cells to continue to add sarcomeres in series, beyond what physical space constraints would be permissive *in vivo*.

hCT1 stimulates beneficial cardiomyocyte remodeling through a constrained activation of caspase 3

The morphologic variation in ventricular cardiomyocytes during pathologic versus physiologic hypertrophy suggests that distinct signaling mechanisms control these divergent cell adaptations. This is a generally accepted hypothesis and robust evidence exists to support this proposition, i.e., activation of Akt-mediated signals induces a physiologic hypertrophy and offers protection against pressure overload pathology, while calcineurin-mediated signals are largely regarded as pathologic growth cues [3, 8]. The primary limitation with this concept is that the early stages of pathologic growth are often compensatory or beneficial in nature in response to a stress adaptation [1]. As such, a reasonable nuance to the prevailing hypothesis is that the divergent forms

Figure 1 Human cardiotrophin 1 (hCT1) induces morphologic changes in primary cardiomyocytes with reversion upon removal of hCT1 stimulation. **(A)** Primary neonatal cardiomyocytes were stimulated for 24 h with hCT1 (0.5 nM), PE (100 μM), hCT1 and PE, or control serum-free medium (Ctrl, SF) followed by morphometric analysis (cell area and length:width ratio). Cells were stained with α-actinin (red) and nuclei were stained with DAPI (blue). Scale bar, 40 μm. **(B**, **C)** Morphometric analysis of **(A)** above. Treatment with hCT1, PE, and hCT1+PE induced a significant increase in cell area versus control (n = 3; *P < 0.05 and **P < 0.01). However, only hCT1 (or hCT1+PE) stimulation resulted in elongated/eccentric growth versus control (n = 3; *P < 0.05 and **P < 0.01). **(D)** Cardiomyocytes were stimulated as in **(A)** above, but for 2 days followed by removal for 4 days. After 2 days, both hCT1 and PE induced hypertrophy versus control at day 2 (n = 3; *P < 0.05 and ****P < 0.0001). Cells reverted to pre-treatment dimensions upon removal of hCT1, whereas removal of PE caused cells to remain hypertrophied versus Control at day 6 (n = 3; ***P < 0.001). **(E**-**G)** Length:width ratio population frequency analysis of **(D)** above. The majority of cardiomyocytes (~ 60%) display a length:width ratio of 1.0-2.0 (Day 0); however, upon treatment with hCT1 (Day 2), a significant shift in length:width ratio of 3.0-9.0 was observed versus control at day 2 (n = 3; **P < 0.01 and ***P < 0.001) with reversion occurring at day 6 upon hCT1 removal.

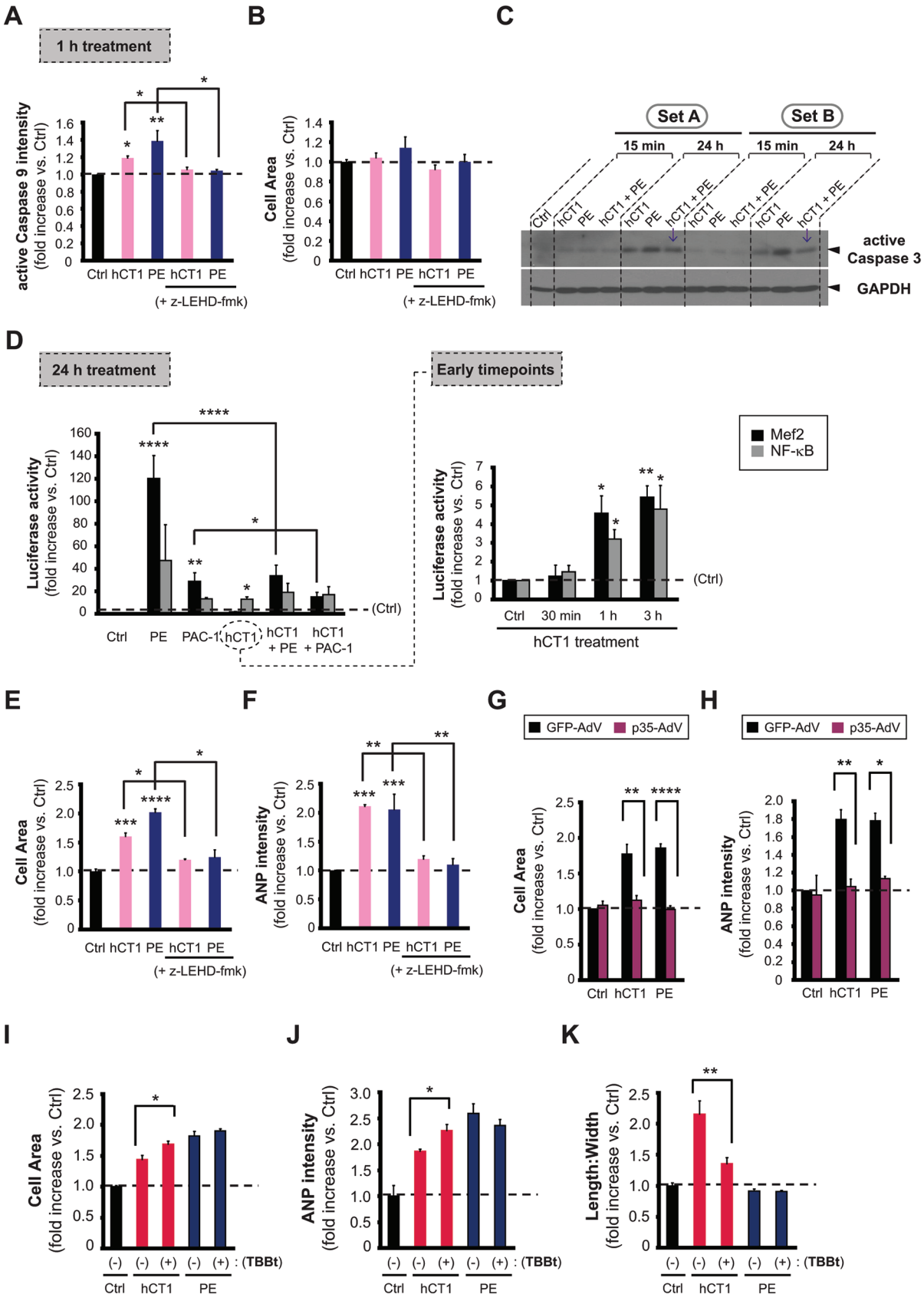

A
(2 weeks)
Ctrl (PBS)
hCT1 (6 μg/kg/h)
ISO (1 mg/kg/d)
RVFW
Septum
RVID
LVID
Reduced LVID
B
(2 weeks)
RVFW (fold increase vs. Ctrl)
Ctrl hCT1 ISO
C
(2 weeks)
RVID:LVID (fold increase vs. Ctrl)
Ctrl hCT1 ISO
D
(2 weeks)
RVFW (fold increase vs. Ctrl)
Ctrl hCT1 PE
E
(2 weeks)
RVID:LVID (fold increase vs. Ctrl)
Ctrl hCT1 PE
F
(6 weeks post-withdrawal)
Ctrl (PBS)
hCT1 (6 μg/kg/h)
PE (10 mg/kg/d)
10 mm
50 μm
G
HW:BW (fold increase vs. Ctrl)
Ctrl hCT1 PE
H
RVFW (fold increase vs. Ctrl)
Ctrl hCT1 PE
I
RVID:LVID (fold increase vs. Ctrl)
Ctrl hCT1 PE
J
Cross-sectional Area (μm²)
Ctrl hCT1 PE
K
PBS hCT1 PE
n.s.
Cardio. Length (μm)
L
PBS hCT1 PE
Cardio. Width (μm)
M
PBS hCT1 PE
n.s.
Cardio. Length:Width (units)
N
(2 weeks)
DAPI Phalloidin
50 μm
PBS hCT1 PE

of hypertrophy may share a common molecular origin, where the more extreme form of growth (pathologic hypertrophy) derives from an unconstrained molecular signal. For example, the Mef2 transcription factor family has been noted to have elevated activities in both pathologic and maturational cardiac growth programs [27-29].

To address this supposition we examined whether hCT1-induced cardiomyocyte remodeling was associated with a blunted activation of the mitochondrial-/intrinsic-mediated cell death pathway. This sequential proteolytic cascade was initially defined as a hallmark of apoptosis, yet this pathway is now widely recognized as a signaling cascade that confers a variety of essential non-death cell adaptations [30-32]. Prior observations from our laboratory have demonstrated that agonists producing pathologic hypertrophy engage robust activation of the intrinsic cell death pathway and distal pathway activation alone (caspase 3) is essential and sufficient to induce hypertrophy without attendant apoptosis [33]. We noted that hCT1 treatment of cardiomyocytes resulted in a rapid proximal activation of this signal cascade, with increased caspase 9 activity (Figure 3A-3B; Supplementary information, Figure S1A). Caspase 3 activity was effectively engaged by hCT1, yet was notably decreased when compared with that in the presence of the hypertrophy agonist PE, with a similar reduction in caspase 3 activity when cardiomyocytes were treated with both hCT1 and PE (Figure 3C). hCT1-treated cardiomyocytes also rapidly engaged caspase 3-sensitive transcriptional responses, including the activation of Mef2- and NF-κB-dependent reporters (Figure 3D). However, unlike exposure to standard pathologic agonists such as PE and ISO, the activation of Mef2 and NF-κB in response to hCT1 was limited in duration (Figure 3D). hCT1 also selectively engaged a robust STAT3-dependent reporter activity unlike PE, which preferentially activated STAT1 (Supplementary information, Figure S2A and S2B). Interestingly, STAT1 and STAT3 appear to have opposing roles in regulating survival and inflammation: STAT1 acts as a pro-inflammatory factor and induces apoptosis, whereas STAT3 is anti-inflammatory and promotes cell survival [34]. It is the intricate balance between STAT1 and STAT3 activation that may determine the outcome of PE or hCT1 treatment. In this case, hCT1 stimulation is likely cardioprotective due to preferential activation of STAT3 over STAT1 (Supplementary information, Figure S2A and S2B). Finally, blockade of caspase 9 activity (through exposure to peptide inhibitors) or caspase 3 activity (through adenoviral delivery of the biologic effector caspase inhibitor p35) completely abrogated hCT1-induced cell growth and hCT1-induced upregulation of pro-hypertrophic markers such as ANP (Figure 3E-3H; Supplementary information, Figure S1B and S1C). ANP expression increases in both pathologic and physiologic hypertrophy settings, as such production and secretion of this natriuretic peptide provides a robust measure of a global hypertrophy response [35]. Although we provide evidence that caspase 9 and 3 activity are required for hypertrophy induction by both hCT1 and PE, the extent of caspase activity is not as robust during hCT1 stimulation when compared to PE. Importantly, this limited caspase activation in response to hCT1 is still significant enough to engage a beneficial hypertrophic response that is sensitive to caspase inhibition.

These observations suggest that hCT1 engages a restricted activation of the intrinsic cell death pathway to

Figure 2 Administration of hCT1 *in vivo* induces beneficial cardiac growth, while withdrawal of hCT1 causes reversion to baseline cardiac dimensions. **(A**-**J)** Osmotic minipumps were implanted subcutaneously in rats containing PBS control (Ctrl), hCT1 (6 μg/kg/h), and isoproterenol (ISO, 1 mg/kg/d) or phenylephrine (PE, 10 mg/kg/d) to induce hypertrophy over 2 weeks. After 2 and 6 weeks post treatment, M-mode echocardiography analysis was used to assess myocardial structure/function. **(A)** Echocardiography images. Arrows and arrowheads (upper panels) point to the right ventricle free wall (RVFW) and septum. Dotted lines (lower panels) span the right and left ventricle internal diameter (RVID and LVID, respectively) of the inner chambers. **(B**-**E)** Both hCT1 and ISO (or PE) induced a significant increase in cardiac hypertrophy versus control (n = 6; *P < 0.05, **P < 0.01 and ****P < 0.0001). However, only rats treated with ISO or PE exhibited an increase in the RVID:LVID ratio (n = 6; *P < 0.05 and **P < 0.01). **(F**-**J)** 6 weeks post withdrawal, hCT1-treated rats displayed reversion of heart growth, whereas PE-treated rats maintained a significant increase in HW:BW (heart weight to body weight ratio), RVFW wall thickness, cardiomyocyte cross-sectional area, and RVID:LVID ratio versus control (n = 6; *P < 0.05, **P < 0.01 and ****P < 0.0001). **(F)**, Whole hearts (left panel; scale bar, 10 mm), Hematoxylin and Eosin-stained sections (middle and right panels; scale bars, 10 mm and 50 μm, respectively). **(K**-**N)** Similar procedure as in **(A)** above, however, adult murine cardiomyocytes were analyzed. After 2 weeks of treatment, hCT1 significantly increased the length of cardiomyocytes versus PBS control or PE (**K**; n = 6, ***P < 0.001 and ****P < 0.0001) while PE significantly increased the width versus PBS control and hCT1 (**L**; n = 6, ****P < 0.0001). The length to width ratio of PE-treated cardiomyocytes was significantly decreased versus PBS control and hCT1 (**M**; n = 6, ****P < 0.0001), whereas no significant difference (ns) was observed between PBS control and hCT1. Representative images **(N)** of murine cardiomyocytes were stained with Alexa Fluor-488 Phalloidin (F-actin, green) and DAPI (nuclei, blue). Scale bar, 50 μm.


A
1 h treatment
active Caspase 9 intensity (fold increase vs. Ctrl)
Ctrl hCT1 PE hCT1 PE
(+ z-LEHD-fmk)
B
Cell Area (fold increase vs. Ctrl)
Ctrl hCT1 PE hCT1 PE
(+ z-LEHD-fmk)
C
Set A
Set B
15 min
24 h
15 min
24 h
Ctrl
hCT1
PE
hCT1 + PE
active Caspase 3
GAPDH
D
24 h treatment
Luciferase activity (fold increase vs. Ctrl)
Ctrl PE PAC-1 hCT1 hCT1 + PE hCT1 + PAC-1
(Ctrl)
Early timepoints
Mef2
NF-κB
Luciferase activity (fold increase vs. Ctrl)
Ctrl 30 min 1 h 3 h
hCT1 treatment
(Ctrl)
E
Cell Area (fold increase vs. Ctrl)
Ctrl hCT1 PE hCT1 PE
(+ z-LEHD-fmk)
F
ANP intensity (fold increase vs. Ctrl)
Ctrl hCT1 PE hCT1 PE
(+ z-LEHD-fmk)
G
GFP-AdV
p35-AdV
Cell Area (fold increase vs. Ctrl)
Ctrl hCT1 PE
H
GFP-AdV
p35-AdV
ANP intensity (fold increase vs. Ctrl)
Ctrl hCT1 PE
I
Cell Area (fold increase vs. Ctrl)
(-) (-) (+) (-) (+) : (TBBt)
Ctrl hCT1 PE
J
ANP intensity (fold increase vs. Ctrl)
(-) (-) (+) (-) (+) : (TBBt)
Ctrl hCT1 PE
K
Length:Width (fold increase vs. Ctrl)
(-) (-) (+) (-) (+) : (TBBt)
Ctrl hCT1 PE

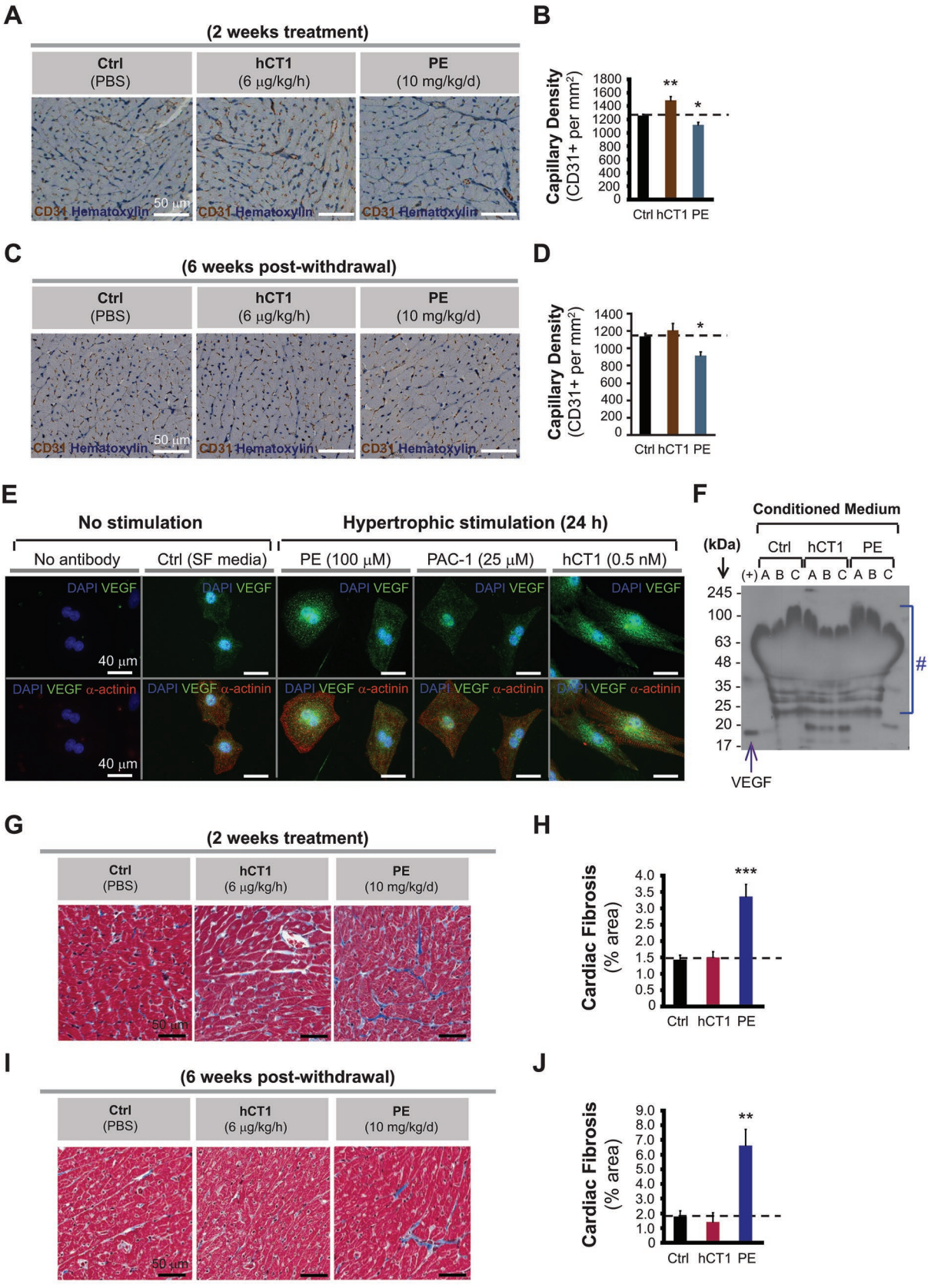
initiate the beneficial remodeling of cardiomyocytes. There are numerous examples in the literature regarding concurrent signals or feedback mechanisms that limit caspase 3 activation and we surmised that such a pathway was operant during hCT1-induced hypertrophy. Here, we examined whether hCT1 was coincident with the activation of CK2, a kinase that phosphorylates both caspase 3 and its cognate substrates, effectively squelching protease activity and limiting proteolytic cleavage [36, 37]. Inhibition of CK2 (via exposure to TBBt) during hCT1 stimulation of cardiomyocytes resulted in a significant increase in cell size and ANP expression when compared to cardiomyocytes treated with hCT1 alone (Figure 3I-3J; Supplementary information, Figure S3). Treatment of cardiomyocytes with both PE and the CK2 inhibitor did not lead to any additional increase in cell size or ANP expression compared to PE alone, suggesting that CK2 activation is not a feature of pathologic signaling cascades. The inhibition of CK2 activity during hCT1 stimulation also resulted in a morphologic alteration, where the affected cardiomyocytes displayed a growth phenotype more characteristic of exposure to pathologic agonists such as PE (i.e., a reduction in the length to width ratio, Figure 3K; Supplementary information, Figure S3). These observations imply that hCT1 mediated a constrained activation of caspase 3 activity via CK2-targeted phosphorylation and that this biochemical step is a key feature of beneficial cardiomyocyte remodeling, instrumental in preventing a transition to fulminant pathologic hypertrophy.

hCT1 stimulates a cardiomyocyte-derived paracrine signal to enhance angiogenesis and limit fibrosis

Physiologic cardiac hypertrophy is associated with an increase in capillary density, whereas pathologic hypertrophy is characterized by a relative decline or no change at all [9, 38]. Indeed, this compensatory vascular growth/angiogenesis is permissive for the increased workload that accompanies physiologic hypertrophy. The intra-dependence of these tissue adaptations suggests that the myocardium and its supporting vasculature may engage in a paracrine or autocrine signal to match myocardial growth with an improved blood supply. In support of this premise, vascular endothelial growth factor (VEGF) has been demonstrated to be produced and secreted by cardiomyocytes and gene targeted deletion of this growth factor leads to prominent cardiac pathology [39, 40]. Alternatively, a beneficial remodeling agent may act concurrently but independently on myocardial and vascular cells to spur organ growth.

To begin to address this supposition we initially examined capillary density in the myocardium of hCT1-treated versus control and PE-treated animals (a similar 14-day treatment regime as noted in Figure 2). hCT1-treated animals displayed a significant increase in the number of CD31-positive capillaries compared to control or PE-treated animals, indicative of beneficial remodeling of the myocardium (Figure 4A and 4B). Discontinuation of hCT1 treatment led to a reversion of capillary density to control values (Figure 4C and 4D), suggesting that the angiogenic properties of hCT1 are fully reversible,

Figure 3 hCT1 engages a restricted activation of the intrinsic caspase-mediated cell death pathway. **(A**, **B)** Primary cardiomyocytes were treated for 1 h with control serum-free medium (Ctrl), hCT1 (0.5 nM), or PE (100 μM) in the presence or absence of the caspase 9 inhibitor (z-LEHD-fmk, 20 μM). Caspase 9 was significantly activated with hCT1 and PE versus control (n = 3; *P < 0.05 and **P < 0.01) and this was decreased in the presence of z-LEHD-fmk (n = 3; *P < 0.05). **(C)** Cardiomyocytes were treated with hCT1 (0.5 nM), PE (100 μM), or hCT1+PE for 15 min and 24 h and analyzed by western immunoblotting. hCT1 caused a moderate increase in caspase 3 activity compared to PE at 24 h. Caspase 3 activity also decreased with combined PE and hCT1 stimulation (arrows). GAPDH was the loading control. **(D)** Cardiomyocytes were transfected with reporter plasmids under the control of NF-κB or Mef2 promoters and luciferase activity was measured after treatment with: control serum-free medium (Ctrl), hCT1 (0.5 nM), PE (100 μM), or procaspase 3-activating compound 1 (PAC-1; 25 μM). hCT1 treatment resulted in NF-κB and Mef2 activation at 1 and 3 h versus control (n = 4; * P< 0.05 and **P < 0.01); and at 24 h, only NF-κB activity was sustained (n = 4; *P < 0.05). However, PE and PAC-1 treatment caused significant activation of Mef2 after 24 h (n = 4; **P < 0.01 and ****P < 0.0001). Co-stimulation of hCT1/PE and hCT1/PAC-1 significantly reduced Mef2 activity compared to PE and PAC-1 alone (n = 4; ****P < 0.0001 and *P < 0.05, respectively). **(E**, **F)** Similar procedure as in **(A)** above; however, with 24 h treatment. hCT1 and PE significantly increased cell area and the pro-hypertrophic marker ANP versus control (n = 3; ***P < 0.001 and ****P < 0.0001) and this was significantly attenuated in the presence of z-LEHD-fmk (n = 3;*P < 0.05 and **P < 0.01). **(G**, **H)** Cardiomyocytes were infected for 24 h with an adenovirus (AdV) encoding the caspase inhibitor, p35-AdV, prior to inducing hypertrophy with hCT1 or PE for 24 h. GFP-AdV was used as a control. p35-AdV significantly inhibited hCT1 and PE induced hypertrophy (n = 3; **P < 0.01 and ****P < 0.0001, respectively) and inhibited ANP expression (n = 3; **P < 0.01 and *P < 0.05, respectively). Both p35-AdV and GFP-AdV were used at a mean of infectivity (MOI) of 20. **(I-K)** Similar procedure as in **(E**, **F)** above; however, casein kinase 2 (CK2) activity was blocked using TBBt (50 μM). CK2 inhibition significantly increased cell size and ANP expression (n = 3; *P < 0.05) while reducing length:width ratio (n = 3; **P < 0.01) when compared to hCT1 treatment alone.


A
(2 weeks treatment)
Ctrl (PBS)
hCT1 (6 μg/kg/h)
PE (10 mg/kg/d)
CD31 Hematoxylin
50 μm
B
Capillary Density (CD31+ per mm²)
1800
1600
1400
1200
1000
800
600
400
200
0
**
*
Ctrl hCT1 PE
C
(6 weeks post-withdrawal)
Ctrl (PBS)
hCT1 (6 μg/kg/h)
PE (10 mg/kg/d)
CD31 Hematoxylin
50 μm
D
Capillary Density (CD31+ per mm²)
1400
1200
1000
800
600
400
200
0
*
Ctrl hCT1 PE
E
No stimulation
Hypertrophic stimulation (24 h)
No antibody
Ctrl (SF media)
PE (100 μM)
PAC-1 (25 μM)
hCT1 (0.5 nM)
DAPI VEGF
DAPI VEGF α-actinin
40 μm
F
Conditioned Medium
(kDa)
Ctrl hCT1 PE
(+) A B C A B C A B C
245
100
63
48
35
25
20
17
#
VEGF
G
(2 weeks treatment)
Ctrl (PBS)
hCT1 (6 μg/kg/h)
PE (10 mg/kg/d)
50 μm
H
Cardiac Fibrosis (% area)
4.0
3.5
3.0
2.5
2.0
1.5
1.0
0.5
0
***
Ctrl hCT1 PE
I
(6 weeks post-withdrawal)
Ctrl (PBS)
hCT1 (6 μg/kg/h)
PE (10 mg/kg/d)
50 μm
J
Cardiac Fibrosis (% area)
9.0
8.0
7.0
6.0
5.0
4.0
3.0
2.0
1.0
0
**
Ctrl hCT1 PE

akin to hCT1-mediated growth alterations in cardiomyocytes and the myocardium proper (Figures 1 and 2). Next, we sought to identify whether the hCT1 pro-angiogenic activity was associated with a cardiomyocyte-derived paracrine signal. Comparative gene expression analysis revealed that hCT1-treated cardiomyocytes exhibited robust induction of angiogenic factors including angiopoietin-like 4 (Angpt14), Fms-related tyrosine kinase 4 (Flt4), von Willebrand factor 5A (Vwa5a), with modest but significant increases in VEGF expression (Supplementary information, Table S1). Stimulation of cardiomyocytes with hCT1 led to a rapid increase of VEGF protein within the cell, yet treatment with pathologic hypertrophy agonists such as PE or the caspase 3 small molecule activator, PAC-1 resulted in a minimal increase (Figure 4E). In addition, blockade of caspase 3 activity (through adenoviral delivery of the biologic effector caspase inhibitor p35) significantly inhibited the hCT1-induced increase in VEGF, whereas the minimal increase in intracellular VEGF with PE was also inhibited with p35 adenovirus (AdV) (Supplementary information, Figure S4A and S4B). This suggests that VEGF expression induced by hCT1 or PE is mediated, in part, by caspase signaling. In addition, western analysis of media derived from hCT1-treated cardiomyocytes demonstrated that the increased production of VEGF protein was associated with an increased release of the growth factor (Figure 4F). It is interesting to note that the minimal cellular VEGF expression induced by PE was not detected in the media after 24 h (Figure 4F). Presumably, pathologic stimulation with PE impedes any robust secretion of VEGF from the cell thus hindering angiogenesis such that it cannot keep pace with hypertrophy. Indeed, others have detected minor amounts of secreted VEGF in the media after prolonged (48 h) stimulation with PE [41]. These results suggest that hCT1 promotes cardiomyocyte secretion of angiogenic factor(s) via a signaling mechanism that is concurrent to and dependent on caspase 3.

Given that angiogenesis can promote the transport of oxygen and nutrients to cardiomyocytes, we next explored the metabolic effect of inducing hypertrophy with hCT1 or PE. Under normal conditions, the majority of energy (ATP) generated in the heart is derived from mitochondrial oxidative phosphorylation and, during hypertrophy, there is an increased metabolic demand to compensate for the increased workload [42]. Thus, oxygen consumption of cardiomyocytes is an important indicator of normal cellular function where unhealthy cells with dysfunctional mitochondria display a lower oxygen consumption compared to healthy cells and exercise adapted cardiomyocytes display rates of oxygen consumption above baseline values. Accordingly, we measured the rate of oxygen consumption and observed that treatment with hCT1 for 24 h resulted in a significantly higher rate of oxygen consumption compared to pathologic stimulation with PE (Supplementary information, Figure S5). Moreover, the microarray data indicated a slight, yet significant, compensatory decrease at the gene expression level of a wide array of oxidative mitochondrial enzymes (Supplementary information, Table S1). This observation suggests that hCT1 may increase the efficiency of oxidative mitochondrial energy metabolism during physiological hypertrophy and would provide further support that hCT1 can model the benefits of increased aerobic fitness (oxygen consumption rate) observed during endurance exercise training. It should also be noted that hCT1 results in increased expression of anti-oxidant regulatory factors (i.e., mitochondrial superoxide dismutase 2 and metallothionein 2A), a mechanism that is consistent with enhanced metabolic control (Supplementary information, Table S1). Finally, studies have shown that CT1 can significantly improve mitochondrial dysfunction leading to neuroprotection in a mouse model by increasing mitochondrial cytochrome oxidase activity and ATP energy

Figure 4 hCT1 enhances angiogenesis and limits fibrosis during cardiac hypertrophy. **(A-D)** Rats were treated with hCT1 or PE for 2 weeks followed by withdrawal for 6 weeks. Capillary density was assessed by staining for CD31 (brown) and counterstaining with Hematoxylin (blue). hCT1-treated rats displayed a significant increase in CD31-positive capillaries (n = 4;$^{**}P$ < 0.01) at 2 weeks with reversion at 6 weeks post withdrawal; whereas PE-treated rats displayed a significant decrease at 2 weeks post treatment and 6 weeks post withdrawal (n = 4; $^{*}P$ < 0.05). Scale bar, 50 μm. **(E)** Primary cardiomyocytes were incubated with control serum-free medium (Ctrl, SF medium), hCT1 (0.5 nM), PE (100 μM), or PAC-1 (25 μM) for 24 h. hCT1 treatment resulted in a greater increase in vascular endothelial growth factor (VEGF) expression compared to PE or PAC-1. Immunofluorescence was used to detect α-actinin (red), VEGF (green), and nuclei were stained with DAPI (blue). Scale bar, 40 μm. **(F)** Similar procedure as in **(E)** above, however, conditioned medium was harvested at 24 h and expression of secreted VEGF protein was detected upon immunoblotting with anti-VEGF antibody. A significant increase in VEGF was observed in hCT1-treated samples (sets A-C) when compared to PE or Ctrl. (+), recombinant VEGF protein (40 ng) used as positive control. (#), cross-reactivity bands of antibody to components in conditioned medium. **(G-J)** Rats were treated as in **(A)** above and fibrosis/collagen was assessed using Masson's Trichrome staining (blue deposits). Rat hearts exposed to PE exhibited a significant increase in collagen/fibrosis at 2 weeks post treatment as well as 6 weeks post withdrawal (n = 4; $^{***}P$ < 0.001 and $^{**}P$ < 0.01, respectively). Scale bar, 50 μm.

levels, while decreasing reactive oxygen species production [43], observations that are consistent with the data presented here.

In addition to elevated vascularity and metabolic profile, we assessed whether hCT1 limited fibrosis/fibrotic deposition, a phenotypic change that is consistent with pathologic hypertrophy [44]. We noted that hCT1-treated animals had no appreciable increase in fibrotic deposition compared with PE-treated animals, which displayed robust elevations in collagen deposits (Figure 4G-4J). hCT1-treated cardiac fibroblasts were also devoid of the robust increase in Galectin-3 that occurs during exposure to PE (Supplementary information, Figure S6A-S6C). Collectively, these data support the contention that CT1 induces multiple cellular adaptations to ensure a matched organ level response to maintain and augment cardiac function.

hCT1 stimulation improves cardiac function in a model of severe right heart failure

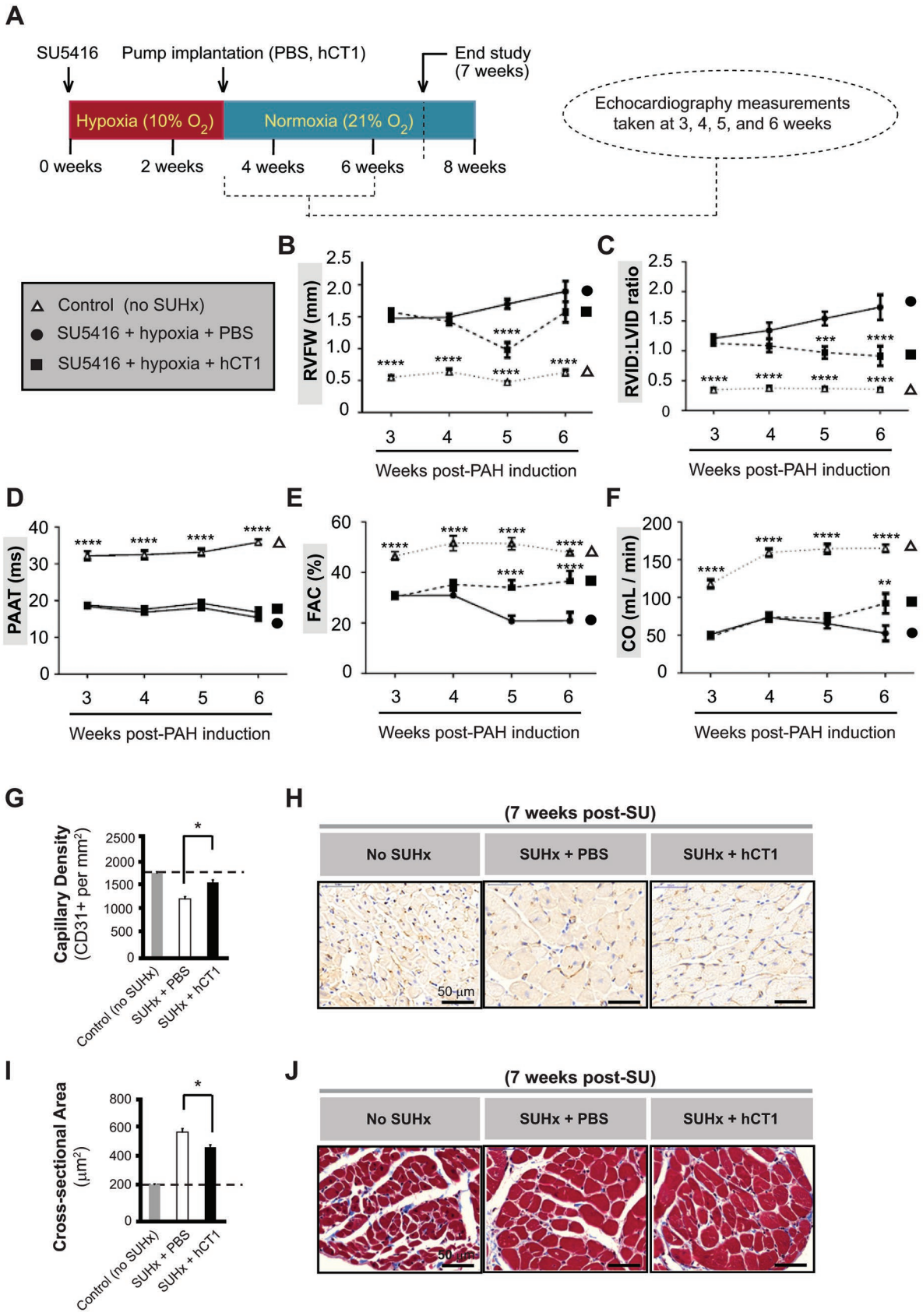
The capacity for hCT1 to induce beneficial myocardial remodeling suggests that this protein may provide a tractable means to limit the progression of cardiac pathologies. To test this general premise, we examined whether hCT1 administration could limit and/or improve cardiac performance in a model of RHF due to severe pulmonary arterial hypertension (PAH)-induced inhibition of VEGFR2 with SU5416 (SU) followed by a 3-week exposure to hypoxia (Hx). The SUHx model faithfully reproduces many of the features of human PAH, which develops from a generalized thickening and obliteration of distal lung arterioles [45-47]. The severity of symptoms and the prognosis in PAH is largely driven by the degree to which the RV can adapt to the marked increases in afterload, and inability to compensate results in progressive RHF, reduced cardiac output, and ultimately death.

Our initial experiments revealed that systemic delivery of hCT1 protein during early stages of hypoxia exposure (prior to the development of RHF) provided an effective means to prevent the onset of RHF (Supplementary information, Figure S7A and S7B). However, this was associated with improvements in pulmonary hemodynamics, possibly due to the beneficial effects of the pro-angiogenic actions of hCT1 on the development of this disease. Therefore, we tested whether hCT1 protein delivery would mitigate RHF at later stages of disease in the SUHx model, when the severe PAH was fully established and RHF was already present. Here, we observed that delivery of hCT1 protein (beginning after 3 weeks of hypoxia exposure) was sufficient to reverse the RHF pathology, where hCT1-treated SUHx animals displayed significant improvement in both contractile function (cardiac output, fractional area change) and structural dimensions of the heart (RVID:LVID ratio) (Figure 5A-5C; 5E and 5F). In addition, hCT1-treated SUHx animals displayed increased RV vascularity (increased capillary density as measured by CD31 staining) and reduced RV cardiomyocyte cell size with a characteristic eccentric growth phenotype, when compared to sham-treated SUHx animals (Figure 5G-5J). Importantly, hCT1 treatment did not mitigate or lessen the elevated pulmonary pressures in the SUHx model (Figure 5D), strongly suggesting that hCT1 improved cardiac function by inducing heart/myocardial specific remodeling events.

Discussion

Here, we demonstrate the capacity of a single exogenously delivered protein, CT1, to produce beneficial remodeling of the heart. The cardiac adaptations elicited by CT1 display the essential characteristics and benefits that are associated with endurance exercise adaptation, all of which are fully reversible when CT1 protein delivery is discontinued. Remarkably, administering CT1 alone achieves an organ level reorganization of the heart, impacting the myocardial and vascular cell components through a cardiomyocyte instructed response, i.e., CT1 stimulates both cell growth and a pro-vascular paracrine signal in the cardiomyocyte population.

Heart failure is a leading cause of morbidity and mortality in affluent societies and a growing epidemic worldwide [48]. The most intensely studied form of the disease, congestive HF, can be effectively managed with combinatorial interventions that enhance contractile performance, while reducing afterload on the weakened muscle (through diuretic-mediated reduction in fluid levels) [49]. RHF, which occurs when the right heart cannot adapt to an increase in afterload, has emerged as an equal if not greater public health crisis. This results from an increase in pulmonary arterial pressure or pulmonary hypertension (PH). Pulmonary arterial hypertension (PAH) is a rare but serious form of PH; however, by far the most common cause of PH is HF with preserved ejection fraction (HFpEF). Despite the important progress in the treatment of left HF with reduced ejection fraction, effective pharmacologic management of RHF, particularly in the context of HFpEF, has proven to be an intractable problem [50]. In addition, patients with RHF, regardless of etiology, have a very limited capacity to engage in and derive the myocardial benefits that are associated with aerobic exercise programs [50]. Our observations suggest that CT1 can dramatically improve cardiac performance in RHF, whereby the failing myocardium is functionally reprogrammed at the whole organ level.


A
SU5416
Pump implantation (PBS, hCT1)
End study (7 weeks)
Hypoxia (10% O2)
Normoxia (21% O2)
0 weeks
2 weeks
4 weeks
6 weeks
8 weeks
Echocardiography measurements taken at 3, 4, 5, and 6 weeks
Control (no SUHx)
SU5416 + hypoxia + PBS
SU5416 + hypoxia + hCT1
B
RVFW (mm)
Weeks post-PAH induction
C
RVID:LVID ratio
Weeks post-PAH induction
D
PAAT (ms)
Weeks post-PAH induction
E
FAC (%)
Weeks post-PAH induction
F
CO (mL / min)
Weeks post-PAH induction
G
Capillary Density (CD31+ per mm2)
Control (no SUHx)
SUHx + PBS
SUHx + hCT1
H
(7 weeks post-SU)
No SUHx
SUHx + PBS
SUHx + hCT1
50 μm
I
Cross-sectional Area (μm2)
Control (no SUHx)
SUHx + PBS
SUHx + hCT1
J
(7 weeks post-SU)
No SUHx
SUHx + PBS
SUHx + hCT1
50 μm

The myocardial remodeling activity of CT1 is relayed through a complex and self-adjusting molecular signal cascade. For example, CT1 engages a temporally brief upregulation in the mitochondrial intrinsic cell death pathway, culminating in a pulse of caspase 3 activation. Robust activation of this signal cascade is a key feature of pathologic hypertrophy [33], yet CT1 appears to deploy the cellular remodeling capacity of caspase 3 as a conduit to initiate physiologic growth. Our observations imply that caspase 3 stimulates an overlapping gene expression program during physiologic and pathologic hypertrophy, i.e., Mef2-dependent transcription, and that varying the duration of this biologic signal may be a primary mechanism to manage the divergent outcomes (Figure 6). CT1 activation of CK2 appears to be central to the process of restrained caspase signaling, as inhibition of this kinase leads to more robust caspase activity and a pathologic hypertrophy phenotype. How CT1 signals to CK2 is not entirely clear, although a post gp130-mediated cascade is a likely conduit. In the erythroleukemic cells, cytokine stimulation has been shown to promote a direct physical interaction between CK2 and the gp130 scaffold kinases JAK1/JAK2, resulting in an autoactivation loop between the JAKs and CK2 [51]. Whether this regulatory network is operant in CT1-stimulated cardiomyocytes will require further investigation. Our experiments strongly suggest that CT1 stimulation of CK2 function is critical to limit caspase activation, a key molecular step in establishing the physiologic hypertrophy phenotype. CK2 is a holoenzyme that is constitutively active [36, 37], as such our data suggest it is most likely that CT1 stimulation limits the interaction between the kinase complex and caspase 3 and or the relevant caspase 3 substrates, rather than directly increasing CK2 activity. We have noted that during hypertrophy stimulation, the caspase 3 activation pattern is tightly scripted within the cell, forming discrete foci in peri-nuclear locations [36]. We attempted to monitor a CK2/caspase 3 interaction via proximity ligation assay (PLA), but were unable to establish an interaction between these enzymes using this methodology. The activated caspase 3 protein foci suggest that the protease may exist within aggregated structures, a condition that would not be conducive to monitoring protein interactions via PLA.

This variable signal hypothesis is consistently demonstrated in the developmental biology literature, where temporal activation of caspase 3 acts as a critical inductive cue for cell differentiation, while sustained activation leads to cell death within the same cell population [30, 31]. Certainly, a temporal removal of Mef2 repression by caspase targeting of HDAC3 (as we have noted in [33]) would provide an amenable mechanism to titrate Mef2 activity, with a more robust activation of this pathway a characteristic of pathologic hypertrophy. Indeed, prior observations have shown that complete deletion of HDAC3 is synonymous with unrestrained pathologic myocardial growth [52]. Nevertheless, caspase 3 cleavage of HDAC3 is unlikely to solely account for the profound phenotypic variation between physiologic versus pathologic hypertrophy. Here, we favor the supposition that sustained caspase 3 activation leads to the targeting of a cohort of substrates that alter the structural integrity of the cardiomyocyte, and that these substrates are either inaccessible or subject to very limited proteolytic targeting when caspase 3 is transiently engaged by CT1. Indeed, caspase cleavage of contractile proteins such as Troponin T and myosin light chain have been noted in nonapoptotic cardiomyocytes during progression to dilation and failure [53, 54], consistent with the CT1-inspired limited caspase activation model we favor (Figure 6).

It is generally accepted that prolonged pathological cardiac hypertrophy frequently transitions to HF, which causes eccentric hypertrophy with chamber dilation and

Figure 5 hCT1 attenuates the morphologic and hemodynamic effects of pulmonary arterial hypertension (PAH) in the Sugen/hypoxia (SUHx) rat model. **(A)** PAH was induced by administering a single subcutaneous injection of SU5416 (SU) at 20 mg/kg (VEGF receptor antagonist) followed by exposure to chronic hypoxia (Hx) at 10% oxygen for 3 weeks. Rats were recovered for 24 h in normoxia before subcutaneous implantation of osmotic minipumps containing hCT1 (6 μg/kg/h) or phosphate-buffered saline (PBS). Echocardiography was conducted and the following parameters were measured: right ventricle free wall thickness (RVFW; **B**), right to left ventricle internal diameter ratio (RVID:LVID; **C**), pulmonary artery acceleration time (PAAT; **D**), fractional area change (FAC; **E**), and cardiac output (CO; **F**). Control rats were not exposed to SU5416 or hypoxia. **(B-F)** Significant differences were observed between the PAH-induced SUHx rat groups (hCT1 or PBS) and the control rat group (n = 3; ****P < 0.0001). At 5-6 weeks, hCT1-treated SUHx animals showed a significant increase in CO **(F)** and FAC **(E)**, and a decrease in RVID:LVID **(C)** and RVFW **(B)** versus the PBS-treated SUHx group (n = 3; **P < 0.01, ***P < 0.001 and ****P < 0.0001). **(G**, **H)** hCT1 treatment significantly increased capillary density versus PBS-treated SUHx animals (n = 3; *P < 0.05). **(H)** Capillaries stained with endothelial-specific CD31+ antibody followed by chromogenic detection (DAB, brown). Nuclei counterstained with Hematoxylin. Scale bar, 50 μm. **(I**, **J)** hCT1 treatment significantly decreased cardiomyocyte cross-sectional area in the right ventricle versus PBS-treated SUHx animals (n = 3; *P < 0.05). **(J)** Masson's Trichrome staining of heart cross-sectional area. Scale bar, 50 μm.

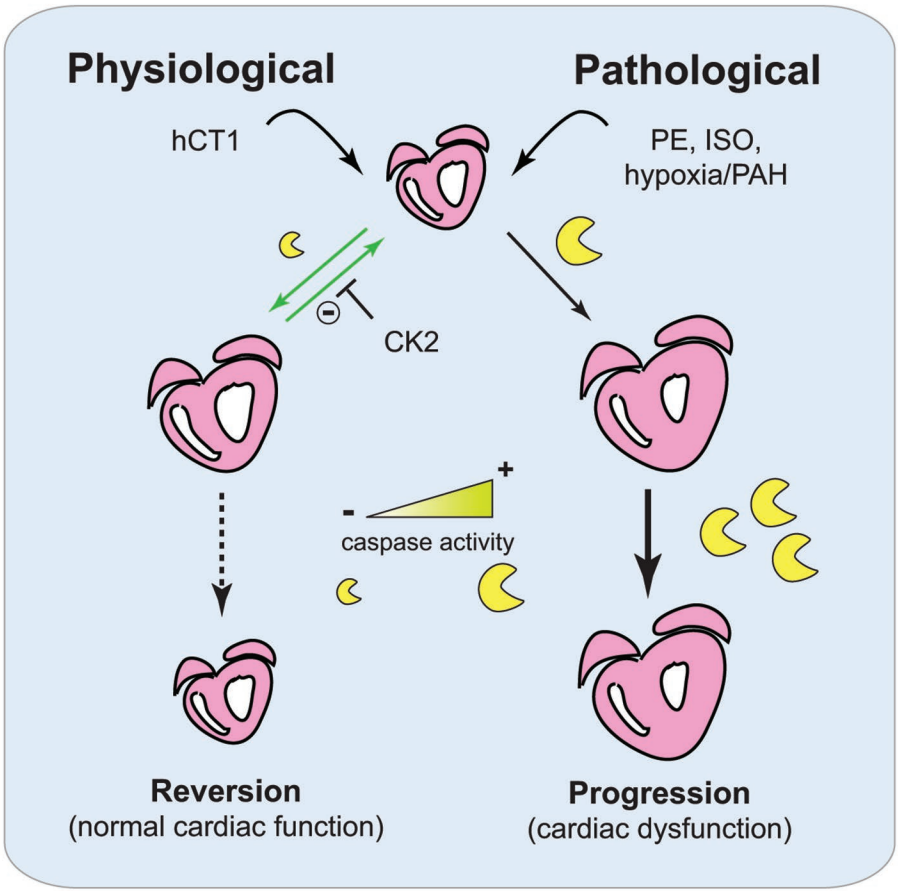


Figure 6 Proposed model of hCT1-mediated physiologic cardiac hypertrophy. hCT1 promotes reversible and beneficial cardiac remodeling by restraining caspase activation via CK2; whereas pathological stimulation (with PE, ISO, or hypoxia/PAH) causes unrestricted caspase activation with progression to cardiac dysfunction. Heart (pink), caspases (yellow), hCT1 (human cardiotrophin 1), PE (phenylephrine), ISO (isoproterenol), CK2 (casein kinase 2), PAH (pulmonary arterial hypertension).

thinning of the myocardium [3]. Although studies have shown that increased cardiomyocyte lengthening contributes to chamber dilation and myocardial thinning in HF [55], there is an appreciable number of studies that provide compelling evidence that exercise training also induces a beneficial cardiomyocyte response, in both morphology and function, by means of cardiomyocyte lengthening/elongation [56-59]. For example, low-intensity endurance training in rats resulted in eccentric hypertrophy of the left ventricle (LV) with increased length to width ratio of cardiomyocytes [57]. Although RV cardiomyocytes showed no change in length to width ratio, the authors postulate that the adaptive response of RV cardiomyocytes might depend on a more prolonged or intense exercise regimen such as high-intensity endurance training. Furthermore, cardiomyocyte lengthening was positively correlated with aerobic fitness in rats exposed to exercise treadmill training and detraining [59]. With training, cardiomyocyte length increased along with aerobic fitness. However, most of the aerobic fitness gained over 2-3 months was lost within 4 weeks of detraining, including regression of cardiomyocyte length back to sedentary control values [59].

It is also important to note that programmed cell death (apoptosis) of cardiomyocytes is an essential process in the progression of dilated cardiomyopathy (DCM) and HF, and patients with DCM and HF have significantly higher apoptosis than control patients [60, 61]. It is reasonable to conjecture that much of the eccentric hypertrophy and cardiomyocyte lengthening seen in the progression of DCM and HF is likely attributed to the indirect stretching of a weakened myocardium, which is a secondary effect to the direct loss of cardiomyocytes due to apoptosis. In the context of our study and our proposed model (Figure 6), we show that hCT1 stimulation does not lead to cell death, but rather, the observed cardiomyocyte lengthening is a result of specific engagement of a beneficial and reversible physiological hypertrophy

process.

Moreover, there is plausible evolutionary evidence indicating that cellular elongation (or length to width ratio increase) provides a survival advantage to a cell or an organism [62]. Remarkably, some cells respond to stress (nutrient deprivation) by changing shapes via elongation (i.e., similar to eccentric growth and increased length to width ratio with hCT1 stimulation), which maximizes the "surface area to volume ratio" and this allows for efficient nutrient uptake during times of stress. On the contrary, spherical cells (i.e., similar to concentric growth and reduced length to width ratio with PE) have the worst possible shape for efficient nutrient/substrate uptake. This could partly account for the effects seen with pathological hypertrophy due to the inability of the hypertrophied cardiomyocyte to meet metabolic demands.

We have noted that CT1 engages signals that are proto-typical of the larger IL-6 cytokine family and are not conserved responses to pathologic hypertrophy agonists *per se*, i.e., gp130-mediated activation of STAT-dependent transcriptional activity. The STAT transcriptional response was sustained and likely contributes to the unique phenotypic outcome that characterizes physiologic hypertrophy and its beneficial remodeling events. At this stage we do not understand precisely how STAT-dependent signaling manifest change within the adapting cardiomyocyte. There is evidence to suggest that STAT activity can modify contractile protein content through upregulation of angiotensin gene expression, while promoting a pro-survival anti-apoptotic response [63]. This observation is certainly consistent with our studies, where CT1 stimulates a restricted caspase activation pattern. STAT transcriptional activity may also be a primary mechanism by which CT1 engages the cardiomyocyte production of angiogenic factors, i.e., STAT3 has been shown to be essential for promoting pro-angiogenic activity/capillarization within the myocardium [64, 65].

The myocardial and vascular remodeling capacity of CT1 implies that it may be effective in combating myopathies and ischemic heart disease in general. For example, the scalable and reversible hypertrophy that derives from CT1 stimulation may improve the contractile function of the post-infarct myocardium, while the pro-angiogenic and anti-fibrotic activities would curtail the loss in functional myocardium that occurs in the weeks following the initial ischemic damage. Indeed, preliminary experiments demonstrate that hCT1 protein can reduce scar size and improve contractile performance in a rodent infarct model up to 8 weeks from the initial insult (ligation of the left descending coronary artery; Supplementary information, Figure S7A and S7B). The rodent myocardium is more robust in the formation of collateral vessels compared to the human heart, nevertheless these observations provide a strong impetus to explore CT1 as a viable myocardial rejuvenation therapy in ischemic disease settings. Collectively, our studies suggest that CT1 protein therapy may provide a tractable means to improve cardiac function across a broad range of myopathic and ischemic disease.

Although pathologic hypertrophy frequently becomes irreversible and transitions to HF [66], the phenotype can be reversed under limited circumstances. For example, inhibition of cGMP phosphodiesterase 5A (PDE5A) has been shown to prevent and reverse pressure overload-induced pathologic cardiac hypertrophy [67]. Also, calcineurin-dependent pathologic cardiac hypertrophy is partially reversible upon removal of calcineurin activity [68]. Furthermore, common anti-hypertensive treatments (e.g., β-blockers and angiotensin receptor blockers) can lead to partial reversion of pathologic hypertrophy in patients with hypertension [69]. Although these treatments reverse pathologic cardiac growth, the reversion is not complete as there is remnant fibrosis present. One of the most essential features distinguishing physiological from pathological hypertrophy is the capacity for complete growth reversion without residual fibrotic pathology [70]. As such, our observations are consistent with the hypothesis that hCT1 induces reversible physiological hypertrophy.

Finally, it is germane to note that therapeutic strategies designed to interdict or block caspase 3 activity, as a means to reduce myocardial cell death, are destined to fail. The transient activation of caspase 3 is a key step in the beneficial remodeling process afforded by CT1, and may also be central to exercise and pregnancy-associated myocardial adaptation. As such, indiscriminate disruption in the baseline activity of this protease will lead to a decline in adaptive capacity of the myocardium, while exacerbating disease progression.

Materials and Methods

Rats and mice

All animal studies (primary cell retrieval and *in vivo* analysis) were approved by the University of Ottawa Animal Care Committee. Sprague-Dawley rats, Fischer rats, and C57BL/6 mice were obtained from Charles River Laboratories (Wilmington, MA, USA).

Neonatal rat primary cardiomyocytes

Primary neonatal rat cardiomyocytes were freshly isolated from hearts of 2-day-old Sprague-Dawley rats (Charles River Laboratories). Hearts were excised and placed in Joklik's-modified Eagle medium (JMEM). Ventricles were separated from the atria, minced with scalpel blades, and transferred to a 50 ml Falcon tube for digestion with 200 units per ml of Collagenase II (Worthington) in a

total of 10 ml JMEM at 37 °C with gentle agitation. After 15 min, use a 25 ml pipet to slowly triturate (pipet up and down) the tissue and media about 2-3 times and then briefly wait for the tissue to settle at the bottom of the pipet. Then, pipet out ("spit") the tissue into a clean tube for further Collagenase digestions while discarding the supernatant remaining in the pipet ("Digestion #0"), which contains mostly red blood cells and cell debris.

Perform another 4-5 rounds of Collagenase digests of the minced/digested heart tissue (as above); however, this time, the supernatant (containing an appreciable amount of primary cardiomyocytes) is transferred to a tube containing 10 ml of fetal bovine serum to stop the Collagenase reaction. This tube is centrifuged at 100× *g* for 5 min at room temperature to pellet the cells. The supernatant is discarded and the cells are resuspended in 1 ml Dulbecco's Modified Eagle Medium (DMEM) growth medium. Pool all the individual 1 ml cardiomyocyte fractions from the Collagenase digests into one tube. Transfer the volume of pooled cardiomyocytes onto a 70 μm filter pore size cell strainer (CellTreat) assembled on top of a 50 ml Falcon tube to help further remove cell clumps and cell debris. Wash the cell strainer with an additional 25 ml of DMEM growth medium.

Conduct a pre-plating step (to separate out cardiac fibroblasts and enrich for cardiomyocytes) by transferring the entire volume of flow-through onto a sterile 15 cm tissue culture dish and incubate at 37 °C for 30 min. Fibroblasts will adhere to the dish while cardiomyocytes remain in the media. Carefully collect the media using a 25 ml pipet and transfer to a new sterile 15 cm tissue culture dish for another round of pre-plating to further enrich for cardiomyocytes. After the second pre-plating incubation, transfer media to a sterile tube and centrifuge at 100× *g* for 5 min at room temperature. Discard the supernatant and resuspend the ventricular pellet in 5 ml of DMEM growth medium and this is the primary cardiomyocyte stock.

Count the number of cardiomyocytes using a Hemocytometer (cells per ml), then seed the desired number of cells directly onto collagen-coated tissue culture dishes and allow cells to recover overnight in DMEM growth medium in an incubator at 37 °C with 5% CO_2. The next day, DMEM growth medium was replaced with serum-free (SF) medium and incubated for another day (up to 24 h) at 37 °C prior to conducting specific experiments.

Adult mouse primary cardiomyocytes

Adult C57BL/6 mice (Charles River Laboratories) at 9 weeks of age were anesthetized using Avertin (0.4 mg/g) intraperitoneally. Thoracic cavity was then opened to expose the heart. Using a syringe pump, pre-warmed (37 °C) perfusion solution (126 mM NaCl, 4.4 mM KCl, 1 mM $MgCl_2$, 4 mM $NaHCO_3$, 30 mM 2,3-butanedione monoxime, 10 mM HEPES, 11 mM glucose, 0.5 mM EDTA, 0.09% Collagenase Type 2, 0.125% trypsin, 25 μM $CaCl_2$ pH 7.4) was pumped through a 26G needle at a rate of 4 ml/min. The needle was inserted into the LV through the apex of the heart and the right atrium was cut. The mouse was then perfused for 5 min. The heart was then carefully removed and placed into a stop solution (126 mM NaCl, 4.4 mM KCl, 1 mM $MgCl_2$, 4 mM $NaHCO_3$, 30 mM 2,3-butanedione monoxime, 10 mM HEPES, 11 mM glucose, 0.5 mM EDTA, 100 μM $CaCl_2$, 2% BSA pH 7.4) at 37 °C for 10 min. The heart was then cut into small pieces and gently triturated about 20-30 times using a wide-bore pipette in a petri dish. A 100 μm nylon mesh filter was used to remove large debris. Formalin (20%) was added in a 1:1 ratio to obtain a final concentration of 10% formalin. Cells were fixed for 15 min. The solution was then spun at 50× *g* for 5 min to pellet cardiomyocytes. Supernatant was disposed and cardiomyocytes were resuspended in PBS prior to conducting fluorescence cell staining.

Recombinant hCT1 protein production

BL21 (DE3) cells (New England Biolabs) were transformed with a plasmid encoding wild-type hCT1. A fresh starter culture prepared from the transformed cells was diluted by 25-fold into 0.5 L Overnight Express autoinduction medium (EMD Millipore) prepared in 2×YT supplemented with 100 μg/ml kanamycin. The culture was grown in a shaking incubator at 37 °C for overnight. Cells were harvested and washed by PBS.

Cell pellet was resuspended in lysis buffer (50 mM Tris-HCl, pH 8.0, 100 mM NaCl, 1 mM EDTA, 10 mM DTT) supplemented with complete protease inhibitor cocktail (Roche) and 0.1% w/v sodium deoxycholate. Cells were lysed by sonication. The inclusion bodies contained in the pellet were washed three times by Triton wash buffer (50 mM Tris-HCl, 100 mM NaCl, 0.5% Triton X-100, 1 mM EDTA, and 1 mM DTT, pH 8.0) followed by three times by Tris wash buffer (50 mM Tris-HCl, 1 mM EDTA, and 1 mM DTT, pH 8.0).

Washed inclusion bodies were solubilized in solubilization buffer (100 mM sodium acetate, 2 M urea, 2 mM DTT, pH 3.5) at room temperature and centrifuged at 22 000× *g* for 30 min. The supernatant was dialyzed against Refolding buffer (20 mM HEPES, 2 mM DTT, pH 7.5) overnight at 4 °C . The refolded protein was centrifuged at 22 000× *g* for 30 min and filtered through a 0.22 μm filter and loaded to a HiTrap CM FF column (5 ml, GE Life Sciences) pre-equilibrated with solvent A (10 mM sodium phosphate, pH 7.5). Column was washed by 5 column volumes of solvent A, and the bound proteins were eluted stepwise by solvent A in 0.1 M NaCl then by solvent A in 1 M NaCl. The 0.1 M NaCl eluate was pooled and dialyzed against PBS overnight at 4 °C . Protein purity was estimated by SEC-HPLC to be > 95%. Mass spectrometry and Edman degradation indicated that the purified protein has a sequence of Ser2-Ala201 of the wild-type hCT1.

Neonatal rat cardiomyocyte treatments

To induce hypertrophy, cardiomyocytes were treated for 24 (or 48) h with the following hypertrophic agonists diluted in SF control medium (SF, Ctrl): hCT1 recombinant protein at 0.5 nM (10 ng/ml) and PE at 100 μM. Serum-free control medium was also used as a non-hypertrophic control.

For caspase 9 inhibition, cardiomyocytes were pre-treated with N-benzyloxycarbonyl-Leu-Glu-His-Asp-fluoromethylketone (z-LEHD-fmk, 20 μM; BioVision) for 2 h before the induction of hypertrophy when fresh inhibitor was added. For effector caspase inhibition, cardiomyocytes were infected for 24 h with an AdV encoding the biologic effector caspase inhibitor p35 upstream of a GFP reporter (p35-AdV) prior to inducing hypertrophy with hCT1 or PE for a further 24 h. A GFP expressing reporter (GFP-AdV) was used as a control and both p35-AdV and GFP-AdV were infected at a mean of infectivity of 20 prior to hypertrophic stimulation. For Casein kinase 2 (CK2) inhibition, cardiomyocytes were pre-treated with 4,5,6,7-tetrabromobenzotriazole (TBBt, 50 μM; EMD Millipore) for 1 h before the induction of hypertrophy when fresh inhibitor was added.

To obtain conditioned medium for detection of the secreted angiogenic factor – VEGF, cardiomyocytes were seeded at a density of 1.0×10^6 cells directly onto 60 mm diameter tissue culture dishes. Hypertrophy was induced with hCT1 (0.5 nM) or PE (100 μM) diluted in a total volume of 3 ml of control SF medium. After 24 h, the conditioned medium was transferred onto an Amicon Centrifugal Filter Device with a 3 kDa cut-off (EMD Millipore) and centrifuged at 4 000× *g* for 30 min at room temperature. The concentrated conditioned medium was analyzed by western immunoblotting. Recombinant VEGF protein (Abcam) was used as a positive control.

Luciferase assays

Primary rat cardiomyocytes were seeded onto collagen-coated 48-well tissue culture plates (0.7×10^5 cells/well) in DMEM growth medium. The following day, cells were transfected using Lipofectamine 2000 (Invitrogen), SF Opti-MEMα (Thermo Fisher), 4 ng of Renilla luciferase internal control plasmid, and 200 ng of Firefly luciferase reporter DNA plasmid under the control of: pro-hypertrophic gene promoters (NF-κB or Mef2), or a pro-survival gene promoter (Stat3), or a pro-inflammatory gene promoter (Stat1) for 5 h at 37 °C with 5% CO_2. The medium was replaced with SF medium and cells were incubated overnight at 37 °C with 5% CO_2. The next day, cardiomyocytes were treated with: non-hypertrophic SF medium control (Ctrl), hCT1 (0.5 nM), PE (100 μM), or procaspase 3-activating compound 1, PAC-1 (25 μM). Treatments were conducted at early time points (30 min, 1 h, and 3 h) and at a later time point (24 h). Luciferase activity (pro-hypertrophic reporter activation) was measured using the Dual Luciferase Assay System as per manufacturer's instructions (Promega). Luciferase values were normalized to the Renilla internal control values and to the SF medium control values.

Oxygen consumption rate assay

Primary rat cardiomyocytes were seeded onto collagen-coated 98-well tissue culture plates (0.9×10^5 cells/well) in DMEM growth medium. The next day, cell culture medium was replaced with SF medium for 24 h. Cardiomyocytes were treated for 1 or 24 h with the following hypertrophic agonists diluted in SF control medium (SF, Ctrl): hCT1 recombinant protein at 0.5 nM (10 ng/ml) and PE at 100 μM. Serum-free control medium was used as a non-hypertrophic control. The MitoXpress – Xtra Oxygen Consumption Rate (OCR) Assay kit was used to measure oxygen consumption according to manufacturer's instructions (Cayman Chemical). Glucose Oxidase enzyme was used as a positive control. The phosphorescent oxygen probe (MitoXpress – Xtra) was used to measure the rate of oxygen consumption in whole cells by standard fluorescence intensity analysis using an excitation of 380 nm and emission of 650 nm.

Immunocytochemistry

Fluorescent cell staining was conducted on primary rat cardiomyocytes (or cardiac fibroblasts) that were seeded at a density of 2.7×10^5 cells directly onto 25 mm diameter collagen-coated glass coverslips. Cells were washed three times in PBS (3 min each) followed by fixation in 4% paraformaldehyde for 30 min. Cells were then permeabilized in Blocking buffer (1% bovine serum albumin – BSA, 2% normal goat serum, 0.4% Tx-100 in PBS) for 15 min. Cells were then incubated for 2 h at room temperature with primary antibody (diluted in Blocking buffer) followed by three successive washes in PBS at 3 min each. Cells were then blocked again in Blocking buffer for 15 min followed by a 1 h incubation in fluorescently conjugated secondary antibody (diluted in Blocking buffer). Cells were then washed again in PBS (five times at 5 min each). Nuclei were counterstained with 4',6-diamidino-2-phenylindole (DAPI) and cells were mounted onto microscope slides with DakoCytomation fluorescent mounting medium (Dako). Digital fluorescent images were obtained using the Zeiss AxioVision SE64 Imaging software (Zeiss).

Primary antibodies used: mouse anti-α-actinin (Sigma), rabbit anti-atrial natriuretic peptide (ANP; Abcam), rabbit anti-active caspase 9 (Abcam), rabbit anti-VEGF (Abcam), rabbit anti-vimentin (Abcam), mouse anti-Galectin-3 (Abcam).

Secondary antibodies used: goat anti-mouse-Cy3 and donkey anti-rabbit-Cy3 (EMD Millipore), Alexa Fluor-488 goat anti-rabbit and Alexa Fluor-647 donkey anti-mouse (ThermoFisher).

Fluorescent cell staining was also conducted on isolated adult primary mouse cardiomyocytes; however, a high-affinity fluorescently labeled phallotoxin probe was used to detect filamentous F-actin: Alexa Fluor-488 conjugated Phalloidin (ThermoFisher). Nuclei were counterstained with DAPI. Digital images were acquired by fluorescence microscopy and cells were analyzed using ImageJ.

Western blotting

Cells were washed in PBS and harvested by centrifugation. Cells were then resuspended in lysis buffer supplemented with protease inhibitors (50 mM HEPES pH 7.5, 150 mM NaCl, 10% glycerol, 1% Tx-100, 1 mM EGTA, 1.5 mM $MgCl_2$, 20 mM NaF, 10 mM sodium pyrophosphate, 0.3 mM PMSF, 2.5 mM sodium orthovanadate) and incubated at 4 °C with gentle rotation for 1 h. Crude lysate was centrifuged at 17 000× *g* for 10 min. Equal amounts (20 μg) of protein were separated by SDS-PAGE and transferred to PVDF membrane for immunoblotting. After blocking the membrane with TBST-milk (10 mM Tris pH 7.4, 150 mM NaCl, 0.05% Tween-20, 5% non-fat powdered milk), membranes were incubated with primary antibody overnight at 4 °C followed by incubation with horseradish peroxidase (HRP)-conjugated secondary antibody for 1 h. Protein expression was detected using the ECL detection kit (GE Healthcare).

Primary antibodies used: rabbit anti-active caspase 3 (Cell Signaling), rabbit anti-glyceraldehyde-3-phosphate dehydrogenase (GAPDH; Cell Signaling), rabbit anti-VEGF (Abcam).

Secondary antibodies used: goat anti-mouse IgG-HRP and goat anti-rabbit IgG-HRP (Bio-Rad).

In vivo analysis

Reversion study and 2-week-only analysis (i) Preparation and surgical implantation of osmotic minipumps. Osmotic minipumps (Model 2002, Alzet; Durect) were used to infuse the following over 2 weeks: hCT1, PE, ISO, or PBS as a non-hypertrophic control. Alzet minipumps (Model 2002) have a reservoir volume of 200 μl and infuse at a steady rate of 0.5 μl/h for 2 weeks. hCT1 was diluted accordingly in PBS based on the average rat weight per group to give a final infusion dose of 6 μg/kg/h. Similarly, the infusion doses for PE and ISO were 10 and 1 mg/kg/d; respectively. All prepared minipumps (PBS, hCT1, PE, and ISO) were pre-equilibrated in normal saline (0.9% NaCl) overnight at 37 °C

in order to reach a steady-state pumping rate of 0.5 µl/h at the time of subcutaneous implantation into Sprague-Dawley rats. Rats were anesthetized with a mixture of 2% Isoflurane and pure oxygen (at 1L per min). Under sterile conditions, a subcutaneous incision was made between the shoulder blades in the upper back using a scalpel blade and an osmotic minipump was gently inserted under the skin. The incision area was then firmly stapled and rats were placed back into their respective cages to recover.

(ii) For the Reversion study, osmotic minipumps (Model 2002) were implanted into three groups of rats. PBS control, hCT1 at 6 µg/kg/h, or PE at 10 mg/kg/d. Rats weighed an average of 300 g at time of surgery. After 2 weeks, cardiac echocardiography was performed, minipumps were then surgically removed, and rats were allowed to recover. At 6 weeks post withdrawal (i.e., at 8 weeks of the study), rats were subjected to another round of cardiac echocardiography and rats were killed and heart tissues were excised for analysis. Of note, the 2-week-only rat study group was divided into the following three groups: PBS control, hCT1 at 6 µg/kg/h, or ISO at 1 mg/kg/d.

(iii) Tissue analysis and histology. All excised hearts were placed in 10% formalin for at least 48-72 h prior to embedding in paraffin and sectioning. The following immunohistochemical analyses were conducted on sectioned tissues: hematoxylin and eosin (H&E) for general morphology, Masson's Trichrome for collagen/fibrotic deposition, and CD31+ (platelet endothelial cell adhesion molecule) staining for angiogenesis and capillary density. Analysis for CD31+ was antibody-based and utilized the colorimetric detection of a 3',3'-Diaminobenzidine (DAB) chromogen (brown precipitate) according to manufacturer's instructions (MACH4 Detection System; BioCare Medical). Immunohistologic analyses were also conducted by the Pathology and Laboratory Medicine (PALM) Histology Core Facility at the University of Ottawa, Canada.

Sugen/hypoxia (SUHx) rat analysis (i) SUHx study outline. PAH was induced by administering a single subcutaneous injection of SU5416 (SU) at 20 mg/kg (a potent VEGFR – VEGFR antagonist) into Fischer rats followed by exposure to chronic hypoxia (CH; 10% oxygen) for 3 weeks. At 3 weeks, rats were recovered for 24 h under normoxic conditions (21% oxygen) before subcutaneous implantation of Osmotic minipumps (Model 2ML4) containing either hCT1 (6 µg/kg/h) or PBS. Cardiac echocardiography analysis was conducted weekly up to the end of study at 7 weeks at which time rats were killed and heart tissues excised for analysis and histology.

(ii) Preparation of osmotic minipumps for SUH analysis. After 3 weeks induction of PAH in Fischer rats followed by 24 h of recovery under normoxic conditions, osmotic minipumps (Model 2ML4, Alzet; Durect) were used to infuse hCT1. PBS was infused for the control rat group. Osmotic minipumps (Model 2ML4) have a reservoir volume of 2 ml and infuse at a steady rate of 2.5 µl/h for 4 weeks. hCT1 was diluted accordingly in PBS based on the average rat weight per group (150 g) to give a final infusion dose of 6 µg/kg/h. All prepared minipumps (PBS and hCT1) were pre-equilibrated in normal saline (0.9% NaCl) overnight at 37 °C in order to reach a steady-state pumping rate of 2.5 µl/h at the time of subcutaneous implantation.

Adult mouse primary cardiomyocyte morphology analysis (i) Study outline. Adult C57BL/6 mice (9 weeks of age) were subcutaneously implanted with Osmotic minipumps (Model 1002) containing: hCT1, PE, or PBS as a non-hypertrophic control. After 2 weeks of infusion, the mice were anesthetized and adult mouse primary cardiomyocytes were isolated by perfusing and digesting whole hearts (see protocol for isolating adult mouse cardiomyocytes). Cardiomyocytes were then stained using immunocytochemistry and analyzed for morphological changes.

(ii) Preparation and surgical implantation of osmotic minipumps. Osmotic minipumps (Model 1002, Alzet; Durect) were used to infuse the following over 2 weeks: PBS (control), hCT1 (6 µg/kg/h), and PE (10 mg/kg/d). Alzet minipumps (Model 1002) have a reservoir volume of 100 µl and infuse at a steady rate of 0.25 µl/h for 2 weeks All prepared minipumps (PBS, hCT1, and PE) were pre-equilibrated in normal saline (0.9% NaCl) overnight at 37 °C in order to reach a steady-state pumping rate of 0.25 µl/h at the time of subcutaneous implantation.

Myocardial infarction analysis Ligation of the left anterior descending coronary artery (LAD) was used to induce a myocardial infarct in rats. Male Sprague-Dawley rats weighing 250 g at the time of surgery were subjected to LAD ligation surgery or were sham operated (open cavity, no LAD). Following ligation, animals were given an intracardiac injection of hCT1-AdV at 7.5×10^5 infectious particles per gram weight, administered into the middle region of the LV. A separate group of animals were given saline following LAD surgery. The animals were allowed to recover for 2 weeks followed by a second intracardiac booster injection of either hCT1-AdV or saline (as above).

At 8 weeks post myocardial infarction, LV function was measured for each animal using a 2 F high-fidelity micro-manometer catheter (Millar Institute) inserted into the LV through the right carotid artery. A Harvard Data Acquisition system (Harvard Apparatus) was used to acquire data and processed using AcqKnowledge III software (ACQ 3.2) for measurement of left ventricular end-diastolic pressure, a critical hemodynamic measurement of ventricular performance. Immediately after acquisition, animals were injected with a 2 M KCl solution to stop the heart in diastole. The heart was excised and fixed in 10% formalin prior to paraffin embedding. Approximately 5-8 µm sections were stained with H&E and counterstained with Masson's Trichrome to visualize the infarct area.

Microarray analysis

Primary neonatal rat cardiomyocytes (previously seeded at 2.5×10^6 onto collagen-coated 10 cm tissue culture dishes) were treated for 24 h with hCT1 (0.5 nM) or with control SF medium. Total RNA was isolated using a TRIzol reagent extraction method. Briefly, 2 ml of TRIzol (ThermoFisher) was added per dish and gently agitated for 5 min at room temperature to lyse cells. The lysate was transferred to a 15 ml Falcon tube and 0.4 ml of chloroform was added. The tube was vortexed for 20 s, left to rest/settle for 3 min, and centrifuged at 3 200× *g* for 25 min, all at room temperature. The clear upper aqueous layer (containing RNA) was transferred to a sterile eppendorf tube and an equal volume of isopropanol was added to precipitate RNA overnight at −20 °C. The RNA pellet was centrifuged at 10 000× *g* for 15 min at 4 °C, washed in 70% ethanol (RNase-free), and resuspended in 100 µl of sterile water (RNase-free).

The RNA was cleaned with the RNeasy MinElute Cleanup kit

(Qiagen) and 300 ng of RNA was processed for microarray using the Affymetrix GeneChip WT PLUS Reagent Kit (Affymetrix) according to manufacturer's instructions. The microarray processing and bioinformatics analysis was conducted at the StemCore Facility of The Ottawa Hospital Research Institute, Canada. Raw data files for the microarray analysis have been deposited in the NCBI Gene Expression Omnibus under accession number GSE87521.

Statistical analysis

All data are expressed as mean ± SEM. Statistical significance for multiple-group comparisons was determined using one-way ANOVA followed by post-hoc statistical analysis (GraphPad Prism software). Dunnett's test was used for pairwise comparisons of treatment groups with control groups and Tukey's test was used for pairwise comparisons between treatment groups. $P < 0.05$ was considered significant.

Acknowledgments

We thank Michael Rudnicki and Jeff Dilworth for insightful discussion. We would also like to thank Monir Ahmad (for performing the myocardial infarction surgeries) and the Ottawa Bioinformatics Core Facility. This work was supported by grants from the Canadian Institutes of Health Research (to LAM and DJS), the Ontario Research Fund (LAM and DJS), the Heart & Stroke Foundation of Canada (LAM) and through a sponsored research contract with Fate Therapeutics (LAM). LAM has served as a member of the scientific advisory board of Fate Therapeutics (to 2015).

Author Contributions

MA-G, CS, BJ, YD, JJW, CP, SB, PF, TTL, PF, FHHL, PGB, DJS, and LAM designed research; MA-G, CS, BJ, YD, JJW, CP, SB, PF, TTL, PF and PGB performed research; MA-G, CS, BJ, YD, JJW, CP, SB, PF, TTL, PF, FHHL, PGB, DJS, and LAM analyzed data; and MA-G, CS, DJS, and LAM wrote the paper.

Competing Financial Interests

The authors declare no competing financial interests.

References

1 Hill JA, Olson EN. Cardiac plasticity. *N Engl J Med* 2008; **358**:1370-1380.
2 Harvey PA, Leinwand LA. The cell biology of disease: cellular mechanisms of cardiomyopathy. *J Cell Biol* 2011; **194**:355-365.
3 van Berlo JH, Maillet M, Molkentin JD. Signaling effectors underlying pathologic growth and remodeling of the heart. *J Clin Invest* 2013; **123**:37-45.
4 Chung E, Leinwand LA. Pregnancy as a cardiac stress model. *Cardiovasc Res* 2014; **101**:561-570.
5 Roh J, Rhee J, Chaudhari V, Rosenzweig A. The role of exercise in cardiac aging: from physiology to molecular mechanisms. *Circ Res* 2016; **118**:279-295.
6 Bueno OF, De Windt LJ, Tymitz KM, *et al.* The MEK1-ERK1/2 signaling pathway promotes compensated cardiac hypertrophy in transgenic mice. *EMBO J* 2000; **19**:6341-6350.
7 Condorelli G, Drusco A, Stassi G, *et al.* Akt induces enhanced myocardial contractility and cell size *in vivo* in transgenic mice. *Proc Natl Acad Sci USA* 2002; **99**:12333-12338.
8 Maillet M, van Berlo JH, Molkentin JD. Molecular basis of physiological heart growth: fundamental concepts and new players. *Nat Rev Mol Cell Biol* 2013; **14**:38-48.
9 Shiojima I, Walsh K. Regulation of cardiac growth and coronary angiogenesis by the Akt/PKB signaling pathway. *Genes Dev* 2006; **20**:3347-3365.
10 Shiojima I, Yefremashvili M, Luo Z, *et al.* Akt signaling mediates postnatal heart growth in response to insulin and nutritional status. *J Biol Chem* 2002; **277**:37670-37677.
11 Duerr RL, Huang S, Miraliakbar HR, Clark R, Chien KR, Ross J, Jr. Insulin-like growth factor-1 enhances ventricular hypertrophy and function during the onset of experimental cardiac failure. *J Clin Invest* 1995; **95**:619-627.
12 McMullen JR, Shioi T, Huang WY, *et al.* The insulin-like growth factor 1 receptor induces physiological heart growth via the phosphoinositide 3-kinase(p110alpha) pathway. *J Biol Chem* 2004; **279**:4782-4793.
13 Sapra G, Tham YK, Cemerlang N, *et al.* The small-molecule BGP-15 protects against heart failure and atrial fibrillation in mice. *Nat Commun* 2014; **5**:5705.
14 Pennica D, King KL, Shaw KJ, *et al.* Expression cloning of cardiotrophin 1, a cytokine that induces cardiac myocyte hypertrophy. *Proc Natl Acad Sci USA* 1995; **92**:1142-1146.
15 Wollert KC, Taga T, Saito M, *et al.* Cardiotrophin-1 activates a distinct form of cardiac muscle cell hypertrophy. Assembly of sarcomeric units in series VIA gp130/leukemia inhibitory factor receptor-dependent pathways. *J Biol Chem* 1996; **271**:9535-9545.
16 Ishikawa M, Saito Y, Miyamoto Y, *et al.* A heart-specific increase in cardiotrophin-1 gene expression precedes the establishment of ventricular hypertrophy in genetically hypertensive rats. *J Hypertens* 1999; **17**:807-816.
17 Jin H, Yang R, Keller GA, *et al. In vivo* effects of cardiotrophin-1. *Cytokine* 1996; **8**:920-926.
18 Lopez B, Gonzalez A, Querejeta R, Larman M, Rabago G, Diez J. Association of cardiotrophin-1 with myocardial fibrosis in hypertensive patients with heart failure. *Hypertension* 2014; **63**:483-489.
19 Schillaci G, Pucci G, Perlini S. From hypertension to hypertrophy to heart failure: the role of cardiotrophin-1. *J Hypertens* 2013; **31**:474-476.
20 Fischer P, Hilfiker-Kleiner D. Survival pathways in hypertrophy and heart failure: the gp130-STAT axis. *Basic Res Cardiol* 2007; **102**:393-411.
21 Hirota H, Chen J, Betz UA, *et al.* Loss of a gp130 cardiac muscle cell survival pathway is a critical event in the onset of heart failure during biomechanical stress. *Cell* 1999; **97**:189-198.
22 Yoshida K, Taga T, Saito M, *et al.* Targeted disruption of gp130, a common signal transducer for the interleukin 6 family of cytokines, leads to myocardial and hematological disorders. *Proc Natl Acad Sci USA* 1996; **93**:407-411.
23 Calabro P, Limongelli G, Riegler L, *et al.* Novel insights into the role of cardiotrophin-1 in cardiovascular diseases. *J Mol Cell Cardiol* 2009; **46**:142-148.
24 Aguilar-Melero P, Luque A, Machuca MM, *et al.* Cardiotro-

phin-1 reduces ischemia/reperfusion injury during liver transplant. *J Surg Res* 2013; **181**:e83-91.
25 Iniguez M, Berasain C, Martinez-Anso E, *et al.* Cardiotrophin-1 defends the liver against ischemia-reperfusion injury and mediates the protective effect of ischemic preconditioning. *J Exp Med* 2006; **203**:2809-2815.
26 Moreno-Aliaga MJ, Perez-Echarri N, Marcos-Gomez B, *et al.* Cardiotrophin-1 is a key regulator of glucose and lipid metabolism. *Cell Metab* 2011; **14**:242-253.
27 Kolodziejczyk SM, Wang L, Balazsi K, DeRepentigny Y, Kothary R, Megeney LA. MEF2 is upregulated during cardiac hypertrophy and is required for normal post-natal growth of the myocardium. *Curr Biol* 1999; **9**:1203-1206.
28 Naya FJ, Black BL, Wu H, *et al.* Mitochondrial deficiency and cardiac sudden death in mice lacking the MEF2A transcription factor. *Nat Med* 2002; **8**:1303-1309.
29 van Rooij E, Fielitz J, Sutherland LB, *et al.* Myocyte enhancer factor 2 and class II histone deacetylases control a gender-specific pathway of cardioprotection mediated by the estrogen receptor. *Circ Res* 2010; **106**:155-165.
30 Abdul-Ghani M, Megeney LA. Rehabilitation of a contract killer: caspase-3 directs stem cell differentiation. *Cell Stem Cell* 2008; **2**:515-516.
31 Dick SA, Megeney LA. Cell death proteins: an evolutionary role in cellular adaptation before the advent of apoptosis. *Bioessays* 2013; **35**:974-983.
32 Fuchs Y, Steller H. Programmed cell death in animal development and disease. *Cell* 2011; **147**:742-758.
33 Putinski C, Abdul-Ghani M, Stiles R, *et al.* Intrinsic-mediated caspase activation is essential for cardiomyocyte hypertrophy. *Proc Natl Acad Sci USA* 2013; **110**:E4079-4087.
34 Regis G, Pensa S, Boselli D, Novelli F, Poli V. Ups and downs: the STAT1:STAT3 seesaw of interferon and gp130 receptor signalling. *Semin Cell Dev Biol* 2008; **19**:351-359.
35 de Almeida JC, Alves CL, de Abreu LC, *et al.* Involvement of the atrial natriuretic peptide in cardiovascular pathophysiology and its relationship with exercise. *Int Arch Med* 2012; **5**:4.
36 Dick SA, Chang NC, Dumont NA, *et al.* Caspase 3 cleavage of Pax7 inhibits self-renewal of satellite cells. *Proc Natl Acad Sci USA* 2015; **112**:E5246-5252.
37 Duncan JS, Turowec JP, Duncan KE, *et al.* A peptide-based target screen implicates the protein kinase CK2 in the global regulation of caspase signaling. *Sci Signal* 2011; **4**:ra30.
38 Hudlicka O, Brown M, Egginton S. Angiogenesis in skeletal and cardiac muscle. *Physiol Rev* 1992; **72**:369-417.
39 Giordano FJ, Gerber HP, Williams SP, *et al.* A cardiac myocyte vascular endothelial growth factor paracrine pathway is required to maintain cardiac function. *Proc Natl Acad Sci USA* 2001; **98**:5780-5785.
40 Osugi T, Oshima Y, Fujio Y, *et al.* Cardiac-specific activation of signal transducer and activator of transcription 3 promotes vascular formation in the heart. *J Biol Chem* 2002; **277**:6676-6681.
41 Zhou Y, Bourcy K, Kang YJ. Copper-induced regression of cardiomyocyte hypertrophy is associated with enhanced vascular endothelial growth factor receptor-1 signalling pathway. *Cardiovasc Res* 2009; **84**:54-63.
42 Abel ED, Doenst T. Mitochondrial adaptations to physiological vs. pathological cardiac hypertrophy. *Cardiovasc Res* 2011; **90**:234-242.
43 Wang D, Liu X, Liu Y, Shen G, Zhu X, Li S. Treatment effects of Cardiotrophin-1 (CT-1) on streptozotocin-induced memory deficits in mice. *Exp Gerontol* 2017; **92**:42-45.
44 Piek A, de Boer RA, Sillje HH. The fibrosis-cell death axis in heart failure. *Heart Fail Rev* 2016; **21**:199-211.
45 Abe K, Toba M, Alzoubi A, *et al.* Formation of plexiform lesions in experimental severe pulmonary arterial hypertension. *Circulation* 2010; **121**:2747-2754.
46 Jiang B, Deng Y, Suen C, *et al.* Marked strain-specific differences in the SU5416 rat model of severe pulmonary arterial hypertension. *Am J Respir Cell Mol Biol* 2016; **54**:461-468.
47 Ryan JJ, Marsboom G, Fang YH, *et al.* PGC1alpha-mediated mitofusin-2 deficiency in female rats and humans with pulmonary arterial hypertension. *Am J Respir Crit Care Med* 2013; **187**:865-878.
48 Ziaeian B, Fonarow GC. Epidemiology and aetiology of heart failure. *Nat Rev Cardiol* 2016; **13**:368-378.
49 Yancy CW, Jessup M, Bozkurt B, *et al.* 2013 ACCF/AHA guideline for the management of heart failure: a report of the American College of Cardiology Foundation/American Heart Association Task Force on Practice Guidelines. *J Am Coll Cardiol* 2013; **62**:e147-239.
50 Shah SJ, Kitzman DW, Borlaug BA, *et al.* Phenotype-specific treatment of heart failure with preserved ejection fraction: a multiorgan roadmap. *Circulation* 2016; **134**:73-90.
51 Zheng Y, Qin H, Frank SJ, *et al.* A CK2-dependent mechanism for activation of the JAK-STAT signaling pathway. *Blood* 2011; **118**:156-166.
52 Montgomery RL, Potthoff MJ, Haberland M, *et al.* Maintenance of cardiac energy metabolism by histone deacetylase 3 in mice. *J Clin Invest* 2008; **118**:3588-3597.
53 Communal C, Sumandea M, de Tombe P, Narula J, Solaro RJ, Hajjar RJ. Functional consequences of caspase activation in cardiac myocytes. *Proc Natl Acad Sci USA* 2002; **99**:6252-6256.
54 Moretti A, Weig HJ, Ott T, *et al.* Essential myosin light chain as a target for caspase-3 in failing myocardium. *Proc Natl Acad Sci USA* 2002; **99**:11860-11865.
55 Gerdes AM, Kellerman SE, Moore JA, *et al.* Structural remodeling of cardiac myocytes in patients with ischemic cardiomyopathy. *Circulation* 1992; **86**:426-430.
56 Carneiro-Junior MA, Peluzio MC, Silva CH, *et al.* Exercise training and detraining modify the morphological and mechanical properties of single cardiac myocytes obtained from spontaneously hypertensive rats. *Braz J Med Biol Res* 2010; **43**:1042-1046.
57 Carneiro-Junior MA, Primola-Gomes TN, Quintao-Junior JF, *et al.* Regional effects of low-intensity endurance training on structural and mechanical properties of rat ventricular myocytes. *J Appl Physiol* 2013; **115**:107-115.
58 Carneiro-Junior MA, Quintao-Junior JF, Drummond LR, *et al.* The benefits of endurance training in cardiomyocyte function in hypertensive rats are reversed within four weeks of detraining. *J Mol Cell Cardiol* 2013; **57**:119-128.
59 Kemi OJ, Haram PM, Wisloff U, Ellingsen O. Aerobic fitness is associated with cardiomyocyte contractile capacity and endothelial function in exercise training and detraining. *Circulation* 2004; **109**:2897-2904.

60 Glumac S, Pejic S, Kostadinovic S, Stojsic Z, Vasiljevic J. Apoptosis in endomyocardial biopsies from patients with dilated cardiomyopathy. *Folia Biol* 2016; **62**:207-211.
61 van Empel VP, Bertrand AT, Hofstra L, Crijns HJ, Doevendans PA, De Windt LJ. Myocyte apoptosis in heart failure. *Cardiovasc Res* 2005; **67**:21-29.
62 Young KD. The selective value of bacterial shape. *Microbiol Mol Biol Rev* 2006; **70**:660-703.
63 Kunisada K, Negoro S, Tone E, *et al.* Signal transducer and activator of transcription 3 in the heart transduces not only a hypertrophic signal but a protective signal against doxorubicin-induced cardiomyopathy. *Proc Natl Acad Sci USA* 2000; **97**:315-319.
64 Hilfiker-Kleiner D, Hilfiker A, Fuchs M, *et al.* Signal transducer and activator of transcription 3 is required for myocardial capillary growth, control of interstitial matrix deposition, and heart protection from ischemic injury. *Circ Res* 2004; **95**:187-195.
65 Obana M, Maeda M, Takeda K, *et al.* Therapeutic activation of signal transducer and activator of transcription 3 by interleukin-11 ameliorates cardiac fibrosis after myocardial infarction. *Circulation* 2010; **121**:684-691.
66 Bernardo BC, Weeks KL, Pretorius L, McMullen JR. Molecular distinction between physiological and pathological cardiac hypertrophy: experimental findings and therapeutic strategies. *Pharmacol Ther* 2010; **128**:191-227.
67 Takimoto E, Champion HC, Li M, *et al.* Chronic inhibition of cyclic GMP phosphodiesterase 5A prevents and reverses cardiac hypertrophy. *Nat Med* 2005; **11**:214-222.
68 Berry JM, Le V, Rotter D, *et al.* Reversibility of adverse, calcineurin-dependent cardiac remodeling. *Circ Res* 2011; **109**:407-417.
69 Fagard RH, Celis H, Thijs L, Wouters S. Regression of left ventricular mass by antihypertensive treatment: a meta-analysis of randomized comparative studies. *Hypertension* 2009; **54**:1084-1091.
70 Vega RB, Konhilas JP, Kelly DP, Leinwand LA. Molecular mechanisms underlying cardiac adaptation to exercise. *Cell Metab* 2017; **25**:1012-1026.

(**Supplementary information** is linked to the online version of the paper on the *Cell Research* website.)

This work is licensed under a Creative Commons Attribution 4.0 Unported License. The images or other third party material in this article are included in the article's Creative Commons license, unless indicated otherwise in the credit line; if the material is not included under the Creative Commons license, users will need to obtain permission from the license holder to reproduce the material. To view a copy of this license, visit http://creativecommons.org/licenses/by/4.0/

© The Author(s) 2017

Appendix III:

Manuscript:

Dick, SA. et al. (2015) Caspase 3 cleavage of Pax7 inhibits self-renewal of satellite cells. Proceedings of the National Academy of Sciences, USA. 112(38):E5246-52

Caspase 3 cleavage of Pax7 inhibits self-renewal of satellite cells

Sarah A. Dick[a,b], Natasha C. Chang[a], Nicolas A. Dumont[a], Ryan A. V. Bell[a], Charis Putinski[a,b], Yoichi Kawabe[a], David W. Litchfield[c], Michael A. Rudnicki[a,b,d], and Lynn A. Megeney[a,b,d,1]

[a]Regenerative Medicine Program, Sprott Center for Stem Cell Research, Ottawa Hospital Research Institute, Ottawa, ON, Canada K1H 8L6; [b]Department of Cellular and Molecular Medicine, University of Ottawa, Ottawa, ON, Canada K1H 8L6; [c]Department of Biochemistry, Schulich School of Medicine and Dentistry, University of Western Ontario, London, ON, Canada N6A 5C1; and [d]Department of Medicine, University of Ottawa, Ottawa, ON, Canada K1H 8L6

Edited by Eric N. Olson, University of Texas Southwestern Medical Center, Dallas, TX, and approved August 6, 2015 (received for review July 1, 2015)

Compensatory growth and regeneration of skeletal muscle is dependent on the resident stem cell population, satellite cells (SCs). Self-renewal and maintenance of the SC niche is coordinated by the paired-box transcription factor Pax7, and yet continued expression of this protein inhibits the myoblast differentiation program. As such, the reduction or removal of Pax7 may denote a key prerequisite for SCs to abandon self-renewal and acquire differentiation competence. Here, we identify caspase 3 cleavage inactivation of Pax7 as a crucial step for terminating the self-renewal process. Inhibition of caspase 3 results in elevated Pax7 protein and SC self-renewal, whereas caspase activation leads to Pax7 cleavage and initiation of the myogenic differentiation program. Moreover, in vivo inhibition of caspase 3 activity leads to a profound disruption in skeletal muscle regeneration with an accumulation of SCs within the niche. We have also noted that casein kinase 2 (CK2)-directed phosphorylation of Pax7 attenuates caspase-directed cleavage. Together, these results demonstrate that SC fate is dependent on opposing posttranslational modifications of the Pax7 protein.

caspase | satellite cells | Pax7 | casein kinase 2 | self-renewal

Postnatal skeletal muscle retains a robust capacity for compensatory growth and regeneration in response to injury and disease. This physiologic adaptation of skeletal muscle is largely dependent on a resident stem cell population, termed satellite cells (SCs), which exist in a well-defined position juxtaposed to the myofiber (1, 2). In resting skeletal muscle, SCs have low homeostatic turnover and are maintained in a nonproliferative, quiescent state (3). Exogenous activation of SCs may lead to a process of self-renewal, which maintains the stem cell niche, or these cells may commit to the myogenic differentiation program, fusing with existing myofibers to accomplish muscle growth and repair (4, 5). The factors that direct an activated SC to self-renew versus initiate myogenesis are not fully defined, and yet a reasonable hypothesis would envision that acquisition of these divergent cell fates requires a mutually exclusive molecular milieu.

The establishment of the SC lineage is controlled by expression of Pax7, a paired-box transcription factor (6). Targeted deletion of Pax7 results in an almost complete loss of SCs, with a striking deficit in muscle regenerative capacity (6, 7). Although Pax7 is required to instruct the myogenic fate of SCs, continued expression of this protein inhibits the myoblast differentiation program (8, 9). Pax7 has also been reported to regulate distinct panels of genes that promote proliferation and antagonize myogenic differentiation, a function that is consistent with a SC-enriched function for this transcription factor (10). As such, the reduction or removal of Pax7 may denote a key prerequisite for SCs to abandon self-renewal and acquire differentiation competence. How the activated SC retains or eliminates Pax7 protein activity remains unknown.

A probable mechanism that may influence Pax7 protein activity (and by extension SC fate choice) is the restricted deployment of directed proteolysis. The caspase 3 protease, originally identified as the central effector of multiple cell death pathways, has been demonstrated to control cell fate determination independent of inducing cell death (11). Transient activation of caspase 3 is essential for inducing the differentiation program across a broad range of lineage restricted progenitor cells (12). In addition, caspase 3 has been observed to limit self-renewal of embryonic stem cells through direct proteolysis and inactivation of the key pluripotency factor Nanog (13). In skeletal muscle myoblasts, caspase 3 directs a differentiation specific gene expression program by activating the caspase-responsive DNase CAD. Once active, CAD reprograms the genome through targeted DNA damage/strand break events (14).

Previous observations have suggested Pax7 is subjected to caspase/proteasome-dependent regulation (15). Here, we provide evidence that Pax7 is a direct target of caspase 3 at aspartic acid residues D187 and D208. Furthermore, we examined whether limitation of SC self-renewal was dependent on caspase 3-targeted cleavage of Pax7. We noted that loss or inhibition of caspase 3 activity leads to the accumulation of Pax7 protein, expansion of the SC self-renewing compartment, and impeded muscle regeneration. Conversely, small molecule stimulation of caspase 3 depletes Pax7 protein and results in a down-regulation of Pax7 target genes. Moreover, the ability of caspase 3 to target Pax7 is subject to an additional regulatory control via CK2. Here, quiescent and self-renewing SCs maintain elevated CK2 activity, which phosphorylates Pax7 and prevents caspase-mediated degradation of Pax7. Together, these results demonstrate that caspase cleavage of Pax7 is an early and essential step to limit SC self-renewal, thereby establishing a cellular environment that is permissive for muscle differentiation.

Results and Discussion

Inhibition of Caspase 3 Promotes Satellite Cell Self-Renewal. To address the role of caspase 3 activity in SC function, we isolated single muscle fibers from juvenile mice and performed immunofluorescence

Significance

Satellite cells form the resident stem cell population in adult skeletal muscle, providing the foundation for postnatal growth and repair of this tissue. Satellite cell self-renewal is maintained by the paired-box transcription factor Pax7, suggesting that this protein is a key determinant in managing cell fate decisions for this niche. Here, we show activation of caspase 3 protease limits satellite cell self-renewal, through targeted cleavage and inactivation of Pax7 in a casein kinase (CK2)-dependent manner. Temporal regulation of caspase 3 activity may offer a robust mechanism to control the satellite cell compartment and enhance skeletal muscle regeneration.

Author contributions: S.A.D., Y.K., D.W.L., M.A.R., and L.A.M. designed research; S.A.D., N.C.C., N.A.D., R.A.V.B., and Y.K. performed research; D.W.L. and M.A.R. contributed new reagents/analytic tools; S.A.D., R.A.V.B., C.P., and L.A.M. analyzed data; and S.A.D. and L.A.M. wrote the paper.

The authors declare no conflict of interest.

This article is a PNAS Direct Submission.

[1]To whom correspondence should be addressed. Email: lmegeney@ohri.ca.

This article contains supporting information online at www.pnas.org/lookup/suppl/doi:10.1073/pnas.1512869112/-/DCSupplemental.

for active-caspase 3. Isolated and cultured myofibers provide an amenable model that accurately reconstructs the transition of SCs from quiescence to activation/early cell divisions, with well-defined temporal kinetics (T = 0 postculture, quiescence; T = 48 h, early activation; and T = 72 h, full activation) (9). No caspase 3 activity was observed immediately following fiber isolation; however, we observed focal caspase 3 activity in both early and late activated SCs (Fig. 1*A*). This temporal activity pattern is reminiscent of caspase 3 activation in other nondeath settings, which include differentiation of committed skeletal myoblasts and stem cells from a variety of lineages, including neuronal and hematopoietic progenitors (12, 13, 16, 17).

To examine the function of caspase 3 in SC activation and self-renewal, isolated myofibers were incubated with a cell permeable caspase 3 specific peptide inhibitor (20 μM z.DEVD.fmk) and assessed for markers of self-renewal (Pax7) versus commitment to differentiation (MyoD). Sustained Pax7 expression in the absence of myogenic markers is indicative of the self-renewing population (8). Alternatively, SCs with down-regulation of Pax7 and up-regulation of the transcription factors MyoD and myogenin are considered to be a cell population committed to differentiation. SCs expressing both Pax7 and MyoD are understood to be committed cells that remain in a proliferative state. Inactivation of caspase 3 resulted in a significant increase in the number of $Pax7^+/MyoD^-$ SCs on fibers at 3 d postisolation (34.85 ± 3.13% DEVD vs. 15.74 ± 4.61% DMSO; $P < 0.05$) with a corresponding decrease in the number of differentiating cells ($Pax7^-/MyoD^+$; 36.71 ± 3.79% DEVD vs. 54.67 ± 3.85% DMSO; Fig. 1 *B* and *C*). The number of SCs undergoing self-renewal was only found to be significantly increased at 3 and 4 d (38.69 ± 3.77% DEVD vs. 21.93 ± 2.69% DMSO) postisolation (Fig. 1*D*). We saw no significant difference in the number of SCs undergoing self-renewal at 2 d postisolation (Fig. 1*D*), suggesting caspases affect SC fate after the initial division occurs. To confirm this, we used the Myf5-Cre/Rosa-YFP lineage-tracing mouse, which irreversibly labels SCs that have at one time expressed the myogenic transcription factor Myf5. This strategy has been used to identify a population of SCs that are YFP-negative and can undergo a symmetric (producing two YFP- cells) or asymmetric division (producing one YFP^- and one YFP^+ cell) (4). We observed no significant change in these two populations on fibers treated with the caspase 3 inhibitor; however, we did see a decrease in the number of differentiating SCs ($YFP^+/MyoD^-$; 5.30 ± 1.55% in DEVD vs. 12.78 ± 3.44% DMSO) (Fig. S1 *A* and *B*). Importantly, the total number of SCs per fiber did not change with or without caspase 3 inhibition at any of the time points examined (Fig. 1*D* and Fig. S1*B*), confirming that caspase activation in the activated SC population impacts the self-renewal process post Myf5 induction, rather than influencing cell death/cell survival per se.

Caspase 3 Activity Is Required for Skeletal Muscle Regeneration. Muscle regeneration requires proper activation, proliferation, and differentiation of SCs to restore muscle function (18). To determine whether caspase 3 is important to this process, we injected the tibialis anterior (TA) muscle with an adenovirus containing a p35-IRES-GFP vector (or GFP alone as a control). The baculovirus p35 protein is a potent biologic inhibitor of caspase 3/7 activity, which we have previously used for in vivo characterization of caspase activity in the heart (19). Infection with the p35-containing virus (Adp35) at 2 d post-cardiotoxin (CTX) injury resulted in a significant reduction in the minimal Feret's diameter (with the majority of fibers measuring between 10–20 μm; 30.03 ± 2.27%) compared with control (AdGFP)-treated muscle (17.33 ± 4.52% of fibers between 10–20 μm) at 14 d postinjury (Fig. 1*E* and Fig. S1*C*). This was accompanied by a dramatic increase in the number of SCs in the niche (4.49 ± 0.37 GFP^+ cells/field Adp35 vs. 1.7 ± 0.26 GFP^+ cells/field AdGFP; Fig. 1 *F* and *G*), disorganized muscle ultrastructure, and ineffective repair (Fig. S1*D*). In addition, we also examined protein content in TA muscles at 3 and 7 d postinjury to assess the Pax7 protein levels as a proxy for monitoring the SC self-renewal response. We noted a robust increase in Pax7 protein in Adp35-infected muscle at day 7 compared with uninjured control, with a consistent increase in Pax7 protein in the Adp35-treated muscle compared with AdGFP control muscles at day 7 (Fig. 1 *H* and *I*).

Taken together with the isolated myofiber experiments, these observations are consistent with the hypothesis that caspase 3 activity may act as a critical step in the regulation of SC-mediated skeletal muscle repair. At this juncture, it is salient to consider that the in vivo experimental approach (Adp35 infection) may also result in the loss of caspase 3 activity in transduced non-muscle cell types, a condition that could separately influence the outcome of the regenerative process. For example, caspase 3 activity is an essential requirement for both macrophage and T-cell maturation/differentiation (12), and these immune cell types have been demonstrated to infiltrate damaged muscle tissue and enhance regeneration (20). Therefore, the impaired regeneration that follows Adp35 infection may derive from a loss of caspase function in both SCs and critical immune cell subtypes. As such, it will be of considerable interest to parse caspase 3 function within each tissue compartment and determine the relative contribution of each protease signal to the overall repair process.

Pax7 Protein Is Degraded via Caspase 3-Directed Cleavage. The increased numbers of self-renewing SCs following caspase 3 inhibition is consistent with the premise that this protease may act to cleave and inactivate the factor(s) that govern the self-renewal process. Pax7 is a logical target in this regard, because (*i*) the protein content has been shown to decline faster than message content in differentiating myoblasts (21); and (*ii*) simple inspection of the Pax7 protein reveals conserved caspase 3 cleavage sites (Fig. S2*A*). To address a prospective posttranslational regulation of Pax7, we used primary derived myoblasts as a reliable proxy for SCs (which can be harvested in sufficient quantity to conduct accurate biochemical analysis) (22). Pax7 protein is rapidly lost following low serum induction of differentiation, and yet peptide inhibition of caspase 3 maintains elevated Pax7 protein for a 24 h period (Fig. 2*A*). To determine whether caspase 3 directly targets the Pax7 protein, we conducted an in vitro cleavage assay using recombinant active-caspase 3 and recombinant Pax7 proteins. Addition of active-caspase 3 was sufficient to induce an immune-reactive Pax7 cleavage product of ~40 kDa (ΔPax7; Fig. 2*B*). This cleavage event was blocked by addition of the caspase 3 peptide inhibitor, confirming the specificity of Pax7 as a caspase 3 substrate.

Next, we sought to identify the caspase 3 cleavage site(s) within Pax7 and whether the cleavage event is consistent with producing a loss of function for Pax7. Importantly, we observed both a 40-kDa band on a silver-stained gel, which corresponded to the immune-reactive fragment identified via Western blot analysis, as well as a 20-kDa fragment, as predicted, upon addition of active-caspase 3 (Fig. 2*C*, arrows). These two bands were excised and processed for liquid chromatography-tandem mass spectrometry (LC-MS/MS), identifying peptides that clustered to either the N terminus (and within the paired domain) in the case of the 20-kDa fragment or the C terminus (including the homeodomain) for the 40-kDa fragment (Fig. S2*B*). This analysis suggested a physiologic cleavage event that parsed these two regions. To identify the precise caspase 3 cleavage site (an exposed C-terminal aspartic acid), we subjected aliquots of the whole cleavage reaction to enzymatic digestion using three different endoproteases (Chymotrypsin, Trypsin, GluC). Analysis of the Pax7 cleavage reaction products revealed a number of peptides produced following cleavage at D187 that could not be attributed to cleavage via the selected diagnostic endoproteases (Table S1).

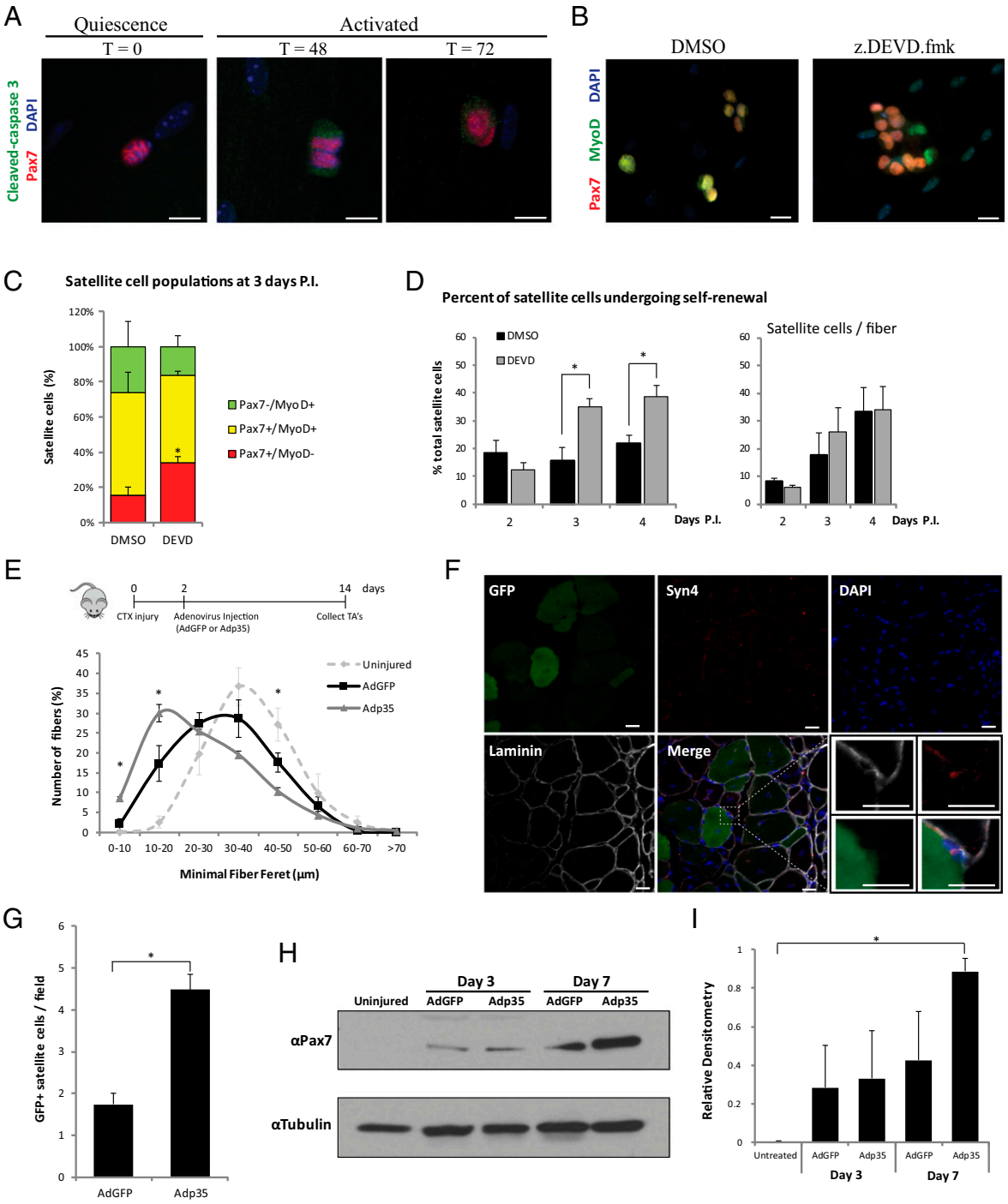


Fig. 1. Caspase 3 activity is required during early satellite cell fate decisions. (*A*) Fibers were stained for cleaved-caspase 3 (green), Pax7 (red), and DAPI (blue) at 48 and 72 h following isolation. Active caspase 3 was observed at a low frequency in fiber-associated SCs at 48 and 72 h but not at time 0 in quiescent SCs. (*B*) Fibers were cultured in z.DEVD.fmk (DEVD; 20 μM) (*Right*) or DMSO (control) (*Left*) for 3 d and stained for Pax7 (red), MyoD (green), and DAPI (blue). (Scale bars: 10 μm.) (*C*) Quantification of the number of SCs expressing each marker at 3 d postinjury (P.I.) expressed as a percentage of the total number of SCs (>30 fibers per treatment per mouse; $n = 4$ mice). (*D*) Quantification of the number of self-renewing SCs ($Pax7^+/MyoD^-$) at 2, 3, and 4 d postinjury (*Left*) and the total number of SCs per fiber (>30 fibers per treatment per time point per mouse; $n = 4$ mice) (*Right*). The percentage of SCs undergoing self-renewal was significantly increase in DEVD-treated fibers compared with control at 3 and 4 d postinjury (*$P < 0.05$). (*E*) Mouse TA muscle was injured with CTX and injected with AdGFP or Adp35 at 2 d postinjury. TAs were embedded and 10-μm-thick frozen sections were stained for immunofluorescence (IF) analysis (Fig. S1C), the minimal fiber Feret's diameter was calculated for GFP^+ fibers, and the frequency of fibers in each bin size was expressed as a percentage of total number of fibers counted (>100 fibers/mouse; $n = 3$ mice/condition; *$P < 0.05$ AdGFP vs. Adp35). (*F*) Representative IF of muscle sections stained for GFP (green), Syn4 (red), laminin (white), and DAPI (blue). (Scale bars: 100 μm.) (*G*) The number of $GFP^+/Syn4^+$ SCs were counted per field indicating an increase in the number of infected SCs in Adp35 infected muscle compared with AdGFP control (*$P < 0.05$; $n = 3$). (*H*) Western blot of whole TA lysate isolated from 3 and 7 d regenerating muscle injected with AdGFP or Adp35 at 1 d postinjury. (*I*) Densitometry results were quantitated from the Western blot (*G*) and averaged from three separate experiments. Pax7 levels were only found significantly increased in day 7 Adp35 mice compared with uninjured control (ANOVA, $P < 0.05$). Error bars ± SEM.

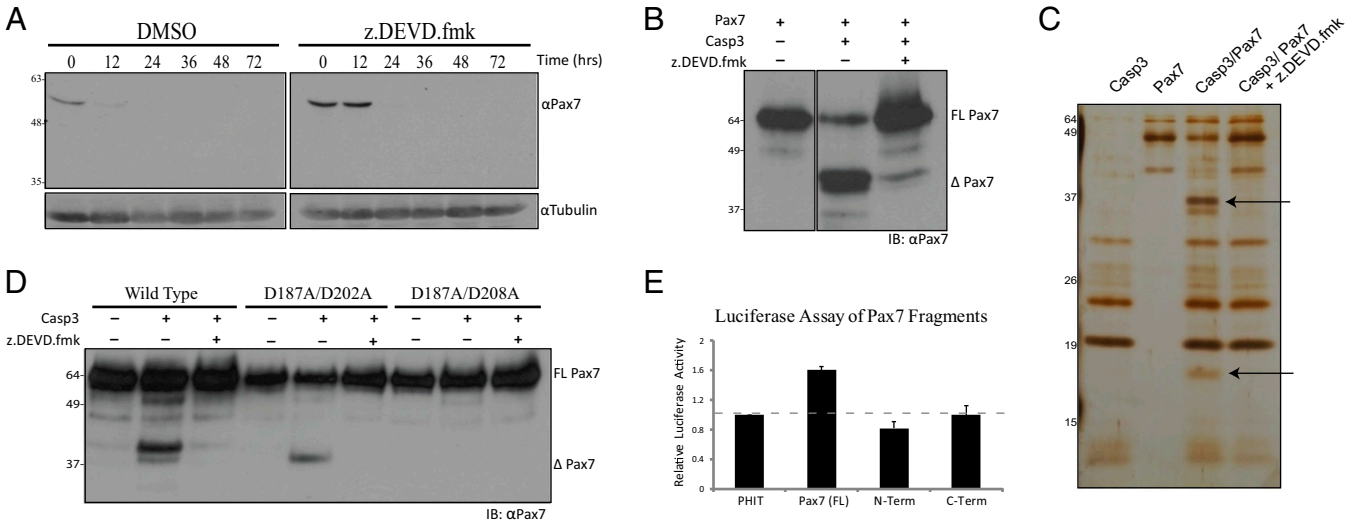


Fig. 2. Pax7 protein is cleaved by caspase 3 at a cryptic cleavage site. (*A*) Differentiation time course of primary myoblasts treated with the caspase 3 peptide inhibitor z.DEVD.fmk (20 μM) or DMSO control. Lysates were probed for αPax7 (upper blots) and α-alpha-tubulin (lower blots; loading control). (*B*) Recombinant Pax7 protein and recombinant active caspase 3 were incubated for 3 h in standard cleavage assay conditions containing either DMSO or z.DEVD.fmk (20 μM) as indicated. Reactions were then subjected to SDS/PAGE and Western blot analysis using αPax7 indicating a caspase 3-specific cleavage event (ΔPax7). (*C*) Pax7 was subjected to caspase 3 cleavage as in *B*, followed by SDS/PAGE and silver stained using silver nitrate. Arrows indicate the Pax7 cleavage fragments (corresponding to ∼40 and ∼20 kDa). (*D*) Recombinant Pax7 protein containing aspartic acid to alanine point mutations at site D187 and D202 or D187 and D208 were subjected to caspase 3 cleavage, followed by Western blot analysis. Pax7 containing D187A/D202A was cleaved; however, D187A/D208A was completely blocked compared with wild type. (*E*) Luciferase Assay performed in COS cells cotransfected with a Pax7 containing plasmid and a luciferase reporter plasmid containing the *Myf5* promoter. Error bars ± SEM; $n = 3$.

D187 mapped to a region that was not detected in either the 40-kDa or the 20-kDa fragments and was localized between the paired and the homeodomain in which the respective peptides clustered (Fig. S2*B*, underlined).

Interestingly, a recombinant Pax7 protein with an alanine substitution at D187 (D187A) displayed partial cleavage via caspase 3, suggesting that Pax7 contained additional cleavage site(s) (Fig. S2*C*). Examination of the Pax7 amino acid sequence indicated two additional aspartic acid residues (D202 and D208) that retain prototypical caspase 3 recognition sites (23). To test the caspase targeting of these residues, we generated the single aspartic acid to alanine Pax7 mutations (D202A and D208A), as well as the relevant Pax7 double mutants (D187A/D202A and D187A/D208A) for use in the caspase cleavage assay. Recombinant Pax7 containing the D187A/D202A double mutant, or any of the single mutants, did not provide effective blockade of caspase directed cleavage (Fig. 2*D* and Fig. S2*C*). However, Pax7 protein containing the dual D187A/D208A aspartic acid to alanine mutations was completely protected from caspase 3 cleavage (Fig. 2*D*), establishing these aspartic acids as de facto caspase target sites. Finally, we examined whether caspase cleavage of Pax7 resulted in loss of function for the resulting Pax7 fragments. COS cells were cotransfected with either full-length [Pax7 (FL)] or truncated Pax7 constructs and a Pax7-responsive promoter linked to a luciferase reporter (*Myf5*-57.5). COS cells transfected with Pax7 (FL) induced expression of the *Myf5*-linked reporter, whereas COS cells expressing either caspase-generated Pax7 fragment [amino acids 1–208 (N terminus) or 209–503 (C terminus)] did not activate the reporter (Fig. 2*E*). These results suggest that caspase cleavage of Pax7 results in the generation of nonfunctional Pax7 fragments.

Exogenous Activation of Caspase 3 Results in Loss of Pax7 and SC Differentiation. The combination of caspase inhibitor experiments and in vitro cleavage assays indicate that caspase activity is necessary to inactivate Pax7 and limit SC self-renewal. To determine whether caspase 3 activation is a dominant (sufficient) signal in determining SC fate, we used a specific small molecule activator of caspase 3, termed procaspase 3-activating compound 1 (PAC-1), to engage protease activity. PAC-1 is a potent and specific procaspase 3-targeted molecule that chelates the inhibitory zinc ions from the catalytic site of the enzyme, leading to autoactivation (24). We have successfully used PAC-1 to produce nonlethal levels of caspase 3 activation, confirming a role for this protease in the induction of cardiac hypertrophy (19). Isolated myofibers treated for 3 h with PAC-1 (50 μM) displayed a significant increase in the number of differentiating SCs (56.41 ± 1.00% $Pax7^{-}$/$Myogenin^{+}$) compared with control (40.81 ± 1.39%), suggesting caspase activation is sufficient to induce differentiation of SCs (Fig. 3 *A* and *B*). We also noted PAC-1 treatment caused a reduction in the number of Pax7 positive cells compared with control treated myofibers ($Pax7^{+}$/$syndecan4^{+}$ cells; Fig. S3 *A* and *B*). To independently confirm these observations, we also tested the capacity of PAC-1 to alter Pax7 levels and the commitment of FACS isolated SCs. Western blot analysis revealed that SCs treated with 25 or 50 μM PAC-1 (a nonlethal concentration in myoblast cultures; Fig. S3*C*) displayed a dramatic reduction in Pax7 protein in growth media conditions, a loss that was comparable to cells exposed to low serum induction of differentiation (Fig. 3 *C* and *D*). Moreover, the PAC-1–induced loss of Pax7 was concurrent to a reduction in the expression of the Pax7 target gene, *Myf5* (Fig. 3*E*). Collectively, these results support the hypothesis that caspase 3 is necessary and sufficient to limit SC self-renewal and establish the molecular conditions that are conducive for differentiation.

Phosphorylation of Pax7 via CK2 Prevents Caspase 3 Cleavage and Promotes SC Self-Renewal. The standalone capacity of caspase 3 to alter self-renewal implies that the SC may have evolved or coopted a mechanism(s) to restrain the protease targeting of Pax7. Interestingly, casein kinase 2 (CK2) has been shown to produce a steric inhibition on caspase 3 cleavage events via phosphorylation of serine residues that reside in close proximity to the caspase 3 cleavage site (25). Indeed, comprehensive proteomic analysis has

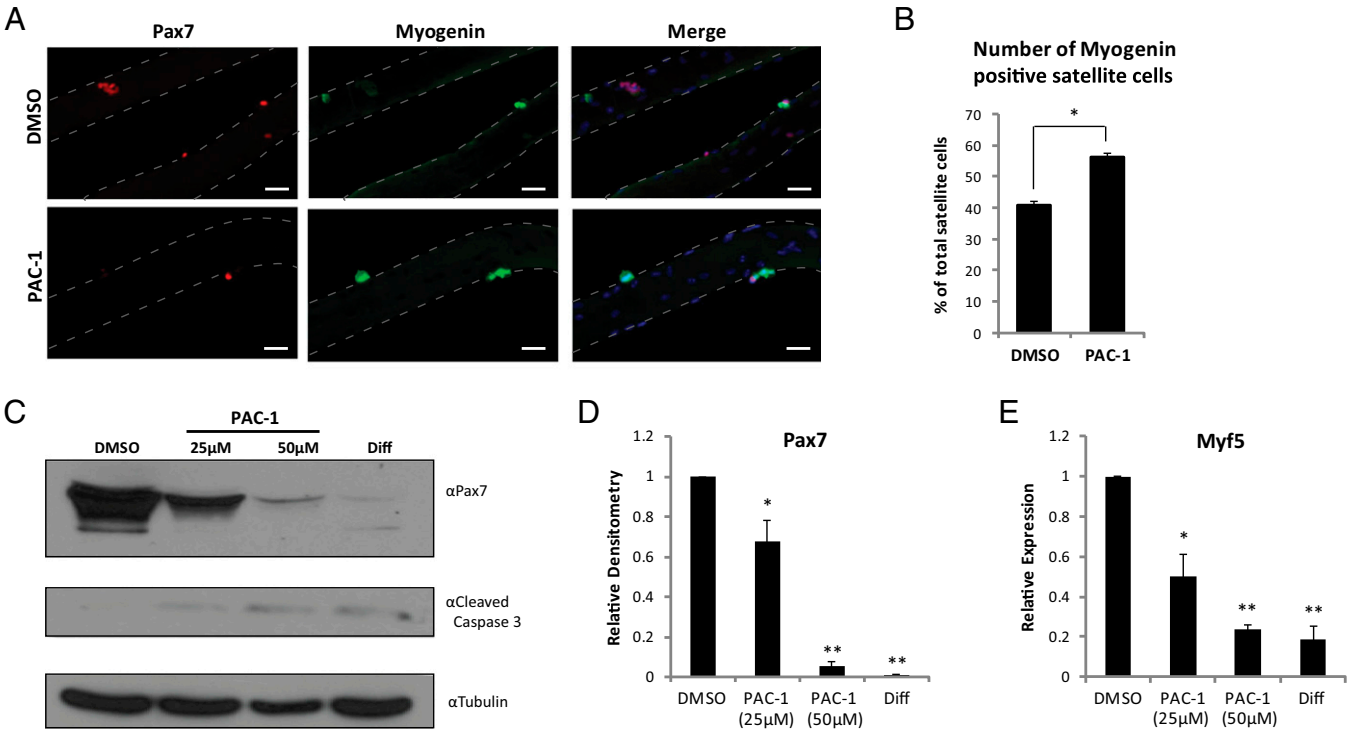


Fig. 3. Small molecule (PAC-1) activation of caspase 3 induces cleavage of Pax7 and loss of SC self-renewal. (*A*) Single fibers were treated with either 50 μM PAC-1 or DMSO 60 h postisolation for 3 h, washed with fresh fiber media, and left for an additional 9 h. At 72 h postisolation, fibers were fixed and stained for Pax7 (red), Myogenin (green), and DAPI (blue). (Scale bars: 20 μm.) (*B*) The number of SCs expressing each marker was counted and the number of myogenin positive SCs ($Pax7^{-}$/$Myogenin^{+}$) was expressed as a percentage of total number of SCs (>30 fibers per treatment per mouse; $n = 3$ mice; $^{*}P < 0.05$). (*C*) Western blot analysis of primary myoblasts treated with PAC-1 at the indicated concentrations for 24 h or differentiation media (Diff). Lysates were probed with αPax7, αCleaved-Caspase3, and αTubulin. (*D*) Densitometry analysis of Pax7 protein levels normalized to tubulin (loading control) shows a decrease similar to that seen in differentiation conditions ($n = 3$). (*E*) Primary myoblasts treated with 25 μM or 50 μM PAC-1, DMSO (control) or differentiation media (diff) for 24 h. RT-quantitative PCR (RT-qPCR) analysis using primers to *Myf5* show a decrease in *Myf5* expression in all treatment groups compared with DMSO control ($n = 3$; $^{*}P < 0.05$; $^{**}P < 0.005$). Error bars ± SEM.

established that caspase 3 cleavage sites and CK2 phosphorylation sites strongly overlap (25, 26). Here, we show that the constitutively active CK2 is present in all activated SCs and the majority (73.0 ± 3.5%) of quiescent SCs (Fig. 4*A*). To address the physiological relevance of CK2 activity and whether this kinase modulates SC self-renewal, we tested the effect of the CK2 specific inhibitor tetrabromobenzotriazole (TBBt) on single fiber cultures. We observed an increase in the differentiation potential of SCs when treated with TBBt (33.55 ± 4.89%) compared with vehicle control (DMSO; 23.68 ± 5.44%), as indicated by the increase in $Pax7^{-}$/$MyoD^{+}$ SCs at 3 d postisolation (Fig. 4 *B* and *C*). There was no significant difference in the number of SCs per fiber, indicating that inhibition of CK2 activity does not impair cell survival.

The Pax7 amino acid sequence contains two serine residues (S201 and S205), which are consistent with a CK2 consensus sequence and in close proximity to the caspase-targeted aspartic acid residue at position D208 (Fig. 4*D*). To confirm Pax7 is a direct target of CK2, we performed an in vitro kinase assay (Fig. 4*E*), observing phosphorylation of Pax7 protein that was completely blocked by addition of the CK2 inhibitor TBBt (Fig. S4*A*). Point mutations of Pax7 at S201 or S205 revealed that only S201 in recombinant Pax7 protein was directly phosphorylated by CK2 in vitro (Fig. 4*F*). The specificity of this phosphorylation event was confirmed via MS peptide mapping of Pax7 protein following incubation with CK2 (Fig. S4*B*).

Next, we tested whether prior CK2 phosphorylation of recombinant Pax7 was sufficient to inhibit cleavage via active caspase 3. Interestingly, CK2 phosphorylation of Pax7 resulted in the generation of a single cleavage fragment of wild-type Pax7 (Fig. 4*G*, †), compared with the two cleavage products generated from unphosphorylated Pax7 protein (Fig. 4*G*, † and ‡). This result suggested that CK2 mediated phosphorylation of Pax7 S201 may shield only one of the caspase-directed cleavage sites. To identify the CK2 protected caspase cleavage site, we tested the D187A and D208A single Pax7 mutants in the same serial kinase/cleavage assay used above. CK2 phosphorylation followed by caspase 3 incubation of the D187A mutant displayed a similar cleavage pattern to uncleaved Pax7 (Fig. 4*G*), whereas the caspase cleavage products generated from the D208A mutant were unaffected by a prior CK2-mediated phosphorylation event (Fig. 4*G*, *Center*). This experiment revealed that CK2 phosphorylation at S201 was sufficient to block Pax7 cleavage at a single cleavage site, D208. Together these results demonstrate a physiologic interaction between CK2 and caspase 3 in the control of Pax7 protein stability.

The persistence of CK2 in cells throughout differentiation is related to the cell survival functions attributed to this kinase (27). Moreover, the CK2 holoenzyme is constitutively active (28), suggesting that the subcellular localization and binding partners of CK2 are the primary determining factor in its substrate-targeting capacity. To investigate the functional interplay between Pax7 and CK2, we performed proximity ligation assay (PLA) on primary myoblasts during a differentiation time course. We observed strong CK2:Pax7 interactions in a perinuclear position during growth (1.85 ± 0.13 puncta/cell) and at 6 h postdifferentiation (1.51 ± 0.14 puncta/cell), which was rapidly dissipated as the differentiation program proceeded (0.68 ± 0.10 puncta/cell by 24 h postdifferentiation) (Fig. 4*H*). The temporal loss of the CK2:Pax7 interaction coincides precisely with the

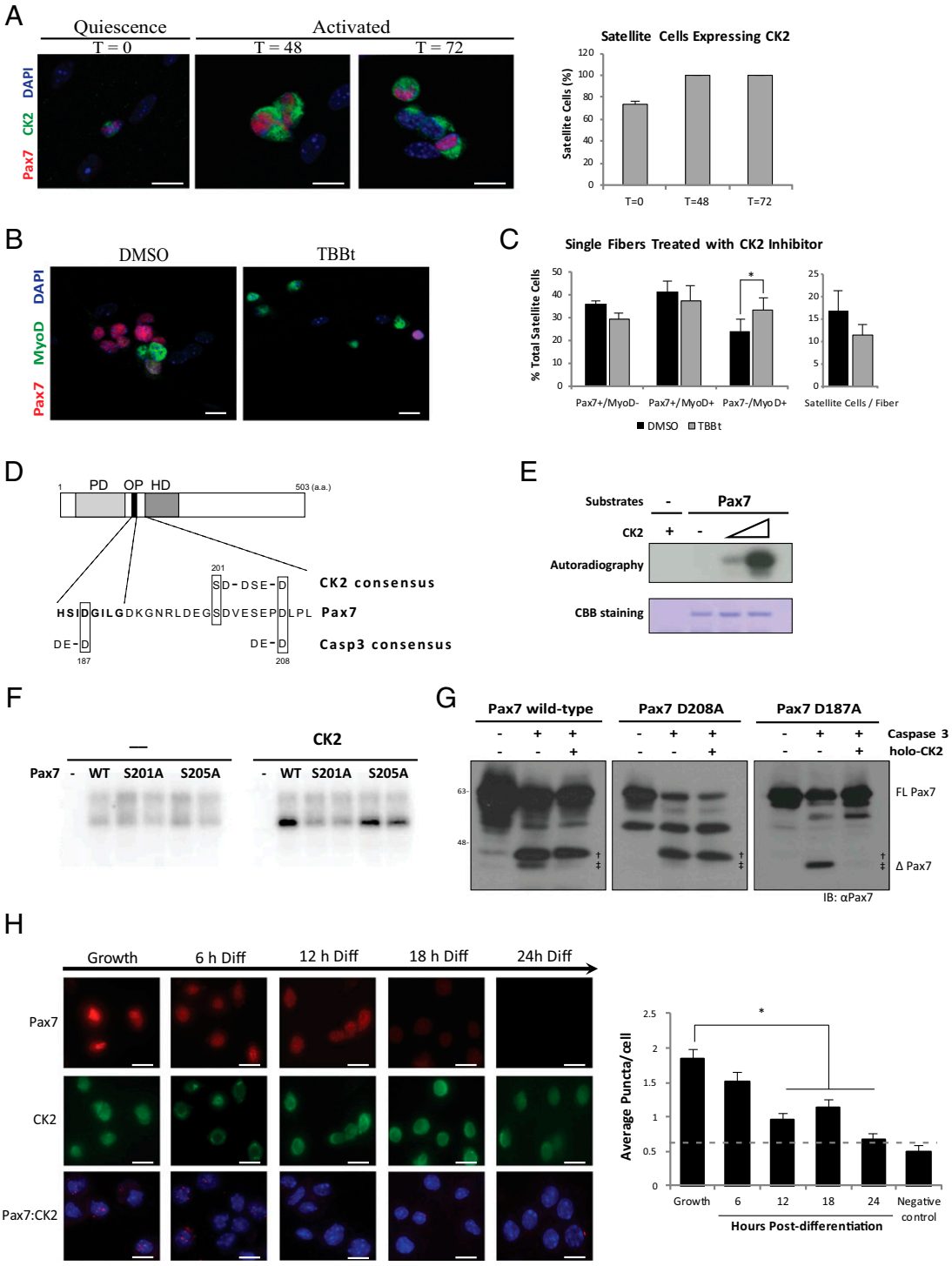


Fig. 4. CK2 phosphorylates Pax7 and restricts SC differentiation. (*A*) Fibers were stained for CK2α (green), Pax7 (red), and DAPI (blue) (*Left*). CK2 is expressed by fiber associated SCs at all time points tested ($n = 3$) (*Right*). (*B*) Fibers were cultured in the presence of the CK2 inhibitor TBBt (50 μM) or DMSO for 3 d and stained for Pax7 (red), MyoD (green), and DAPI (blue). (*C*) Quantification of the number of SCs expressing each marker expressed as a percentage of total SCs. Fibers treated with TBBt contained more differentiating $Pax7^{-}/MyoD^{+}$ SCs compared with DMSO control ($n = 4$; $^{*}P < 0.05$). (*D*) Schematic of Pax7 protein indicating the caspase 3 cleavage sites, as well as the CK2 phosphorylation site located between the paired domain (PD) and the homeodomain (HD) of Pax7. The octapeptide (OP) sequence is bolded. (*E*) In vitro kinase assay of CK2 and Pax7. Autoradiography indicates Pax7 is phosphorylated by CK2 in a dose-dependent manner. (*F*) In vitro kinase assay of wild-type Pax7 or Pax7 with site mutations at S201A or S205A. Autoradiography indicating loss of phosphorylation in the S201A mutant only. (*G*) Recombinant Pax7 was subjected to an in vitro kinase assay as in *E*. Aliquots from each reaction were then subjected to caspase 3 cleavage, SDS/PAGE, and Western blot analysis using αPax7. Production of the Pax7 cleavage fragments (ΔPax7, † and ‡) was impaired in the D187A mutant following preincubation with CK2. (*H*, *Left*) Primary myoblasts were fixed at the indicated times and stained for Pax7 (red) (*Top*), CK2 (green) (*Middle*), or PLA [red dots indicate PLA reaction, costained with DAPI (blue)] (*Bottom*). (*H*, *Right*) PLA showed a positive interaction between CK2 and Pax7 at growth and 6 h following differentiation (6 h Diff). The number of PLA-positive puncta per cell was quantified (80–150 cells/treatment; $n = 3$). Error bars represent ± SEM. $^{*}P < 0.05$. (Scale bars: 10 μm.)

endogenous caspase 3 activation profile (29) and the consequent loss of Pax7 protein. Additionally, we performed PLA on isolated single fibers to verify the CK2 and Pax7 interaction in SCs in situ. We detected a clear PLA signal in SCs at 48 h following myofiber isolation, a time point that coincides with SC activation/proliferation and before the initiation of the differentiation program (Fig. S4*C*). These results in combination with the results obtained using the CK2 inhibitor TBBt (Fig. 4 *B* and *C*) suggest that CK2 ensures protein stability of Pax7 in proliferating/self-renewing SCs and loss of this kinase function is a key step in initiating myogenic differentiation.

Caspase 3 activation is an essential cue for promoting differentiation of committed progenitor cells (12). Our study demonstrates that caspase 3 also acts at a much earlier step in the life cycle of muscle stem cells, by limiting the self-renewal process. Caspase 3 blocks SC self-renewal by cleavage inactivation of Pax7 protein, a mechanism that is counter balanced by CK2-mediated phosphorylation of Pax7. Blockade of caspase activity extends self-renewal in the SC pool, whereas inhibition of CK2 leads to increased numbers of differentiation committed cells, revealing that SC fate is strongly influenced by competing post-translational modifications of Pax7.

The mechanisms involved in the posttranslational regulation of Pax7 protein stability during myoblast differentiation has only been briefly analyzed (15). However, its close paralogue, Pax3, has been demonstrated to be regulated by ubiquitin-mediated degradation (30). Although these studies ruled out a role for the ubiquitin/proteasome pathway in the regulation of Pax7, a role for CK2 has never previously been examined. Here, we provide, to our knowledge, the first evidence that CK2 mediates Pax7 stability during muscle differentiation and is important for SC self-renewal. This mechanism may also have implications in the regulation of the Pax7-FOXO1 fusion protein, the overexpression of which plays a causative role in the tumorigenicity of the skeletal muscle cancer, alveolar rhabdomyosarcoma (31). Indeed, CK2 phosphorylation of Pax3-FOXO1 enhances its protein stability in transformed cells (32). This study did not address the mechanism of Pax3 degradation; however, we predict a similar mechanism involving caspase 3, as we have demonstrated here for Pax7.

In summary, our study is, to our knowledge, the first to demonstrate that caspase 3 limits self-renewal of a lineage restricted stem/progenitor cell. Caspase 3 has been previously reported to inhibit ES cell self-renewal through targeted cleavage of the pluripotency factor Nanog (13). Therefore, it is reasonable to conclude that a similar dichotomous phosphorylation/cleavage modification of Nanog controls ES cell self-renewal, with CK2 and caspase 3 acting as the respective competing enzymes. We speculate that the caspase 3/CK2 targeting of self-renewal factors is a broadly conserved phenomenon, affecting cell fate determination across all lineages.

Materials and Methods

For a more detailed discussion of the materials and methods, see *SI Materials and Methods*. All animal studies were approved by the University of Ottawa Animal Care Committee.

Fibers were isolated from 6- to 8-wk-old mice and cultured in DMEM Fiber Media with z.DEVD.fmk (20 μM; BioVision), TBBt (20 μM; Chemicon), PAC-1 (25–50 μM; Abcam), or DMSO (control). Inhibition of caspase 3 in vivo was accomplished by infecting TA muscles with adenovirus containing a p35-IRES-GFP cassette (or IRES-GFP control) at 1 or 2 d post-CTX injury, and tissue was collected at 3 and 7 d for Western blot analysis or fixed at 14 d for sectioning and immunostaining. For in vitro cleavage assays, recombinant Pax7 protein (100–300 ng) and recombinant active-caspase 3 (0.5 μg; Chemicon) were incubated at 37 °C for 3 h in cleavage assay buffer containing either DMSO or z.DEVD.fmk (20 μM; BioVision) as indicated. Kinase assays were performed by combining recombinant Pax7 (100 ng) with increasing concentrations of purified GST-CK2 in standard kinase assay conditions containing γ[^{32}P]ATP (0.04 μCi/μL) for 1 h at 30 °C. Reactions were stopped by addition of Laemmli sample buffer, subjected to SDS/PAGE, and either Western blot analysis using αPax7 primary antibody or autoradiography. All data are expressed as means ± SEM. The Student *t* test was used for comparisons between treatments unless specified, with $P < 0.05$ considered significant.

ACKNOWLEDGMENTS. We thank members of the L.A.M. laboratory for technical help and insightful discussions; Dr. Lawrence Puente for the mass spectrometry work and data analysis; and Dr. Fabien LeGrand for scientific discussions. This work was supported by grants from The Muscular Dystrophy Association USA, The Canadian Institute of Health Research, and the Ontario Research Fund (to L.A.M.). L.A.M. held the Mach Gaennslen Chair in Cardiac Research, and S.A.D. is supported by Queen Elizabeth II Graduate Scholarship in Science and Technology.

1. Mauro A (1961) Satellite cell of skeletal muscle fibers. *J Biophys Biochem Cytol* 9:493–495.
2. Bentzinger CF, von Maltzahn J, Rudnicki MA (2010) Extrinsic regulation of satellite cell specification. *Stem Cell Res Ther* 1(3):27.
3. Yin H, Price F, Rudnicki MA (2013) Satellite cells and the muscle stem cell niche. *Physiol Rev* 93(1):23–67.
4. Kuang S, Kuroda K, Le Grand F, Rudnicki MA (2007) Asymmetric self-renewal and commitment of satellite stem cells in muscle. *Cell* 129(5):999–1010.
5. Chargé SB, Rudnicki MA (2004) Cellular and molecular regulation of muscle regeneration. *Physiol Rev* 84(1):209–238.
6. Seale P, et al. (2000) Pax7 is required for the specification of myogenic satellite cells. *Cell* 102(6):777–786.
7. von Maltzahn J, Jones AE, Parks RJ, Rudnicki MA (2013) Pax7 is critical for the normal function of satellite cells in adult skeletal muscle. *Proc Natl Acad Sci USA* 110(41):16474–16479.
8. Olguin HC, Olwin BB (2004) Pax-7 up-regulation inhibits myogenesis and cell cycle progression in satellite cells: A potential mechanism for self-renewal. *Dev Biol* 275(2):375–388.
9. Zammit PS, et al. (2004) Muscle satellite cells adopt divergent fates: A mechanism for self-renewal? *J Cell Biol* 166(3):347–357.
10. Soleimani VD, et al. (2012) Transcriptional dominance of Pax7 in adult myogenesis is due to high-affinity recognition of homeodomain motifs. *Dev Cell* 22(6):1208–1220.
11. Abdul-Ghani M, Megeney LA (2008) Rehabilitation of a contract killer: Caspase-3 directs stem cell differentiation. *Cell Stem Cell* 2(6):515–516.
12. Dick SA, Megeney LA (2013) Cell death proteins: An evolutionary role in cellular adaptation before the advent of apoptosis. *BioEssays* 35(11):974–983.
13. Fujita J, et al. (2008) Caspase activity mediates the differentiation of embryonic stem cells. *Cell Stem Cell* 2(6):595–601.
14. Larsen BD, et al. (2010) Caspase 3/caspase-activated DNase promote cell differentiation by inducing DNA strand breaks. *Proc Natl Acad Sci USA* 107(9):4230–4235.
15. Olguín HC (2011) Regulation of Pax7 protein levels by caspase-3 and proteasome activity in differentiating myoblasts. *Biol Res* 44(4):323–327.
16. Fernando P, Brunette S, Megeney LA (2005) Neural stem cell differentiation is dependent upon endogenous caspase 3 activity. *FASEB J* 19(12):1671–1673.
17. Janzen V, et al. (2008) Hematopoietic stem cell responsiveness to exogenous signals is limited by caspase-3. *Cell Stem Cell* 2(6):584–594.
18. Sambasivan R, et al. (2011) Pax7-expressing satellite cells are indispensable for adult skeletal muscle regeneration. *Development* 138(17):3647–3656.
19. Putinski C, et al. (2013) Intrinsic-mediated caspase activation is essential for cardiomyocyte hypertrophy. *Proc Natl Acad Sci USA* 110(43):E4079–E4087.
20. Aurora AB, et al. (2014) Macrophages are required for neonatal heart regeneration. *J Clin Invest* 124(3):1382–1392.
21. Dey BK, Gagan J, Dutta A (2011) miR-206 and -486 induce myoblast differentiation by downregulating Pax7. *Mol Cell Biol* 31(1):203–214.
22. Pasut A, Oleynik P, Rudnicki MA (2012) Isolation of muscle stem cells by fluorescence activated cell sorting cytometry. *Methods Mol Biol* 798:53–64.
23. Thornberry NA, et al. (1997) A combinatorial approach defines specificities of members of the caspase family and granzyme B. Functional relationships established for key mediators of apoptosis. *J Biol Chem* 272(29):17907–17911.
24. Putt KS, et al. (2006) Small-molecule activation of procaspase-3 to caspase-3 as a personalized anticancer strategy. *Nat Chem Biol* 2(10):543–550.
25. Duncan JS, et al. (2011) A peptide-based target screen implicates the protein kinase CK2 in the global regulation of caspase signaling. *Sci Signal* 4(172):ra30.
26. Turowec JP, et al. (2014) An unbiased proteomic screen reveals caspase cleavage is positively and negatively regulated by substrate phosphorylation. *Mol Cell Proteomics* 13(5):1184–1197.
27. Duncan JS, et al. (2010) Regulation of cell proliferation and survival: Convergence of protein kinases and caspases. *Biochim Biophys Acta* 1804(3):505–510.
28. Turowec JP, et al. (2010) Protein kinase CK2 is a constitutively active enzyme that promotes cell survival: Strategies to identify CK2 substrates and manipulate its activity in mammalian cells. *Methods Enzymol* 484:471–493.
29. Fernando P, Kelly JF, Balazsi K, Slack RS, Megeney LA (2002) Caspase 3 activity is required for skeletal muscle differentiation. *Proc Natl Acad Sci USA* 99(17):11025–11030.
30. Boutet SC, Disatnik MH, Chan LS, Iori K, Rando TA (2007) Regulation of Pax3 by proteasomal degradation of monoubiquitinated protein in skeletal muscle progenitors. *Cell* 130(2):349–362.
31. Barr FG (2001) Gene fusions involving PAX and FOX family members in alveolar rhabdomyosarcoma. *Oncogene* 20(40):5736–5746.
32. Dietz KN, Miller PJ, Iyengar AS, Loupe JM, Hollenbach AD (2011) Identification of serines 201 and 209 as sites of Pax3 phosphorylation and the altered phosphorylation status of Pax3-FOXO1 during early myogenic differentiation. *Int J Biochem Cell Biol* 43(6):936–945.